PHOSPHORUS/ANTIMONY AND PHOSPHORUS/H-BOND DONOR AMBIPHILIC LIGANDS: INCORPORATION INTO LATE TRANSITION METAL COMPLEXES AND THE REACTIVITY THEREOF

A Dissertation

by

SROBONA SEN

Submitted to the Office of Graduate and Professional Studies of
Texas A&M University
in partial fulfillment of the requirements for the degree of

DOCTOR OF PHILOSOPHY

Chair of Committee,	François P. Gabbaï
Committee Members,	Marcetta Y. Darensbourg
	Oleg V. Ozerov
	Sreeram Vaddiraju
Head of Department,	Simon W. North

December 2017

Major Subject: Chemistry

ABSTRACT

Z-type ligands based on main group Lewis acids like Sb(V), B(III) and Al(III) etc. have heralded a new direction in the coordination chemistry of transition metals. Although ambiphilic ligands featuring group 13 and 14 main group elements have been explored in the realm of coordination chemistry of late transition metals, utilization of heavy group 15 elements remains mostly limited to L-type spectator ligands. Recent research on transition metal/antimony platforms has shown that the electronic properties of the transition metal centers can be successfully modulated with the help of carefully crafted Lewis acidic ligands due to their versatile redox and coordination non-innocent properties. In this dissertation, I have studied the structure-property correlation in a series of heterobimetallic platforms featuring antimony-based Z-ligands with tunable stereo-electronic properties.

This dissertation delineates the investigation of the effects of strongly Lewis acidic antimony center on the coordination chemistry and the reactivity of the ligated metal center in a series of [Sb-M] compounds. A systematic analysis of the Lewis acidity, coordination properties and the catalytic activities of the Sb-M complexes proved that the variation of the substituents at antimony and phosphorus plays a significant role in the bonding and electron distribution between the Lewis acid and the transition metal center and this modulation of electronic properties has been exploited for electrophilic catalysis as well as for the photoreductive elimination of halogens.

My second project is inspired by the basic concept that the metal-ligand cooperativity plays an important role in enhancing the catalytic activities of the metal

centers. Recent development in gold catalysis focusses on new methods to bypass the use of silver salt metathesis by introducing metal-ligand cooperativity in gold complexes. I have discovered a novel route to self-activate the gold center and overcome the synthetic difficulties posed by the use of light- and moisture-sensitive silver salts in gold catalysis by introducing a H-bond donor functional group in the ligand framework to provide.

DEDICATION

Ma, Baba, Bhai

and

Arghya

ACKNOWLEDGEMENTS

First and foremost I thank Prof. François P. Gabbaï for giving me the opportunity to be a part of his group when I came to Texas A&M University. His ideas, encouragement and support are the true foundation upon which my Ph.D. career is built.

I thank Prof. Marcetta Y. Darensbourg, Prof. Oleg V. Ozerov and Prof. Sreeram Vaddiraju for sitting in my committee and being a constant source of encouragement and constructive criticism.

I thank my Masters' advisor Prof. R. N. Mukherjee at IIT Kanpur, who is undoubtedly the best inorganic chemistry teacher I have ever had, for his guidance and tutelage. His teaching rejuvenated my interest in inorganic chemistry.

I am indebted to my teachers at Presidency College for teaching me and opening a whole new exciting world of chemistry in front of me. They are the most inspiring teachers in this world and it is because of their teaching of chemistry and encouragements, I am what I am today.

I am deeply thankful to the past and present members of the Gabbaï group. Dr. Casey Wade, Dr. Iou-Sheng Ke, Dr. Baofei Pan, Dr. Kewei Huang, Dr. Boris Vabre, Dr. Daniel Tofan, Dr. Guillaume Bélanger-Chabot, Dr. Sumit Sahu, Dr. Kantapat Chansaenpak, Dr. Masato Hirai, Dr. James (Stuart) Jones, Lauren Leamer, Dr. Anna Marie Christianson, Ahmed Ali, Mengxi (Moncy) Yang, Chang-Hong Chen (Eric), Elham Tabei, , Ying-Hao Lo (Russell), Di You, Gregory Day, Christina Lollar, Kevin Jack and L. Chase

Elrod. Very special thanks goes to Dr. Iou-Sheng Ke, Dr. Masato Hirai and Dr. James Stuart Jones for their mentorship and guidance during the early years of my Ph.D.

I would like to thank my brother Mr. Subham Sen, who is my biggest critic yet my greatest friend, for his unwavering support, compassion and playful mischief, without which I would not have survived this journey.

My heartfelt thanks goes to my best friend Mr. Arghya Sarkar who has been by my side my entire adult life through all the ups and downs. His unconditional love and friendship has been the most cherished treasure of my life. It will be an honor to spend the rest of my life with him.

I would like to thank Mr. Sayan Saha for all the wonderful time that we spent together. It is my privilege to be his sister and friend. I thank all my class mates in Presidency College who accepted me with open arms despite my many flaws and continue to be my closest friends. I am truly grateful to Mr. Satrajit Indu whose friendship and sense of humor always makes a day brighter. I am incredibly lucky to have him as a friend and a brother. The friendship and compassion of Ms. Pradipta Das is something that I will cherish forever.

I thank Ms. Arpita Mitra for helping me through numerous difficult cross-roads of my life…both figuratively and literally!

I thank the Bengali Community of College Station for being a surrogate family and making this city a home away from home. I thank Dr. Yindrila Chakraborty for being a mentor in every sense of the word. Ms. Deepika Das, Mr. Rajat Maji, Dr. Vangmayee Sharma are the most wonderful friends and colleagues anyone could ask for. The

friendship of Ms. Ananya Dasgupta, Ms. Isita Jhulki, Mr. Sanjoy Adak, Dr. Sharmila Ghosh, Mr. Shachin Patra, and Mr. Pokhraj Ghosh has been the brightest highlights of the past five years. I am grateful to Ms. Ratnamala Mandal for tolerating my chatter and making the third floor of '72 wing a much more enjoyable place!

It was an honor to be a part of Women in Science and Engineering at TAMU and work with truly awesome and talented ladies from different departments. I am also grateful to serve as an officer in the Organization for Cultural Diversity in Chemistry.

I am indebted to the Department of Chemistry at Texas A&M University for providing the funding, resources and travel awards which were the most important part of my Ph.D.

I thank the wonderful and caring doctors and nurses of Brazos Valley Women's Center and St. Joseph's Hospital for taking care of me when I was at my worst health.

Last but not the least, I thank my parents Dr. Rana Sen and Dr. Soma Sen, from whom I inherited the 'Chemistry Gene'! My first exposure to chemistry happened when I accompanied them to their respective labs as a little kid and they showed me colorful test tube reactions to keep me entertained. Their insistence, encouragement and support in pursuing a career in Chemistry has been the biggest motivation behind my academic pursuits.

CONTRIBUTORS AND FUNDING SOURCES

Contributors

This work was supervised by a dissertation committee consisting of Professor François P. Gabbaï (advisor), Professor Marcetta Y. Darensbourg and Prof. Oleg V. Ozerov of the Department of Chemistry and Professor Sreeram Vaddiraju of the Department of Chemical Engineering.

The crystal structures of complex **58** mentioned in the introduction of Section 2 was reported by Dr. Iou-Sheng Ke. The PGSE measurements on complex **76** was performed by Ms. Chia-Hsiu Chen from the group of Professor Christian Hilty of the Department of Chemistry.

All other work conducted for dissertation was completed by the student independently.

Funding Sources

This graduate work was supported by the National Science Foundation (CHE-1566474), the Welch Foundation (A-1423), and Texas A&M University (Arthur E. Martell Chair of Chemistry).

NOMENCLATURE

COD	Cyclooctadiene
COE	Cyclooctene
DCM	Dichloromethane
DFT	Density functional theory
DMAP	4-Dimethylaminopyridine
DMF	N,N-dimethylformamide
DMSO	Dimethylsulfoxide
ESI	Electron spray ionization
GC	Gas chromatography
HOMO	Highest occupied molecular orbital
LUMO	Lowest unoccupied molecular orbital
MeCN	Acetonitrile
MLCT	Metal-to-ligand charge transfer
MS	Mass spectrometry
NBO	Natural bond orbital
NFSI	N-fluorodiphenylsulfonimide
NLMO	Natural localized molecular orbital
NMR	Nuclear magnetic resonance
PGSE	Pulse gradient spin echo
TBAT	Tetra-n-butylammonium triphenyldifluorosilicate

TBAF	Tetra-n-butylammonium fluoride
TD-DFT	Time-dependent density functional theory
TFA	Trifluoroacetic acid
THF	Tetrahydrofuran
tht	Tetrahydrothiophene
TM	Transition metal
XRD	X-ray diffraction

TABLE OF CONTENTS

Page

LIST OF FIGURES

Page

LIST OF TABLES

1. INTRODUCTION TO THE COORDINATION CHEMISTRY OF ANTIMONY BASED Z-LIGANDS AND THEIR APPLICATIONS

1.1 Coordination chemistry of main group Lewis acids

1.1.1 A brief introduction to main group Lewis acids

Lewis acids are defined as chemical compounds that can accept an electron pair from a Lewis base into its empty orbital.[1] The fundamental concept of the formation of a thermodynamically stable dative bond between an electron pair donor and an acceptor has formed the basis of modern organometallic chemistry.[2] Since the identification of the simplest Lewis acid-base adduct $H_3N{\rightarrow}BH_3$, the chemistry of Lewis acids has been dominated by group 13 elements (B, Al, Ga, In, Tl) due to the presence of an empty p_z-orbital capable of accepting electron density from a donor moiety (Figure 1). Amongst the group 13 elements, boron has attracted the most attention because of its intrinsic Lewis acidity.[3] By virtue of the strong anion affinity resulting from the electron unsaturation, borane-based Lewis acids have been at the forefront of the anion sensing chemistry. [4-5] In addition to their application in the field of anion-recognition, boranes have also found use in organic synthesis as electrophilic catalysts[6-9] and as external activators for organometallic polymerization pre-catalysts.[10-12] With the advent of 'frustrated Lewis pair' (FLP) chemistry, boranes have been extensively used in small molecule activation.[13] The heavier group 13 elements (Al, Ga and In) also show impressive Lewis acidity and constitute a significant part of FLP chemistry. Compared to the extensive study of group 13 Lewis acids, the exploration of Lewis acidity of hypervalent heavy group 14

compounds (Si, Ge, Sn and Pb) which arises from the presence of vacant *d* orbitals is a relatively new yet fast growing field (Figure 1).[14-15]

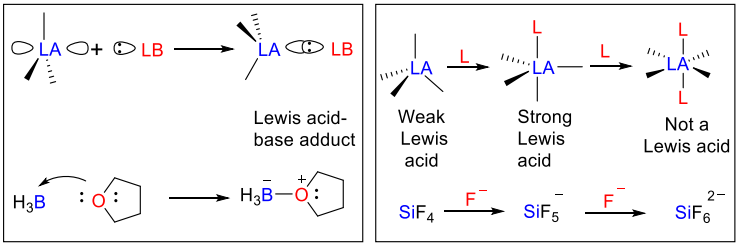

Figure 1. Lewis acidity of group 13 (left) and group 14 (right) elements.

While it may be a general perception that strong Lewis acidity is an unique property of group 13 elements such as boron, the work of Olah has shown that strong Lewis acidity can also be expressed by group 15 elements, especially antimony in its +V oxidation state.[16-18] Early experimental work by Gutmann shows that the chloride ion affinity of $SbCl_5$ exceeds that of BCl_3, suggesting that the former is a stronger Lewis acid.[19] The following trend in Lewis acidity was established by Gutmann:

$$SbCl_5 > SnCl_4 > ZnCl_2 > SbCl_3 > PCl_5$$

A similar conclusion can be derived from a comparison of the computed gas phase fluoride ion affinity (FIA) of SbF_5 (489 kJ/mol) and BF_3 (338 kJ/mol), with the former exceeding the latter by more than 150 kJ/mol.[20]

In contrast to group 13 elements where an empty *p*-orbital acts as the electron acceptor, the Lewis acidity of antimony arises from low-lying σ*-orbital as depicted in Figure 2. Remarkable Lewis acidity of antimony(V) was attributed to its large size that

supports higher coordination number and the resulting polarizability. and also to the electropositive nature of antimony. Antimony(III) compounds are also known to be Lewis acidic when substituted with strong electron-withdrawing ligands as in the examples depicted in Figure 2. Compounds **1**,[21-22] **2**[23] and **3**[24] all feature electron-withdrawing chloride ligands bound to antimony leading to strong N-Sb dative bonds. It has also been demonstrated that the Lewis acidity of stibines increases with the number of halogen substituents. Perhaps, the most interesting feature of these derivatives is their capability to undergo two-electron oxidation which augments their Lewis acidity due to the formation of the corresponding highly electron deficient Sb(V) species as a neutral stiborane or cationic stibonium (Figure 2).

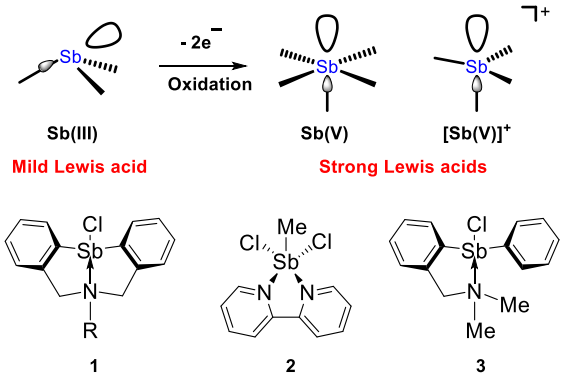

Figure 2. Top: Acceptor orbitals of Sb(III) and Sb(V) compounds. Bottom: Lewis acidic nature of halostibines.

While antimony halides are moisture-sensitive which limits their use as anion sensors, aryl antimony compounds provide viable route to explore the practical

applications of antimony Lewis acids in the domain of anion sensing and catalysis. Our group has pioneered in developing air- and moisture-stable neutral and cationic aryl antimony(V) derivatives which show exceptional fluoride affinity and can be used as efficient fluoride sensors at ppm level in water.[25-29]

1.1.2 Coordination chemistry of group 13 and group 14 ligands

The use of electron deficient compounds as ligands in coordination chemistry is counter-intuitive to the traditional description of a metal-ligand bond where the ligand is either an anionic one electron donor (X-) or a neutral two electron donor (L-type) ligand.[30] Yet, the electron affinity of main group Lewis acids have been utilized to develop a new class of ligand called Z-type ligand which can accept an electron pair from a metal fragment into an empty orbital (Figure 3).[31-33] The bonding scenario in these complexes takes advantage of the ambivalent nature of a transition metal center which arises from the presence of partially filled *d*-orbitals capable of accepting electron density from ligands and also establishing back-donation to vacant orbital on the ligand.[34-37] In the case of *p*-block Lewis acids and late transition metals, the M→Z bonding has predominantly σ character (Figure 3). This unique bonding situation involving a reversal of classical donor-acceptor interaction has attracted attention within the organometallic community because of the resulting stability that can be imparted to an electron rich metal center in low oxidation states.

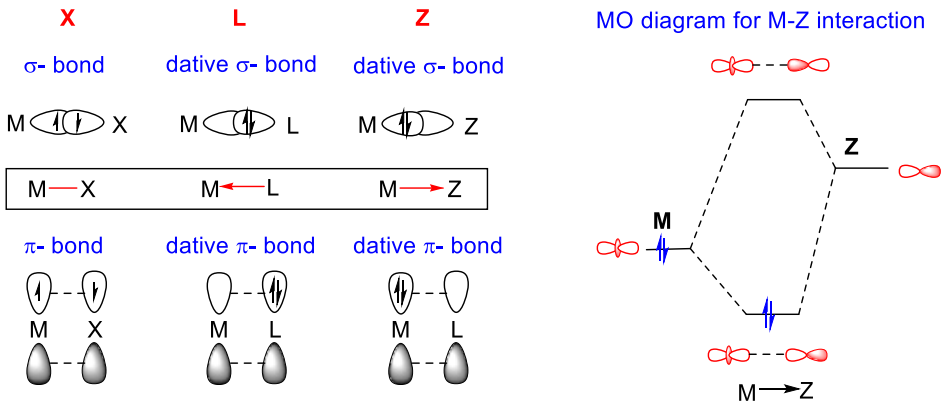

Figure 3. Orbital description of metal-ligand bonding for X-, L- and Z- type ligands.

The benefits of such complexes featuring M→Z interaction were first observed with simple main group Lewis acids such as $AlCl_3$, $AlPh_3$, $GaCl_3$ and SO_2 (Figure 4).[38-41] More recently, Z-type ligands have been incorporated in ambiphilic ligands which usually contain a L-type σ-donor (usually N, P and S) and a Z-type σ-acceptor moiety within the same ligand scaffold (Figure 12). The latter imposes structural restraint to the resulting metal complex and stabilizes the M→Z interaction by bringing the interacting partners in close proximity to each other.

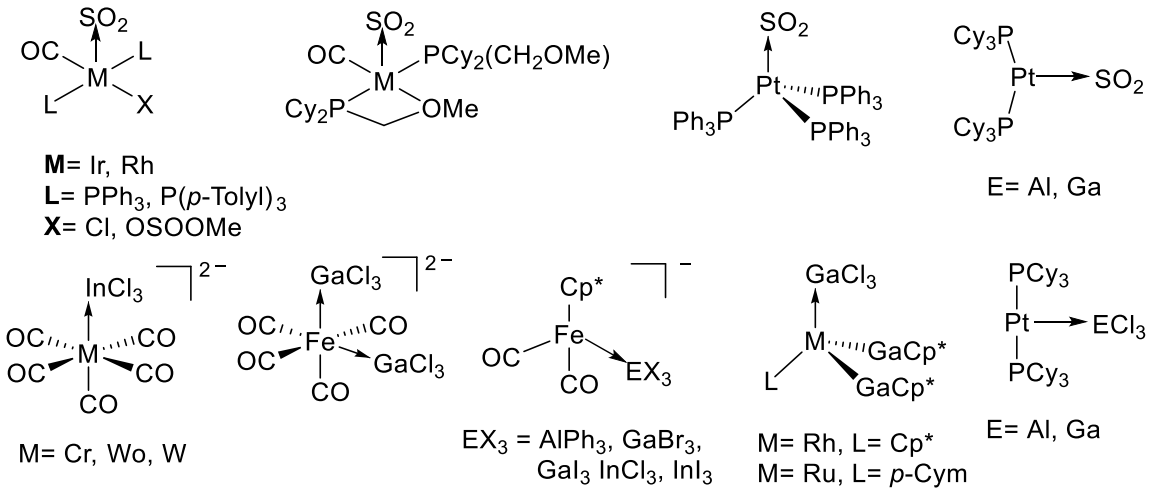

Figure 4. Representative examples of complexes with M→Z interaction

The coordination of ambiphilic ligands to the metal center shows four possible coordination mode as depicted in Figure 5 based on the propensity of the bifunctional moiety to participate in bonding.[33] It is of no surprise that boron based ambiphilic ligands have dominated the coordination chemistry with σ-accepting Z-ligands due to their well-established history of strong Lewis acidity. The works of Bourissou and Ozerov have advanced the field of group 13 Z-ligands by introducing new borane-based ambiphilic ligands with one, two or three phosphine donor buttresses (Figure 5) which has helped the organometallic community to gain insights into the nature and influence of the coveted M→Z interaction on the stability and reactivity of such complexes. These phosphinoborane ligands were successfully introduced in the coordination sphere of group 9-11 transitional metals.[42-46] Computational and crystallographic analysis have provided

useful insights into the electronic influence of the M→Z interaction on the stability of these complexes. The M-Z distance is regarded as an indicator for the strength of the M→Z dative bonding which can also be analyzed by Natural Bond Orbital (NBO) analysis. Transition metal complexes of ambiphilic ligands based on heavier group 14 elements (Si, Ge, Sn) have shown unique bonding situation where the coordinately saturated group 14 elements become hypervalent upon coordination and behaves as σ-acceptors towards metals.[47-52] The bonding situation in these complexes, effectively depletes the electron density from the metal center which may result in interesting structural modifications and enhancement of electrophilicity of the metal center that have been exploited in stoichiometric as well as catalytic activation of small molecules. From this discussion, it can be concluded that the tendency of these main group Lewis acids to attract electron density from the proximal Lewis basic site is the dominating factor behind the rich and diverse chemistry of these electrophilic compounds.

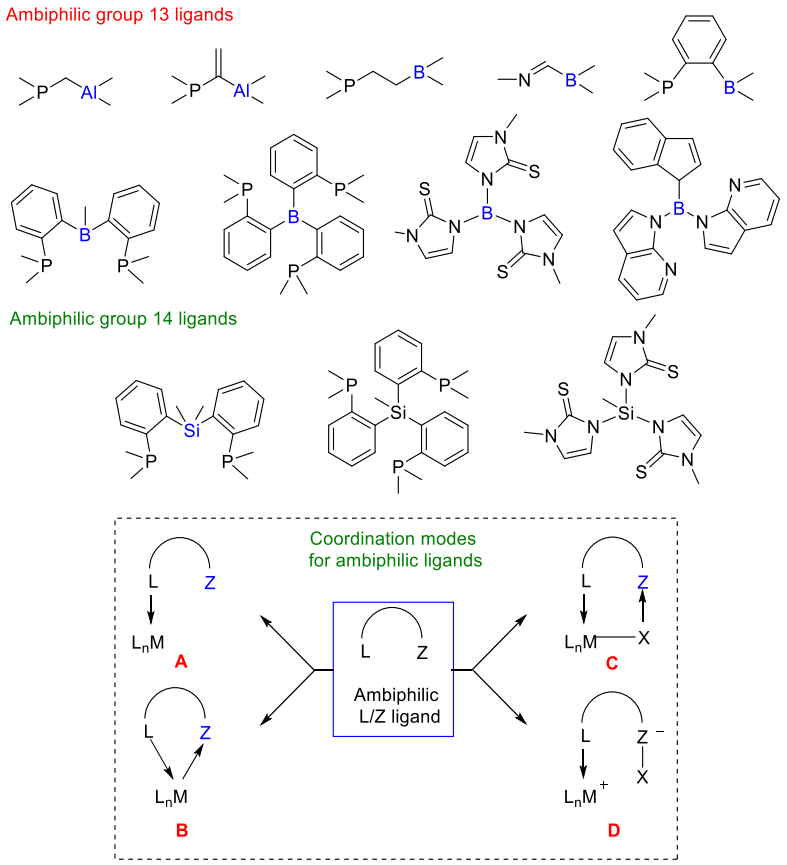

Figure 5. Examples of ambiphilic ligands featuring group 13 and group 14 Lewis acids and their probable coordination modes.

1.1.3 Organoantimony compounds as Z-ligands

Coordination chemistry of group 15 elements has been dominated by phosphines which are mostly used as two-electron donor spectator ligands in transition metal complexes. While stibines have been considered similar in properties to phosphines, their use as ligands in organometallic chemistry has been neglected due to their weaker donating property and the inherent instability of Sb-C bond.[53-54] In the majority of the chemistry involving stibines which bind to the metal center in an end-on fashion via σ-

bonding, they are used as labile spectator ligands suitable for reactions which require ligand displacement.[55-57] Although Alkyl- and arylstibine compounds are Lewis basic in nature, halostibines (R_2SbX or $RSbX_2$) show significant Lewis acidity due to the presence of electron withdrawing substituents.[58-59] An alternative strategy for the development of highly Lewis acidic antimony based ligands requires the oxidation of Sb(III) to Sb(V) which transforms a basic stibine into an acidic stiborane. It can be argued that when these Sb(V) ligands are introduced in the coordination sphere of a metal center, they will imitate the behavior of Lewis acidic organoboranes in modulating the coordination geometry and reactivity of the metal center. Based on this rationale, our group has explored the use of σ-accepting antimony ligands in coordination chemistry.

Our foray into antimony chemistry began with the synthesis of the gold- and the mercury-stibonium complexes **4** and $\mathbf{5}^+$ (Figure 6)[60-61] both of which showed evidence of strong M→Sb interaction in solid state structure. Perhaps the most intriguing feature of these complexes is the enhancement of the Lewis acidity of the Au and Hg center which is a direct influence of the adjacent, strongly electron withdrawing stibonium moiety. The Lewis acidic nature of the Hg center in complex $\mathbf{5}^+$ was demonstrated by its ability to coordinate Lewis bases such as F, Cl, Br, I, DMAP, THF and PF_6 (Figure 6) whereas the unsupported $HgPh_2$ do not show such behavior in presence of Lewis bases.[61]

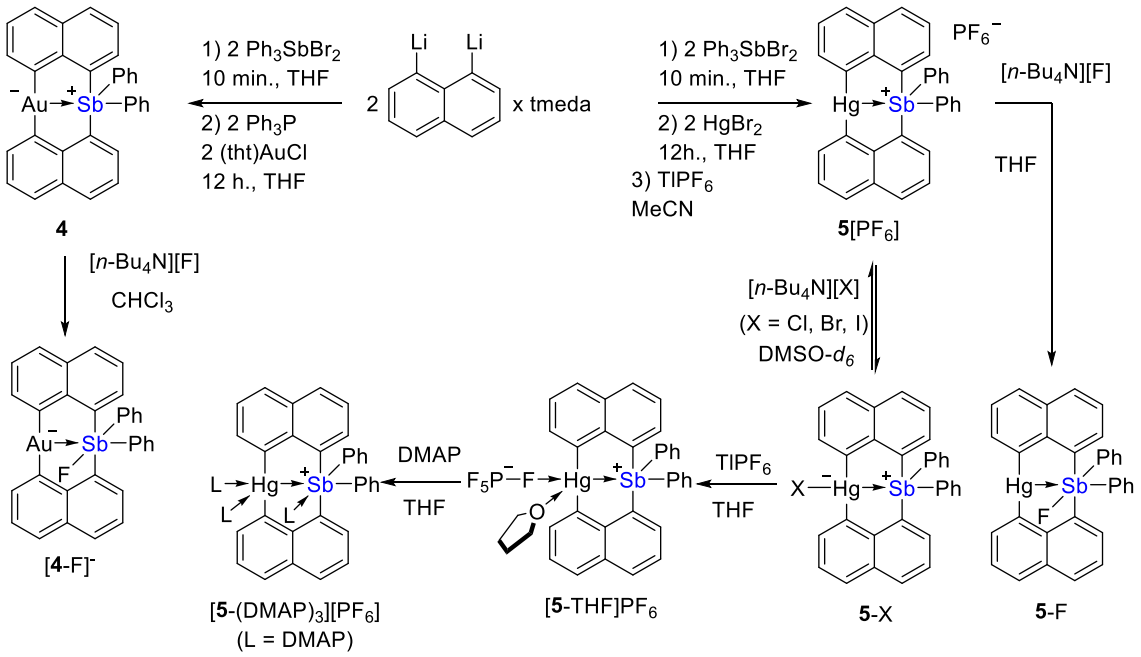

Figure 6. Synthesis of **4** and **5**$^{+}$ and their coordination with Lewis bases.

Interestingly, the reactivity of these bimetallic platforms is not limited to transition metal centers. The stibonium centers can engage in Lewis acid-base interactions when fluoride is used to afford the corresponding fluorostiborane complexes [**4**-F]$^{-}$ and **5**-F. These studies demonstrated that the incorporation of a Lewis acidic antimony center into the coordination sphere of a d-block metal center can modulate the electronic properties of the adjoining metal by polarizing its electron density and the antimony center is coordinately unsaturated and may potentially bind anionic or neutral ligands. These unique capability of Z-type antimony ligands to modulate the properties of a metal center while retaining its own reactivity, piqued our interest in the coordination chemistry of high valent antimony ligands.

The use of chlorostibines as ligands also showed unique Sb-M bonding situations. In 2013, we reported the gold complex **6** supported by a chlorostibine ligand $\mathbf{L}^{\mathbf{P}i\mathbf{Pr}}$-Cl (Figure 7)[62], which revealed strong lp(Au)→σ*(Sb-Cl) interactions when subjected to NBO analysis. The σ-acceptor behavior of the chlorostibine in **6** can be attributed to the presence of an electron withdrawing chloride substituents, which has been observed in the cases of other halostibines. A more unambiguous situation has been demonstrated for the arylstibine analog **7**, which shows both lp(Sb)→6p(Au) and lp(Au)→σ*(Sb- C_{Ph}) interactions. Interestingly, the NBO analysis also revealed that the Au→Sb interaction in **6** is comparable to that of Au→B interaction in $((P i Pr_2C_6H_4)_2BPh)AuCl$ pointing to the high Lewis acidity of chlorostibines.

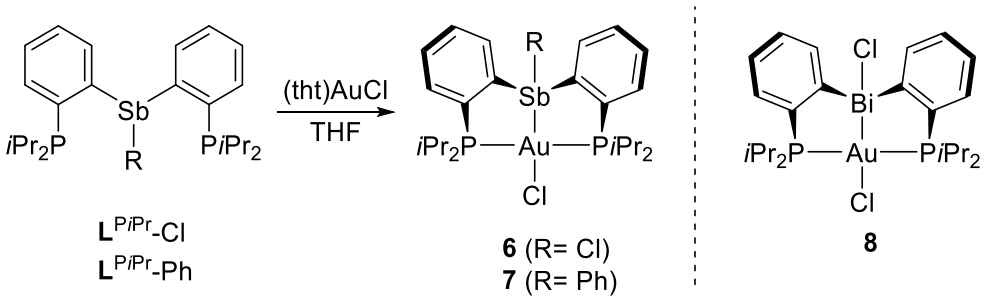

Figure 7. Synthesis of **6** and **7**.

The above mentioned results validated the notion that the chlorostibine moiety acts as a pure Z-type ligand whereas the arylstibine can be considered as 'σ-donor/acceptor confused' ligand when coordinated to the gold atom. The bonding situation for the

chlorostibine is identical to the σ-acceptor behavior of the related bis(phosphinyl)bismuthine complex **8**.[62]

1.2 Coordination non-innocence in antimony-transition metal complexes

The ability of organoantimony moiety to retain its residual Lewis acidity and engage in secondary bonding interactions in the coordination sphere of a transition metal has been coined as 'coordination non-innocence'. Fluoride affinity of **4** and $\mathbf{5}^{+}$ is an example of such coordination non-innocent behavior of the antimony centers involved. The coordination non-innocence of antimony(V) as well as coordinated antimony(III) species is speculated to arise from low-lying Sb-M σ* orbitals which can accept electron density from an incoming Lewis base (Figure 8). Similar phenomenon has also been observed in the case of first row transition metal complexes with halostibine ligands such as **9** and **10**. In these examples, the antimony center display enhanced Lewis acidity due to the presence of halogen substituents and the low-lying Sb-Br σ* orbitals act as electron accepting site to coordinate the oxygen atom of the triflate counter anion.

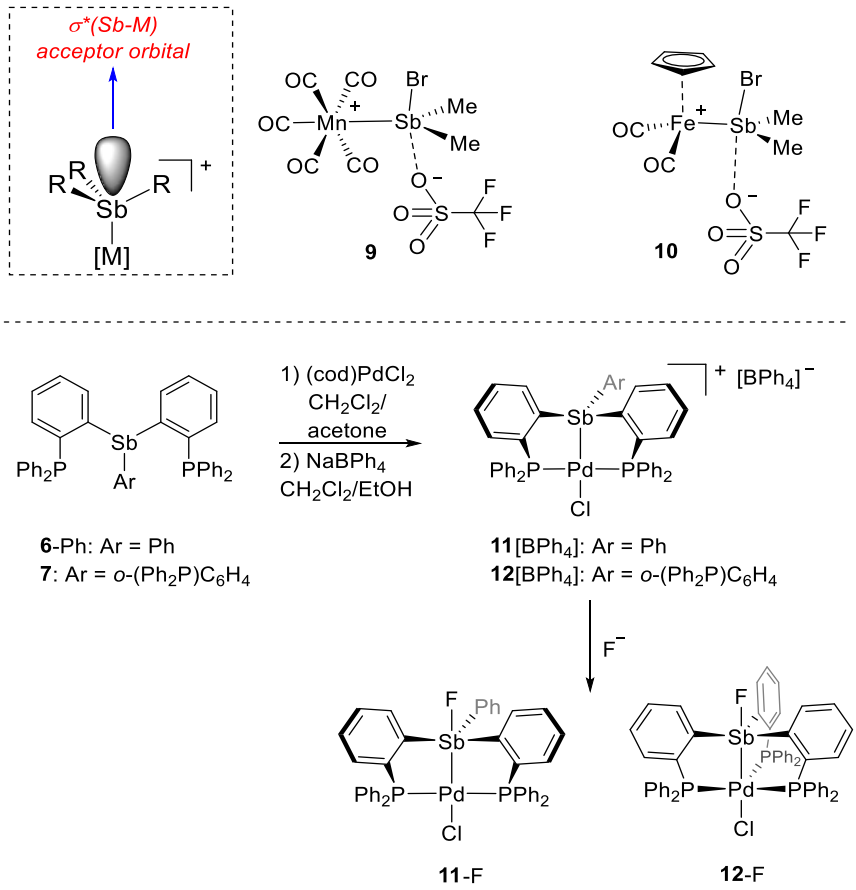

Figure 8. Top: Coordination non-innocence demonstrated by $[(R_2SbX)M]^+$ and $[(R_3Sb)M]^+$ type complexes. Bottom: Synthesis of **11**[BPh_4] and **12**[BPh_4].

Inspired by the coordination non-innocence of antimony in the coordination sphere of a metal, we surmised its possible implication in the domain of anion-sensing which has been an on-going research interest in our group. In 2012, we developed cationic stibine-palladium complexes $\mathbf{11}^+$ and $\mathbf{12}^+$ which can be synthesized by complexation of (COD)$PdCl_2$ (COD = 1,5-cyclooctadiene) with the corresponding poly(phosphinyl)stibine ligands, followed by chloride abstraction with $NaBPh_4$ (Figure 8).[63] The crystal structure of both $\mathbf{11}^+$ and $\mathbf{12}^+$ shows that in both cases, a square planar palladium center is bound to

a four-coordinate stibine moiety. In complex $\mathbf{12}^+$ the third phosphine arm does not bind to the palladium center. To test the coordination non-innocence of the palladium-bound antimony center, $\mathbf{11}^+$ and $\mathbf{12}^+$ were treated with TBAF in CH_2Cl_2, which showed immediate formation of the corresponding fluorostiboranyl complexes **11**-F and **12**-F as evidenced from the appearance of the corresponding fluorine resonances (**11**-F: -121.61 ppm, $3J_{F\text{-}P}$ = 26.7 Hz, **12**-F: -129.72 ppm, $3J_{F\text{-}P}$ = 20.7 Hz) in the ^{19} F NMR spectra. The formation of the fluoride adduct **12**-F resulted in a rapid color change from pale yellow to deep orange. The crystal structure of **12**-F revealed that the formation of the fluoride adduct was accompanied by the coordination of a third phosphine arm to the palladium center leading to a trigonal bipyramidal geometry whereas the palladium center in **11**-F remains square planar. Both of these phenomena are assumed to arise from the change in the ligand field transitions.

The coordination non-innocence of coordinated antimony center has been extended to platinum complexes as shown in a more recent paper by our group.[64] A dicationic platinum complex $\mathbf{14}^{2+}$ can be prepared by abstraction of two chlorides from the parent stibine-platinum complex **13** with $AgSbF_6$ (Figure 9). Complex $\mathbf{14}^{2+}$ readily binds stoichiometric amount of fluoride to afford the monofluoro-antimony analogue $\mathbf{15}^{+\cdot}$. A direct chloride—fluoride exchange can be performed by anion abstraction with TlF in presence of CyCN which results in the formation of the difluorostiborane complex **16** which can also be prepared by the addition of one equivalent of fluoride to $\mathbf{15}^+$. Solid state structures of this series of complexes showed that the Sb-Pt distance increases with the progressive addition of fluoride to antimony (Sb-Pt: (2.4706(5) for for **14**, 2.6236(3) for

15^{+}, and 2.6568(6) for **16**) suggesting a weakening of the Sb-Pt interaction. NBO and QTAIM analysis carried out on these complexes revealed a progressive polarization of the Sb-Pt bond with the stepwise coordination of fluoride anions.

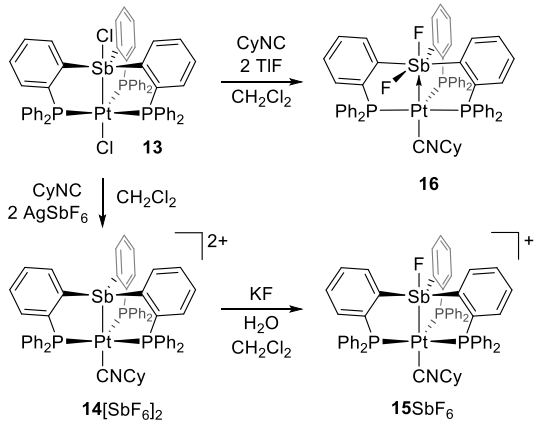

Figure 9. Synthesis of complexes **14**$^{2+}$, **15**$^{+}$ and **16**.

Altogether, these results validates the concept of coordination non-innocence of antimony bound to a metal center and demonstrates the retention of strong fluoride affinity of the said antimony center. This phenomenon also affects the polarization of the M-Sb bond.

1.3 Redox chemistry of antimony-transition metal complexes

The redox chemistry of organoantimony compounds is a well-documented field of study. Oxidation to Sb(V) is usually accompanied by a sharp increase in the Lewis acidity. Intrigued by the unique electronic and coordination properties of metal-bound antimony

centers, we turned our attention to the redox properties of coordinated antimony centers in heterobimetallic Sb-TM complexes.[65] However, rather surprisingly, the redox chemistry of antimony-transition metal complexes had been largely neglected and is limited to a handful of reported complexes. Malisch and coworkers provided important insights into this field by studying the synthesis and reactivity of transition metal stibido complexes which undergo a variety of redox processes.[66] Redox reactions of coordinated stibines were non-existent until we studied the reversible two electron redox process of a gold- trisphosphinylstibine complex **17**.[67] Complex **17** can be cleanly oxidized with $PhICl_2$ to afford the dichlorostiborane gold complex **18**, the formation of which was accompanied by a decrease in the Sb-Au distance from 2.8374(4) Å in **17** to 2.7086(9) Å in **18** as indicated by the XRD analysis of the solid state structures. The strengthening of the Sb-Au core was indicative of the enhanced Lewis acidity of the antimony center upon oxidation. A downfield shift in the ^{31}P NMR resonance upon the formation of **18** along with the square planar geometry of gold (common for the trivalent state of gold) suggested a partial oxidation of the gold center. NBO analysis performed on **17** and **18** revealed that the oxidation of the Sb-Au core is accompanied by a reversal of the Au→Sb donor-acceptor interaction which changes from predominantly Sb→Au in **17** to Sb→Au in **18**. It was interesting to note that the oxidation of **17** was reversible since **18** can be reduced by the treatment of NaI.

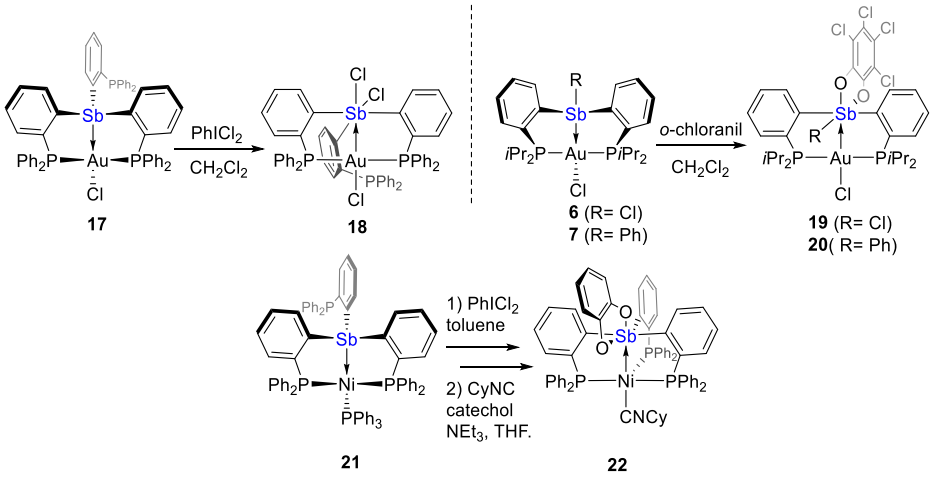

Figure 10. Synthesis of complexes **18, 19, 20** and **22.**

A similar two-electron oxidation protocol has been implemented for the diphosphinylstibine gold complexes **6** and **7** which can be converted to their oxidized analogs **19** and **20** with *o*-chloranil. In both cases, the oxidation was accompanied by a strengthening of the Sb-Au core as indicated by an NBO analysis performed on the optimized geometries. A downfield shift in the ^{31}P NMR resonance from the parent complexes and a change of coordination geometry at gold from trigonal pyramidal to distorted square planar in the case of **20** again validated the hypothesis that the oxidation is not entirely localized on antimony.

In a related effort we have successfully demonstrated a catechol-based oxidation of a Sb-Ni core in a triphosphinylstibine nickel complex **21**. Complex **21** can be oxidized with $PhICl_2$ followed by the substitution of chlorides with catechol to afford the complex **22**. Gratifyingly, as in the case with Sb-Au complexes, an umpolung of the Sb-M bond was observed via computational and spectroscopic analysis. The experimental and

theoretical studies pointed towards the conversion of the antimony ligand from L-type in **21** to Z-type in **22**. The oxidation was also accompanied by the coordination of the third phophine arm to the nickel center.

In conclusion, coordination non-innocence and redox properties of antimony when coordinated to a transition metal center can modulate the electronic and structural properties of the tethered metal center which often leads to versatile reactivity such as anion coordination.

1.4 Application of main group Z-ligands in catalysis

1.4.1 Background

With the advent of ambiphilic ligands featuring main group Lewis acids, the significance of M→Z interaction on the cooperative activation has attracted the attention of organometallic chemists. In 2012, the Peters group provided the seminal example of transition metal-Lewis acid cooperativity in the activation of H_2.[68] The diphosphinoborane nickel complex **23** activated H_2 efficiently and reversibly under 1 atm at 25°C to produce the corresponding dihydro nickel complex **24** which features a B-H-Ni bridge (Figure 11). Complex **24** was found to catalytically deliver hydrogen to styrene under ambient conditions. Computational and spectroscopic analysis revealed the importance of the M-Z cooperation during the catalytic process which is reminiscent of the frustrated Lewis pair reactivity model.[68] Complex **23** also proved to be an efficient catalyst for the hydrosilylation of a variety of para-substituted benzaldehydes.[69] Similar bridged M-Z compounds have been observed by Figueroa upon the activation of H_2, HX or PhCCH by

the Pt-B complex **25** (Figure 11). In this case, the borane ligand provides the necessary structural flexibility for the activation of the incoming substrates.[70]

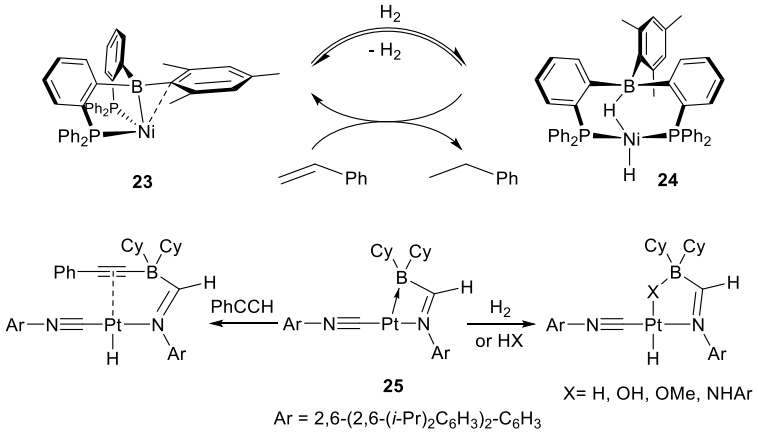

Figure 11. Hydrogen activation via metal-Lewis acid cooperation

In addition to the above mentioned examples, metal complexes supported by ambiphilic ligands have demonstrated diverse reactivity in the past few decades including additions across M-Z bond, activation of H-H, C-H, C-O, Si-H bonds and fixation and transformation of N_2.[71]

1.4.2 Application of B and Sb ligands in gold catalysis

Gold-catalyzed homogeneous organic reactions have gained widespread interest during the past decade due to the mild, relatively carbophilic Lewis acidic nature of the gold center. Since 2004, great progress has been made in developing efficient and selective Au-catalysts. The vast majority of reactions developed with homogeneous gold catalysts have exploited the propensity of gold to activate carbon-carbon π-bonds as electrophiles.

In most of these catalytic reactions, the active catalyst is a cationic monoligated $[LAu]^+$ species where L is a two electron donor). Two or three coordinate gold(I) complexes of the type $[L_2Au]^+$ and $[L_3Au]^+$ show no catalytic activity due to the quenching of Lewis acidity of the gold center by electron rich donor atoms. It can be argued that in these complexes, modification of the ligand L can play an important role in tuning the Lewis acidity of the gold center. The ability of a coordinated Lewis acid to withdraw electron density from the adjoining metal center was exploited by Inagaki who isolated the air-stable gold(I) cation [**26**]$^+$, a complex which showed excellent reactivity and selectivity in the cyclization of enynes.[72] Although this report provided the proof of concept that a Lewis acidic center can activate an adjacent metal center, no unambiguous characterization data was provided for the supposed catalyst.

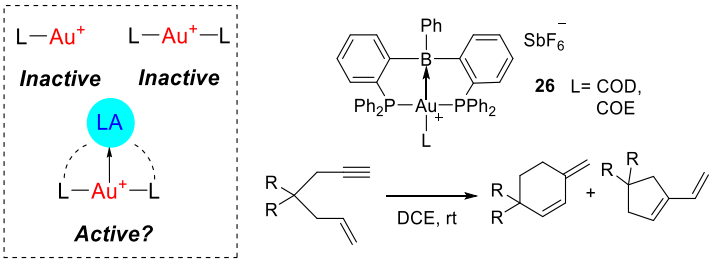

Figure 12. Activation of a gold cation by Lewis acid

Inspired by these findings, we questioned whether a PSbP ligand could impart similar electronic effect on the proximal metal center. Previous work in our group has already shown that dinuclear cationic complexes featuring a Lewis acidic antimony(V) moiety adjacent to a mercury center enhances the Lewis acidity of the transition metal

center to a great extent as compared to the unfunctionalized analog.[61] Additionally, we have already established the superior Lewis acidity of antimony over boron via a series of anion-binding studies.[25, 29] These results alluded to the fact that the M→Z interaction will be stronger if Sb(V) is used in the ligand scaffold instead of boron leading to a highly electron poor metal center, with enhanced catalytic activity in reactions necessitating alkyne activation. Apart from an enhancement in Lewis acidity, other advantages of using antimony-based ligands instead of boron include: i) the greater air and moisture stability of Sb-C bonds when compared to B-C bonds in arylboranes; ii) the pentavalent nature of the antimony center which will provide access to a larger degree of substitution pattern at the main group element.

To this end, we studied the chlorostibine gold complex **27** in which the Sb(III) center shows significant Lewis acidic character due to the presence of electron withdrawing chloride substituent. Conversion of the gold chloride complex with $AgSbF_6$ afforded the corresponding cationic gold species **28**[SbF_6] (Figure 13). When the reactivity of complex **28**[SbF_6] was evaluated with respect to hydroamination of phenyacetylene with p-toluidine, it showed poor reactivity with only 2.7% conversion in 3 h while the unfuctionalized anlog [$(Ph_3P)_2Au$]SbF_6 failed to catalyze the reaction. This enhancement of reactivity due to the presence of the chlorostibine moiety validated our hypothesis that an antimony based Z-ligand may activate an otherwise inert metal center.

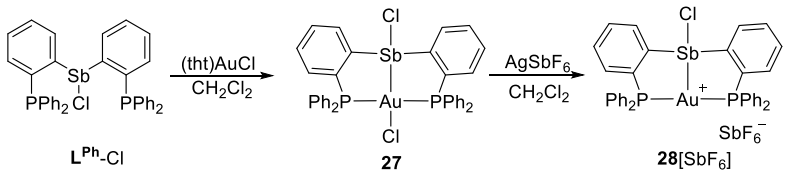

Figure 13. Synthesis of **28**[SbF_6].

To further improve the catalytic activity, we considered the two-electron oxidation of the antimony center which in general 'turns on' the Lewis acidity of the said moiety. Oxidation of **27** with $PhICl_2$ afforded the trichlorostiborane gold complex **29** (Figure 14). To increase the Lewis acidity of the stiborane we performed a halide exchange reaction with TBAF which produced the corresponding trifluorostiborane gold complex **30**. Next, a chloride abstraction protocol was performed with $AgSbF_6$ to generate the cationic gold species [**31**]SbF_6. The Au→Sb interactions in this series of complexes were studied by X-ray crystallography as well as by theoretical methods.

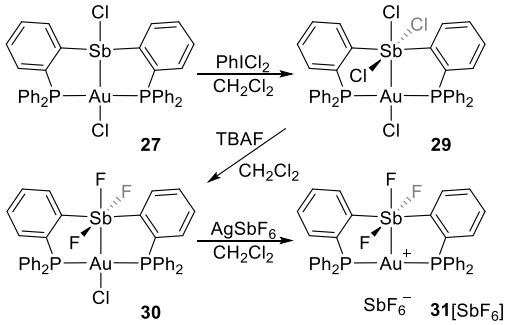

Figure 14. Synthesis of **31**[SbF_6].

The Lewis acidity of **28**[SbF_6], **31**[SbF_6] and [$(PPh_3)_2Au$][SbF_6] was evaluated by the Gutmann-Beckett method using triphenylphosphine oxide (Ph_3PO, ^{31}P NMR (CH_2Cl_2): δ = 27.3 ppm) as the Lewis base probe. While [$Au(PPh_3)_2$][SbF_6] failed to show any change in the ^{31}P NMR resonance of Ph_3PO, both **28**[SbF_6] and **31**[SbF_6] showed downfield shift of 30.6 and 32.9 ppm, respectively. This experiment provided the proof of concept that the gold center becomes more Lewis acidic when coordinated to a strong electron withdrawing stiborane.

The effectiveness of such a bimetallic system was further established, when the catalytic activity of **31**[SbF_6] was investigated using the hydromaination reaction of alkynes. **31**[SbF_6], showed remarkable activity towards alkyne activation at ambient conditions as depicted in Table 1. It should be noted that a typical hydroamination of alkyne usually requires very harsh condition and inert atmosphere. The reaction of phenyacetylene with *p*-toluidine was complete in 40 min. Electron-withdrawing substituent on arylamines resulted in a decreased activity.

Table 1. Hydroamination of alkynes catalyzed by 31[SbF_6],

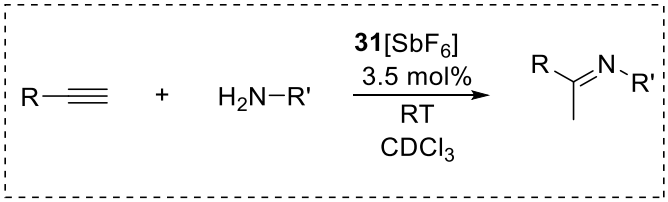

R	R'	Time	Conversion (%)
Ph	*p*-tolyl	40 min	98
Ph	2,6-diisopropylphenyl	70 min	93
Ph	pentafluorophenyl	48 h	68
Ph	hydrazine	30 min	86
*t*Bu	*p*-tolyl	60 min	61

The enhancement of reactivity of a gold center upon coordination to a strongly Lewis acidic antimony moiety, as compared to its unfunctionalized analog, demonstrated the potential of these bimetallic complexes in organometallic catalysis.

1.5 Application of main group Z-ligands in the photoreductive elimination of halogens

1.5.1 Background

With the rise in global energy consumption as well as the CO_2 level in atmosphere due to the excessive use of fossil fuel, a search for renewable carbon-neutral energy source

to has been the most important scientific challenge for the past few decades.[73] Among other alternative energy sources such as wind, geothermal and biomass, solar energy has attracted the most attention due to the prospect of storage of solar energy in the form of chemical bonds, an idea similar to the fundamental concept behind photosynthesis which produces almost all the energy to sustain our planet.[74-76] The implementation of effective storage of solar energy requires a highly distributed storage medium which can be realized by the sunlight-driven water splitting reactions to generate hydrogen.[77] Although the water-splitting reaction provides a logical path to produce a carbon-neutral solar fuel and storage of considerable amount of solar energy, it has its own drawbacks. The requirement of a complex redox process involving four electrons and four protons, often counter-balances the otherwise vast potential of water-splitting reactions in the domain of solar-energy storage and necessitate the use of metal catalysts to facilitate such transformations.[73] A simpler and more viable route to store solar energy is the photocatalytic cleavage of H-X bond present in easily available hydrohaloacids (HX where X= Cl, Br) to afford H_2 and X_2. The amount of solar energy stored during the process of H-X splitting is comparable to that involved in water splitting, yet the oxidative half reaction of H-X involves only two electrons coupled to H_2 generation (Figure 15).[78-79]

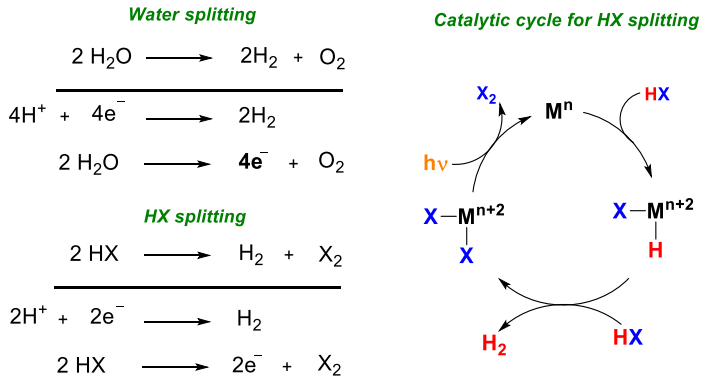

Figure 15. Half reactions involved in H_2O and HX splitting (left). Catalytic cycle for HX splitting involving two-electron photoreduction of a metal dihalide.

Three main steps involved in a successful photocatalytic HX splitting with metal complexes are: 1) HX oxidative addition to produce metal hydride complexes, 2) H_2 generation either by protonolysis or reductive elimination, or 3) photoinduced elimination of X_2 to regenerate the starting catalytic complex (Figure 15).[80] It was realized early on that the most crucial barrier in this simplistic formulation of HX splitting is the photocatalyzed M-X bond cleavage which dictates the turnover frequency of metal photocatalysts. Although, implementation of photo-induced HX splitting by mononuclear species has proved to be challenging, the Nocera group has successfully developed a variety of homo- and heterobimetallic scaffolds with late transition metals (Ni, Ru, Rh, Ir, Pt and Au) which are promising platforms for halogen photo-elimination (Figure 16).[74, 78-83] The reactivity of these complexes, featuring two metal centers linked by polydentate ligands, depends on their ability to oxidatively add and photo-reductively eliminate halogens to regenerate their original reduced form. The most efficient scaffolds are those in which the metal core can survive two electron redox processes and ligands can

destabilize the high valent metal centers to facilitate the reductive elimination of halogen by virtue of their electron withdrawing properties.

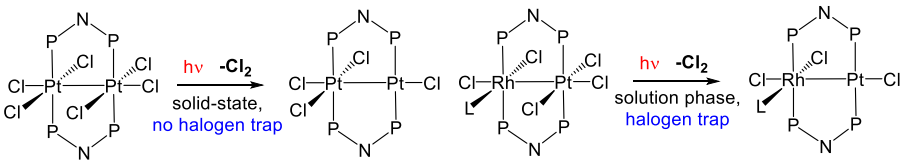

Figure 16. Examples of bimetallic complexes capable of photoinduced elimination of chlorine.

1.5.2 Photoreductive elimination of halogen from Te platforms

Recent advances in redox chemistry of main group elements has found interesting applications in photoelimination of halogens. The ability of heavy main group elements to sustain reversible two electron redox process points to their potential as photocages for halogens. Although the photochemistry of main group elements is still a relatively new field, several encouraging discoveries have been made in the past decade.

Oxidation of tellurium compounds with a variety of oxidants including halogens were known for a long time[84-87] yet the reductive elimination process was mostly limited to thermal or chemical stimulation. The Seferos group has recently reported several Te(IV)-based systems which have emerged as efficient platforms for the light-driven elimination of halogens.[88-91] Incorporation of Te(IV) atom within π-conjugated scaffold of tellurophenes provided compounds which can sustain two-electron redox processes that accompany the addition and elimination of halogens. 2,5-Diphenyltellurophene **32** can be

oxidized by bromine, chlorine, and fluorine and the halogens can be eliminated upon photolysis to regenerate the reduced tellurophene.[89] Excellent quantum yield of Φ= 42% for the photoelimination process was obtained when highly electron withdrawing pentafluorophenyl was incorporated in the tellurophene scaffold.

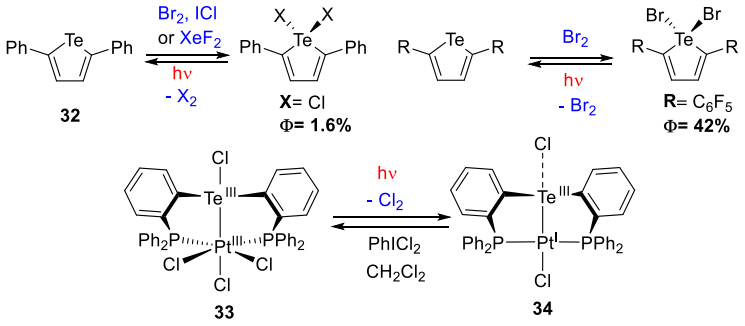

Figure 17. Photoredox chemistry of tellurophene compunds.

Our contribution to this field was initiated by a study of the Te^{III}/Pt^{III} complex **33**. This complex supported the photo-driven elimination of chlorine with a maximum quantum yield of 4.4% in presence of the radical trap 2,3-dimethyl-1,3-butadiene to regenerate the reduced precursor **34**. The halogen elimination from the redox active Te/Pt platform is assumed to be facilitated by the ability of hypervalent tellurium to act as an electron reservoir. Despite the low quantum yield as compared to its transitional metal analogs, this was the first time a main group/late transition metal complex was evaluated in its capacity to support the light-driven elimination of halogens. The effectiveness of this Te/Pt binuclear platform has since inspired us to delve deeper into the realm of photoreductive chemistry of main group/transition metal complexes.

1.5.3 Photoreductive elimination of halogen from Sb

Motivated by the success of the previously discussed Te/Pt complex **33**, we have explored the possibility of using antimony ligands to develop new bimetallic platforms suitable for photoreductive elimination of halogens. As part of our contribution to the redox chemistry of antimony based complexes, we developed pincer stiboranyl complexes with platinum (**35**)[92] and palladium (**36**),[93] both of which undergo oxidation with $PhICl_2$ in CH_2Cl_2 to afford complexes **37** and **38**. The crystal structure of **37** showed that the platinum center is formally oxidized by the incoming "Cl_2" equivalent, whereas in **38**, the trihalostiborane moiety and the palladium center is bridged via a chloride (Figure 18).

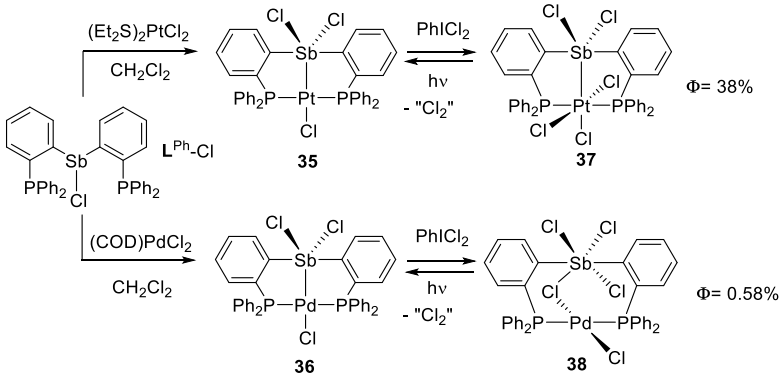

Figure 18. Synthesis and photolysis of **37** and **38.**

When complex **37** was irradiated at 320 nm in the presence of 2,3-dimethyl-1,3-butadiene (DMBD) as a radical trap, it underwent clean elimination of a Cl_2 equivalent to regenerate the parent complex **35** with a maximum quantum yield of 38%. The photoreductive elimination was monitored by both UV-vis and ^{31}P NMR spectroscopy.

Interestingly, photo irradiation of **37** in the solid state in absence of a trap, produced impressive results with the evolution of ~70% of the predicted chlorine.

Upon irradiation with a Hg lamp in the presence of 1 M DMBD, complex **38** eliminates a chlorine equivalent to produce complex **36** within 30 minutes. A maximum quantum yield of 0.58% was obtained when 2.0 M Ph_2S was used. While the quantum yield was rather low as compared to **37**, the photoreduction of **38** is the first example where the elimination of chlorine is based on antimony rather than the transition metal center. It should also be noted that the photoreductive elimination results in the reestablishment of the Sb-Pd bond. Overall, these results validated the potential of antimony-transition metal complexes as suitable platforms for the photoreductive elimination of halogens, which can be explored further in the context of solar energy storage.

1.6 Metal-ligand cooperativity in self-activation of metal catalysts

1.6.1 Metal-ligand cooperation by ambiphilic ligands

Inspired by the seminal contributions of Noyori and Shvo, the concept of metal-ligand cooperation has been exploited to a remarkable extent in the area of transition metal catalysis.[94-95] Contrary to the case of traditional spectator ligands, Lewis acidic Z-type ligands show metal-ligand cooperativity in activating small molecules.[71] Examples of such M/Z synergistic effects are well studied in transitional metal-boron complexes featuring ambiphilic ligands.[68, 96-99] In the reactions involving H_2 activation, the M→Z interaction cleaves to produce an exposed metal center while the Lewis acidic boron actively participates in the activation of the substrate.

This general concept can be put to broader use in the field of organometallic catalysis by taking advantage of the coordination mode L→M→X→Z offered by ambiphilic ligands featuring pendant group 13 Lewis acids. The Bourissou group has encountered this coordination mode in a palladium complex **39** where the pendant borane moiety engages in P→Pd→Cl→B interaction with the Pd-bound chloride (Figure 19).[42] The rare Cl→B contact[100] was supported by the Short C-B distance (2.16 Å) and by the significant pyramidalization of the boron center. The extent of such interaction determines the strength of the M-Cl bond, one extreme of this scenario being the complete cleavage of the bond resulting in the formation of a zwitterionic species. In fact, zwitterions resulting from strong X→Z interaction have been identified with a variety of metals (Ni, Ru, Rh, Au) and ambiphilic ligand platforms featuring group 13 elements, namely B, Al, Ga and In (Figure 19).[101-109]

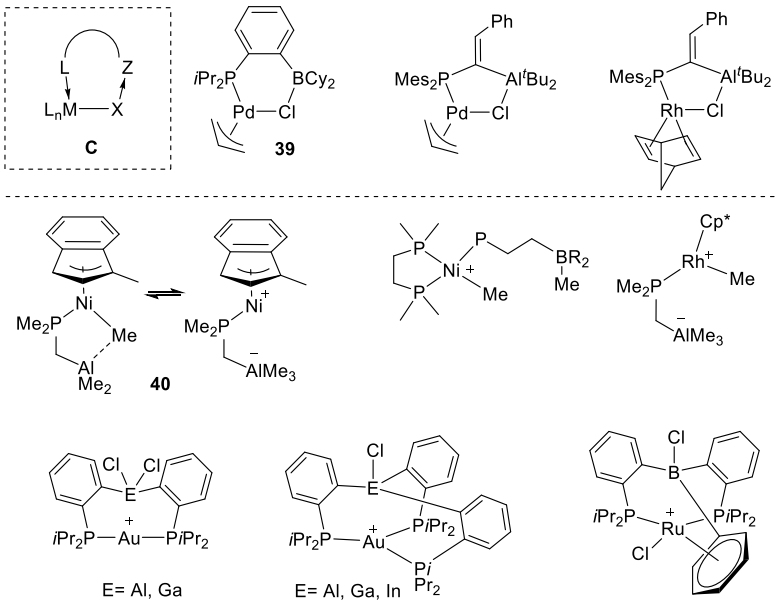

Figure 19. The L→M→Cl→Z coordination mode present in metal complexes supported by ambiphilic ligands (top) and Zwitterionic complexes derived from M-X bond activation by such bonding interactions (bottom two rows).

The significance of such zwitterions in organometallic chemistry was first reported by Zargarian who identified the formation of the bridged Ni^{II} complex **40** when $Me_2PCH_2AlMe_2$ was used as a cocatalyst in the dehydrogenative oligomerization of $PhSiH_3$ reaction.[108] Recently, Bourissou and coworkers have successfully employed the concept metal-ligand cooperation in designing a gold(I) catalyst for the cyclization of propargylamides.[110] When $Mes_2PC(=CHPh)Al\textit{t}Bu_2$ was treated with an equivalent of (tht)AuCl, a novel zwitterionic aluminate-phosphine gold complex **41** was obtained. Formation of this complex resulted from the activation of the Au-Cl bond by the pendant alane center. Complex **41** was found to be a good catalyst for the cyclization of

propargylamides due to the presence of a pre-formed cationic gold center masked only by a labile tht ligand (Figure 20).

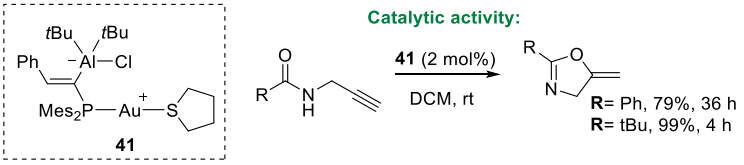

Figure 20. Catalytic activity of a zwitterionic alane-gold complex.

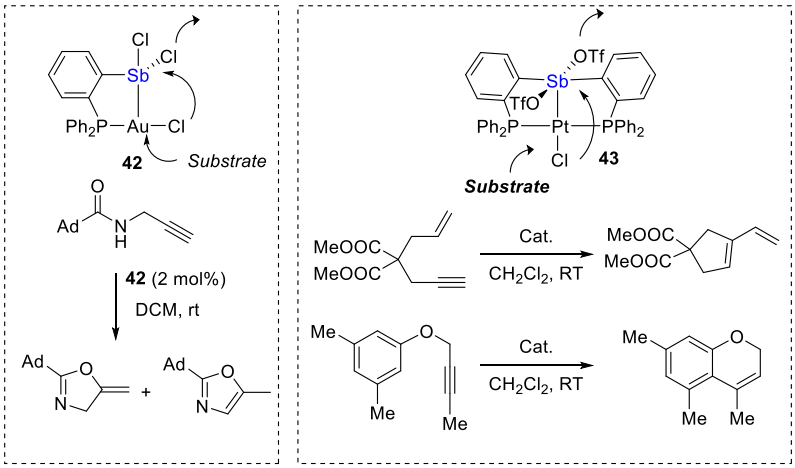

Figure 21. Activation of M-Cl bond by a dichlorostibine and a stiboranyl ligand.

Building on the idea of non-innocent ligand assisted reactivity, our group has developed Sb/Au (**42**) and Sb/Pt (**43**) platforms which demonstrates good catalytic activity towards alkyne activation without requiring any external activating agent (Figure 21)[111-112] In these examples of self-activation of the catalytic species, the strong anion affinity of antimony promotes the displacement of chloride from the metal center, thus allowing for substrate coordination.

1.6.2 M-Cl bond activation by H-bond donors

An alternate approach to activate M-Cl bond can be conceived by establishing direct non-covalent interaction with the halide, such as H-bonding. Catalytic reactions initiated by halide abstraction via H-bonding interaction has emerged as a promising new direction for organocatalysis due to its broad application in organic transformations. The seminal works of Jacobsen on anion-abstraction catalysis using dual H-bond donor chiral ureas and thioureas have shown that covalently bound halides can be activated by dual H-bond donors as illustrated in Figure 22.[113-115]

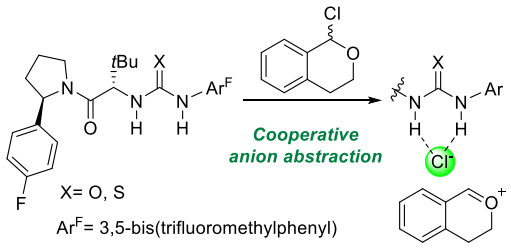

Figure 22. Left: an example of cooperative anion abstraction by dual H-bond donors.

The importance of bifunctional ligands featuring H-bond donors in tuning the geometry and reactivity of the metal center has been elucidated by Szymczak *et al*. in his works with Ru and Cu complexes.[116-119] The presence of the pendant H-bond donor OH functionality in the ligand framework of the Ru(II) complex **44** (Figure 23) results in an enhanced selectivity and reactivity in transfer hydrogenation catalysis as compared to its non-functionalized counterpart **45**. H-bond donor groups present in the ligand can also enforce uncommon metal geometries as depicted by the square planar Cu(I) complex **46**

(Figure 23) by establishing H-bonding interaction with the Cu-bound chloride. In complex **47** the H-bonding interaction between the pendant H-bond donor hydroxyl group with the fluoride anion present in the outer coordination sphere of Cu(I) center allows for the chemical reduction of the corresponding tripodal Cu(II)-F complex.[120]

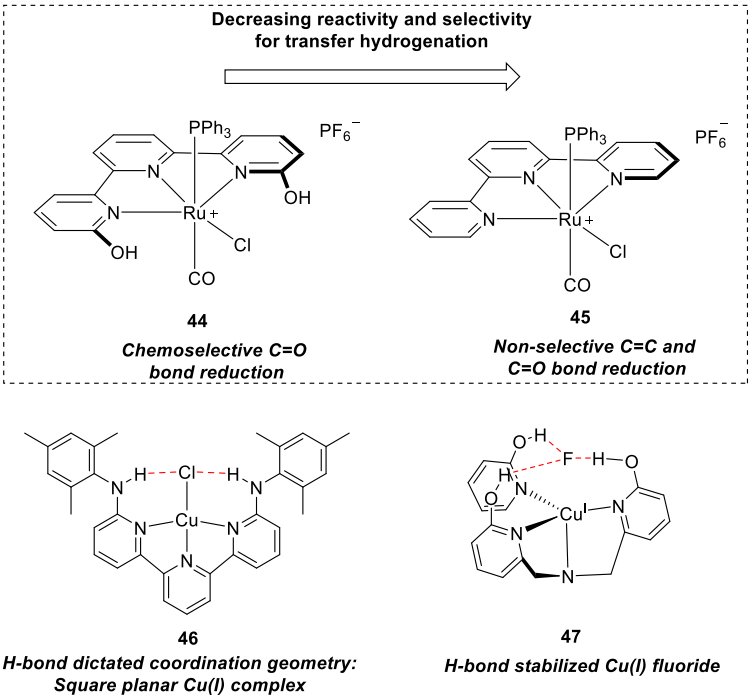

Figure 23. Ru and Cu complexes featuring H-bond donor ligands.

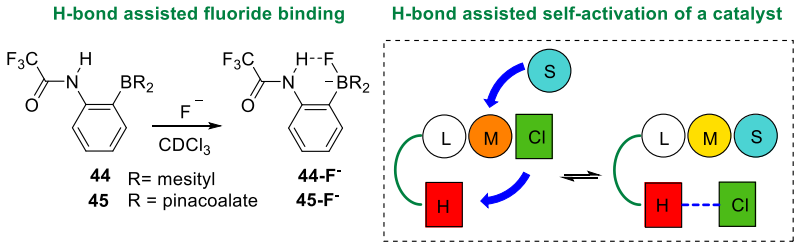

Figure 24. H-bond assisted fluoride binding by bifunctional ambiphilic boranes.

In our group, we have used this approach in the realm of fluoride sensing where a borane receptor **48**, with trifluroacetamide group appended to it, have been developed (Figure 24).[121] Compound **48** showed enhanced fluoride binding capability (stability constant of the 1:1 complex K= 10^7 M^{-1}) compared to a simple $BMes_3$ (K= 3.3 (0.4) x 10^5 M^{-1}). The increase in fluoride affinity in **48** was attributed to the formation of strong H-bonding between the highly acidic trifluoroacetamide functionality and the hard F^- anion bound to the Lewis acidic boron center. The spectroscopic (^1H and ^{19}F NMR) and solid state structural analysis of such complexes showed evidence for the aforementioned H-bonding. Similar H-bond assisted fluoride adduct formation has been illustrated by complex **49** which features a trifluoroacetamide decorated pinacolateborane.[122] These instances of versatile reactivity imparted by bifunctional ambiphilic compounds authenticates the potential of H-bonds in activating M-Cl bonds which may lead to the design of new self-activating catalysts, paving a new path in the domain of transition metal catalysis.

1.7 Objectives

The main focus of this dissertation is to study the influence of ambiphilic Z-type ligands featuring antimony on the structure and reactivity of the harnessed metal center.

1.7.1 Structural influence of Sb-M bonding

To investigate the structural influence of M→Sb interactions in heterobimetallic

systems, we plan to study a series of gold-stiborane complexes which feature a variety of substituents on antimony and gold, via spectroscopic, crystallographic and computational methods.

1.7.2 Influence of peripheral ligands on the reactivity metal-stiborane complexes

Stiborane ligands have been shown to impart interesting catalytic activity to coordinated gold centers. Motivated by the reactivity of such gold/stiborane complexes, we propose to synthesize a series of new gold/stiborane complexes which differ by the nature of substituent on the pendant phosphine arm. A thorough inspection of the catalytic activity of such complexes via experimental and theoretical methods will give us insights about the influence of peripheral ligands on the catalytic properties of the Z-ligand supported metal centers.

1.7.3 Photoreductive elimination of halogens from metal-stiborane complexes

Inspired by the photochemistry of antimony-platinum and antimony-palladium complexes whose core can be reversibly oxidized by two electrons, we intend to explore the possibility of the light-driven elimination of a halogen equivalent from the antimony center in the related gold-stiborane complexes.

1.7.4 Activation of Au-Cl bond by H-bond donor functionalities

Motivated by the anion-binding catalysis observed with H-bond donors, we sought

to investigate the prospect of extending the concept of ligand cooperativity to metal complexes supported by ambiphilic H- bond donor ligands. To this end, we plan to design a gold complex supported by a phosphine-based ligand with a pendant H-bond donor functional group which will provide a way to activate the Au-Cl bond via H-bonding interaction.

2. ANION-CONTROLLED POSITIONAL SWITCHING OF A PHENYL GROUP ABOUT THE DINUCLEAR CORE OF A Au/Sb COMPLEX[1]

2.1 Introduction

The field of anion recognition is dominated by the design of molecular platforms which respond to the presence of the analyte by a perturbation of their photophysical or electrochemical properties.[123-129] An approach that has gained interest in the past decade is based on the use of Lewis acids which engage the anion in the formation of a polar covalent interaction as in the case of boron-based sensors.[4, 130-134] After contributing to this area of chemistry extensively,[5, 135-136] our group became interested in the use of antimony(V) Lewis acids for the complexation of the potentially toxic fluoride anion.[64, 137-138] Our engagement in this new direction was prompted by the realization that antimony(V) compounds are inherently more Lewis acidic than the corresponding boron(III) compounds.[16-19] This situation is reflected by the greater fluoride ion affinity of SbF_5 *vs.* that of BF_3[20] as well as by the greater resistance of SbF_6^- to hydrolysis than BF_4^-.[139]

Drawing inspiration from the chemistry of $B(C_6F_5)_3$[3, 10, 140-141] which is more Lewis acidic[20] and yet much more resistant to hydrolysis than BF_3, we decided to consider the

[1] Reprinted with permission from Sen, S.; Ke, I. S.; Gabbaï, F. "Anion-Controlled Positional Switching of a Phenyl Group about the Dinuclear Core of a AuSb Complex" *Inorg. Chem*. **2016**, *55*, 9162-9172. Copyright 2017 American Chemical Society.

introduction of organic substituents in antimony(V) compounds as a means to tame the inherent reactive and corrosive nature of antimonypentahalides. Our efforts in this directions were further motivated by a series of reports showing that both neutral and cationic organoantimony(V) species form adducts with neutral and anionic Lewis bases.[142-150] The validity of this approach is illustrated by the anion binding properties of neutral and cationic antimony(V) derivatives[26, 151-152] such as **50** and **51**$^{+}$ which display a fluorescence turn-on response upon fluoride anion binding to the antimony atom (Figure 1).[25, 27, 29] This chemistry, which takes place in aqueous solvent, demonstrates that despite the introduction of organic substituents, the antimony(V) center retains considerable Lewis acidity.

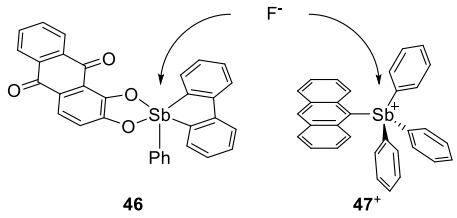

Figure 25. Fluoride sensors featuring Sb(V)

With the view of generalizing this phenomenon, we have also tested whether a similar anion binding behavior could be observed when the antimony center is positioned in the coordination sphere of a transition metal. A first system considered for these studies is the stiboranyl platinum complex **52** (Figure 25). This complex, which can also be

described as a metallostiborane derivative, reacts with aqueous fluoride anions under biphasic conditions to afford the divalent platinum - fluorostiborane complex (**53**). Formation of this complex is the result of a unique internal redox reaction during which the Pt-Sb covalent bond of **52** is cleaved as a result of fluoride binding to antimony. In addition of changes in the valence of the platinum center, this platform also responds to the presence of the anion colorimetrically. Related results have been obtained with the zwitterionic gold complex **4** (Figure 26). As in the case of **52**, the antimony(V) center of this complex is reactive toward fluoride anions as shown by the rapid conversion of this complex into the corresponding fluorostiborane complex 4-F^- when in the presence of fluoride anions. In this case however, the platform shows very minimal structural perturbations, with no notable lengthening to the Au-Sb and no major reorganization.

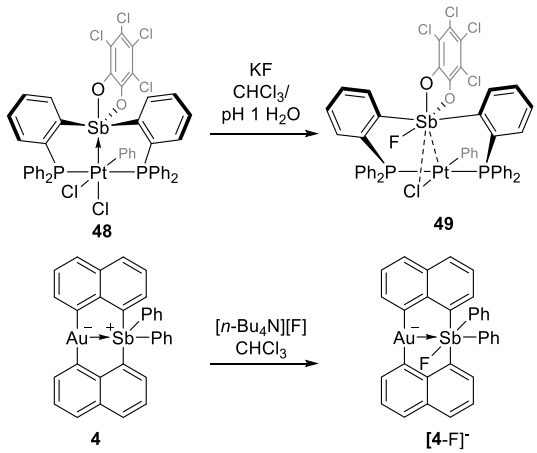

Figure 26. Fluoride anion binding by **52** and **4.**

The high fluoride ion affinity displayed by the above mentioned complexes led us to question if anion complexation would also occur at the antimony center of a triarylstibine/transition-metal complex such as $\mathbf{4}^{+}$, a cationic palladium complex with a Pd-Sb bond supported by two ancillary phosphine ligands (Figure 27).[63] Encouraged by a series of recent reports which show that coordinated stibines may display Lewis acidic properties,[58-59, 64, 153] we investigated the reaction of $\mathbf{12}^{+}$ with fluoride anions and observed the formation of the corresponding fluorostiboranyl–palladium species. Remarkably, this transformation is accompanied by a change in the denticity of the triphosphine unit, leading to a bright-orange trigonal-bipyramidal d^8 lantern complex (**12**-F).

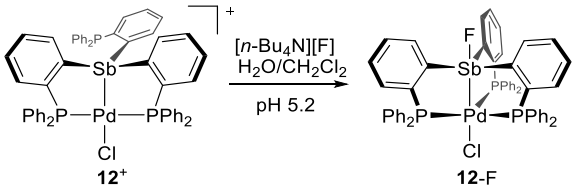

Figure 27. Fluoride anion binding by $\mathbf{12}^{+}$.

The structural reorganization observed upon fluoride binding to complexes such as **52** and $\mathbf{12}^{+}$ led us to speculate that anion binding could also be signaled by a mechanical rather than a photophysical response, a possibility that has been formulated by others who have used anions to actuate molecular switches.[154]

2.2 Previous results

As part of our contribution to this area of chemistry, we became interested in the unique case of a dinuclear AuSb platform which can be regarded as a molecular analog of a mechanical three-way switch. The switching element is a phenyl group whose position about the dinuclear core can be precisely controlled by the nature of the halide substituents. As depicted in Figure 4, the three positions adopted by the phenyl group are defined according to three distinct stages (stage 1-3). Dr. Iou Sheng Ke has described these three stages in his thesis as illustrated in Figure 28.[155]

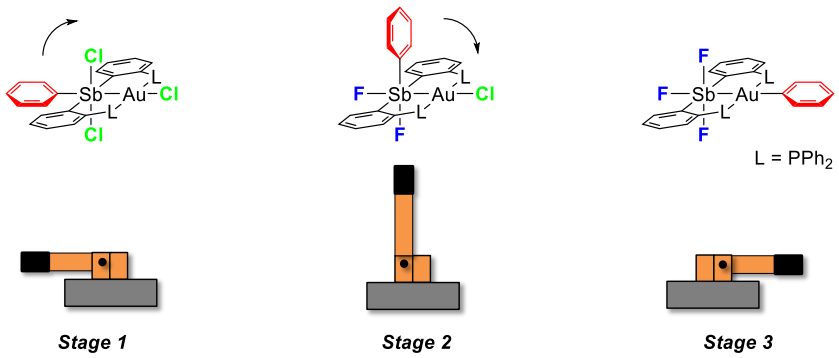

Figure 28. The three positions or stages adopted by the phenyl group about the dinuclear core of the title AuSb platform. The analogy with a mechanical three-way switch is also illustrated.

The synthesis of the gold-stiborane complexes **54** (Stage 1), **55** (Stage 2), **56** (an intermediate between stages 2 and 3) and **57** (Stage 3) performed by Dr. Ke is shown in Scheme 1.

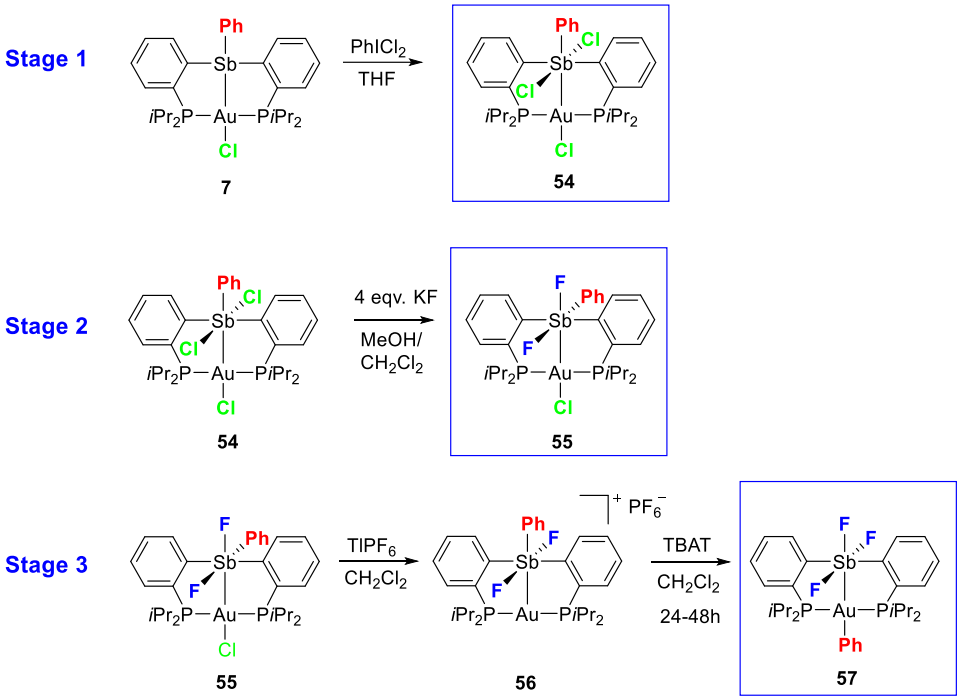

Scheme 1. Syntheses of the complexes of **54-57**.

Dr. Ke determined the structures of these complexes using X-ray crystallography and studied their NMR spectra in great details. The important parameters of the corresponding crystal structures are shown in Table 2.

Table 2. Relevant structural parameters for 54-57.

	Sb-Au (Å)	P-Au-P (°)	Sb-Au-X (°)	Σ_{α}Au (°)
54	2.8651(4)	166.03(3)	160.217(18)	364.89
55	2.7450(14)	163.82(5)	164.18(3)	364.13
56	3.0708(13)	178.70(11)	-	-
57	2.6886(5)	171.84(5)	177.14(19)	360.17

2.3 Objective

The phenomenon of the positional switching of ligands in a heterobimetallic platform is another example of the influence of the M→Z interaction on these systems. Intrigued by these observations, we were motivated to further study the interconversion between the different stages to fully explore the potential of this molecular switch. We were particularly interested in the reversibility of these reactions and the isolation and characterization of the probable intermediates. Our main objective was to investigate the Ph group migration from antimony to gold which we expect to proceed through the intermediacy of a zwitterionic fluoride adduct.

2.4 Reversibility of stages 2 and 3

The conversion of **54** into **55** and hence the 90^{o} switch of the phenyl group is reversible. Indeed, when **55** is treated with two equivalents of TBDMSCl (*t*-butyldimethylsilyl chloride) in CH_2Cl_2, fluoride abstraction occurs, leading to the formation of TBDMSF and regeneration of the antimony dichloride complex **54**.

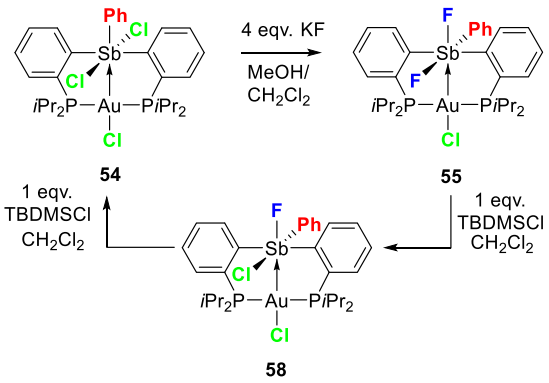

Scheme 2. Conversion of **55** to **54** by the consecutive addition of TBDMSCl.

Monitoring this reaction by ^{31}P NMR spectroscopy points to the intermediacy of a new species (**58**) characterized by ^{19}F NMR resonance at -136 ppm which, by analogy with the chemical shift of F_{ax} in **55**, suggested the presence of a fluoride anion *trans* to the gold center. The ^{31}P NMR spectrum displayed a peak at 95 ppm, the value of which is in between the corresponding signals for **54** and **55**. The reaction of **55** and TBDMCl proceeds slowly and a complete consumption of **55** was observed after 18h (Figure 29). Interestingly, a complete conversion of **58** in to **54** was not observed even after 26 h and the reaction mixture contains both **54** and **58**.

This observation led us to speculate that **58** was a mixed halide complex in which one fluoride and one chloride are bound to antimony. Isolating an analytically pure sample of **58** proved to be impossible because its formation could never be completely decoupled from that of the complex **54**, even when one equivalent of TBDMSCl was used (Figure 37- Figure 38).

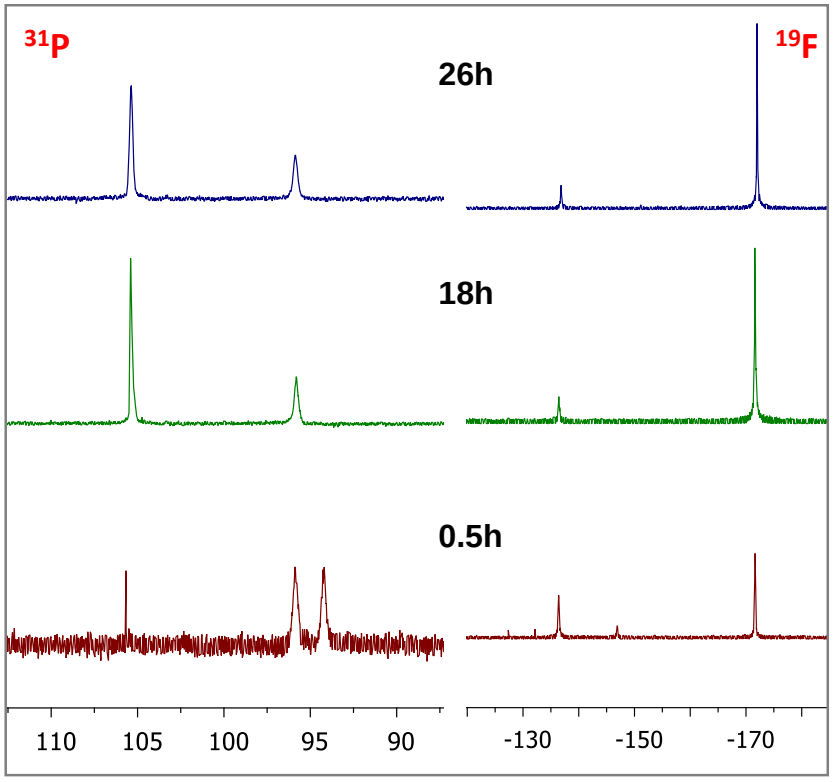

Figure 29. Reaction of **55** with 2 eqv. of TBDMSCl monitored by ^{31}P and ^{19}F NMR.

However, through systematic screening of single crystals grown from a CH_2Cl_2 solution containing an equimolar amount of **55** and TBDMSCl, we succeeded in the structural characterization of **58** (Figure 30) which confirmed that it is the mixed halide derivative. This structural assay confirmed that the phenyl group is in the equatorial plane, indicating that the presence of a single fluoride ligand is enough to induce a 90° switch. The structure of **58** is very similar to that of **55**, with the fluoride and phenyl ligands positioned *trans* and *cis* from the gold atom, respectively. The Sb1-F1 bond distance of 1.966(3) Å was comparable to that found in **55** (1.968(3) Å) whereas the Sb1-Cl1 bond distance (2.467(2) Å) was similar to the Sb-Cl bond in **54** (2.4757(8) Å). The Sb1-Au1

distance of 2.7327(9) Å in **58** is also very close to that in **55** (2.7450(14), indicating a stronger Au→Sb interaction (Figure 8).

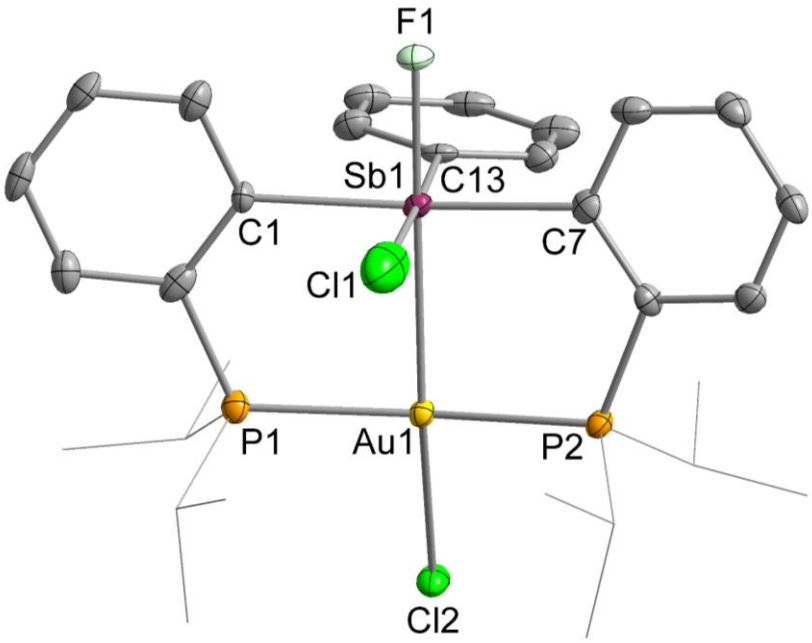

Figure 30. Crystal structure of **58**. Displacement ellipsoids are scaled to the 50% probability level. Hydrogen atoms are omitted for clarity. Selected bond lengths (Å) and angles (deg) for **58**: Au-Sb 2.7327(9), Au-Cl1 2.5021(5), Sb-F1 1.966(3), Sb-Cl1 2.467(2); P1-Au-P2 165.37(5), Cl1-Au-Sb 164.65(3), Au-Sb-F1 178.58(10), Cl1-Sb-C13 177.68(15), C1-Sb-C7 166.38(19).

2.5 Identification and characterization of a zwitterionic intermediate leading to stage 3

Conversion of **56** into **57** triggered by the addition of fluoride anion is undoubtedly the most interesting part of this study. We envisioned that the added fluoride anion could bind to the strongly Lewis acidic antimony center and force phenyl group migration to gold. Previously, the attempts to isolate or characterize such intermediates were

unsuccessful and only the existence of the rearranged product after the Ph migration could be experimentally confirmed. In order to characterize the probable intermediate, we decide to look more carefully into the conversion of **56** into **57.** In fact, the identity of **59** was misassigned by Dr. Ke in his thesis in which he speculated that the added fluoride anion was bound to the gold atom.

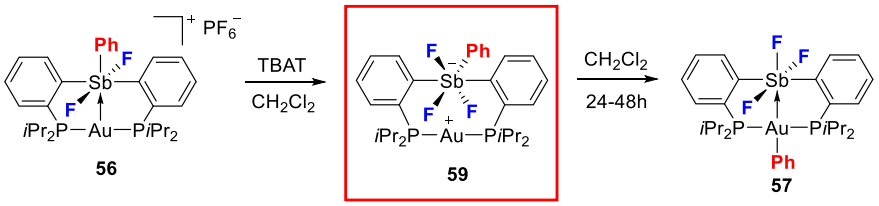

Scheme 3. Reaction of **56** with TBAT: migration of Ph from the antimony to the gold atom via the intermediacy of **59**.

To revisit this chemistry, **56** was treated with one equivalent of $[^{n}Bu_4N][Ph_3SiF_2]$ (TBAT) which is a dry source of fluoride anion, in CH_2Cl_2 under inert conditions. This reaction led to the formation of a zwitterionic intermediate (**59**) which could not be isolated in bulk amount because of it instability (Scheme 4). The ^{31}P NMR spectrum of **59** shows a pseudo-triplet at 69.5 ppm (Figure 39) with $J_{P\text{-}F}$ = 14 Hz while the ^{19}F NMR showed three signals at -2.72 ppm (ddt, $J_{F\text{-}F(cis)}$ =60 Hz, $J_{F\text{-}F(cis)}$ =32 Hz, $J_{P\text{-}F}$ = 14Hz), -71.43 ppm (ddt, $J_{F\text{-}F(trans)}$ = 80 Hz, $J_{F\text{-}F(cis)}$ = 32 Hz, $J_{P\text{-}F}$ =14Hz) and -128.65 ppm (dd, $J_{F\text{-}F(trans)}$ = 80 Hz, $J_{F\text{-}F\,(cis)}$= 60Hz), in 1:1:1 intensity ratio (Figure 31). For detailed spectra see Figure 40. Upon standing in solution, this intermediate slowly rearranges to give a new complex identified as the target gold(I) aryl complex **57** (*vide supra*).

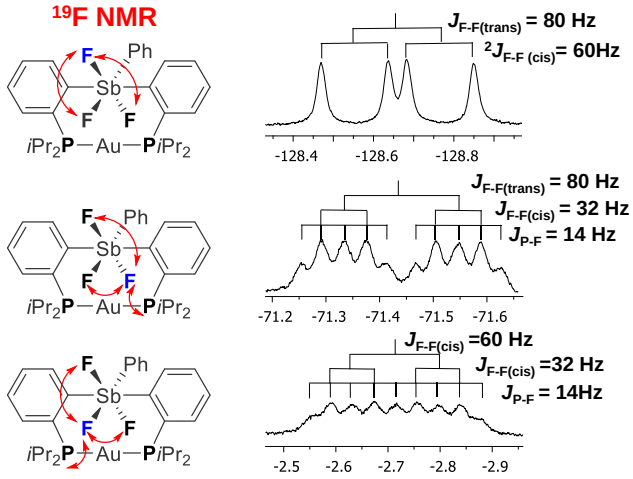

Figure 31. The ^{19}F NMR resonances of **59** in CH_2Cl_2.

Unambiguous characterization of **59** came a structural elucidation of single crystals obtained by layering the reaction mixture with pentane shortly after mixing the reagents. Examination of the structure of **59** reveals its zwitterionic nature (Figure 32). The antimony is incorporated in an octahedral triaryltrifluoroantimonate anion that sits in proximity to the bis-phosphine gold(I) cation (Figure 12). The formation of this zwitterion is reminiscent of the behavior of other group 13-containing ligands[107, 110, 156-158] such as (*o*-(*i*Pr$_2$P)C$_6$H$_4$)$_2$AlCl which form related zwitterionic structures when coordinated to gold(I) chloride.[110]

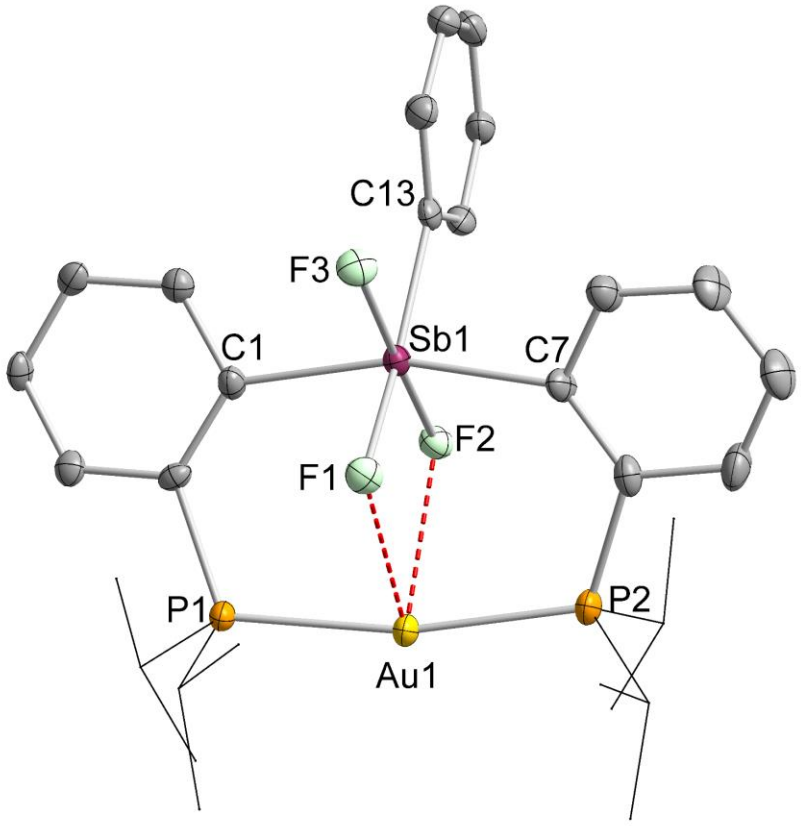

Figure 32. Solid state structure of **59**. Displacement ellipsoids are scaled to the 50% probability level. Hydrogen atoms are omit-ted for clarity. Selected bond lengths (Å) and angles (deg) for **59**: Au1---Sb1 3.3918(4), Sb1-F1 2.010(3), Sb-F2 2.009(3), Sb-F3 1.973(3), Sb1-C13 2.158(5), Au1-F1 2.6644(32), Au2-F2 2.6755(28); P1-Au-P2 168.20(5).

The most interesting feature in the structure of **59** are the short Au-F1 (2.6644(32) Å) and Au-F2 (2.6755(28) Å) distances which show that two of the fluorine atoms are in forced proximity to the gold(I) center. These distances, which are comparable to those observed in [((*o*-(Ph_2P)C_6H_4)$_2F_3Sb$)Au][SbF_6] (2.728(4) Å),[159] are noticeably longer than the Au-F bonds of known molecular gold fluoride complexes (2.0281(17)Å for (SIDipp)AuF[160] and 2.060(1) Å for [((SIDipp)Au)$_2$(μ-F)][BF_4] with SIDipp = 1,3-bis(2,6-

diisopropylphenyl)-4,5-dihydroimidazol-2-ylidene)[161] and only correspond to weak and geometrically constrained Au-F interactions. Finally, the Sb-Au distance of 3.3918(4) Å rules out any direct interaction between the gold and antimony center

It is interesting to note that this phenyl group migration can only be initiated by the addition of fluoride anion. The addition of TBACl to a solution of this salt in $CDCl_3$ leads to the clean formation of **55**, as confirmed by ^{31}P and ^{19}F NMR spectroscopy. This observation is another proof of the strong fluoride affinity of hard Sb(V) center over the soft Lewis acidic Au(I) center.

2.6 DFT analysis of the three stages of the positional switch

To gain insight into the variation of Au→Sb bonding in different stages, we have computed the structures of **54-59** using Density Functional Theory (DFT) methods (Gaussian09: BP86 with 6-31g for H, C; 6-31+G(d') for F; 6-31G(d') for P, Cl; cc-pVTZ-PP with Stuttgart relativistic small core for Au and Sb). Dr. Ke had carried out such calculations on complexes **54-57.** However these calculation were repeated at a different level of theory to allow comparison with the new complexes isolated in my work. Optimization of the geometry of these complexes reproduced the trend observed experimentally (Table 3). In accordance to the stronger electron withdrawing effect of fluoride than chloride, the computed Sb-Au distance in **54** (2.88 Å) was found to be longer than in **55** (2.79 Å). The calculated Sb-Au bond distance in **58** was also in good agreement with the crystal structure and correctly predicted the effect of the replacement of one

fluoride with chloride on antimony. The lengthening of the Sb-Au bond upon conversion of **55** into **56** was also reflected in the computed bond distance of 3.06 Å in Table 3.

Table 3. Selected bond lengths (Å) and angles (°) for complexes 54, 55, 56, 57 and 58 as determined crystallographically and optimized computationally. (* denotes the calculated parameters)

Complex	Sb-Au (Å)	P-Au-P (º)	Sb-Au-X (º)	Σ_{α}Au (º)
54	2.8651(4)	166.03(3)	160.217(18)	364.89
54*	2.8808	174.993	167.832	361.054
55	2.7450(14)	163.82(5)	164.18(3)	364.13
55*	2.7971	170.779	168.463	361.703
58	2.7327(9)	165.37(5)	164.65(3)	363.64
58*	2.7946	172.212	168.607	361.422
56	3.0708(13)	178.70(11)	-	-
56*	3.0608	175.313	-	-
57	2.6886(5)	171.84(5)	177.14(19)	360.17
57*	2.7989	170.061	179.996	359.99

Table 4. . Selected bond lengths (Å) and angles (°) for complex 59 as determined crystallographically and optimized computationally. (* denotes the calculated parameters)

	Sb---Au (Å)	Au---F1 (Å)	Au---F2(Å)	Sb-F1 (Å)	Sb-F2 (Å)	Sb-F3 (Å)	P-Au-P (º)
59	3.3918(4)	2.6644(32)	2.6755(28)	2.010(3)	2.009(3)	1.973(3)	168.19(5)
59*	3.37593	2.6646	2.6785	2.0845	2.0751	2.010	168.261

The computed structure of the zwitterion **59** reproduced the experimental geometry with good precision. It revealed the absence of a Sb-Au interaction as indicated by the

long Sb-Au separation of 3.37 Å (Table 4). The Au-F distances also corroborated well with the solid state structure as delineated in Table 4. Although the optimized geometry of **57** showed the re-establishment of Sb-Au bonding interaction, the calculated bond distance (2.79 Å) was longer than what was found experimentally (2.6886(5) Å) (Table 3).

2.7 Quantum Theory of Atoms In Molecules Analysis

The variation of the Sb-Au bonding in these complexes were also investigated by a Quantum Theory of Atoms In Molecules (QTAIM) analysis, which identifies the bond paths and bond critical points (BCPs) between atoms in a molecule. We have analyzed the topology of the electron density using the Atoms in Molecules method as implemented in AIMAll. For both complexes **54** and **55**, this analysis identifies a bond path connecting the two heavy atoms thereby confirming the presence of a bonding interaction. The value of the Laplacian of the electron density ($\nabla^2\rho(r)$) at the Sb-Au bond critical point (BCP) of both **54** and **55** is positive, in agreement with the donor-acceptor nature of the Au→Sb bonding (Table 5).[162]

Table 5. Selected parameters for the Sb-Au BCPs

Compound	ρ(r) e Bohr^{-3}	$\nabla^2\rho$(r) e Bohr^{-5}	δ(A,B)
54	4.99×10^{-2}	2.69×10^{-2}	0.46
55	5.63×10^{-2}	2.94×10^{-2}	0.50
58	5.67×10^{-2}	3.02×10^{-2}	0.52
56	3.13×10^{-2}	3.71×10^{-2}	0.27
57	6.08×10^{-2}	1.40×10^{-2}	0.54

It is interesting to note that the value of the electron density at the Sb-Au BCP is lower in **54** (ρ(BCP) = 4.99 10^{-2} e Bohr^{-3}) than in **55** (ρ(BCP) = 5.63 10^{-2} e Bohr^{-3}) (Table 1). This difference, which correlates with the shorter Au-Sb bond measured experimentally for **55** indicates that the latter has a stronger Au→Sb interaction than **54**, a phenomenon that we rationalize by the presence of an apical fluoride atom *trans* to the gold atom. It can also be argued that the phenyl group in **54** exerts a strong *trans* influence thereby weakening the Au→Sb interaction. A similar conclusion is derived from the delocalization index which is higher for **55** (δ(A,B) = 0.50) than for **54** (δ(A,B) = 0.46).[163] A complementary picture emerges from the visualization of the localized orbital locator (LOL) function, a function that maps the electron kinetic energy within a molecule.[164-165] For both complexes, the LOL function as implemented in Multiwfn displays a basin with LOL values close to 0.5 between the gold and antimony atom (Figure 33). As previously

explained for other late transition metal complexes,[166-167] such a situation corresponds to a slow electron region and is indicative of a bonding interaction between these two atoms.

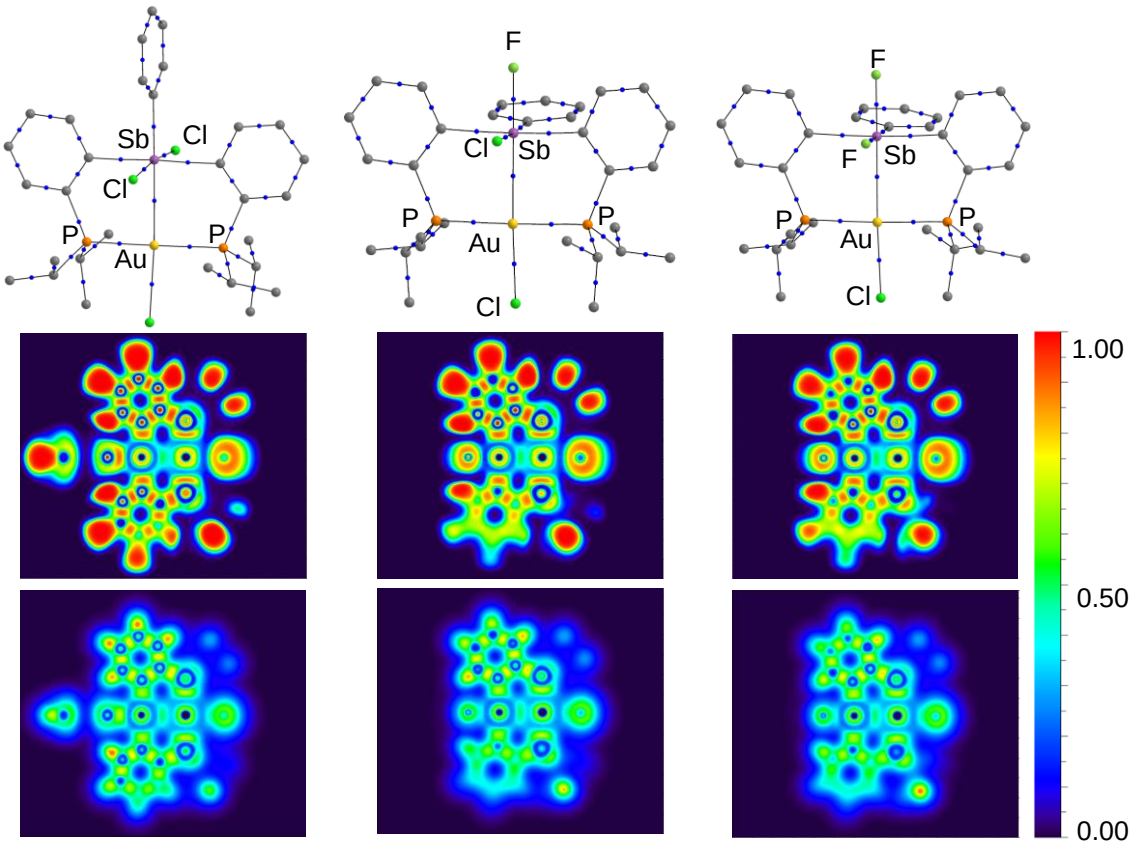

Figure 33. Top: QTAIM bond paths and bond critical points analysis for **54**, **55** and.**58** Hydrogen atoms and bond critical points featuring ρ(r) values less than 0.02 e Bohr^{-3} and their corresponding bond paths are omitted for clarity. Electron localization function (middle) and localized orbital locator map (bottom) of the complexes **54**, **55** and **58** in the plane of Sb-Au-P.

The weakening of the Au→Sb donor-acceptor interaction in **56** is also reflected by the computational results. Indeed, the AIM analysis reveals that both the electron

density ρ(r) at the Sb-Au BCP (3.13 10^{-2} e Bohr^{-3}) and the delocalization index δ(A,B) in **56** (0.27) are significantly lower than in **55** (ρ(r) = 5.63 10^{-2} e Bohr^{-3}, δ(A,B) = 0.50). The LOL map of **56** is also very diagnostic with a clear shrinking of the slow electron region between gold and antimony (Figure 34). The weakening of the Au→Sb interaction results from the removal of the chloride trans to antimony, a phenomenon that we have recently observed upon conversion of ((*o*-(Ph_2P)C_6H_4)$_2F_3$Sb)AuCl into [((*o*-(Ph_2P)C_6H_4)$_2F_3$Sb)Au]$^+$.[159] Similar effects have also been observed upon by Bourrisou who found that Au→B interaction of ((*o*-(*i*Pr_2P)C_6H_4)$_3$B)AuCl is stronger and shorter than in [((*o*-(*i*Pr_2P)C_6H_4)$_3$B)Au]$^+$.[168]

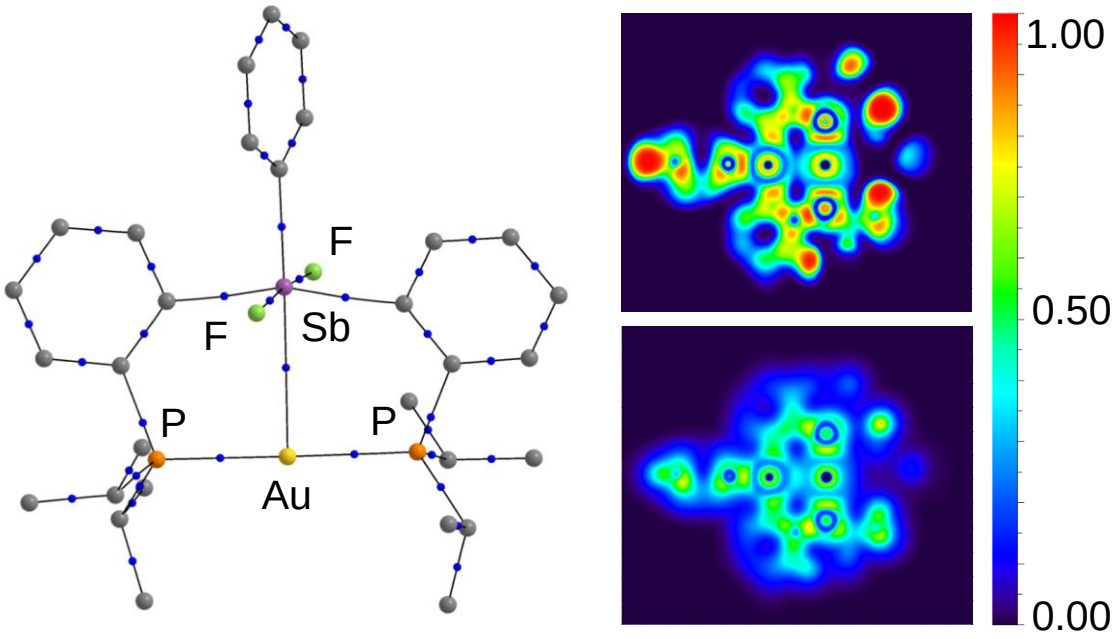

Figure 34. Top: QTAIM bond paths and bond critical points analysis for **56.** Hydrogen atoms and bond critical points featuring ρ(r) values less than 0.02 e Bohr^{-3} and their corresponding bond paths are omitted for clarity. Electron localization function (top right) and localized orbital locator map (bottom right) of **56** in the plane of Sb-Au-P.

The loss of bonding interaction between the heavy atoms upon the coordination of fluoride on antimony is confirmed by the results of the AIM and LOL analysis which show no bond path and no slow electron basin, respectively, between the two heavy atoms in **59** In turn, one can easily conclude that addition of a third fluoride anion to the antimony center neutralizes the Lewis acidity of the later and no longer allows for donor-acceptor bonding between gold and antimony. On the other hand, the presence of Au-F interactions is confirmed by the presence of bond paths connecting the gold atom to the two fluorine atoms with very similar values of the density at the BCP (av. ρ(r) = 2.85 10^{-2} e $Bohr^{-3}$) (Figure 35).

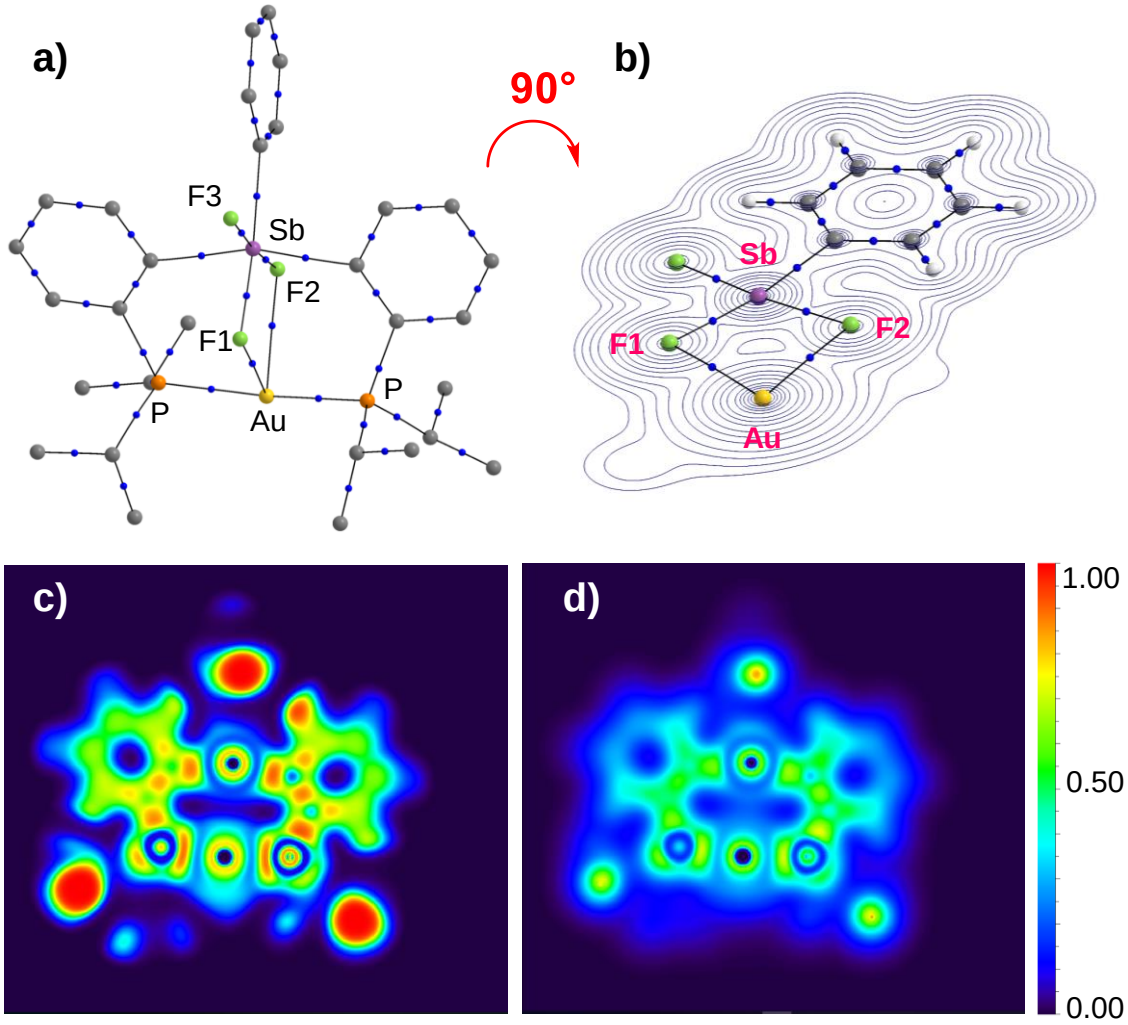

Figure 35. a) QTAIM bond paths and bond critical points analysis for **59.** Hydrogen atoms and bond critical points featuring ρ(r) values less than 0.02 e Bohr^{-3} and their corresponding bond paths are omitted for clarity b) QTAIM bond paths and bond critical points analysis for **59** projected in the Au-F1-F2 plane. The topology of the electron density is also shown. c) ELF map for **59** d) LOL map for **59**.

The strengthening of the Sb-Au core upon the migration of Ph group to gold, can be assigned to the increased acidity of the trifluorodiarylstiborane unit and the increased metallobasicity of the gold center, which is now substituted by a strong trans-influencing phenyl substituent. These effects are also reflected in the AIM results which show the

highest electron density ρ(r) at the Sb-Au BCP (6.086 10^{-2} e $Bohr^{-3}$) and the highest delocalization index (δ(A,B)= 0.54) of the series of complexes described in this paper (Table 5). The LOL map of **57** is also unambiguous, with a very developed slow electron region between gold and antimony atoms (Figure 36). The stability of this structure is also reflected by its reluctance to revert back into **55** when treated with TMSCl. Finally, the Au-C13 distance (2.149(6) Å) is significantly longer than the average Au-C_{Ph} bond distance of 2.054 Å which could be derived from an analysis of the Cambridge Structural Database for complexes featuring a gold-phenyl substructure (see the experimental section).[169] In fact, the Au-C_{Ph} bond of **57** appears to be the longest such bond ever measured. We propose that this unusually long bond distance is the result of the unusual square planar geometry assumed by the gold center.

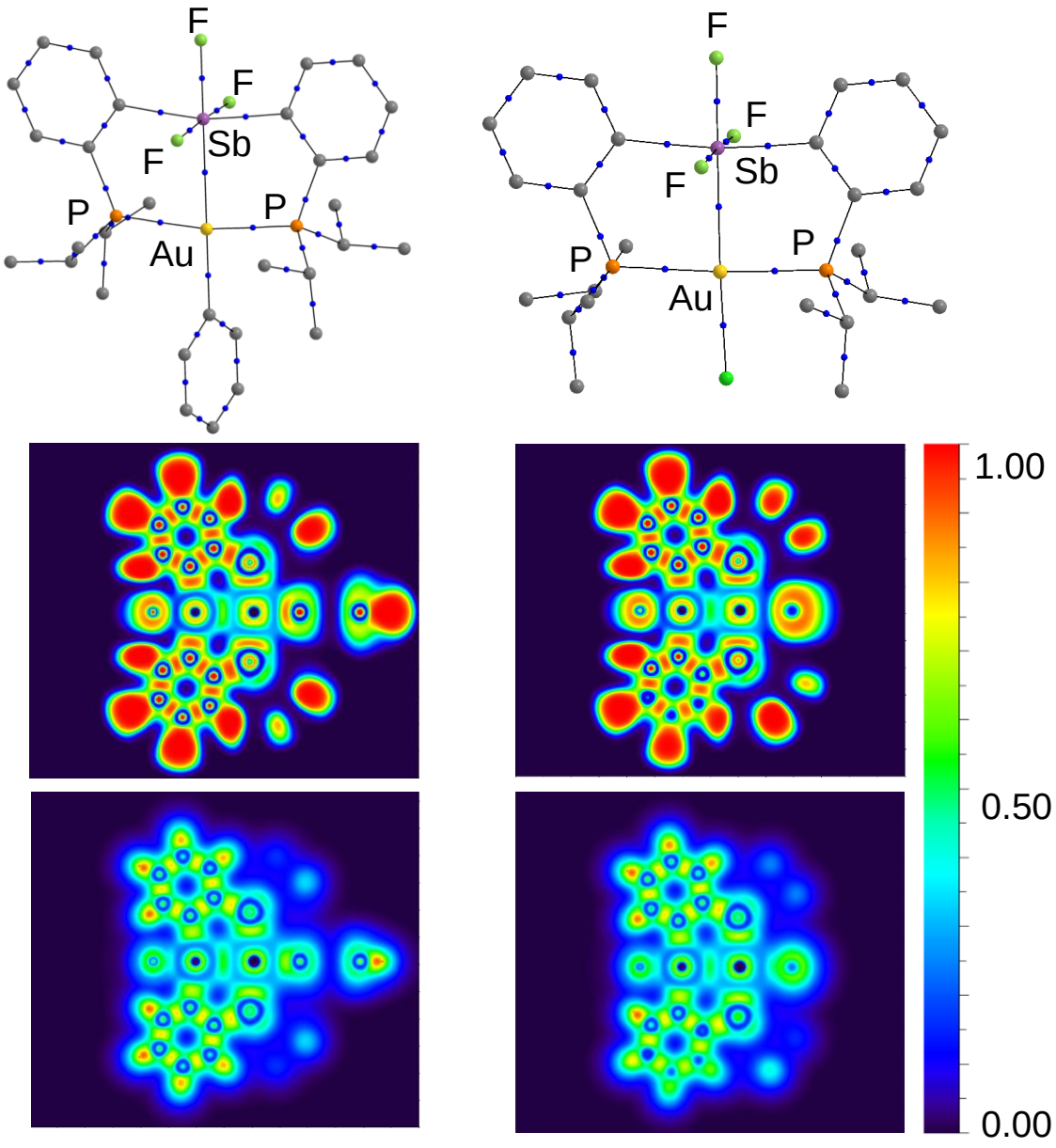

Figure 36. QTAIM bond paths and bond critical points analysis for **57** (top left) and **60** (top right)**.** Hydrogen atoms and bond critical points featuring ρ(r) values less than 0.02 e Bohr^{-3} and their corresponding bond paths are omitted for clarity. ELF (middle) and LOL (bottom) maps for **57** (left) and **60** (right).

To obtain a comparison between phenyl and chloride as ligands on gold, we performed the DFT optimization and AIM calculation on the imaginary structure where the Ph group on gold is replaced by a chloride. The optimized structure showed that the Sb-Au bond distance in **60** is longer than that of **57** which can be explained by the higher trans-influencing effect of the phenyl group over chloride.

AIM analysis on **60** showed similar electron density ρ(r) at the Sb-Au BCP (6.079 10^{-2} e $Bohr^{-3}$) and the delocalization index (δ(A,B)= 0.51) as in **57**. The ELF and LOL map indicated slow electron region between gold and antimony atoms comparable to **57** (Figure 9). This observation shows that the electron donating effect of phenyl anion is almost as strong as chloride and the strong electron withdrawing effect of the trifluorostibonium moiety plays an important role in strengthening the Sb-Au core.

2.8 Conclusion

In summary, we have described how simple fluoride-chloride anion exchange reactions can be used to precisely dial in the position of a phenyl substituent about the dinuclear core of a AuSb complex. While in all three stages, the platform retains a Au→Sb interaction whose presence is unambiguously established using both experiment and theory, two of the observed intermediates involved between stage 2 and stage 3 have a disrupted transannular bond. The first one is the cationic derivative **56** in which the absence of an anionic ligand at gold reduces the metallobasicity of the later drastically weakening the Au→Sb. The second one is the zwitterionic derivative which no longer possesses a Au→Sb interaction as a result of fluoride anion addition to the antimony

center. Altogether, these results allow us to introduce a unique mechanical three way switch actuated by anions. In addition to possible applications in mechanochemistry, we propose that such switches could also be of used in the domain of anion sensing, a direction that we are further exploring.

2.9 Experimental section

General considerations. (tht)AuCl (tht = tetrahydrothiophene)[170], *o*-(*i*Pr_2P)C_6H_4Br,[171] $PhICl_2$,[172] $PhSbCl_2$,[173] were prepared according to the reported procedures. Solvents were dried by passing through an alumina column (n-pentane and CH_2Cl_2) or by reflux under N_2 over Na/K (Et_2O and THF). All other solvents were used as received. All commercially available chemicals were purchased and used as provided ($SbCl_3$, ^{n}$Bu_4NF\cdot 3H_2O$ and [^{n}Bu_4N][Ph_3SiF_2] from Aldrich, $TlPF_6$ from Strem, TBDMSCl from Chem Impex Int'l Inc. and TBACl from Acros). All air and moisture sensitive manipulations were carried out under an atmosphere of dry N_2 employing either a glove box or standard Schlenk techniques. Ambient temperature NMR spectra were recorded on a Varian Unity Inova 500 FT NMR (499.42 MHz for ^{1}H, 125.58 MHz for ^{13}C, 202.17 MHz for ^{31}P, 469.93 MHz for ^{19}F) spectrometer. Chemical shifts (δ) are given in ppm and are referenced against residual solvent signals (^{1}H, ^{13}C) or external H_3PO_4 (^{31}P) and $BF_3.Et_2O$ (^{19}F). Elemental analyses were performed at Atlantic Microlab (Norcross, GA).

Crystallography. All crystallographic measurements were performed at 110(2) K using a Bruker SMART APEX II diffractometer with a CCD area detector (graphite monochromated Mo Kα radiation, λ = 0.71073 Å, ω-scans with a 0.5° step in ω) at 110 K.

In each case, a specimen of suitable size and quality was selected and mounted onto a nylon loop. The semi-empirical method SADABS was applied for absorption correction. The structures were solved by direct methods and refined by the full-matrix least-square technique against F^2 with the anisotropic temperature parameters for all non-hydrogen atoms. All H atoms were geometrically placed and refined in riding model approximation. Data reduction and further calculations were performed using the Bruker SAINT+ and SHELXTL NT program packages.

Theoretical calculations. Density functional theory (DFT) calculations (full geometry optimization) were carried out on starting from the crystal structure geometries with Gaussian09 program (BP86[174-175] with 6-31G for H, C; 6-31+G(d') for F; 6-31G(d') for P, Cl, cc-pVTZ-PP with Stuttgart relativistic small core for Au[176-177] and Sb[178-179]). Frequency calculations performed on the optimized geometries found no imaginary frequency except in the case for **56** for which a weakly imaginary frequency (-8.17 cm^{-1}) associated to the rotation of the PF_6 anion was observed. QTAIM calculations were carried out on the wave functions derived from the optimized structures using the AIMAll program.[180] The LOL (Localized Orbital Locator) plots were obtained using Multiwfn, version 3.3.8.[181-182]

Characterization of 58. A solution of TBDMSCl (1.9 mg, 0.012 mmol) in dry CH_2Cl_2 (0.2 mL) was added to a solution of **55** (10.8 mg, 0.012 mmol) in dry CH_2Cl_2 (0.4 mL). The reaction mixture was transferred to an NMR tube and the formation of **58** was monitored by the heteronuclear NMR. The color changed from colorless to yellow within 2 hours indicating the conversion of **55** into **54** via the formation of **58**. After 24 hours,

the reaction reached an equilibrium with **54**, **58** and **55** present in the solution in 1.9:8.2:1 ratio. Single crystals of **58** suitable for X-ray diffraction were obtained by layering the reaction mixture with pentane. $^{31}P\{^{1}H\}$ NMR (202.17 MHz; $CDCl_3$): δ 95.89 (bs, 2P, P*i*Pr$_2$), ^{19}F NMR (469.93 MHz; $CDCl_3$): -136.42 (bs, 1F)

Characterization of 59. A solution of TBAT (11.18 mg, 0.02 mmol) in $CDCl_3$ (2 mL) was added dropwise to a solution of **56 (**20 mg, 0.02 mmol) also in $CDCl_3$ (1 mL). It was left to stir for 10 min and an aliquot of 0.5 ml was transferred to an NMR tube. Single crystals of **59** suitable for X-ray diffraction were obtained by layering a 1:1 mixture of **56** and TBAT in CH_2Cl_2 with pentane. $^{31}P\{^{1}H\}$ NMR (202.17 MHz; $CDCl_3$): δ 69.5 (t, $^{3}J_{P\text{-}F}$ = 14 Hz). ^{19}F NMR (469.93 MHz; $CDCl_3$): δ -2.72 ppm (ddt, 1F, $^{3}J_{P\text{-}F}$ = 14 Hz, $^{2}J_{F\text{-}F(cis)}$ = 32 Hz, $^{2}J_{F\text{-}F(cis)}$ = 60 Hz), -71.43 (ddt, 1F, $^{2}J_{F\text{-}F(trans)}$ = 80 Hz, $^{2}J_{F\text{-}F(cis)}$ = 32 Hz, $^{3}J_{F\text{-}P}$ = 14 Hz), -128.65 (dd, 1F, $^{2}J_{F\text{-}F(trans)}$ = 80 Hz, $^{3}J_{F\text{-}P}$ = 60 Hz).

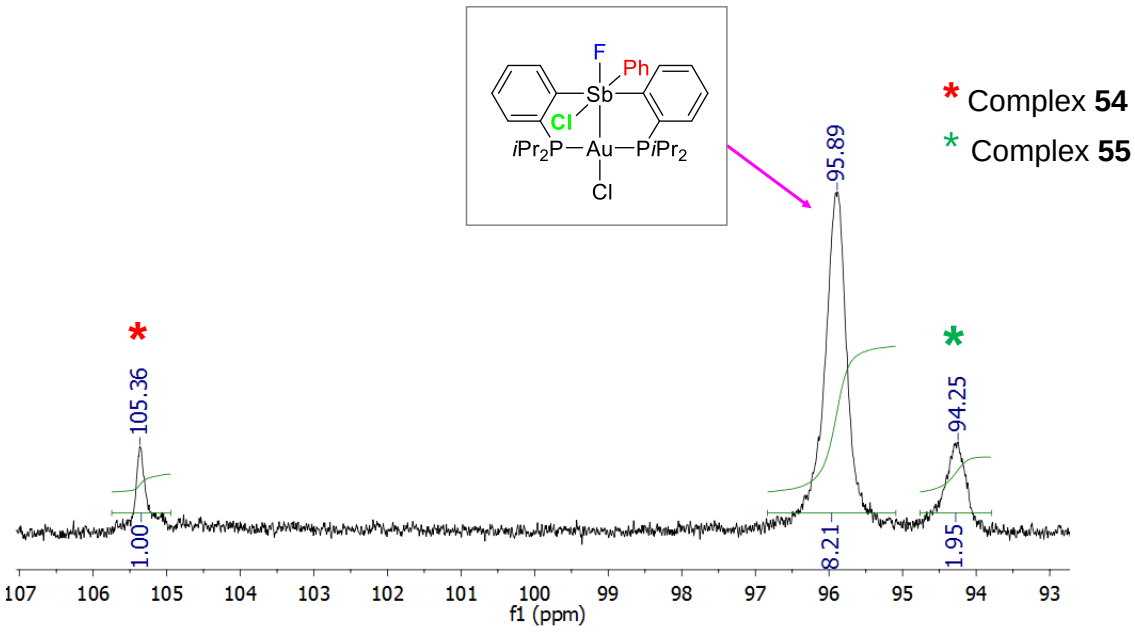

Figure 37. ^{31}P NMR of an equimolar mixture of complex **55** and *t*-Butyldimethylsilyl fluoride in CH_2Cl_2 after 24 hr.

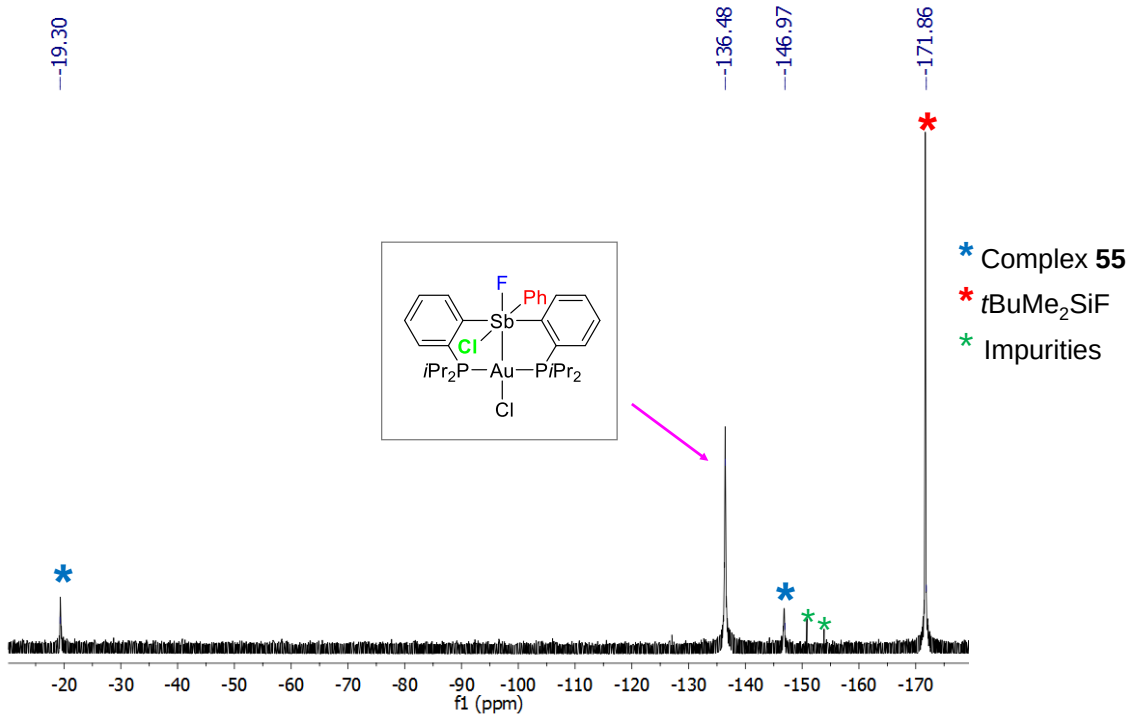

Figure 38. ^{19}F NMR of an equimolar mixture of complex **55** and *t*-Butyldimethylsilyl fluoride in CH_2Cl_2 after 24 hr.

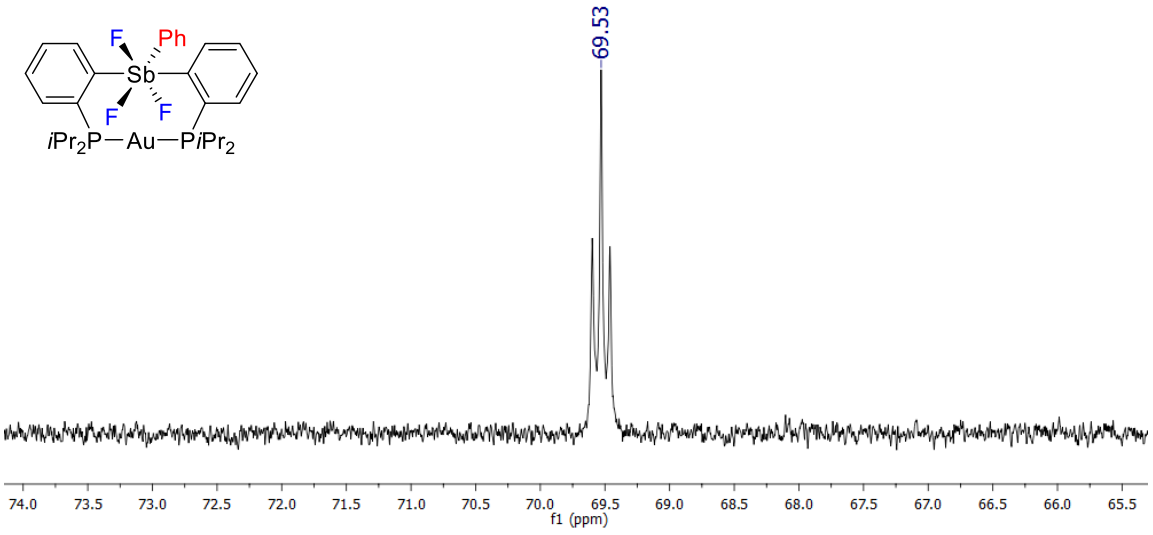

Figure 39. ^{31}P NMR spectrum of **59** in $CDCl_3$

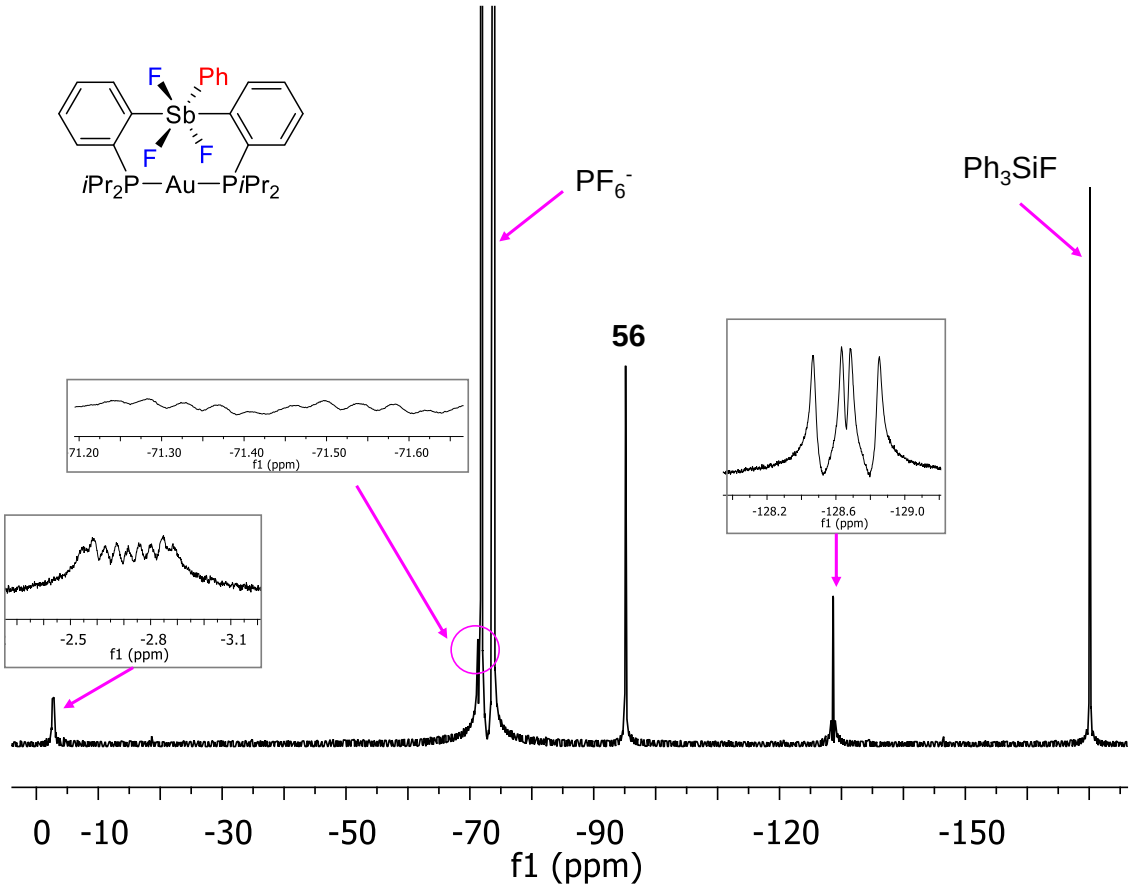

Figure 40. ^{19}F NMR spectrum of **59** in $CDCl_3$.

3. T-SHAPED GOLD→STIBORANE COMPLEXES AS CARBOPHILIC CATALYSTS: INFLUENCE OF THE PERIPHERAL SUBSTITUENTS[2]

3.1 Introduction

Introduction of a Lewis acidic main group ligand in the coordination sphere of a transition metal is emerging as a powerful tool to control and sometimes enhance the catalytic reactivity of the transition metal center.[183-192] While extensive efforts have been devoted to complexes featuring group 13 and 14 elements,[193-201] recent advances in the Lewis acid chemistry of group 15 compounds[25-26, 28-29, 137-138, 142, 147, 202-211] led us to speculate that ligands featuring heavy pnictogens[58-59, 153] may present new opportunities for the exploration of synergistic effects between a transition metal center and a main group Lewis acid. As part of these efforts, we discovered that stibine ligands could be oxidized within the coordination sphere of a metal to afford metal-stiborane complexes[63, 212-215] in which the stiborane functions as a Z-type ligand.[216] Using gold as a metal, we showed that the resulting Au→Sb interaction could also provide a handle on the electron density and reactivity of the transition metal center.[62, 217-218] This possibility can be illustrated by the oxidative conversion of the stibine complex **28**[SbF_6] into the stiborane complex **31**[SbF_6] which behaves as an active catalyst in the hydroamination of alkynes

[2] Reprinted with permission from Sen, S.; Ke, I. S.; Gabbaï, F. P. "T-Shaped Gold→Stiborane Complexes as Carbophilic Catalysts: Influence of the Peripheral Substituents" *Organometallics* **2017**, *36*, 4224-4230. Copyright 2017 American Chemical Society.

(Figure 41).[159] The increased reactivity of the gold center in **31**[SbF_6] is directly correlated to the oxidation of the antimony center which enhances the electrophilic character of the gold center because of a strengthening of the Au→Sb interaction.[62, 159, 217-218] These effects are similar to those discussed by Inagaki for related gold complexes whose catalytic activity are enhanced by an adjoining Lewis acidic boron atom.[219-220]

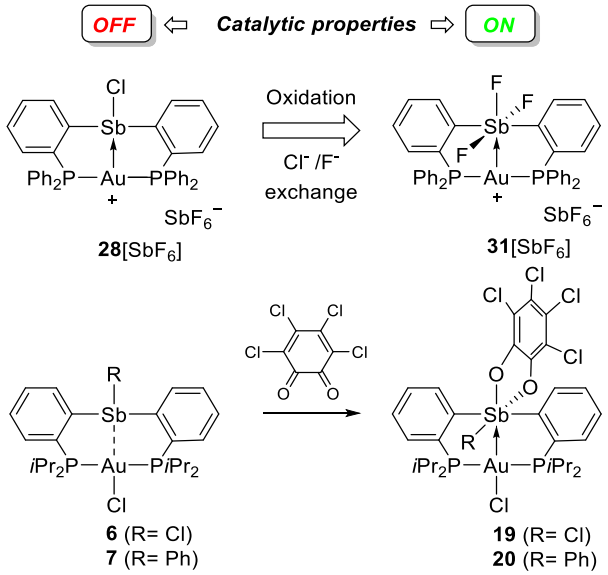

Figure 41. Examples of complexes featuring and Au→Sb interaction.

In another series of papers, we have shown that stibine ligands could be conveniently oxidized by *o*-chloranil when coordinated to transition metals.[62, 213] These reactions proceed by addition of the *ortho*-quinone to the antinomy atom, leading to the formation of a stiborane as in the case of **19** and **20** (Figure 41).[62] Given the ease by which such reactions can be implemented, we have now become interested in exploring

whether *o*-chloranil oxidized gold-antimony complexes would also be catalytically active. In addition to answering this primary question, it is also our more general intention to explore the influence that the ligand structure may have on the properties of such complexes. In this paper we present a series of results that address these questions and objectives.

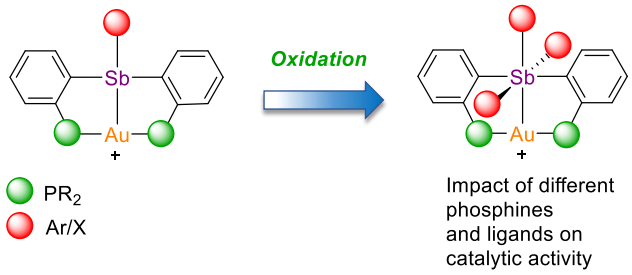

Figure 42. The typical complexes intended for this study

3.2 Synthesis, structure and bonding of cationic stiborane-gold complexes

In this study, we have decided to investigate pincer complexes of the general formula [(*o*-(R_2P)-C_6H_4)$_2$SbPh]AuCl which differ by the nature of the phosphine substituents R. We have previously synthesized the ligand (*o*-(Ph_2P)-C_6H_4)$_2$SbPh (L^{Ph}-Ph) and studied its interaction with precious metals such as palladium and platinum[63, 213] but the synthesis of the corresponding gold complex has not been attempted. We have now observed that L^{Ph}-Ph reacts with one equivalent of (tht)AuCl in CH_2Cl_2 at 0°C to afford the desired complex **61** as an air-stable, yellow powder in 80% yield (Scheme 4).

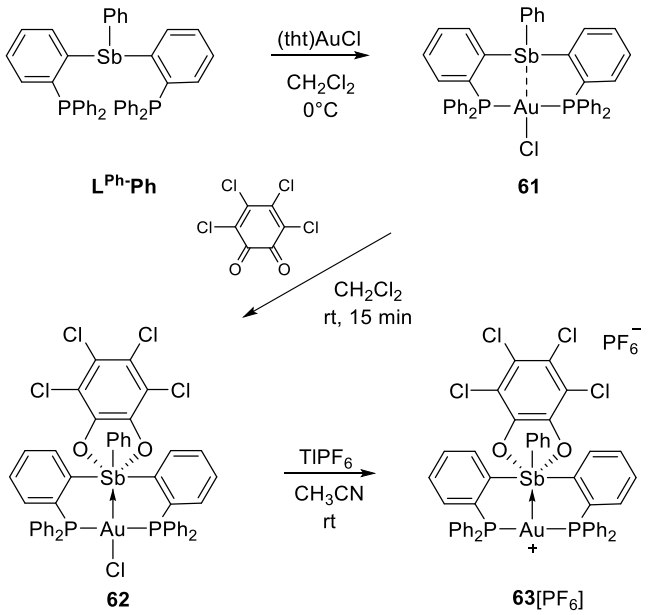

Scheme 4. Synthesis of **61**, **62** and **63**[PF_6].

Complex **61** has been characterized by ^{31}P NMR spectroscopy which showed a sharp peak at 40.92 ppm. The production of complex **61** was often accompanied by the formation of the chlorostibine complex [(*o*-(Ph_2P)-C_6H_4)$_2$SbCl]AuCl which was identified by its characteristic ^{31}P NMR signal at 38 ppm.

While we failed to crystallize **61**, we found that it cleanly reacts with *o*-chloranil in dichloromethane to afford the corresponding tetrachlorocatecholatostiborane gold complex **62** (Scheme 4). Complex **62** was obtained in a 60% yield as a bright orange crystalline solid after purification by column chromatography over silica. The ^{31}P NMR spectrum of the crude product shows a resonance at 83.03 ppm. While this compound was characterized by elemental analysis, its low solubility did not allow for reliable ^{1}H and ^{13}C NMR data to be obtained. When compared to complex **61**, the ^{31}P NMR resonance

is shifted downfield by ~45 ppm, in line with an increased oxidation of the AuSb core.[62, 67]

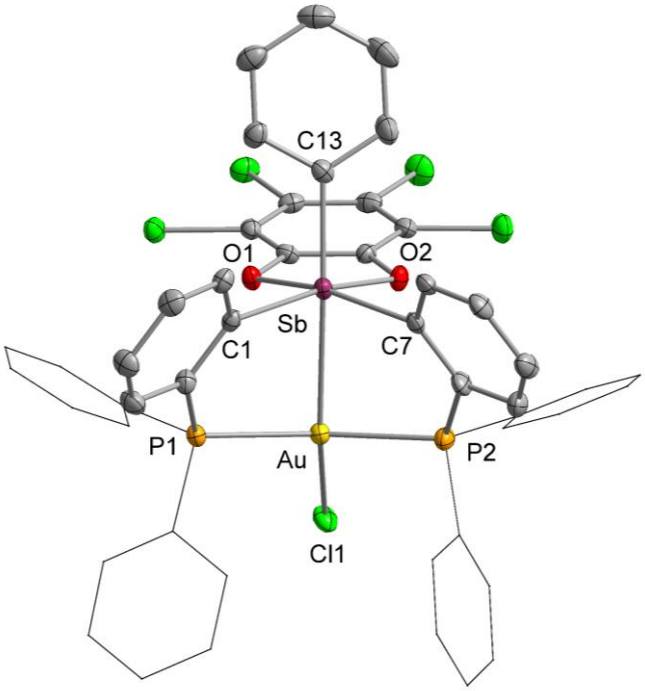

Figure 43. Crystal structure of **62**. Displacement ellipsoids are scaled to the 50% probability level. Hydrogen atoms and the lattice solvent molecules are omitted for clarity. Selected bond lengths (Å) and angles (deg) for **62**: Au-Sb 2.8608(5), Au-Cl1 2.5376(11), Au-P1 2.3161(11), Au-P2 2.3172(12), Sb-C13 2.132(4), Sb-O1 2.078(3), Sb-O2 2.079(3); P1-Au-P2 148.74(4), P1-Au-Cl1 104.71(4) and P2-Au-Cl1 98.14(4), Sb-Au-Cl1 150.96(3), C13-Sb-Au 163.99(12), O1-Sb-O2 79.29(11), C1-Sb-C7 100.20(16).

The crystal structure of complex **62** has been determined (Figure 43). The Au-Sb bond distance of 2.8608(5) Å is considerably longer than that in the analogous complex **20** (2.6833 (3) Å). This longer distance may be correlated to the fact that the positon trans to the gold atom is occupied by a phenyl ligand (C_{Ph}-Sb-Au = 163.99(12)°) rather than an

electron withdrawing oxygen atom as in the case of **20**. The catecholate ligand lies in a plane approximately perpendicular to the C_{Ph}-Sb-Au axis, with the two oxygen atoms positioned trans from the *ortho*-phenylene linkers. The strain imposed by the five-membered SbO_2C_2 ring leads to an acute O1-Sb-O2 angle of 79.29(11)°. By contrast the C1-Sb-C7 angle of 100.20(16)° involving the two *ortho*-phenylene linkers is relaxed by about ~10° when compared to the ideal value of 90°. In the absence of an Au→Sb interaction, the sum of the P1-Au-P2, P1-Au-Cl1, and P2-Au-Cl1 should be equal to 360°. However, the sum of these angles in **62** is equal to 351.6° suggesting some degree of electron donation from gold to antimony. The structural differences observed between **62** and **20** may originate from steric effects or even weak interactions between the peripheral ligands. We speculate that, in the case of **62**, the observed structure is stabilized by weak interactions occurring between the phosphorus-bound phenyl group and the tetrachlorophenylene ring of the catecholate ligand.[221] Such arene-arene stabilizing interaction would be absent with the bulkier di-*iso*-propyl phosphine units leading to the conformation observed in **20**.

Next, we decided to convert **62** into a potentially catalytically active species by abstraction of the gold-bound chloride. Salt **63**[PF_6] was generated by treating **62** with one equivalent of $TlPF_6$ in CH_2Cl_2/CH_3CN at room temperature. The product was obtained as a dark orange crystalline powder in 80% yield. Complex **63**[PF_6] gives rise to a ^{31}P NMR resonance at 56.34 ppm in CH_2Cl_2 and 56.09 in $CHCl_3$ (See Figure 51-Figure 54) However, the use of the more coordinating ligand CH_3CN produces a peak at 61.86 ppm, suggesting solvent coordination to the gold center. Addition of excess 4-

dimethylaminopyridine (DMAP) to a CH_2Cl_2 solution of **63**[PF_6] results in a ^{31}P NMR resonance a 67.63 ppm, again suggesting coordination of the DMAP to the gold atom. However, no notable changes in the ^{31}P NMR resonance of **63** [PF_6] was induced by addition of phenylacetylene indicating that this substrate is too weakly basic to shift the equilibrium in favor of the corresponding complex.

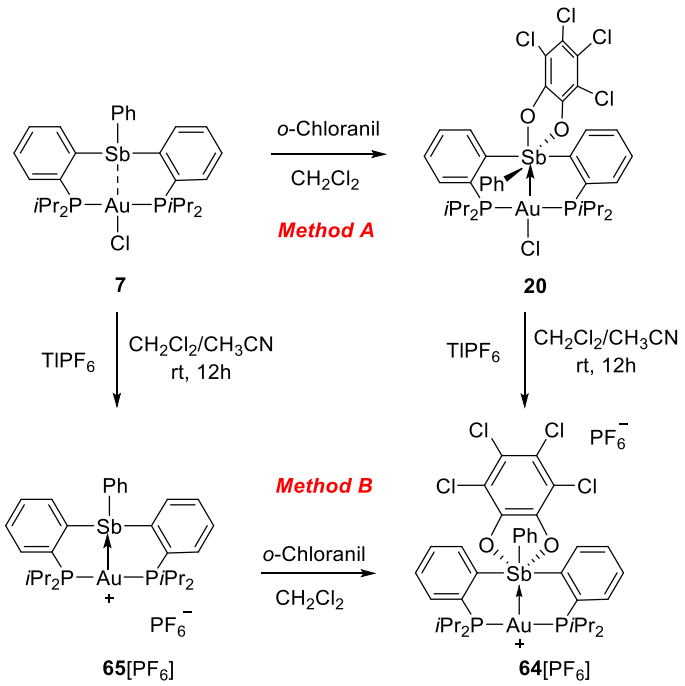

Scheme 5. Synthesis of **64**[PF_6] from **20** and **65**[PF_6]

In our pursuit of exploring the effect of ligands on the metal center, we decided to modify the phosphine arms that coordinate the gold center. Phosphine-supported gold catalysts usually feature phenyl derivatives on phosphines and the use of alkyl derivatives are almost non-existent. We became curious to compare the reactivity of an alkyl-

substituted phosphine to that of the diphenylphosphino derivate **63**[PF_6]. With this goal in mind, we also generated the di-*iso*-propylphosphino derivative **64**[PF_6] starting from the previously reported complex **20** (Scheme 5, Method A). Salt **64**[PF_6] was also obtained as a dark orange powder which showed a single ^{31}P NMR peak at 81.86 ppm in $CDCl_3$ (See Figure 55-Figure 58). Interestingly, ^{31}P NMR measurements indicated that **64**[PF_6] does not appear to interact with CH_3CN or DMAP as observed for **63**[PF_6].

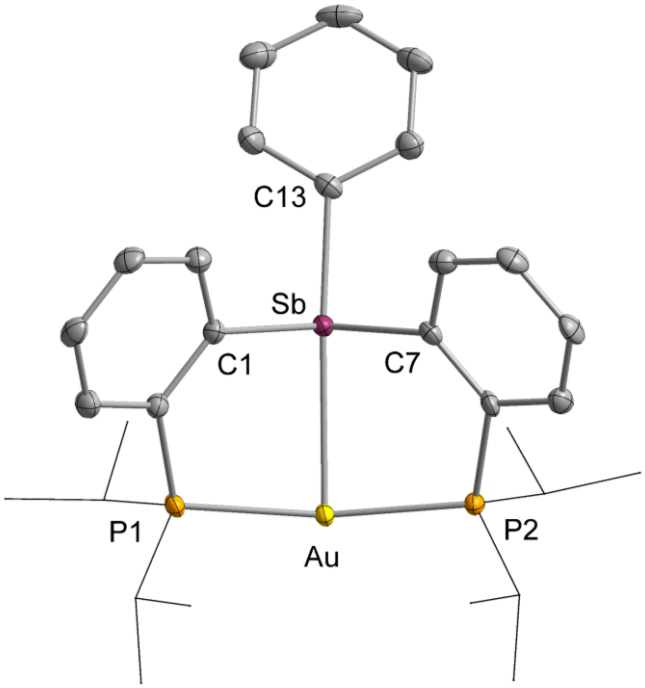

Figure 44. Crystal structure of **65**$^+$. Displacement ellipsoids are scaled to the 50% probability level. Counter anion PF_6^- and hydrogen atoms are omitted for clarity. Selected bond lengths (Å) and angles (deg) for **65**$^+$: Au-Sb 2.8820(4), Au-P1 2.3069(9), Au-P2 2.3065(9), Sb-C13 2.146(4); P1-Au-P2 162.48(3), Sb-Au-P1 86.40(2), Sb-Au-P2 86.65(2), C13-Sb-Au1 174.54(9), C1-Sb- C7 98.91(13).

Salt **64**[PF_6] can also be obtained from **65**[PF_6] via Method B (Scheme 5). Treatment of **7** with one equivalent of $TlPF_6$ in CH_3CN produces complex **65**[PF_6] as a pale yellow powder in 80% yield and was characterized by the downfield shift of the ^{31}P NMR (80.46 ppm) from the parent complex **7** (69 ppm). The single crystal structure of **65**[PF_6] obtained by X-ray diffraction showed that Au center displays a distorted T-shaped geometry with P1-Au-P2, Sb-Au-P1 and Sb-Au-P2 angles of 162.48(3)°, 86.40(2)° and 86.65(2)° respectively (Figure 44). The Sb center adopts a see-saw geometry very similar to that observed in case of the complex **31**[SbF_6]. The Sb center features a close to linear C13-Sb-Au angle of 174.54(9)° and a compressed C1-Sb-C7 angle of 98.91(13)°. The Sb-Au distance was found to be 2.8820(4) Å which is longer than the Sb-Au distance in the parent complex **7** (2.8669(4) Å).

Single crystals of **63**[PF_6] and **64**[PF_6] were obtained from $CDCl_3$/pentane and CH_2Cl_2/pentane, respectively. Both structures feature a core similar to that of **2** (Figure 45), with the phenyl group trans from the gold center (C13-Sb-Au = 168.9(4)° for $\mathbf{63}^+$ and 169.9(4)° for $\mathbf{64}^+$). The Sb-Au distances in $\mathbf{63}^+$ (2.9948(7) Å) and $\mathbf{64}^+$ (2.971(3) Å) are significantly longer than in the corresponding gold chloride complexes **62** (2.8608(5) Å) and **20** (2.6833(3) Å), respectively. This increased separation is explained the decreased Au→Sb donation that results from the formation of a cationic gold center. The same trend is observed upon conversion of borane-gold chloride complexes into their cationic counterparts.[168] It is also interesting to note that the Au-Sb bond length (2.971(2) Å) in **64**[PF_6] was found to be significantly longer than **65[**PF_6] (2.8820(4) Å which can be rationalized by the increase of coordination number of antimony from four to six.

In both **63**$^+$ and **64**$^+$, the gold atom is linearly coordinated to the two phosphine ligands (P1-Au-P2 = 165.04(9)° for **63**$^+$ and 165.83(12)° for **64**$^+$), with the antimony atom positioned along a direction essentially perpendicular from the P-Au-P vector. It is interesting to note the positional switching of the phenyl ligand upon conversion of **C** into **64**$^+$. Again, as noted above, we propose that the formation of a more electron deficient gold center is at the origin of this change.

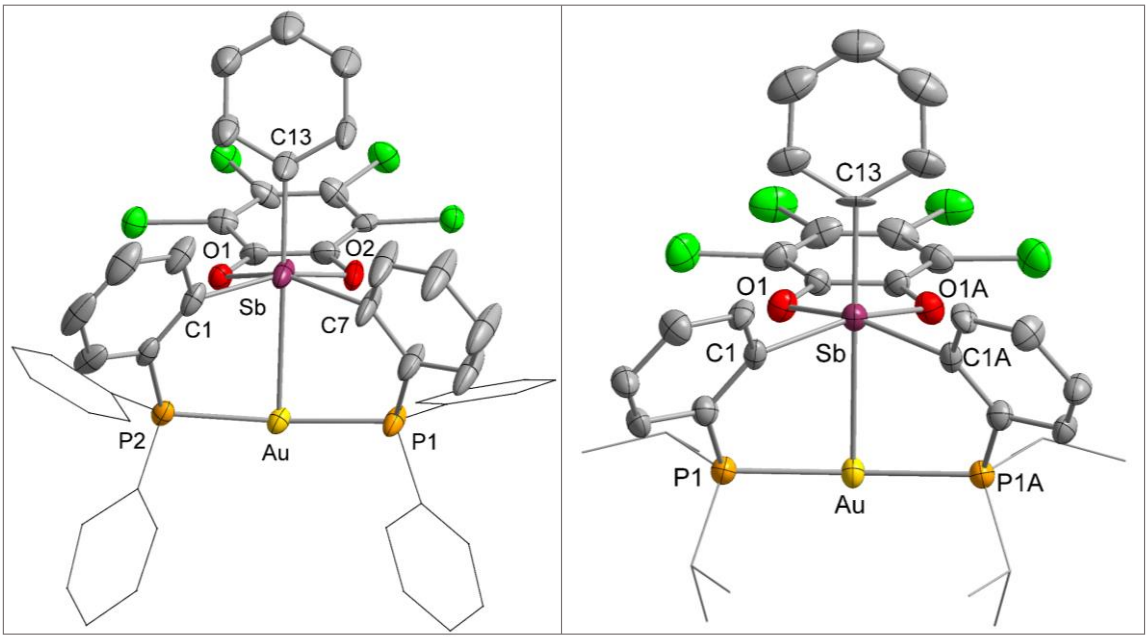

Figure 45. Crystal structures of **63**$^+$ (left) and **64**$^+$ (right). Displacement ellipsoids are scaled to the 50% probability level. Counter anion PF_6^- and hydrogen atoms are omitted for clarity. The symmetry generated atom in 4$^+$ were denoted by suffix A. Selected bond lengths (Å) and angles (deg) for **63**$^+$: Au-Sb 2.9948(7), Au-P1 2.305(3), Au-P2 2.309(3), Sb-C13 2.127(10), Sb-O1 2.055(6), Sb-O2 2.063(8); P1-Au-P2 165.04(9), Sb-Au-P1 86.60(6), Sb-Au-P2 86.40(6), C13-Sb-Au 168.9(4), O1-Sb-O2 79.5(3), C1-Sb-C7 107.0(5); for **64**$^+$: Au-Sb 2.971(3), Au-P1 2.318(3), Au-P1A 2.318(3), Sb-C13 2.101(12), Sb-O1 2.083(6), Sb-O1A 2.083(6); P1-Au-P2 165.83(12), Sb-Au-P1 87.48(6), Sb-Au-P1A, 87.48(6), C13-Sb-Au 169.9 (3), O1-Sb-O1A 78.2(4), C1-Sb-C1A 107.2(4).

3.2.1 Computational studies on **61**, **62**, **63**$^{+}$, **20** and **64**$^{+}$:

A theoretical study was undertaken on complexes **61**, **62**, **63**$^{+}$, **20** and **64**$^{+}$ to understand how the ligands decorating the core of these complexes influence the Au→Sb interaction and the Lewis acidity of the gold center. The structures were optimized by DFT methods (Gaussian09: BP86 with 6-31g for H, C, O; 6-31G(d') for P, Cl; cc-pVTZ-PP with Stuttgart relativistic small core for Au and Sb) and subjected to Natural Bond orbital (NBO) analysis (See experimental section). The optimized geometries of these complexes corresponded well with those experimentally derived in the cases of complex **62-65**$^{+}$ (Table 6). In the case of complex **61**, the optimized geometry revealed that the Sb center adopts a distorted trigonal pyramidal geometry while coordinated to a distorted tetrahedral Au. This structural feature is similar to that observed in the cases of the previously reported analogous complexes ((*o*-(*i*Pr$_2$P)C$_6$H$_4$)$_2$SbPh)AuCl and *o*-(Ph$_2$P)C$_6$H$_4$)$_2$SbPh)Cl.

The Natural Bond Orbital (NBO) analysis provided further insights into the variation of the Au→Sb bonding interaction with modification of the substituents around Sb and P and the oxidation state of Sb. NBO calculation on **61** identified a strong donor-acceptor interaction between the 5s lone pair of Sb to the vacant 6s orbital of Au as well as a weaker donation of lp(Au) to σ*(Sb-C), in line with the description of the stibine as a Z-ligand.

Table 6. Selected bond lengths (Å) for complexes 62, 63^+, 20 and 64^+ as determined crystallographically and optimized computationally (* denotes the optimized geometry).

Complex	Au-Sb (Å)
62	2.8608(5)
62*	2.82
63^+	2.9948(7)
63^+*	3.02
20[62]	2.6833(3)
20*	2.76
64^+	2.971(2)
64^+*	3.03
65^+*	2.8820(4)
65^+*	2.93

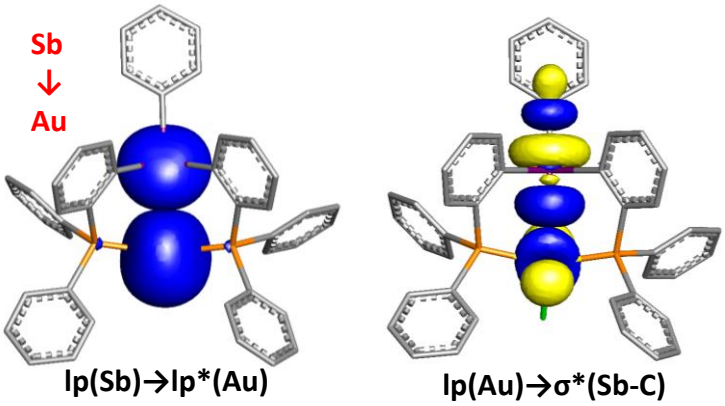

Figure 46. Principal Au→Sb donor-acceptor interactions in **61** obtained from NBO analysis (isodensity value = 0.05). Hydrogen atoms are omitted for clarity**.**

For **62**, the NBO calculations show the presence of multiple Au→Sb interactions involving donation from gold-based lone pair orbitals (lp) of *d* character into vacant orbitals at antimony. The two dominating interactions, which consist of a lp(Au)→lp*(Sb) and a lp(Au)→σ*(Sb-C_{Ph}), are shown in Figure 47. The deletion protocol as implemented in the NBO program suggests that all second order Au→Sb interactions contribute E_{del} = 70.5 kcal/mol to the stability of the complex. We note in passing that an NBO analysis of **61** at the same level of theory shows that the Au-Sb interaction is dominated by Sb→Au character (E_{del} = 19.2 kcal/mol) leading us to conclude that oxidation of the antimony center increases the acidity of the antimony atom and leading to a depletion of electron density from the gold center via formation of an Au→Sb interaction in **62**. Such changes have been described previously in the case of which is also generated by oxidation of a stibine precursor **20**.[62]

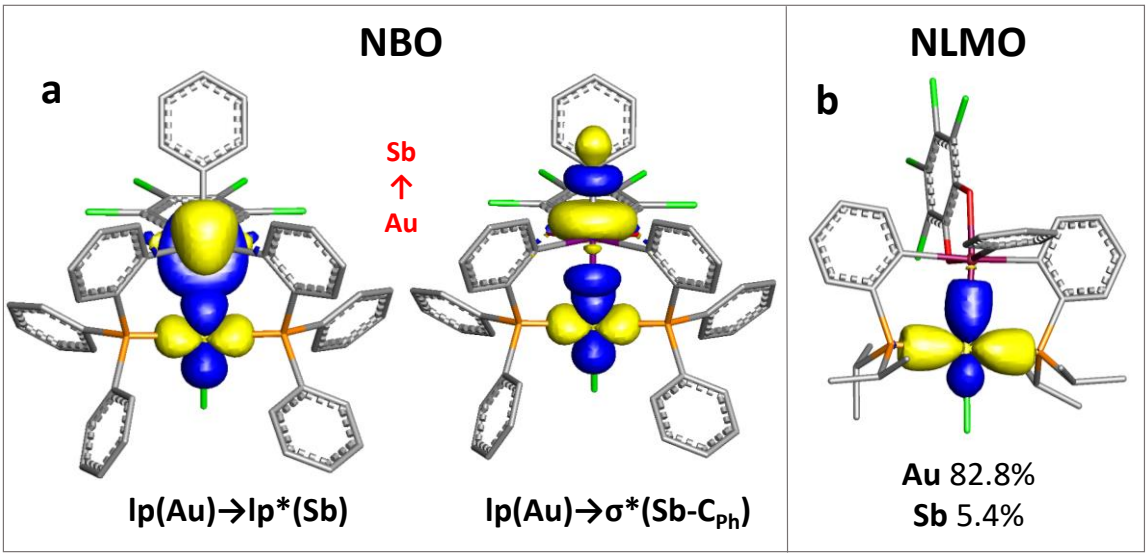

Figure 47. Principal Au→Sb donor-acceptor interactions in **62** (left) obtained from NBO analysis and Au−Sb Natural Localized Molecular Orbital in **20** (right) as observed in NLMO analysis (isodensity value = 0.05). Hydrogen atoms are omitted for clarity.

By contrast to the situation observed for **62**, we found that **20** is described by the NBO analysis as possessing a covalent and inherently stronger Au-Sb interaction. Inspection of the relevant NLMO shows that the Au-Sb interaction retains some Au→Sb character as indicated by the orbital make up (Au, 82.8% / Sb, 5.4%), which shows that gold is the largest contributor (Figure 4). The difference observed between **62** and **20** is assigned to the nature of the antimony ligand trans to the gold atom. In the case of **20**, the electron withdrawing nature of the catecholate oxygen atom increases the acidity of the antimony center leading to a less dative and more covalent Au→Sb interaction. This situation is reminiscent of that observed in (*o*-(*i*Pr$_2$P)C$_6$H$_4$)$_2$SiFPh)AuCl for which a

significant Au→Si interaction is only observed when the silicon-bound fluorine atom is located trans to gold.[49]

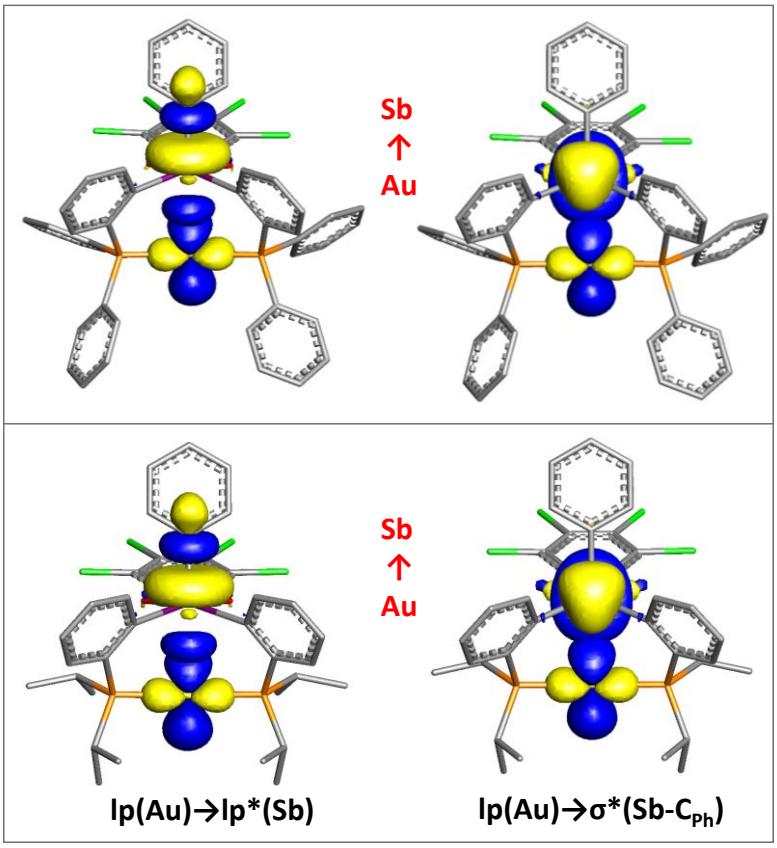

Figure 48. Principal Au→Sb donor-acceptor interactions in 63^+ (top) and 64^+ (bottom) obtained from NBO analysis (isodensity value = 0.05). Hydrogen atoms are omitted for clarity.

Conversion of **62** into **63**$^+$ by abstraction of the chloride ligand attenuates the metallobasicity of the gold center. This effect is reflected by the lower total Au→Sb stabilization energy (E_{del} = 31.5 kcal/mol). The nature of the individual Au→Sb interactions remains similar to those in **62** (Figure 48). As in **62**, a (lp(Au)→lp*(Sb) and

a lp(Au)→σ*(Sb-C_{Ph}) interaction dominate (Figure 48). The NBO analysis of **64**$^+$ shows a situation almost identical to that in **63**$^+$ with a total Au→Sb stabilization energy (E_{del}) of 29.3 kcal/mol (Figure 48). The slightly lower stabilization energy determined for **64**$^+$ is unexpected given the higher donicity of the di-*iso*-propylphosphino substitutents. We assigned this anomaly to the fact that the optimized structure of **64**$^+$ converges to a structure with a longer Au-Sb separation than in **63**$^+$. A last point which deserves comments is the fact that the positional switching of the Ph group observed upon conversion of **20** into **64**$^+$ changes the nature of the Au-Sb interaction, as interpreted by NBO, from a covalent one in **20** to a donor-acceptor one in **64**$^+$. Finally, we note that the NPA charges on the gold atom are very similar in both **63**$^+$ (0.289) and **64**$^+$ (0.282), which incidentally feature very similar Au→Sb deletion energy. In turn, the NBO calculations suggest that electronically, the gold centers of **63**$^+$ and **64**$^+$ are very similar.

3.2.2 Study of the catalytic activity of complexes **63**[PF_6] and **64**[PF_6]:

To conclude this study, we decided to examine the catalytic properties of the cationic complexes in the hydroamination of terminal alkynes[222-228] as well as in the cyclization of propargylic amides.[229-230] Given the electronic similarities existing for the gold centers of **63**$^+$ and **64**$^+$, we expected these two cationic complexes to behave similarly. This assumption was reinforced by the fact that the core structure of these two cations are close to each other as confirmed by the overlay shown in Figure 49. To our surprise, however, we found that **64**$^+$ is inactive in the reaction of *p*-toluidine with phenylacetylene

or in the cyclization of *N*-(prop-2-yn-1-yl)benzamide. By contrast, **63**$^+$ promoted both reactions as indicated in Table 7.

We propose that the differences observed in the catalytic properties of **63**$^+$ and **64**$^+$ originate from steric rather than electronic effects, with the bulkier *iso*-propyl group leading to a less accessible gold center as illustrated in Figure 49. This steric effect also explains why DMAP fails to interact with the gold center of **64**$^+$ as noted earlier. The role played by steric effects in these complexes is further supported by the fact that the cone angle of P(*i*Pr)$_3$ (160°) is larger than that of PPh$_3$ (145°).[231]

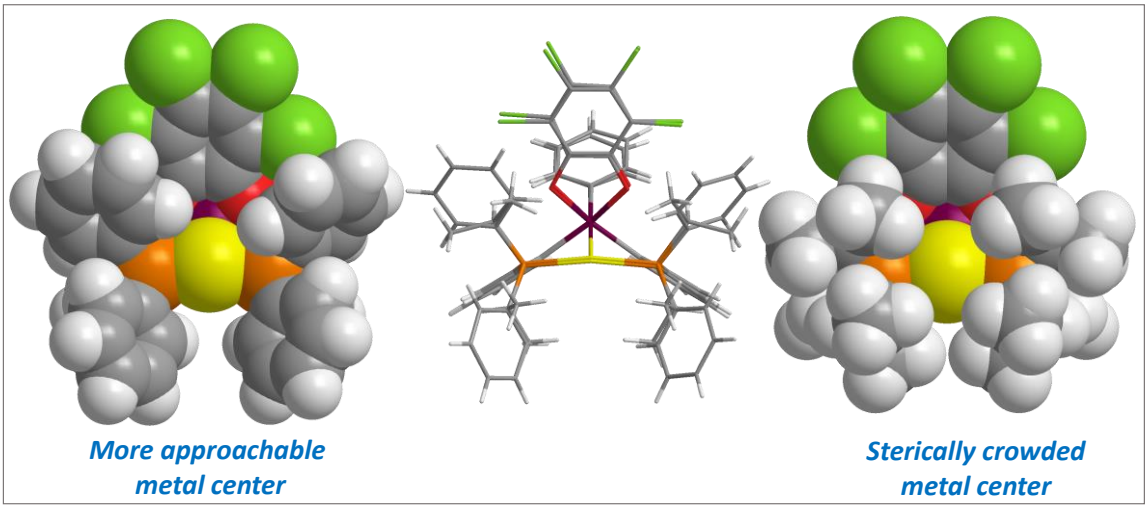

Figure 49. Space-filled model of **63**$^+$ (left) and **64**$^+$ (right) and the overlaid stick models of **63**$^+$ and **64**$^+$ (middle).

Table 7. Catalytic conversion of hydromaination reactions and cyclization of *N*-(prop-2-yn-1-yl)benzamide with 63 [PF_6] in $CDCl_3$ (Conversions are based on NMR).

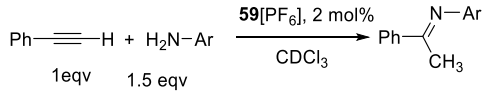

Entry	Ar	Temp.	Time (h)	Conversion
1	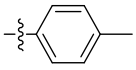	rt	2	100%
2	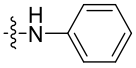	rt	2	76%
3	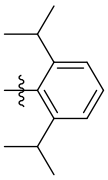	60°C	10	30%
4	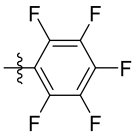	rt	24	n.r.

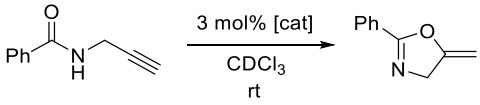

	Catalyst	Temp.	Time (h)	Conversion
5	**31**[SbF_6]	rt	7.5	100%
6	**63**[PF_6]	rt	7.5	35%

As indicated in Table 7, catalyst $\mathbf{63}^+$ is competent for the hydroamination of phenylacetylene with phenylhydrazine. It is however challenged by bulky and electron

deficient anilines as indicated by entries 3 and 4. We had previously observed that the reactions in entries 3 and 4 were efficiently catalyzed by **31**$^+$**.** We assign the lower activity of **63**$^+$ to the fact that its phenyl-tetrachlorocatecholatostiborane moiety is not as Lewis acidic as the trifluorostiborane unit present in **31**$^+$. A similar difference is observed in the cyclization of *N*-(prop-2-yn-1-yl)benzamide with **31**$^+$ being a notably more efficient catalyst than **63**$^+$ (Entries 5 and 6 of Table 7).

3.3 An introduction to stibonium-coordinated gold complexes

We have, so far, discussed the synthesis and application of gold complexes featuring a vacant site on cationic gold center supported by a coordinately saturated neutral stiborane moiety. Traditionally, the reactivity of transition metal catalysts depends on the Lewis acidity of the metal center arising from a vacant site which can either be accessed by predesign or by activating a metal-halide bond by an external reagent. As part of our contribution to this field, we have explored the possibility of bypassing the use of external activators and instead considered different self-activation routes implemented by the Lewis acid buttress. The practical implementation of this concept in the context of transition metal catalysis has been achieved through the gold complex **42** which is able to activate the Au-Cl bond by halide migration from gold to the strongly Lewis acidic and electrophilic antimony center in presence of an organic substrate.[111] A similar approach to unmask the catalytic activity of a platinum(II) center by intramolecular halide migration has been from Pt to Sb has been demonstrated by complex **43**.[112] An extrapolation of this hypothesis to electrophilic gold chemistry can be conceived by synthesizing molecules

where the gold chloride is supported by a cationic stibonium moiety with a vacant coordination site on antimony. We expect that the complexes and will follow the similar activation route in the presence of suitable organic substrates.

3.3.1 Synthesis and characterization of a monocationic gold-stibonium complex

To test the applicability of this hypothesis, we targeted the synthesis of the monocationic antimony/gold pincer complexes **66**[$N(SO_2Ph)_2$] (Scheme 6). This complex could easily be obtained by the oxidation of **61** with N-Fluorobenzenesulfonimide (NFSI) in dry CH_2Cl_2 at room temperature. In these reactions, NFSI serves the dual role of an electrophilic fluorinating reagent and an oxidant.

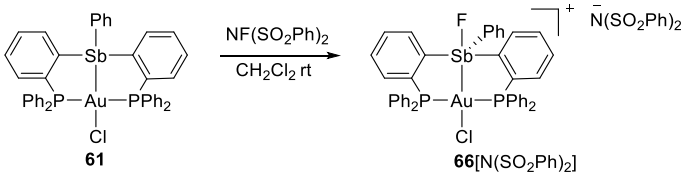

Scheme 6. Synthesis of **66**[$N(SO_2Ph)_2$].

Complex **66**[$N(SO_2Ph)_2$] was obtained as a bright yellow powder with 92% yield. Complete characterization of complex **66**[$N(SO_2Ph)_2$] was obtained by both heteronuclear NMR spectroscopy and X-ray diffraction study. Complex **66**[$N(SO_2Ph)_2$] shows a doublet at 72 ppm in ^{31}P NMR which is shifted downfield from the parent complex **61** (δ 40.92 ppm) indicating an oxidized Sb/Au core. The $J_{P\text{-}F}$ value is consistent with a ^3J coupling observed in the cases of the previously reported fluorostiborane/gold complexes featuring

an axial fluorine on antimony. A broad ^{19}F signal at -150 ppm corroborates with the existence of a fluorine trans to gold.[62, 159, 218]

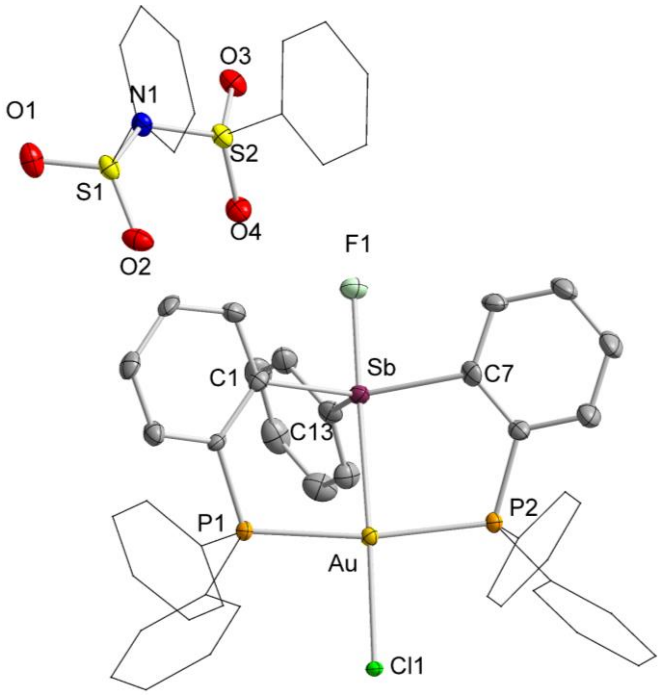

Figure 50. Crystal structures of **66**[$N(SO_2Ph)_2$]. Displacement ellipsoids are scaled to the 50% probability level. The hydrogen atoms are omitted for clarity. Selected bond lengths (Å) and angles (deg) for **66**: Au-Sb 2.7078(4), Au-Cl1 2.4586(11), Sb-F1 1.992(3); P1-Au-P2 170.52(4), Cl1-Au-Sb 172.79(3), F1-Sb-Au 175.85(9), C13-Sb-C7 119.38(19), C1-Sb-C7 133.48(18).

X-ray quality single crystals of **66**[$N(SO_2Ph)_2$] were obtained by the diffusion of Et_2O in a concentrated solution of **66**[$N(SO_2Ph)_2$] in CH_2Cl_2. The solid state structure provided unambiguous proof of the formation of the proposed cationic complex (Figure 50). The antimony center in **66**[$N(SO_2Ph)_2$] can be described as trigonal bipyramidal with fluorine and gold at the apical positions (angle F1-Sb-Au= 175.85(9)°). The gold center

adopts a square planar geometry which is in conformation with the series of gold/stiborane complexes described earlier in this chapter (Figure 50). The structure of **66**[$N(SO_2Ph)_2$] is reminiscent of that of complex **11**-F featuring a similar geometry with antimony and palladium decorating the core and a series of previously reported metal complexes featuring hypervalent group 14 centers.[49, 52, 232-234] An interesting feature of this molecules is the short Au-Sb distance of 2.7078(4) Å, compared to **62** or **20**, which can be attributed to the enhance Au→Sb interaction generated by the electron-deficient fluorostibonium moiety.

3.3.2 Reactivity of **66**[$N(SO_2Ph)_2$]

After obtaining a full characterization of **66**[$N(SO_2Ph)_2$], we decided to test its reactivity. Based on our previous observations regarding monocationic gold/stiborane complexes, we tested the catalytic activity of $\mathbf{66}^+$ with respect to hydromaination of phenylacetylene with *p*-toluidine. To our disappointment, $\mathbf{66}^+$ failed to catalyze the reaction which can be explained by the strong Lewis acidic character and the capability of the stibonium moiety to interact with Lewis bases, leading to the quenching of its reactivity.[235-252] Surprisingly, $\mathbf{66}^+$ catalyzed the cyclization of *N*-(prop-2-yn-1-yl)benzamide (complete conversion in 33 h) but the integrity of the catalytically active species could not be established due to the emergence of several peak in the ^{31}P NMR resonance.

To further probe the accessibility of a catalytically active metal center, we targeted the synthesis of complexes where the electron deficiency at the core will be enhanced by

increasing the overall charge of the complexes from 1^+ to 2^+. We hypothesized that the entry to this chemistry could be achieved by abstracting the halide from the gold center of **66**[$N(SO_2Ph)_2$] thus creating a vacant site on gold attached to a strongly electron-withdrawing stibonium moiety. Unfortunately, the reaction of **66**[$N(SO_2Ph)_2$] with one equivalent of $TlPF_6$ failed to provide any conclusive result. The reluctance of these molecules towards halide abstraction reactions may arise from the strengthening of the Sb-Au core due to the presence of the stibonium moiety and the resultant increase in the stability of the gold-chloride bond stemming from the electronic push-pull effect. We further hypothesized that such dicationic species may be stabilized by introducing another ligand in the coordination sphere of gold to counteract the electronic deficiency of the proposed cationic gold center.

3.3.3 Synthesis and characterization of a dicationic gold-stibonium complex

To access the proposed cationic species we decided to work with complex **67** which has been synthesized by Dr. Casey Wade.[253] He attempted to synthesize the dication **68**[PF_6]$_2$ but it could not be fully characterized at that time. As part of our ongoing research we revisited the synthesis of and were able to prepare it by the treatment of **67** with 4 equivalents of $TlPF_6$ in CH_3CN and single crystals were obtained by diffusion of Et_2O into a solution of **68**[PF_6]$_2$ in CH_3CN (Scheme 7). Complex **68**[PF_6]$_2$ was characterized by the ^{31}P NMR spectroscopy which showed a doublet at δ = 41.37 ppm (d, $^3J_{P\text{-}F}$ = 80 Hz) and ^{19}F NMR showed a broad singlet at δ = - 155.36 ppm.

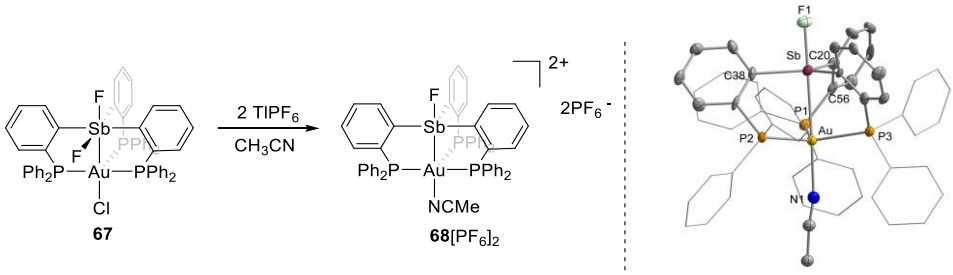

Scheme 7. Left: Synthesis of **68**$[PF_6]_2$ from **67**. Right: Crystal structure of **68**$^+$. Displacement ellipsoids are scaled to the 50% probability level. The PF_6^- counter anions and hydrogen atoms are omitted for clarity.

Interestingly the solid state structure of **68**$^+$ showed that one CH_3CN molecule is coordinated to the Au center which points towards the high Lewis acidity of the gold center. The gold center adopts a pentacoordinated trigonal bipyramidal geometry with the nitrogen of CH_3CN and antimony decorating the apexes of the pyramid and the three phosphorus atoms constituting the base. The Sb-Au distance was found to be 2.7929(8) Å which indicates a strong Au→Sb interaction. The Sb-F distance of 1.947(5) Å is comparable to that of **66**$[N(SO_2Ph)_2]$. This is the first time a dicationic 4-coordinate Au complex has been synthesized and its robust nature and strong Lewis acidity makes it a good candidate to study catalytic reactivity. However, when tested, complex **68**$[PF_6]_2$ showed very poor catalytic activity towards the hydromaination of phenylacetylene with *p*-toluidine (20% in 20 h at 60°C). The lack of reactivity of the gold center in complex **68**$[PF_6]_2$ may attributed to the presence of three electron-donating phosphine ligands around the gold center which partially quenches its electrophilicity. Steric crowding may also block access to the gold center.

3.4 Conclusion

In summary, we have shown that gold chloride complexes supported by stibine ligands can be oxidized using *o*-chloranil to form the corresponding stiborane complexes. This two-electron oxidation induces a depletion of electron density from the gold center in a direct manifestation of the increased σ-accepting properties of the oxidized antimony center. Conversion of these complexes into the cationic ones by abstraction of the gold-bound chloride produces T-shaped complexes $\mathbf{63}^+$ and $\mathbf{64}^+$ which differ by the nature of the phosphine substituents but whose dinuclear core are very similar. Reactivity studies indicate that only $\mathbf{63}^+$ is catalytically active in reactions requiring alkyne activation. Based on this observation and the results of our structural and computational studies, we conclude that the bulk of the ancillary *i*Pr$_2$P ligands present in $\mathbf{64}^+$ are responsible for the catalytic incompetency of the latter. Finally, a comparison of the catalytic properties $\mathbf{3}^+$ with those of $\mathbf{31}^+$ shows that the antimony substituents strongly influence the catalytic properties of the gold center.

In a related work, we have described the synthesis of a novel monocationic gold complex **66**[N(SO$_2$Ph)$_2$] in which the gold center is joined to stibonium moieties. The electrophilic nature of the stibonium center enhances the stability of the gold-chloride bond and thus prevents the displacement of chloride by a substrate. A diacationic gold complex **68**[PF$_6$]$_2$ featuring both a cationic gold canter and a stibonium could only be accessed by the introduction of a third phosphine arm. However, complex **68**[PF$_6$]$_2$ lacks the ability to coordinate alkynes, probably due to the presence of an electronically saturated and sterically crowded gold(I) center.

3.5 Experimental section

General considerations. (tht)AuCl (tht = tetrahydrothiophene)[170], (*o*-$(Ph_2P)C_6H_4)_2SbPh$,[63] (*o*-(*i*$Pr_2P)C_6H_4)_2$(*o*-$C_6Cl_4O_2$)SbPh)AuCl,[62] and the N-(prop-2-yn-1-yl)benzamide were prepared according to the reported procedures. Solvents were dried by passing through an alumina column (n-pentane and CH_2Cl_2) or by reflux under N_2 over Na/K (Et_2O and THF). All other solvents were used as received. All commercially available chemicals were purchased and used as provided ($TlPF_6$ from Strem, *o*-Chloranil from Acros). All air and moisture sensitive manipulations were carried out under an atmosphere of dry N_2 employing either a glove box or standard Schlenk techniques. Ambient temperature NMR spectra were recorded on a Varian Unity Inova 500 FT NMR (499.42 MHz for ^1H, 125.58 MHz for ^{13}C, 202.17 MHz for ^{31}P, 469.93 MHz for ^{19}F) spectrometer. Chemical shifts (δ) are given in ppm and are referenced against residual solvent signals (^1H, ^{13}C) or external H_3PO_4 (^{31}P) and $BF_3.Et_2O$ (^{19}F). Elemental analyses were performed at Atlantic Microlab (Norcross, GA).

Synthesis of 61. A solution of (tht)AuCl (88.87 mg, 0.27 mmol) in CH_2Cl_2 (20 mL) was added dropwise to a solution of (*o*-$(Ph_2P)C_6H_4)_2SbPh$ (200 mg, 0.27 mmol) in CH_2Cl_2 (20 mL) at 0°C. After stirring for an hour in a vessel protected from incident light, volatiles were removed and the residue was washed with Et_2O (5 ml) and pentane (10 mL). Compound **61** was obtained as a yellow powder. Yield: 205 mg, 79%. ^1H NMR (500 MHz, $CDCl_3$) δ 8.02 (s, 2H), 7.87 (d, *J* = 6.0 Hz, 2H), 7.42 (m, 22H), 7.19 – 6.98 (m, 6H), 6.93 – 6.79 (m, 1H). ^{13}C NMR (126 MHz, $CDCl_3$) δ 146.90 (s), 139.08 (s), 136.98 (s),

136.17 (s), 135.36 (d, J = 22.6 Hz), 134.79 – 133.69 (m), 132.87 (d, J = 30.6 Hz), 131.82 (d, J = 24.5 Hz), 131.09 (d, J = 11.0 Hz), 130.75 (s), 129.04 (dd, J = 23.0, 16.7 Hz), 128.25 (s). ^{31}P NMR (202 MHz, $CDCl_3$) δ 40.92 (s). Elemental analysis calcd (%) for $C_{42}H_{33}AuClP_2Sb$: C 52.89, H 3.49; found: C 52.39, H 3.92.

Synthesis of 62. A solution of *o*-chloranil (51.53 mg, 0.21 mmol) in CH_2Cl_2 (5 mL) was added dropwise to a solution of **61** (200 mg, 0.21 mmol) in CH_2Cl_2 (5 mL) at ambient temperature. The reaction was stirred for an hour before removing the solvent under reduced pressure. The resulting orange solid was purified by column chromatography (Silica, 230−400 mesh, 4:1 dichloromethane(dry)/ hexane(dry), R_f= 0.46). The product was obtained as a bright orange solid. Yield: 150 mg, 60%. Single crystals of **62** suitable for X-ray diffraction were obtained by vapor diffusion of Et_2O into a solution of the compound in CH_2Cl_2. Due to the poor solubility and unstable nature of **62** in organic solvent, good quality ^{1}H and ^{13}C could not be obtained. ^{31}P NMR (202 MHz, $cdcl_3$) δ 83.03 (s). Elemental analysis calcd (%) for $C_{48}H_{33}AuO_2P_3Cl_5Sb$: C 48.06, H 2.77; found: C 49.03, H 3.45.

Synthesis of 63[PF_6]. A solution of $TlPF_6$ (54.49 mg, 0.156 mmol) in CH_3CN (5 mL) was added to a solution of **62** (125 mg, 0.104 mmol) in CH_2Cl_2 (5 mL) and stirred at ambient temperature for two hours. Precipitation of a TlCl was observed. The solvent was evaporated and the resulting solid was extracted with CH_2Cl_2, followed by filtration of the resulting solution over Celite. The residual solvent was evaporated and the product was obtained as a dark orange solid after washing with pentane (5mL). Yield: 110 mg, 80%. Single crystals of **63**[PF_6] suitable for X-ray diffraction were obtained by vapor diffusion

of Et_2O into a solution of the compound in CH_3CN. ^1H NMR (499 MHz, $CDCl_3$) δ 7.96 (d, *J* = 7.6 Hz, 1H), 7.80 (t, *J* = 7.5 Hz, 1H), 7.75 (q, *J* = 7.7 Hz, 2H), 7.72 – 7.57 (m, 5H), 7.52 (t, *J* = 6.9 Hz, 2H), 7.47 (dd, *J* = 14.9, 7.4 Hz, 2H), 7.40 (t, *J* = 7.5 Hz, 1H), 7.21 (dd, *J* = 13.6, 6.9 Hz, 2H). ^{13}C NMR (126 MHz, $CDCl_3$) δ 155.80 – 153.87 (m), 142.83 (s), 139.00 (s), 135.43 (s), 134.97 (s), 133.72 (t, J = 7.6 Hz), 133.25 (dd, J = 19.8, 13.0 Hz), 132.63 (s), 132.44 (s), 132.19 (s), 130.42 (t, J = 6.5 Hz), 130.12 – 129.62 (m), 125.10 – 124.21 (m), 121.04 (s), 117.34 (s). ^{19}F NMR (470 MHz, $CDCl_3$) δ -73.75 (PF_6, d, *J* = 713.2 Hz). ^{31}P NMR (202 MHz, $CDCl_3$) δ 56.09 (s), -143.93 (PF_6, septate, *J* = 713.3 Hz). Elemental analysis calcd (%) for $C_{48}H_{33}AuO_2F_6P_3Cl_4Sb$: C 44.04, H 2.54; found: C 45.03, H 2.93.

Synthesis of 64[PF_6]. Method A: A solution of $TlPF_6$ (82.10 mg, 0.235 mmol) in CH_3CN (5 mL) was added to a solution of **20** (125 mg, 0.117 mmol) in CH_2Cl_2 (5 mL) and stirred at ambient temperature for two hours. Precipitation of a TlCl was observed. The solvent was evaporated and the resulting solid was extracted with CH_2Cl_2, followed by filtration of the resulting solution over Celite. The residual solvent was evaporated and the product was obtained as a dark orange solid after washing with pentane (5mL). Yield: 96.5 mg, 70%. Method B: A solution of *o*-chloranil (53.03 mg, 0.216 mmol) in CH_2Cl_2 (5 mL) was added dropwise to a solution of **65**[PF_6] (200 mg, 0.216 mmol) in CH_2Cl_2 (5 mL) at ambient temperature. The reaction was stirred for an hour before removing the solvent in vacuo. The resulting dark orange solid was washed with pentane (5 ml). Yield: 177.38 mg, 70%).Single crystals of **64**[PF_6] suitable for X-ray diffraction were obtained by diffusion of pentane into a solution of the compound in $CDCl_3$ inside an NMR tube. ^1H

NMR (500 MHz, $CDCl_3$) δ 7.81 (ddd, *J* = 8.0, 5.8, 2.5 Hz, 2H), 7.75 (dd, *J* = 6.8, 5.5 Hz, 4H), 7.62 (dd, *J* = 11.2, 3.9 Hz, 2H), 7.49 (ddd, *J* = 14.8, 6.8, 1.3 Hz, 4H), 7.40 (t, *J* = 7.5 Hz, 2H), 3.69 (dp, *J* = 14.5, 7.3 Hz, 2H), 3.57 – 3.44 (m, 2H), 1.47 (dt, *J* = 7.0, 4.8 Hz, 12H), 1.40 – 1.32 (m, 8H), 1.11 – 1.03 (m, 6H). ^{13}C NMR (126 MHz, $CDCl_3$) δ 154.18 (s), 143.22 (s), 135.35 (s), 135.19 – 134.78 (m), 133.41 (s), 132.91 (s), 132.35 (d, *J* = 13.1 Hz), 132.06 (d, *J* = 3.7 Hz), 129.72 (s), 121.62 (s), 116.81 (d, *J* = 42.1 Hz), 116.61 (s), 77.48 (d, *J* = 7.0 Hz), 77.26 (s), 77.00 (s), 29.61 (t, *J* = 14.3 Hz), 24.13 (t, *J* = 14.3 Hz), 22.83 (t, *J* = 3.6 Hz), 20.58 (s), 20.37 (t, *J* = 3.7 Hz), 15.83 (s). ^{19}F NMR (470 MHz, $CDCl_3$) δ -73.74 (PF_6, d, *J* = 713.0 Hz). ^{31}P NMR (202 MHz, $CDCl_3$) δ 81.86 (s), -144.02 (PF_6, septate, *J* = 713.3 Hz). Elemental analysis calcd (%) for $C_{36}H_{41}AuO_2F_6P_3Cl_4Sb$: C 36.86, H 3.52; found: C 36.64, H 3.43.

Synthesis of 65[PF_6]. A solution of $TlPF_6$ (140.96 mg, 0.40 mmol) in CH_3CN (5 mL) was added to a solution of **7** (330 mg, 0.40 mmol) in CH_2Cl_2 (5 mL) and stirred at ambient temperature for two hours resulting in the precipitation of a white TlCl salt. The solvent was evaporated and the resulting solid was extracted with CH_2Cl_2 via the filtration over Celite. The residual solvent was evaporated and the product was obtained as a dark orange solid after washing with pentane (5ml). Yield: 345 mg, 93%. Single crystals of **65**[PF_6] suitable for X-ray diffraction were obtained by vapor diffusion of Et_2O into a solution of the compound in CH_3CN. ^1H NMR (500 MHz, $CDCl_3$) δ 7.94 (d, *J* = 7.4 Hz 2H), 7.67 – 7.58 (m, 4H), 7.55 – 7.48 (m, 2H), 7.46 – 7.38 (m, 3H), 7.36 – 7.30 (m, 2H), 3.29 – 3.14 (m, 2H), 2.77 – 2.63 (m, 2H), 1.56 – 1.47 (m, 6H), 1.43 (dd, *J* = 18.6, 7.2 Hz, 6H), 1.38 – 1.30 (m, 6H), 1.07 – 0.98 (m, 6H). ^{19}F NMR (470 MHz, $CDCl_3$) δ -74.01 (d,

J = 713.0 Hz). ^{31}P NMR (202 MHz, $CDCl_3$) δ 81.02 (s), -143.52 (septate, *J* = 713.3 Hz). Elemental analysis calcd (%) for $C_{30}H_{41}AuF_6P_3Sb$: C 38.86, H 4.46; found: C 39.51, H 4.51

General procedure for the catalyzed hydroamination reactions. All the catalytic reactions were carried out in air. In a typical reaction, one equivalent of phenylacetylene (20 mg, 0.196 mmol) was mixed with 1.5 equivalent of amine (0.293 mmol) in 0.6 ml $CDCl_3$ in a 20 mL vial. Next, 2 mol% catalyst was added to the solution and the reaction mixture was transferred to an NMR tube. The progress of the reaction was monitored by ^{1}H NMR and the conversion was estimated using durene (2, 3, 4, 5-tetramethylbenzene) as an internal standard.

General procedure for catalyzed cyclization of *N*-(prop-2-yn-1-yl)benzamide. All the catalytic reactions were carried out in air. A typical procedure is as follows: *N*-(prop-2-yn-1-yl)benzamide (20 mg, 0.125 mmol) is dissolved in 0.6 mL $CDCl_3$. The selected catalyst (3 mol%) was dissolved in 0.8 mL $CDCl_3$. The solution containing the catalyst was added to the solution of *N*-(prop-2-yn-1-yl)benzamide. The resulting solution was stirred at room temperature. The progress of the reaction was monitored by ^{1}H NMR and the conversion was estimated using durene (2, 3, 4, 5-Tetramethylbenzene) as an internal standard.

Synthesis of 66[$N(SO_2Ph)_2$]. A solution of NFSI (66mg, 0.209 mmol) in CH_2Cl_2 was added dropwise to a solution of **61** (200 mg, 0.209 mmol) in CH_2Cl_2. The resulting bright yellow solution was left to stir for an hour and subsequently evacuated to dryness under reduced pressure. The resulting residue was washed with Et_2O (3 × 5 mL) to afford

crude **66**[$N(SO_2Ph)_2$] as yellow crystalline solid. Yield: 245mg, 92%. Single crystals of **66**[$N(SO_2Ph)_2$] were obtained by slow diffusion of Et_2O into a concentrated CH_2Cl_2 solution. ^{1}H NMR (499 MHz, $CDCl_3$) δ 8.87 (d, *J* = 9.2 Hz, 2H), 7.76 (t, *J* = 7.0 Hz, 2H), 7.68 (dt, *J* = 8.2, 4.1 Hz, 4H), 7.60 (dd, *J* = 15.6, 8.1 Hz, 2H), 7.54 – 7.46 (m, 6H), 7.45 – 7.33 (m, 12H), 7.32 – 7.28 (m, 4H), 7.25 – 7.17 (m, 2H), 7.07 (t, *J* = 7.8 Hz, 4H), 6.94 – 6.84 (m, 3H), 6.59 (t, *J* = 7.7 Hz, 2H). ^{13}C NMR (126 MHz, $CDCl_3$) δ 144.92 (s), 138.01 (s), 135.34 (s), 134.58 (t, *J* = 6.8 Hz), 134.33 (s), 133.88 (s), 133.30 (t, *J* = 6.0 Hz), 132.77 (s), 132.27 (s), 130.41 (s), 129.76 (s), 129.32 (dt, *J* = 12.6, 5.9 Hz), 128.83 (s), 127.49 (s), 126.71 (s), 126.08 (s). ^{19}F NMR (470 MHz, $CDCl_3$) δ -148.45 (t, J_{P-F} = 19.6 Hz). ^{31}P NMR (202 MHz, $CDCl_3$) δ 71.80 (d, *J* = 21.8 Hz). Elemental analysis calcd (%) for $C_{54}H_{43}AuN_2O_4FP_2S_2SbAu$: C 52.17, H 3.84, N 1.07; found: C 50.27, H 3.76, N 1.26.

Crystallography. All crystallographic measurements were performed at 110(2) K using a Bruker SMART APEX II diffractometer with a CCD area detector (graphite monochromated Mo Kα radiation, λ = 0.71073 Å, ω-scans with a 0.5^o step in ω) at 110 K. In each case, a specimen of suitable size and quality was selected and mounted onto a nylon loop. The semi-empirical method SADABS[254] was applied for absorption correction. The structures were solved by direct methods and refined by the full-matrix least-square technique against F^2 with the anisotropic temperature parameters for all non-hydrogen atoms. All H atoms were geometrically placed and refined in riding model approximation. Data reduction and further calculations were performed using the Bruker *Apex2* (2013) and SHELXTL program packages. Structural refinements were performed using Olex2.[255] In the crystal structure of **64**[PF_6], disordered solvent molecules were

identified in the final stages of refinement. The disorder of the solvent molecules could not be modeled. The corresponding residual electron density was handled using the solvent mask routine implemented in Olex2 (Similar to Squeeze[256]/Platon[257]). This approach allows for the mathematical compensation of the electron contribution of disordered solvent molecules to the calculated diffraction intensities. The solvent mask program found a void volume of 585 $Å^3$ (142 electrons) per molecules of **64** [PF_6]. This is in reasonable agreement with the presence of four molecules of pentane[258] (ρ = 0.88 g/cm^3, 548 $Å^3$, 168 electrons) per molecule of **64** [PF_6].

Theoretical calculations. Density functional theory (DFT) calculations (full geometry optimization) were carried out on starting from the crystal structure geometries with Gaussian09 program (BP86[174-175] with 6-31G for H, C, O; 6-31G(d') for P, Cl, cc-pVTZ-PP with Stuttgart relativistic small core for Au[176-177] and Sb[178-179]). Frequency calculations performed on the optimized geometries found no imaginary frequency. The structure of **C** had been previously optimized at a different level of theory. This optimization was repeated for consistency using the above mentioned basis sets. The optimized structures, which are in excellent agreement with the solid-state structures. Bonding was analyzed using NBO 5.9 program.[259] The resulting NBOs and NLMOs were visualized and plotted in Jimp 2 program.[260]

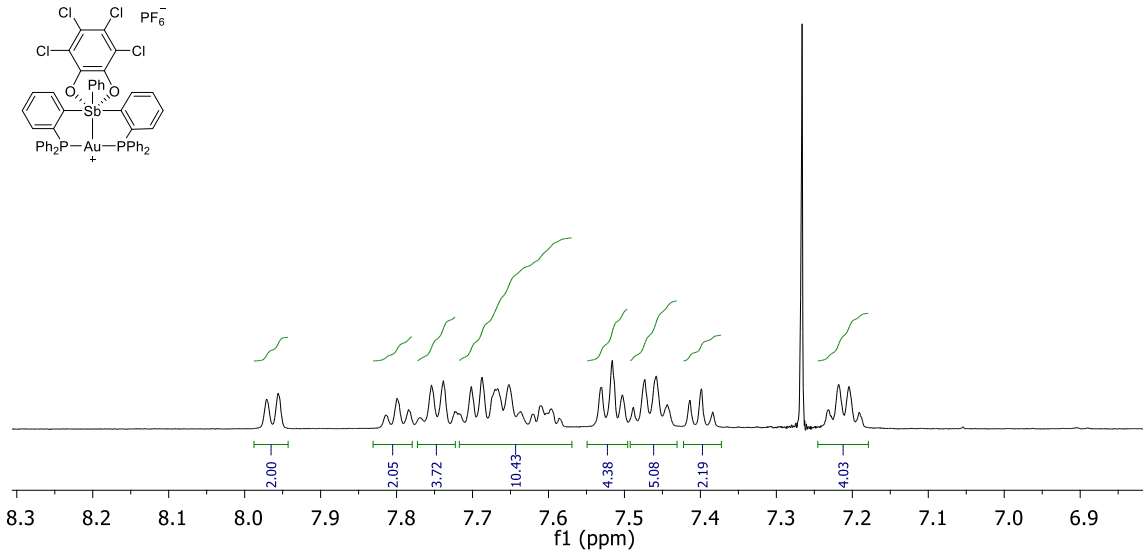

Figure 51. ^{1}H NMR spectrum of **63**[PF_6] in $CDCl_3$. Solvent peak is denoted by *****

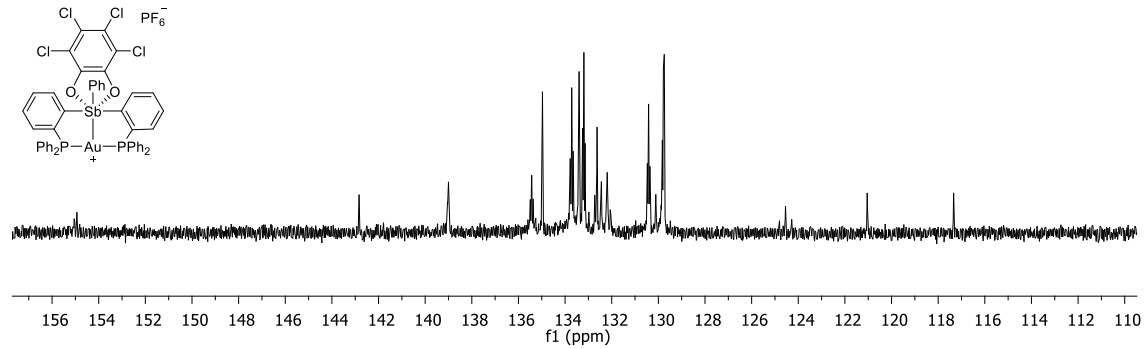

Figure 52. ^{13}C NMR spectrum of **63** [PF_6] in $CDCl_3$.

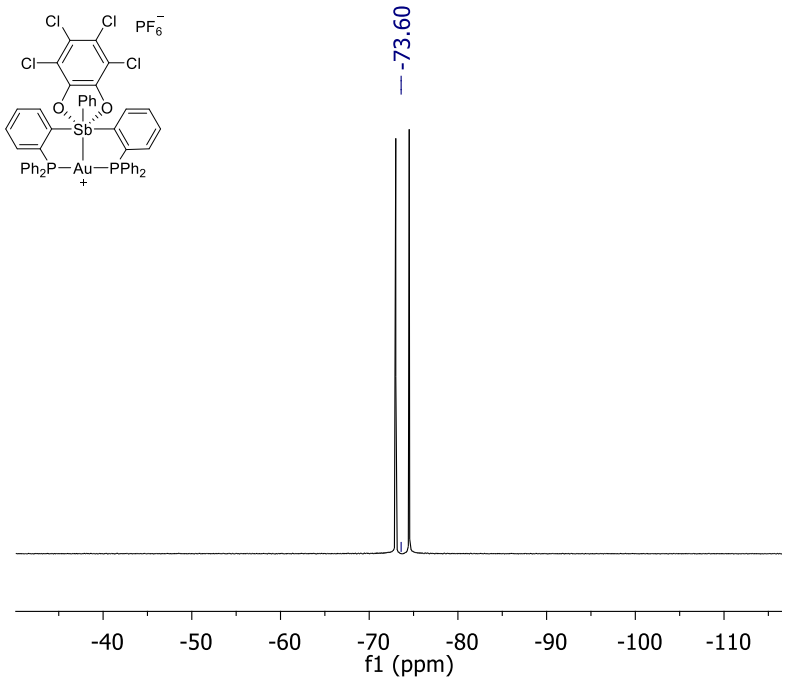

Figure 53. ^{19}F NMR spectrum of **63** [PF_6] in $CDCl_3$

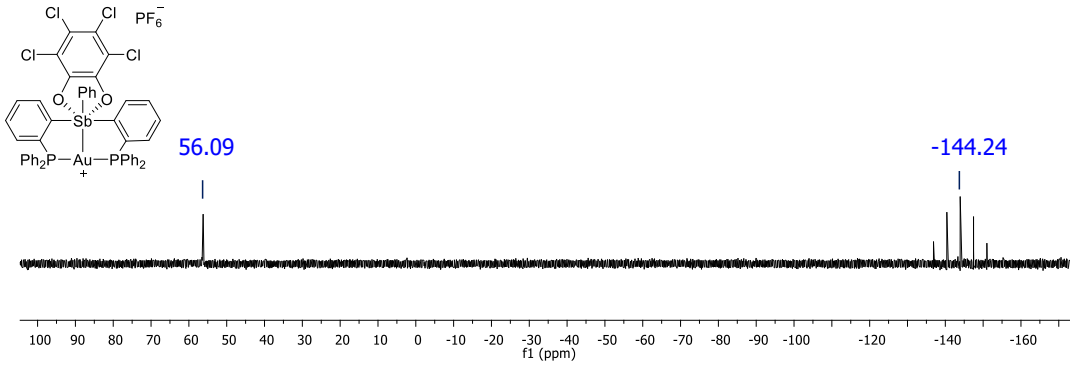

Figure 54. ^{31}P NMR spectrum of **63** [PF_6] in $CDCl_3$.

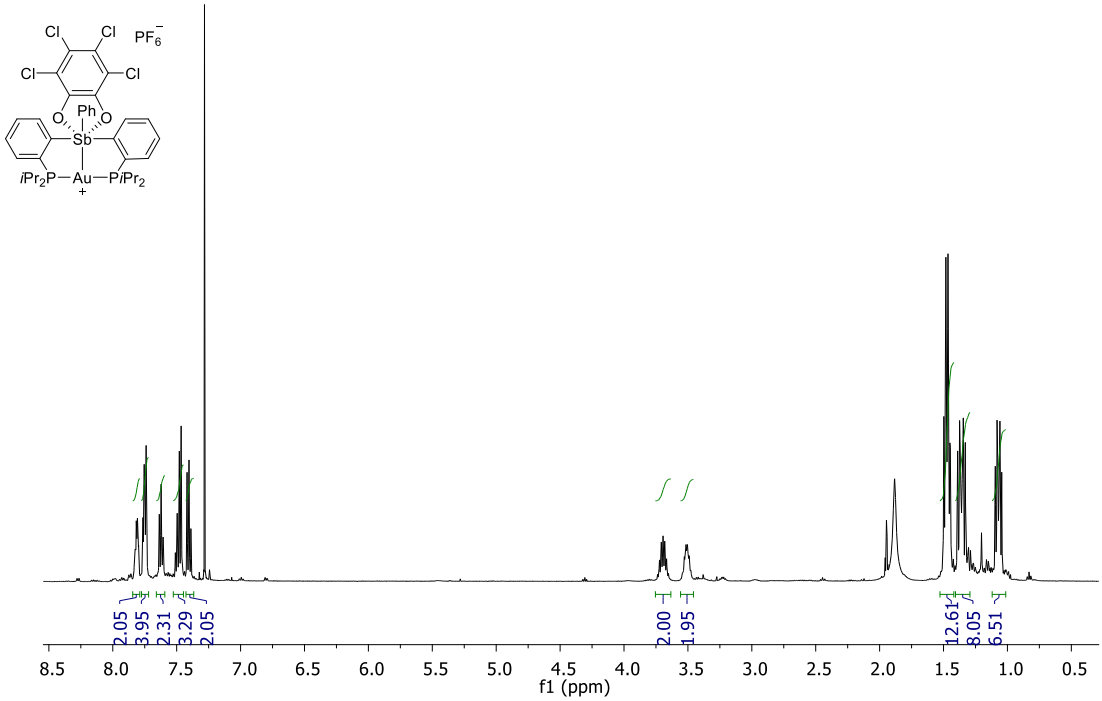

Figure 55. ^{1}H NMR spectrum of **64**[PF_6] in $CDCl_3$. **a)** $CDCl_3$ **b**) CH_3CN.

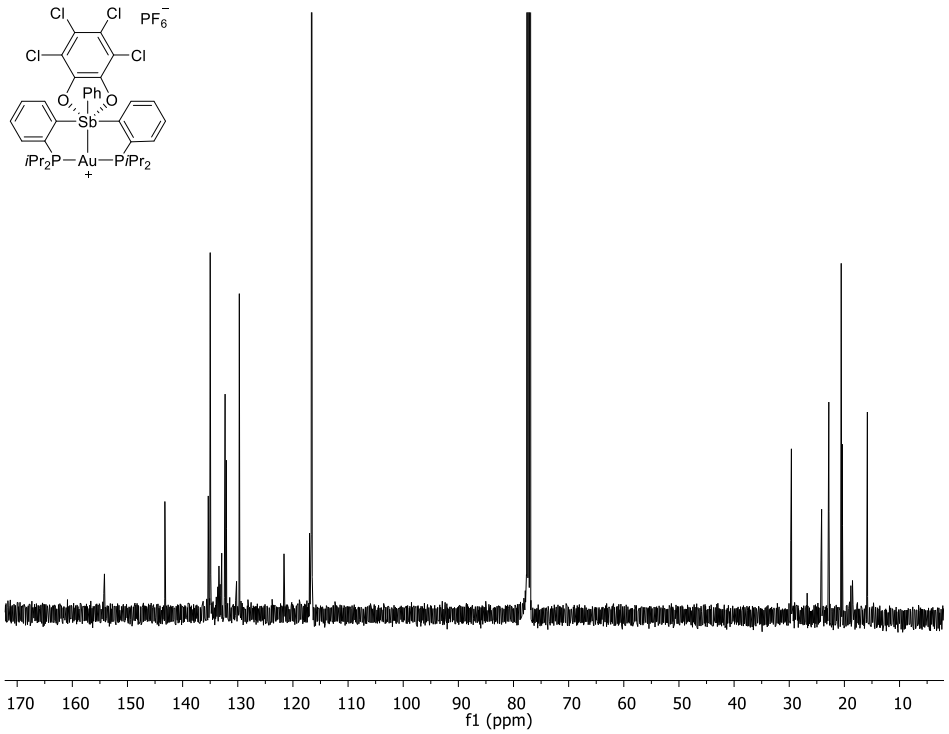

Figure 56. ^{13}C NMR spectrum of **64**[PF_6] in $CDCl_3$.

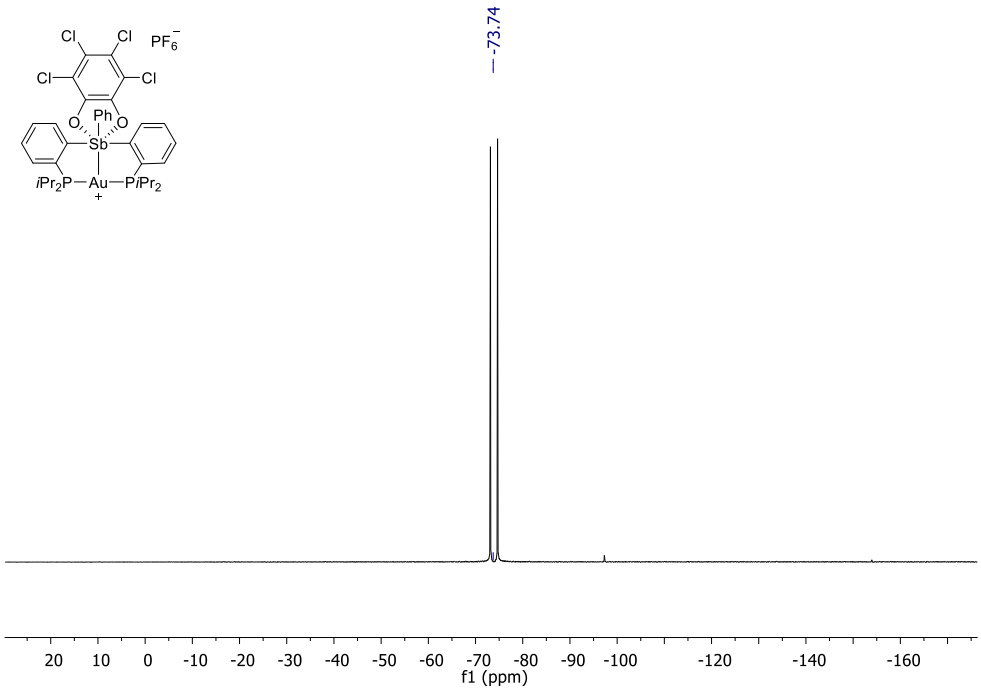

Figure 57: ^{19}F NMR spectrum of **64**[PF_6] in $CDCl_3$.

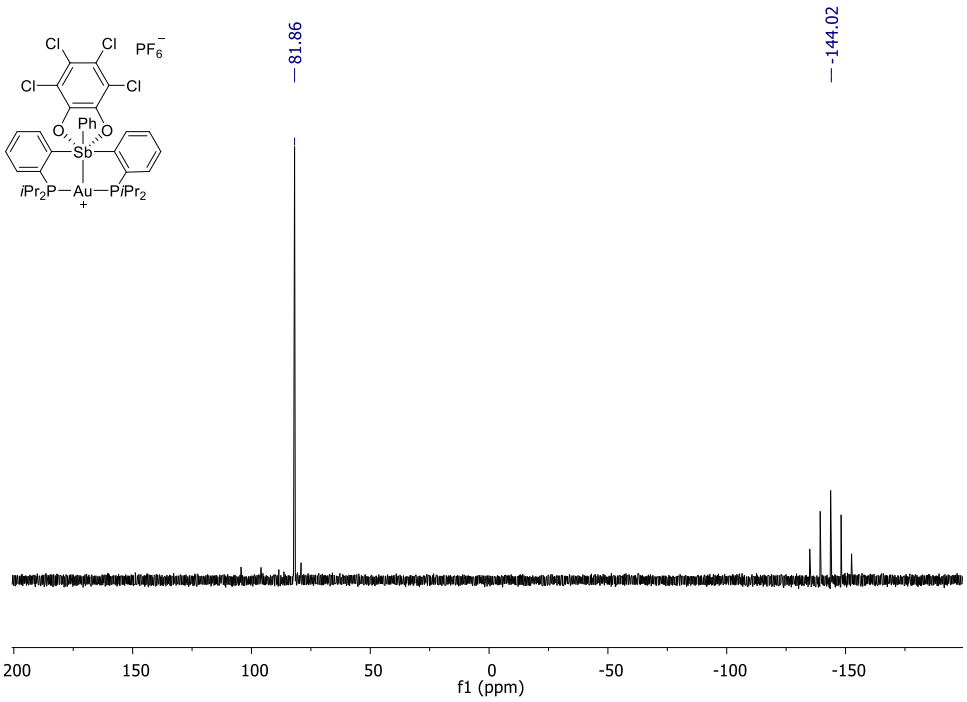

Figure 58. ^{31}P NMR spectrum of **64**[PF_6] in $CDCl_3$.

4. BRØNSTED ACID INDUCED CATALYTIC ACTIVITY OF AN ANTIMONY/PLATINUM COMPLEX

4.1 Introduction

Recent advances in coordination chemistry have shown that di-coordinated Pt(0) complexes of type A[40-41, 70, 261-263] (Figure 59) are metallobasic and readily form adducts of type B with Lewis acids as demonstrated by the work of Braunschweig and Figueroa.

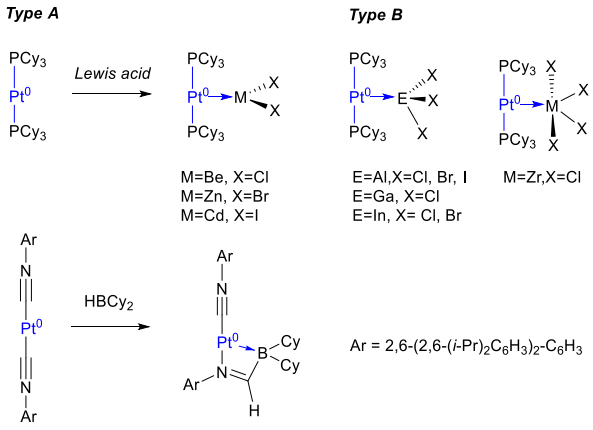

Figure 59. Metallobasicity of di-coordinate Pt(0) complexes.

Because such complexes are core-isoelectronic with the cationic gold complexes such as **31**[SbF_6] and **63**[PF_6] which we found to be catalytically active in reactions involving alkynes, we are now interested in testing if complexes of type B would be active catalysts. In an effort to access such catalytically active Pt(0) center, we have hypothesized

that the electron rich Pt(0) center could be stabilized by a non-innocent Lewis acidic ligand capable of modulating the electron density of the metal center. We have previously discussed, in details, the ability of stiboranyl and stiborane ligands to stabilize coordinately unsaturated metal centers by dative M→Sb interactions. The Sb(V) center, when coordinated to a metal in low oxidation state, can act as an electron acceptor to impart stability to the metal. Formation of this M→Sb bond could also deplete the electron density of the metal center and promote substrate coordination and activation because of a depletion in electron density. Building upon this general idea, we have previously investigated the influence of a trifluorostiborane ligand in the coordination sphere of a zero-valent platinum center.[264-265] The target platinum/stiborane complexes **69** and **70** can be obtained by a chloride-to-fluoride exchange reaction initiated by TlF in presence of Lewis bases such as acetonitrile and cyclohexylisonitrile (Scheme 8). As anticipated, the incoming fluoride anions prefer the hard antimony center rather than the soft metal center which is reminiscent of the formation of complex **59** (discussed in section 2). Dr. Yang was also able to obtain the solid state structures of the corresponding stibonium complexes **71** and **72** (Scheme 8).

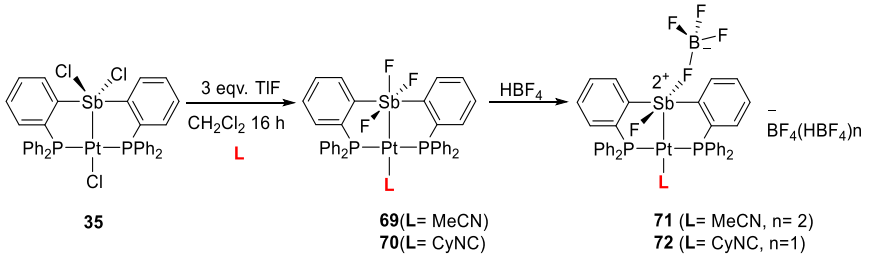

35 **69**(**L**= MeCN) **70**(**L**= CyNC) **71** (**L**= MeCN, n= 2) **72** (**L**= CyNC, n=1)

Scheme 8. Synthesis of **69-72.**

As part of my work, I have been interested in testing whether a similar reaction would occur in the presence of benzonitrile. This objective was chosen because of the difficulty met when Dr. Haifeng Yang attempted to obtain a clean sample of the acetonitrile adduct **69**.

4.2 Synthesis and characterization of a platinum/trifluorostiborane complex

In search of a Lewis base would enhance the stability of the target platinum(0) complex, we decided to use PhCN due to its higher proton affinity in gas phase compared to CH_3CN (196.5kcal/mol for PhCN vs 186.5 kcal/mol for CH_3CN).[266] We speculate that the use of PhCN instead of CH_3CN, will provide us a more practical and economic route to access the trifluorostiborane coordinated Pt(0) center. To this end, the previously reported complex **35** was treated with 4 equivalents of TlF in a mix solvent system of CH_2Cl_2/PhCN (1:1) leading to the precipitation of TlCl and formation of the target complex **73** within 2 h (Scheme 9). Complex **73** was identified by a doublet in the ^{31}P NMR resonance at 71.88 ppm with a Pt-P coupling constant $^1J_{Pt\text{-}P}$ of 3466 ppm which is similar to that observed for **69** ($^1J_{Pt\text{-}P}$ = 3462 Hz) and **70** ($^1J_{Pt\text{-}P}$ = 3131 Hz). The ^{19}F NMR spectrum of **73** also indicated the coordination of three fluoride anions to antimony. Two sets of ^{19}F NMR resonance in 2:1 ratio were observed with the chemical shifts of -84.99 ppm and -114.28 ppm respectively. This pattern is assigned to the presence of two fluorine atoms in trans positions from each other and one fluorine atom trans from the platinum atom. The ease of synthesis and the stability of complex **73** can be attributed to the higher basicity, hence the greater coordinating ability, of PhCN over CH_3CN.

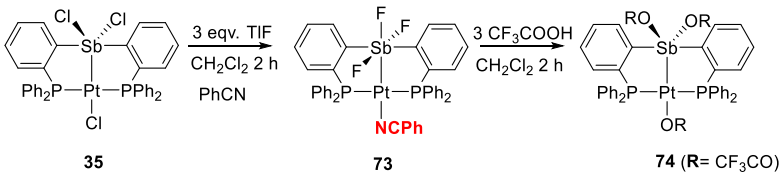

Scheme 9. Synthesis of **73** and **74.**

To determine the structure of complex **73**, single crystals of **73** were obtained from the diffusion of Et_2O into a solution of **73** in CH_2Cl_2 at 0-5°C. Complex **73** crystallizes in trigonal $P3_221$ space group with half a molecule of **73** in the asymmetric unit. X-ray diffraction analysis confirmed that the solid state structure indeed features a trifluorostiborane moiety bound to a Pt center which is coordinated to a molecule of PhCN. The structure of **73** is analogous to those of **69** and **70**, featuring an octahedral antimony and a square planar platinum centers (Figure 60). The Pt-Sb bond distance of 2.645(3) Å is longer than in both complexes **69** (2.57974(19)) Å and **70** (2.6215(11)) which suggests a weaker Sb-Pt bonding interaction.

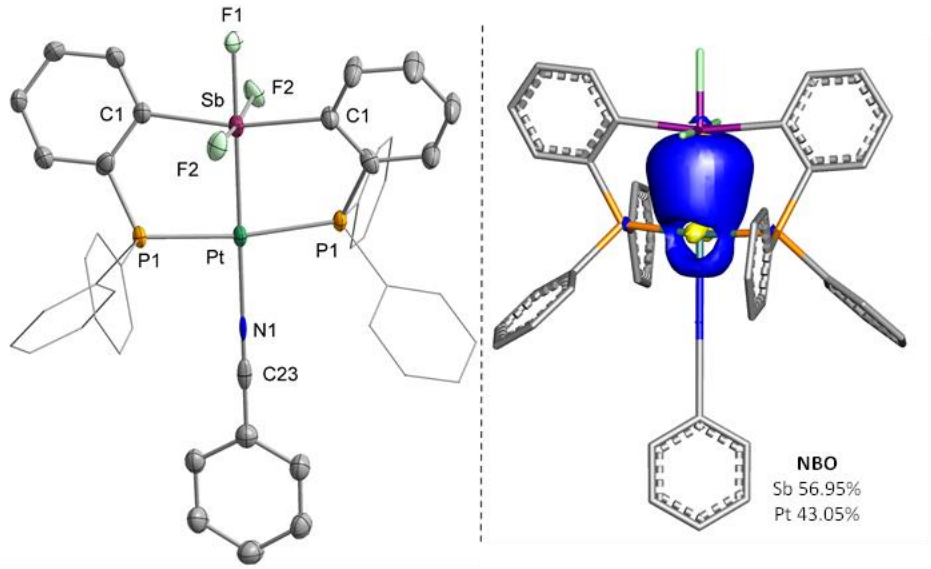

Figure 60. Left: Crystal structure of **73**. Displacement ellipsoids are scaled to the 50% probability level. All the hydrogen atoms except the amide hydrogens are omitted for clarity. Selected bond lengths (Å) and angles (deg) for **73**: Pt-Sb 2.645(3), Pt-N1 2.206(15), Sb-F1 2.018(9), Sb-F2 2.009(6), Sb-C1 2.205(9), N1-C23 1.11(2); P1-Pt-Sb 85.80(6), P1-Pt-P2 171.59(12), N1-Pt-Sb 180.0, F1-Sb-Pt 180.00(8), F2-Sb-F2 171.2(4), C1-Sb-C1 166.9(6). Right: NBO corresponding to Sb-Pt bonding interaction in **73.**

To gain insights into the nature of Sb-Pt bond, the structure of **73** was optimized using DFT methods (Gaussian program, functional: BP86; mixed basis set: Sb/Pt: cc-pVTZ; P: 6-31g(d'); F: 6–31+g(d'); C/H/N: 6-31g). The computed structure was in good agreement with the solid state structure of **73** (Table 8). NBO analysis was performed on the optimized structure to probe the nature of Sb-Pt bond. Similar to the cases of **69** and **70.** NBO analysis identified a covalent interaction between Sb and Pt atoms. The corresponding NBO has 43.05% Sb and 56.95% Pt character.

Table 8. Selected bond lengths (Å) and angles (°) for 73 as determined crystallographically and computationally. (Computed values area denoted with *)

Parameter	73	73*
Sb-Pt	2.645(3)	2.69
Pt-N1	2.206(15)	2.09
P1-Pt-P2	171.59(12)	171.5
F1-Sb-Pt	180.00(8),	179.9
F2-Sb-F3	171.2(4)	177.9
Sb-Pt-N1	180.0	179.9
C23-N1	1.11(2)	1.18

4.3 Reaction of **73** with Brønsted acid

Speculating that complex **73** could be converted into a cationic one by abstraction of a fluoride ligand, we decided to treat complex **73** with Brønsted acids, which we thought could lead to a protonolysis of a Sb-F bond. With this as an objective, we treated **73** with HBF_4•Et_2O.and the reaction was monitored by ^{31}P and ^{19}F NMR spectroscopy. The reaction was instantaneous and an upfield shift in the ^{31}P NMR resonance was observed leading to a new signal at (49.53 ppm, $^1J_{Pt\text{-}P}$= 2359 ppm). This change is consistent with a more oxidized platinum center. The ^{19}F NMR spectrum revealed two sets of peaks in ^{19}F NMR resonances at -151.12 ppm and -153.37 ppm in a 1:4 ratio (Figure 61). The ^{19}F NMR resonance at 153.37 ppm can be attributed to the excess HBF_4 present in the solution whereas the identity of the other ^{19}F NMR resonance at -151.12 ppm could not be assigned.

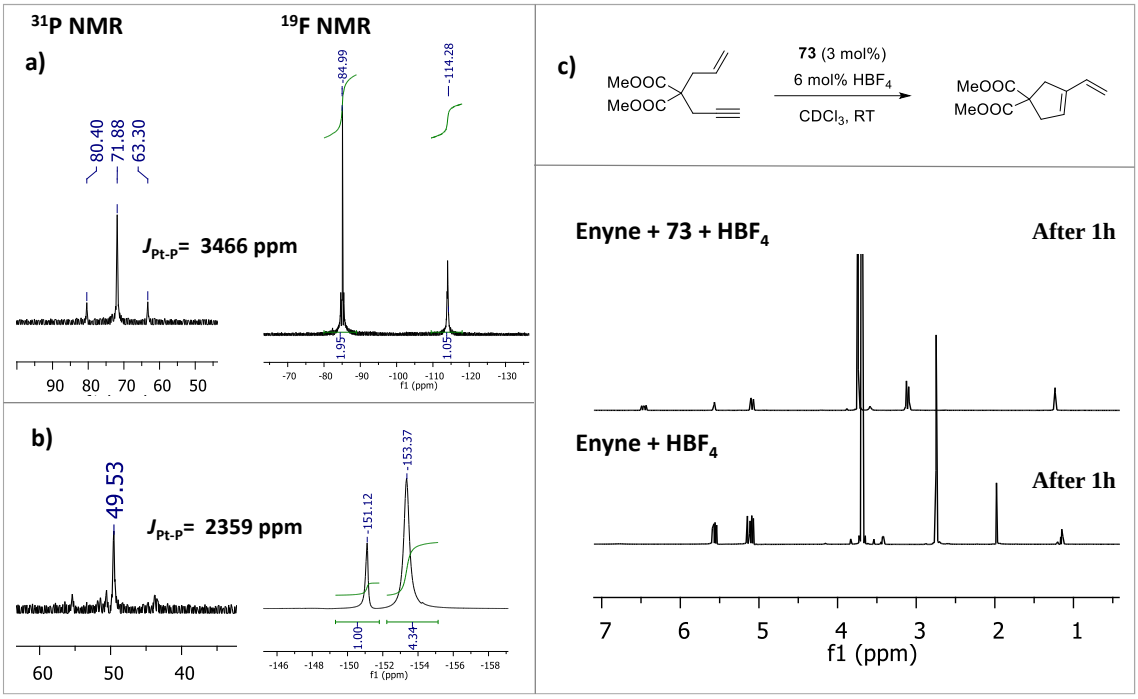

Figure 61. ^{31}P and ^{19}F NMR resonances of **73** (a) and **73** + HBF_4 (b). Enyne cyclization reaction catalyzed by **73** and HBF_4 (c).

Based on our experimental evidences, we became eager to test catalytic properties of **73** after addition of HBF_4, which we believe promotes the protonolysis of a Sb-F bond. We hypothesized that, the σ-accepting capability and Coulombic effect of the resulting stibonium moiety would enhance the electrophilicity of the metal center rendering it catalytic active.[112] To test the validity of this approach, we studied the cyclization of dimethyl 2-allyl-2-(2-propynyl)malonate with 3 mol% of **73** and excess HBF_4 in Et_2O. Gratifyingly, the enyne cyclization reaction was complete in an hour and the stability of the catalyst was confirmed by the ^{31}P NMR spectroscopy. To further establish the nature

of the catalyst, we ran a control reaction with the enyne and HBF_4, which failed to catalyze the cyclization reaction after one hour (Figure 61). Complex **73** alone was also inactive under the same reaction condition. These control reactions led us to conclude that both **73** and HBF_4 are essential components for the catalysis.

In an effort to find a less corrosive and easily available Brønsted acid source, we tested the reactivity of **73** towards trifluoroacetic acid (pKa 0.23). The key features of TFA is that a) it is highly soluble in organic solvents, b) it furnishes relatively weakly coordinating trifluoroacetate anion c) due to its volatile nature (bp 72°C), its removal from the reaction mixture is relatively easy. The reaction of **73** with excess TFA proceeded smoothly in CH_2Cl_2 and the upfield shift in the ^{31}P NMR resonance was indicative of the formation of the product. X-ray diffraction analysis of a single crystal of **74**revealed that the structure is analogous to complex **35** and features a Pt(II)-Sb(IV) bimetallic core (Figure 62). The chlorides in **35** are now replaced with trifluoroacetate ligands, two of which are on Sb and one on Pt. The antimony center in **74** adopts a square pyramidal geometry with the oxygen atoms of the trifluoroacetate anions and the *ortho*-phenylene carbon atoms constituting the base of the square pyramid. The platinum center retains its square planar geometry as indicated by the values of the P1-Pt-P2 (171.14(7)°) and O5-Pt-Sb (170.6(2)°) angles. The Pt-Sb bond distance of 2.438(2) Å was found to be close to that of the starting platinum stiboranyl complex **35 (**2.4407(5) Å which established the structural similarity between the two complexes.

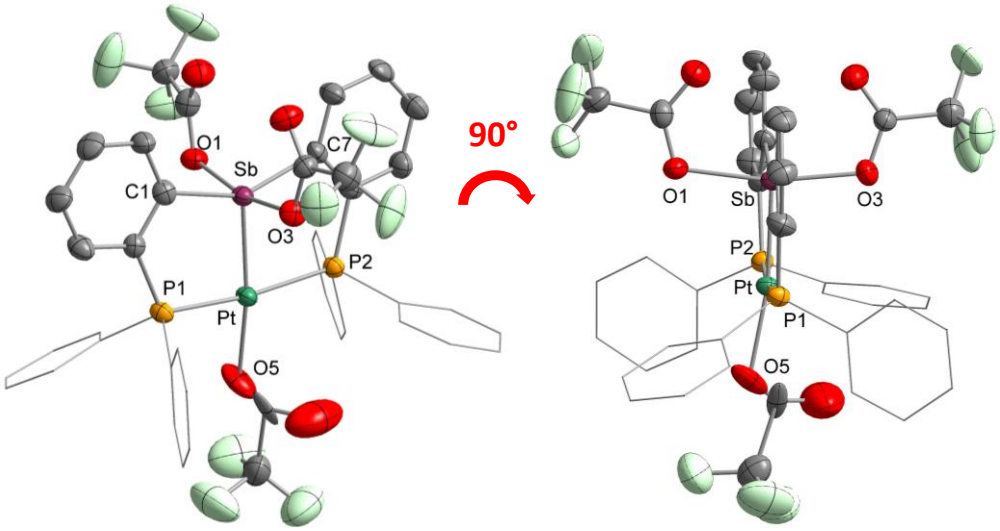

Figure 62. Crystal structure of **74**. Displacement ellipsoids are scaled to the 50% probability level. All the hydrogen atoms except the amide hydrogens are omitted for clarity. Selected bond lengths (Å) and angles (deg) for **74**: Sb-Pt: 2.438(2), Sb-O3: 2.168(5), Sb-O1: 2.196(5), Pt-O5: 2.173(7), P1-Pt-P2: 171.14(7), O5-Pt-Sb: 170.6(2), O3-Sb-O1: 167.96(19), C7-Sb1-C1: 149.1(3)

With this masked tricationic species in hand, we tested the catalytic activity of this molecule in enyne cyclization reaction. Complex **74** showed no catalytic activity in this organic transformation. The lack of reactivity of **74** indicated trifluoroacetate anions are sufficiently strongly bound to antimony center due to the inherent affinity of antimony towards oxygen. Based on these results, we can conclude that the nature of the anionic ligands decorating the core is of utmost importance in determining the reactivity of the platinum center and non-coordinating anions such as triflate are probably better candidates if an exposed platinum center is the goal.

4.4 Conclusion

In this chapter, we elucidated a synthetically viable route to access the trifulorostiborane-platinum complex of the type [F_3R_2SbPtL] where L= PhCN. This complex becomes active as a catalyst in enyne cyclization reactions once treated with HBF_4. NMR measurements suggest that the role of HBF_4 is to induce the protonolysis of the Sb-F bonds, leading to the formation of a more electron deficient complex and a more electrophilic Pt center. Finally, we showed that treatment of **73** with TFAA affords a stiboranyl platinum complex whose structure is analogous to that of **35** at the only difference that the three chloride ligands are replaced by three trifluoroacetate ligands.

4.5 Experimental section

General considerations. Complex **35**[92] was prepared according to the reported procedure. Solvents were dried by passing through an alumina column (pentane and CH_2Cl_2) or by reflux under N_2 over Na/K (Et_2O and THF). All other solvents were used as received. Commercially available chemicals were purchased and used as provided (Commercial sources: Acros Organics for TlF and Strem chemicals for PhCN). Ambient temperature NMR spectra were recorded on a Varian Unity Inova 500 FT NMR (499.42 MHz for ^1H, 125.58 MHz for ^{13}C, 469.89 MHz for ^{19}F and 202.16 MHz for ^{31}P). Chemical shifts δ are given in ppm and are referenced against residual solvent signals (^1H, ^{13}C) or external BF_3–Et_2O (^{19}F) and 85% H_3PO_4 (^{31}P). IR spectra were recorded on a Mattson ATI Genesis FT-IR spectrometer using KBr pellets. Elemental analyses were performed at Atlantic Microlab (Norcross, GA).

Crystallography. All crystallographic measurements were per-formed at 110(2) K using a Bruker SMART APEX II diffractometer with a CCD area detector (graphite monochromated Mo Kα radiation, λ = 0.71073 Å, ω-scans with a 0.5o step in ω) at 110 K. In each case, a specimen of suitable size and quality was selected and mounted onto a nylon loop. The semi-empirical method SADABS was applied for absorption correction. The structures were solved by direct methods and refined by the full-matrix least-square technique against *F*2 with the anisotropic temperature parameters for all non-hydrogen atoms. All H atoms were geometrically placed and refined in riding model approxima-tion. Data reduction and further calculations were performed using the Bruker SAINT+ and SHELXTL NT program packages.

Theoretical calculations. Density functional theory (DFT) calculations (full geometry optimization) were carried out on starting from the crystal structure geometries with Gaussian09 program (BP8635 with 6-31G for H, C; 6-31+G(d') for F; 6-31G(d') for P, Cl, cc-pVTZ-PP with Stuttgart relativistic small core for Pt and Sb). Frequency calculations performed on the optimized geometries found no imaginary frequency. Natural Bond Orbital analysis was performed using NBO 5.9 and the resulting orbitals were visualized and plotted using Jimp 2 program.

Synthesis of 73. Complex **35** (100 mg, 0.105 mmol) was mixed with a 1:1 solution of CH_2Cl_2 (4mL) and PhCN (4mL). After the resulting suspension was stirred for 1 h, solid TlF (94.47mg, 0.422 mmol) was added to it. The reaction mixture was stirred for an additional 4 h resulting in the precipitation of white TlCl, after which the volatiles were removed under vacuum. The resulting solid residue was extracted with CH_2Cl_2 (8 mL) and

the filtered through celite. The filtrate was concentrated to 2 mL under vacuum and the subsequent addition of Et_2O (10 mL) lead to the precipitation of **73** as a pale yellow solid. Compound **73** was collected by filtration and dried under vacuum at room temperature. Yield: 80 mg, 76%. X-ray quality crystals of **73** was obtained by diffusion of Et_2O into a DCM solution of **73** at 0-5°C. ^{1}H NMR (500 MHz, $CDCl_3$) δ 8.78 (d, *J* = 7.6 Hz, 2H), 7.68 – 7.57 (m, 12H), 7.47 (dd, *J* = 9.2, 5.4 Hz, 6H), 7.40 (d, *J* = 6.5 Hz, 16H), 7.30 – 7.27 (m, 4H). ^{13}C NMR (126 MHz, $CDCl_3$) δ 133.99 (d, *J* = 52.6 Hz), 133.19 – 132.85 (m), 132.77 (s), 132.48 (d, *J* = 73.8 Hz), 133.19 – 131.59 (m), 133.19 – 130.64 (m), 130.18 – 129.96 (m), 128.91 (d, *J* = 70.7 Hz), 128.24 (s). ^{31}P{^{1}H} NMR (202.28 MHz; $CDCl_3$): δ 71.88 ($J_{Pt–P}$ = 3466 Hz), ^{19}F{^{1}H} NMR (470.2 MHz; $CDCl_3$): δ -84.99 (bs), -114.28 (s). Elemental analysis calcd (%) for $C_{43}H_{33}NF_3P_2SbPt$: C 51.67, H 3.33, N 1.40; found: C 49.73, H 3.35, N 0.97.

General procedure for the catalytic cycloisomerization. The catalytic cycloisomerization of dimethyl 2-allyl-2-(2-propynyl)malonate was carried out in air at ambient temperature. The malonate (20 mg) was mixed with 3 mol% of complex **73** in $CDCl_3$ and 6 mol% HBF_4 (in Et_2O) was added to the resulting solution. The conversion was estimated using ^{1}H NMR spectroscopy.

5. PHOTOREDUCTIVE ELIMINATION OF CHLORINE AND CHLOROBENZENE FROM ANTIMONY/TRANSITION METAL PLATFORMS

5.1 Introduction

Current demand for carbon-neutral alternative energy sources has inspired a new research field dedicated to the development of chemical strategies to utilize and store solar energy.[80, 267] One of the most efficient way to store solar energy is in the form of a chemical bond which has long been established in nature by the means of photosynthesis. In the chemical realm, analogous conversion of solar energy into fuel can be envisioned by the photo-induced water splitting reaction producing hydrogen and oxygen. To facilitate the formation of alternative fuel from readily available resource, chemical community has focused on developing water-splitting catalysts and study the mechanism of such energy intense processes. Alternatively, recent advances have been made to produce hydrogen by splitting H-X bonds (X= Cl, Br). The success of HX splitting lies in the efficient reduction of proton and oxidation of the halides which can be achieved by a transition metal catalyst capable of facile oxidative addition of H-X and successive reductive elimination of H_2 and X_2.

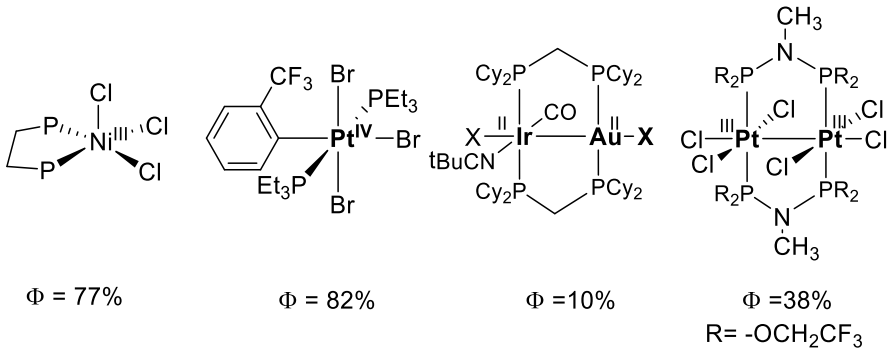

Figure 63. Examples of efficient mono- and bimetallic platforms for photoreductive elimination of halogen.

Recent advances in designing photocatalysts for HX splitting and more specifically the photoreductive elimination of an X_2 equivalent (X = halogen) have been centered around late transition metal complexes featuring metal centers in high oxidation states, capable of undergoing two electron reduction. The challenge involved in such photocatalytic processes arises from the high energy requirement associated to the strong metal-halogen bond which can be mitigated by using a metal platform featuring a low lying M−X σ*- orbital. Population of this low lying M−X σ*- orbitals upon electronic excitation can facilitate the weakening of the bond leading to subsequent homolytic M−X bond cleavage. This strategy has been employed by Nocera in his seminal work in the field of HX splitting and halogen photoelimination by hetero- and homobimetallic transition metal scaffolds, predominantly featuring Pt, Ir, Ni, Au and Rh centers (Figure 63).[82, 268] The presence of two metal centers in close proximity to each other in the molecular scaffold and the cooperative effect on their individual redox states has been stated as the key feature in these photocatalytic systems.

As part of our continuing interest in redox-active main group complexes, we have explored the possibility of the photoreductive elimination of halogens from transition metal complexes supported by redox active main group elements. The use of antimony and tellurium ligands in the coordination sphere of Pt and Pd has proved to be highly successful as discussed in Section 1.5. The ability of both antimony and tellurium to undergo two-electron redox processes without disrupting the bonding interaction with transition metals is crucial for such photo-induced halogen eliminations.

In 2012, we presented the first example of a main group/transition metal platform featuring a TePt core (complex **33)** which underwent a clean elimination of "Cl_2" upon irradiation by UV light with a maximum quantum yield of 4.4% (Figure 17, Section 1.5.2). Similar reactivity has been observed in the case of the Sb/Pt complex **37** (Figure 18, Section 1.5.3) which demonstrated the elimination of "Cl_2". In these cases, the main group Lewis acid predominantly serve as a spectator ligand which supports the reductive elimination of the halogen from the metal center by redox synergy between the heavy atoms. In pursuit of a system which allows the reductive elimination to occur at the main group element rather than the metal center, the Sb/Pd complex **38** was investigated (Figure 18, Section 1.5.3). To our satisfaction, complex **38** illustrated the first reported instance of halogen elimination from the antimony center accompanied by the formal one-electron reduction of both the antimony and palladium centers. It is important to mention here that, while metal-coordinated antimony undergoes facile two electron oxidation, the reduction of the antimony(V) center in metal-stiborane complexes by chemical means has been challenging, only reported example so far being the conversion of **18** into **17**-I by NaI

(Figure 64).[67] Considering this synthetic shortcoming, photolysis reactions provide a promising avenue in the redox chemistry of antimony.

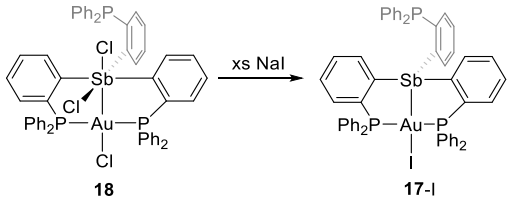

Figure 64. Reduction of **18** with NaI.

Inspired by the possibility of photoreduction of the antimony center, we decided to extend this methodology to other transition metal platforms. Photo-activation of Au-X bond has been performed predominantly on heterobimetallic platforms featuring M^n-Au^{II} motif (M= Rh, Ir, Pt) as shown in Figure 63. Nocera has also explored reductive photoelimination of X_2 from Au^{III} centers of mono- and bimetallic molecules.[269] Despite these examples, the field of photoreductive elimination from gold complexes remains mostly unexplored. Moreover, a comprehensive study of the synergistic relation between main group heavy metal and gold in the context of energy considerations has not been pursued. This has motivated us to investigate the photoredox chemistry of Sb/Au complexes with the aim of discovering efficient photocages.

In addition to the halogen elimination, metal-metal redox cooperation in multinuclear complexes can be utilized for C-X bond forming reactions.[270] Metal-mediated carbon-halogen bond formation has attracted an enormous amount of attention

due to their potential as a starting point to a diverse group of organic transformations.[271] An attempt to extend this strategy has been pursued by Dr. Iou-Sheng Ke[155] and Dr. James Stuart Jones[264] in their dissertations where they investigated a formal elimination of Ph-Cl from a Sb/Pt platform (**B**) (Figure 65).

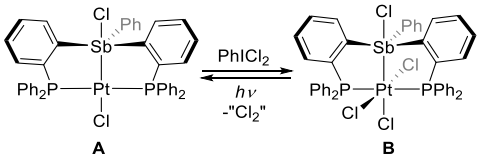

Figure 65. Elimination of a chlorobenzene equivalent from Sb/Pt platform.

Inspired by these precedents, we have now studied the photochemistry of gold and palladium complexes supported by chlorostibine and arylstibine ligands. As part of our investigation, we have synthesized a series of antimony/gold complexes and evaluated their potential as photocages.

5.2 Synthesis and characterization of gold/trihalostiborane complexes

On the basis of these considerations, we carried out the oxidation of (*o*-(*i*Pr$_2$P)C$_6$H$_4$)$_2$SbClAuCl (**6**) [62] with PhICl$_2$ to obtain the gold-stiborane complex **75** (Scheme 10). Complex **75** gives rise to a sharp ^{31}P NMR resonance at 97 ppm. The downfield shift of the ^{31}P NMR resonance from the parent complex (65 ppm) is indicative of the oxidation of the Sb/Au core.[62, 67, 218] In contrast with the insoluble nature of complex **29**, complex **75** is highly soluble in organic solvents such as DCM, chloroform and THF.

The improved solubility of **75** comes from the presence of *i*Pr rather than Ph groups on the phosphorus atoms.

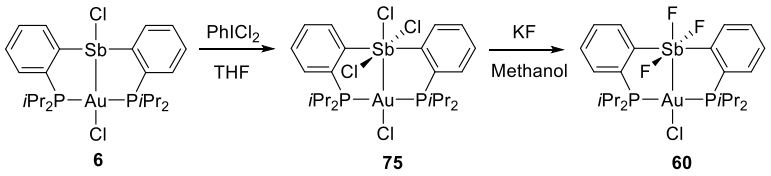

Scheme 10. Synthesis of **75** and **60.**

Elucidation of the solid state structure of **75** was obtained from XRD analysis using single crystals grown by the diffusion of Et_2O into a solution of **75** in DCM. Complex **75** crystallizes in an almost tetrahedral crystal system with a minor amount of pseudo merohedral twining. There are two molecules in the asymmetric unit, only one of them is shown in Figure 66. The bond distance between the heavy atoms was revealed to be 2.679(3) Å which is significantly shorter than the Au-Sb distance of 2.7937(13) Å in the reduced counterpart **6** but comparable to that of **29** (2.6985(14) Å). The decrease in the Sb-Au distance in **75** is indicative of the oxidation of the Sb/Au core and the subsequent strengthening of the Au→Sb interaction which has been observed in previously reported gold/stiborane complexes.[62, 67, 159, 218] The superior Lewis acidic nature of the trichlorostiborane *vs* aryldichlorostiborane was evident from the shorter Sb-Au bond length in **75** as compared to its arylstiborane analog **54** (2.8651(4) Å).

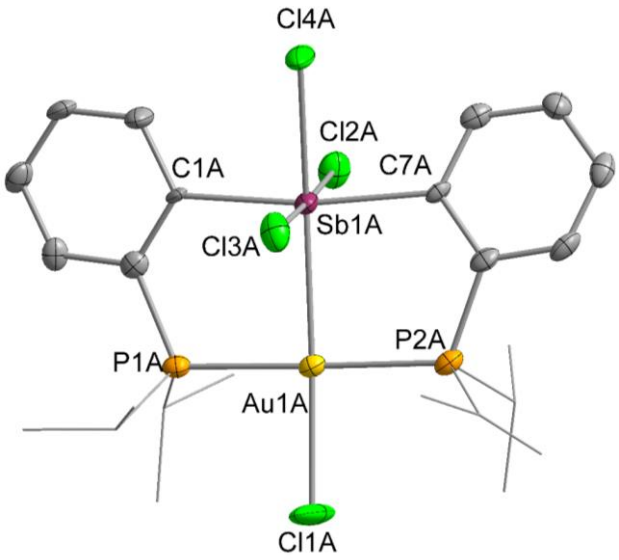

Figure 66. Crystal structure of **75**. Displacement ellipsoids are scaled to the 50% probability level. Hydrogen atoms are omitted for clarity. Selected bond lengths (Å) and angles (deg) for **75**: Au(1A)-Sb(1A) 2.679(3), Au(1A)-Cl(1A) 2.435(4), Sb(1A)-Cl2 2.499 (4), Sb(1A)-Cl(3A) 2.486(4), Sb(1A)-Cl(4A) 2.498(4); P(1A)-Au(1A)-P(2A) 178.47(10), Cl(1A)-Au(1A)-Sb(1A) 174.34(10), Cl(3A)-Sb(1A)-Cl(2A) 178.06(11), Cl(4A)-Sb(1A)-Au(1A) 167.59(10), C(7A)-Sb(1A)-C(1A) 169.9(4)

The solid state structure of **75**, in most part, is very similar to that of **29** (Section 1.4.2). As depicted in Figure 66, the gold atom adopts a square planar geometry with P(1A)-Au(1A)-P(2A) and Cl(1A)-Au(1A)-Sb(1A) angles of 178.47(10)° and 174.34(10)° respectively, which suggests a trivalent character of gold. The antimony center adopts an slightly distorted octahedral geometry, analogous to that observed in the analogous di- or trichlorostiborane gold complexes **29**, with Cl(3A)-Sb(1A)-Cl(2A), Cl(4A)-Sb(1A)-Au(1A) and C(7A)-Sb(1A)-C(1A) angles of 178.06(11)°, 167.59(10)° and 169.9(4) ° respectively.

With complex **75** in hand, the next logical step was to study its interaction with fluoride to obtain the previously discussed model complex **60** (Section 2.7). Successful synthesis of **60** will not only allow us to compare the theoretical results with experiment

observations, but also provide a gold/trihalostiborane complex to investigate in the context of photoinduced reductive elimination. To put our hypothesis to test, we treated **75** with excess KF in THF/MeOH, which to our satisfaction gave rise to the target molecule **60.** The formation of **60** was confirmed by the charateristic doublet in the ^{31}P NMR resonance at ppm with a $^{3}J_{\text{P-Fax}}$= 16 Hz. As in the cases of complexes **30** and **57,** the phosphorus nuclei did not show any coupling with the equatorial fluorine atoms which may be rationalized by invoking the Karplus rule and the orthogonality of the F-Sb-F and P-Au-P vector. ^{19}F NMR spectroscopy provided further proof of the presence of a trifluostiborane moiety. Complex **60** showed two signals in the ^{19}F NMR in a 2:1 ratio corresponding to the two equatorial and one axial fluorine atoms on antimony. The ^{19}F NMR resonance of the equatorial fluorine atoms shows up as a doublet at -69.71 ppm with $^{3}J_{\text{P-Fax}}$= 17 Hz whereas the axial fluorine resonance appears as a pseudo-quintet at -133.78 ppm because of the near degeneracy of $^{3}J_{\text{P-Fax}}$ (16 Hz) and $^{2}J_{\text{Fax-Feq}}$ (17 Hz).

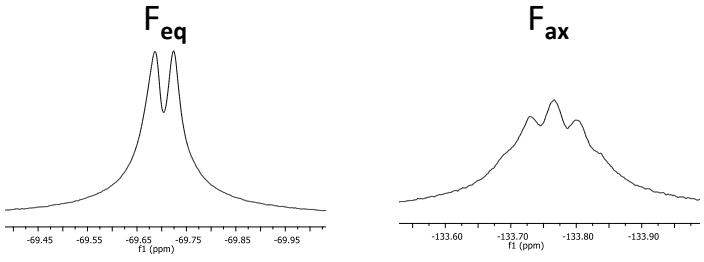

Figure 67. The ^{19}F NMR resonances of **60**.

Single crystals of **60** was obtained from the slow evaporation of a DCM solution. Complex **60** crystallizes in the orthorhombic P_{bca} space group.The structure of **60** was

similar to that of **75** and **30** and features an octadral antimony moiety connected to the square planar gold center. The Sb-Au distance of 2.6874(5) Å is close to that of the previously discussed gold/trifluorostiborane complexes **57** (2.6886(5) Å) and **30** (2.7069(7) Å). Contrary to the shortening of the Sb-Au bond upon conversion of **54** into **55**, the Sb-Au bond distance does not show any significant change upon the replacement of chloride with fluoride in the case of complex **60**. This suggests little perturbation of the Au→Sb interaction when the trichlorostiborane moiety is converted in to the corresponding trifluorostiborane. As in **75**, the gold atom of **60** adopts a square planar geometry with both Cl1-Au-Sb and P1-Au-P2 angles close to linearity (172.90(4)° and 176.98(6)° respectively). The antimony atom, which sits at the center of a trifluorostiborane unit, maintains an octahedral geometry with almost linear F1-Sb-Au, F2-Sb-F3 and C1-Sb-C7 angles of 179.06(13)°, 179.55(16)° and 171.4(2)° respectively.

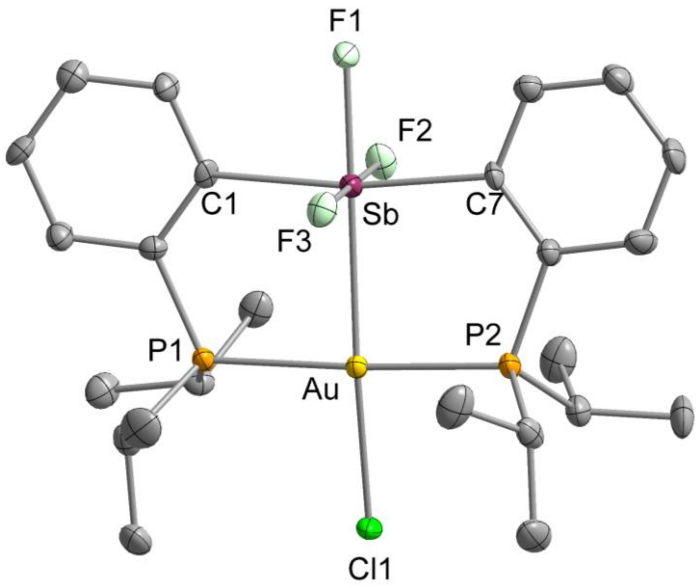

Figure 68. Crystal structure of **60**. Displacement ellipsoids are scaled to the 50% probability level. Hydrogen atoms are omitted for clarity. Selected bond lengths (Å) and angles (deg) for **60**: Au-Sb 2.6874(5), Au-Cl1 2.4703(15), Sb-F1 1.939(4), Sb-F2 1.971(4), Sb-F3 1.963(4); P1-Au-P2 176.98(6), Cl1-Au-Sb 172.90(4), F1-Sb-Au 179.06(13), F2-Sb-F3 = 179.55(16), C1-Sb-C7 = 171.4(2).

5.3 Computational analysis and photophysical properties of **75** and **60**

To comprehend the potential of **75** and **60** in the context of halogen photoreductive elimination, a thorough computational analysis of the structure and bonding of the abovementioned gold/stiborane complexes was undertaken. The structures of **75** was optimized by DFT methods (Gaussian09: BP86 with 6-31g for H, C; 6-31+G(d') for F, 6-31G(d') for P, Cl; cc-pVTZ-PP with Stuttgart relativistic small core for Au and Sb). The optimized geometries of **75** and **60** (the latter was previously discussed in Section 2.7) were then subjected to Natural Bond orbital (NBO) analysis to gain insights into the donor-acceptor interaction between the two heavy atoms. The optimized structure of **75** corresponded well with the solid state structure (Table 9)

Table 9. Selected bond lengths (Å) for complexes 75 and 60 as determined crystallographically and optimized computationally (* denotes the optimized geometry).

Complex	75	75*	60	60*
Au-Sb	2.679(3)	2.78	2.6874(5)	2.76

NBO analysis identified multiple Au→Sb donor-acceptor interactions in both complexes **75** and **60**, involving donation from gold-based lone pair orbitals (lp) of *d* character into vacant orbitals at antimony. The two dominating interactions, which consist of a lp(Au)→σ*(Sb-Cl) and a lp(Au)→σ*(Sb-C*o*-$_{Ph}$) donations, are shown in Figure 69. The deletion protocol as implemented in the NBO program suggests that all second order Au→Sb interactions contribute E_{del} = 108.9 kcal/mol to the stability of complex **75**. NBO analysis of **60** revealed similar Au→Sb dative interaction, involving donation of electrons from lp(Au) to p-orbital of Sb and σ* orbitals of Sb-C*o*-$_{Ph}$ bonds, the dominating interaction being lp(Au)→p (Sb) donation. These interactions contribute a deletion energy of E_{del} = 147.3 kcal/mol to the stability of the molecule. Although NBO analysis predicts that the Au→Sb interaction is stronger in **60** as compared to **75** the Au-Sb bond distances in these complexes do not show any significant changes as described in Table 9. This observation is also corroborated by the solid state structures of **75** and **60** which feature similar Au-Sb bond distances of 2.679(3) Å for **75** and 2.6874(5) Å for **60**. The increase in the deletion energy from **75** to **60** may be attributed to the difference in the nature of acceptor orbitals on antimony in the cases of **75** and **60**.

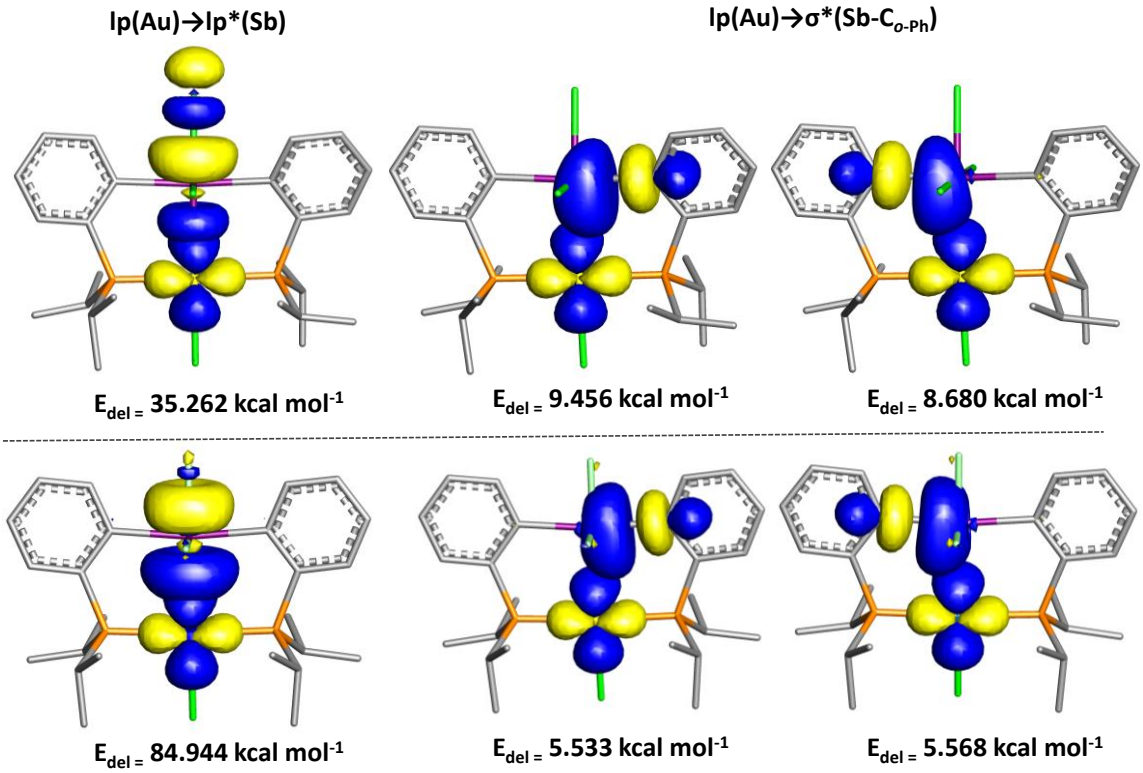

Figure 69. Principal Au→Sb donor-acceptor interactions found in **75** (top) and **60** (bottom). Hydrogen atoms are omitted for clarity. Isodensity value= 0.5.

UV-Vis spectra of **75** shows an intense low energy absorption at 327.4 nm with an extinction coefficient of 14100 M^{-1} cm^{-1}. TD-DFT analysis (implicit solvent model with THF as solvent; MPW1PW91 functional with mixed basis set Sb/Au: cc-pVTZ-PP; P/Cl: 6- 31g(d′); C/H: 6-31g) of **75** was carried out to find the corresponding electronic transitions. According to these calculations, two high oscillator strength (f=0.1685, 348.87 nm and f=0.0502, 339.96 nm) excitations ontribute to the 327 nm band of **75.** Both of these transitions involve the LUMO as the accepting orbitals. From this analysis, we expect that a

light-induced electronic excitation will populate the Sb-Cl σ*-orbital of **75**, resulting in the eventual cleavage of the said bond.

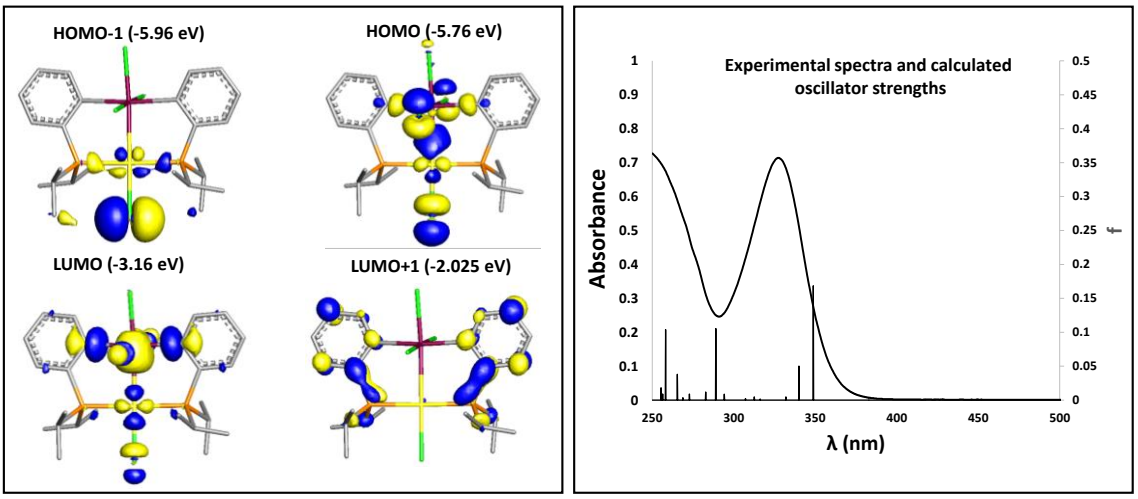

Figure 70. Left: Frontier molecular orbitals of **75 (**Hydrogen atoms are omitted for clarity. Isodensity value= 0.5). Right: UV-Vis spectrum of a 10^{-4}M solution of **75** in THF overlaid with the oscillator strengths.

We also studied the molecular orbitals **54**. The frontier orbitals of **54** was very similar to that of **75.** The LUMO is based on the Sb-Cl σ*-orbital. TD-DFT analysis using the MPW1PW91 functional (mixed basis set: Sb, Pt: cc–pVTZ–PP; P ,Cl: 6–31g(d'); C, H: 6–31g) and the SMD implicit solvation model with THF as a solvent found a low energy transition at 374.49 nm with an oscillator strength of 0.2534. This excitation contribute to the absorption band at 365.4 nm (ε= 21600 M^{-1} $cm^{-}1$) obtained from UV-Vis spectroscopy. Again, the acceptor orbital was the Sb-Cl σ*-orbital which opens up the possibility of chlorine elimination from the antimony center.

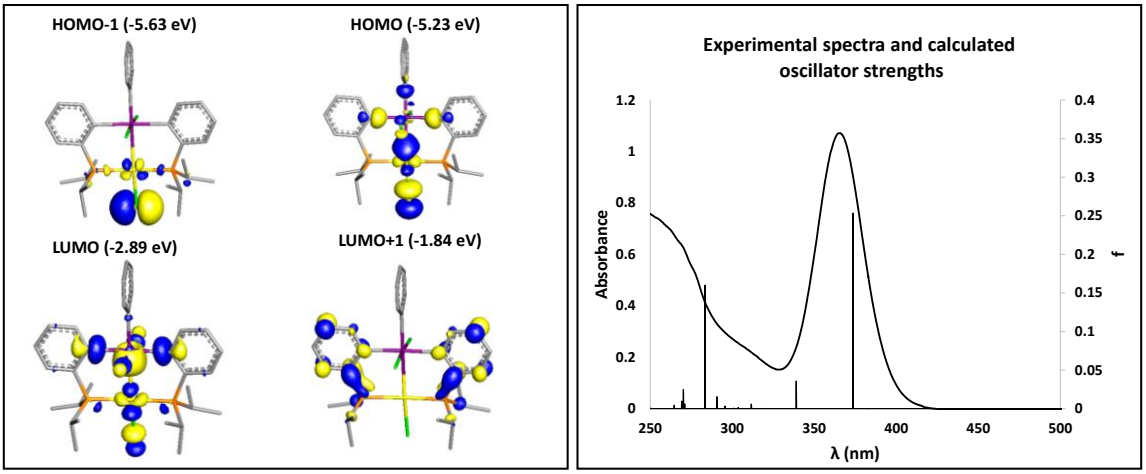

Figure 71. Left: Frontier molecular orbitals of.**54 (**Hydrogen atoms are omitted for clarity. Isodensity value= 0.5)**.** Right: UV-Vis spectrum of a 10^{-4}M solution of **75** in THF overlaid with the oscillator strengths.

5.4 Synthesis and characterization of palladium/stiborane complexes

Motivated by the synthetic advantages of the using (*o*-(*i*Pr$_2$P)C$_6$H$_4$)$_2$SbCl (namely, the enhanced solubility in organic solvents), we decided to synthesize the [Sb/Pd]^V complex analogous to the previously reported complex **36**. Complex **76** was readily synthesized by reacting (*o*-(*i*Pr$_2$P)C$_6$H$_4$)$_2$SbCl with one equivalent of (COD)PdCl$_2$ (cod = 1,5-cyclooctadiene) in DCM at ambient temperature (Scheme 11). Complex **76** was obtained as a yellow solid. This new complex was fully characterized by heteronuclear NMR spectroscopy. Complex **76** showed a sharp singlet at 78.04 ppm in the ^{31}P NMR spectrum which is significantly downfield compared to the free ligand (5.70 ppm).

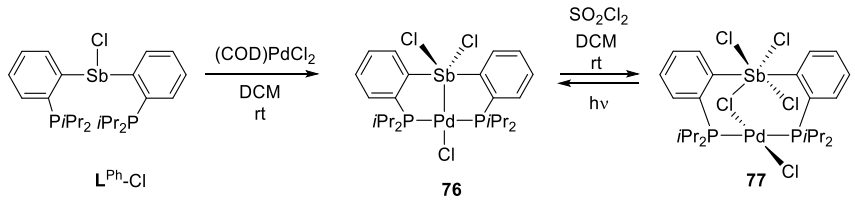

Scheme 11. Synthesis of **76** and **77**.

The solid state structure of **76** is similar to that reported for the palladium and platinum analogues [(*o*-(Ph_2P)C_6H_4)$_2$$SbCl_2MCl$] (M= Pd, Pt). XRD analysis of **76** showed a divalent square-planar palladium center with P2-Pd-P1 angle of 167.44(5)° and Cl1-Pd-Sb angle of 171.30(5)°, which are slightly deviated from linearity (Figure 72). The pentavalent antimony center at the core of the dichlorodiarylstiboranyl moiety is positioned trans from the chloride ligand on palladium and adopts a distorted square pyramidal geometry with C1-Sb-C7 angle of145.3(2)°, Cl3-Sb-Cl2 angle of 162.20(5)° and C1-Sb-Pd angle of 106.90(17)°. The base of the square pyramid is defined by Cl2, Cl3, C1 and C7 and the palladium center sits at the apex of the pyramid. The two antimony-bound chloride ligands are projected in a direction oblique to the Pd−Sb bond resulting in the absence of a trans-influencing effect along the Sb-Pd bond vector. The Sb-Pd bond length of 2.4269(15) Å was close to that found in **36** (2.4230(3)Å) which suggested the similarity of these complexes and prompted us to investigate the oxidation of the Pd/Sb core of **76.**

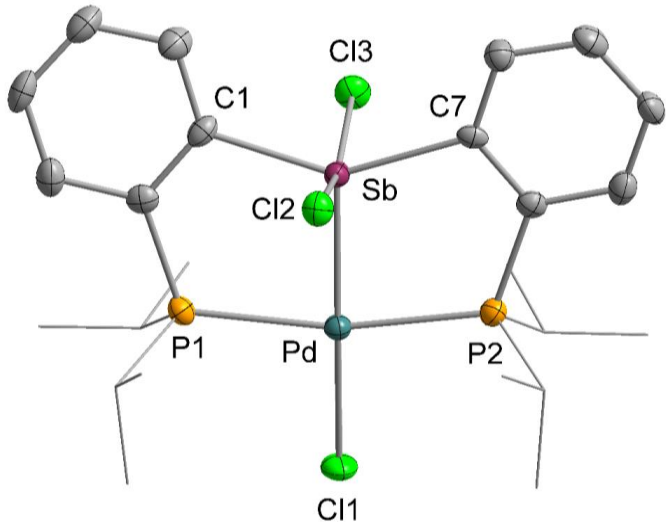

Figure 72. Solid state structure of **76.** Displacement ellipsoids are scaled to the 50% probability level. Hydrogen atoms are omitted for clarity. Selected bond lengths (Å) and angles (deg) for **76**: Sb-Pd 2.4269(15), Sb-Cl3 2.492(2), Sb-Cl2 2.519(2), Pd-Cl1 2.371(2); C1-Sb-C7 145.3(2), Cl3-Sb-Cl2 162.20(5), C1-Sb-Pd 106.90(17), C7-Sb-Pd 107.75(16), P2-Pd-P1 167.44(5), Cl1-Pd-Sb 171.30(5) P2-Pd-Cl1 96.72(8), P1-Pd-Cl1 95.79(8), P2-Pd-Sb 83.37(7), P1-Pd-Sb 84.09(7).

In an attempt to generate an analog of **38**, complex **76** was reacted with $PhICl_2$ in DCM at room temperature. Unfortunately, the reaction with $PhICl_2$ was very slow and did not proceed to completion. A search for an oxidant capable of delivering an equivalent of "Cl_2" prompted us to use SO_2Cl_2 which is capable of oxidizing metal centers by the desired halogen transfer route. Indeed, the reaction of **76** with an excess of SO_2Cl_2 afforded clean conversion of **76** into **77** which was identified by a change in the ^{31}P NMR resonance from 78.04 ppm in **76** to 31.74 ppm in **77**. The upfield shift in the ^{31}P NMR resonance upon oxidation of the [Sb-Pd] core is opposite to that observed in the case of **75** but similar to the case of complex **38** which lead us to speculate that the structure of **77** is in fact analogous to **38**.

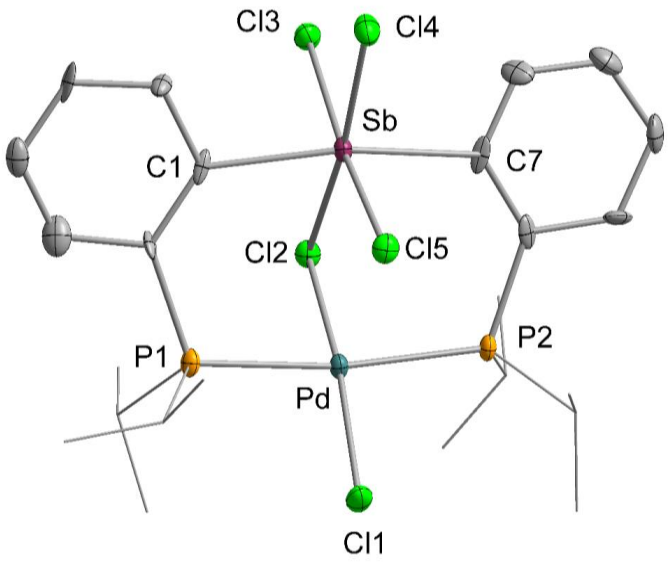

Figure 73. Solid state structure of **77.** Displacement ellipsoids are scaled to the 50% probability level. Hydrogen atoms are omitted for clarity. Selected bond lengths (Å) and angles (deg) for **77**: Sb---Pd 3.3097(10), Sb-Cl2 2.652(4), Sb-Cl3 2.441(4), Sb-Cl4 2.391(4), Sb-Cl5 2.451(4), Pd-Cl1 2.312(4), Pd-Cl2 2.310(4); C1-Sb-C7 166.3(3), Cl2-Sb-Cl4 167.54(8), Cl3-Sb-Cl5 173.27(8), Cl1-Pd-Cl2 167.30(9), P1-Pd-P2 171.71(8).

Our hypothesis was confirmed by the XRD analysis performed on a single crystal of **77.** Complex **77** crystallizes in $P2_12_12_1$ space group. The solid state structure of **77** revealed an absence of Sb-Au interaction suggested by the long Sb---Pd separation of 3.3097(10) Å (Figure 73). The two heavy atoms are bridged asymmetrically by a chloride atom (Cl2) with Sb-Cl2 = 2.652(4) Å and Pd-Cl2 = 2.310(4) Å. The divalent palladium center retains its square planar geometry with Cl1-Pd-Cl2 angle of 167.30(9)° and P1-Pd-P2 angle of 171.71(8)°. The geometry of the antimony center is reminiscent of that in complex **59**, where the hexa-coordinated antimony moiety is decorated with four halides

and two *o*-diphenylene ligands. As expected for a halide-bridged complex, the bridging Sb-Cl2 bond is longer than the other Sb-Cl bonds (Sb-Cl3= 2.441(4) Å, Sb-Cl4= 2.391(4) Å and Sb-Cl5= 2.451(4) Å).

5.4.1 Computational analysis and photophysical properties of **76** and **77**

With the aim of gaining insight into the Sb-Pd bonding interaction in **76** and **77**, their structures were optimized by DFT methods (Gaussian09: BP86 with 6-31g for H, C; 6-31G(d') for P, Cl; cc-pVTZ-PP with Stuttgart relativistic small core for Pd and Sb). No imaginary frequencies were observed for the optimized structures. The optimized geometries of **76** and **77** were then subjected to Natural Bond orbital (NBO) analysis to gain insights into bonding situation between Sb and Pd.

NBO analysis carried out on the optimized geometry of **76**, treated the Sb-Pd interaction as a covalent bond rather than the donor-acceptor interaction which is observed in the cases of the previously discussed gold complexes. The NLMO analysis implemented in NBO was carried out to study the nature of the Sb-Pd bond which revealed that the NLMO corresponding to the Sb-Pd bond has 50.97% Sb character and 42.06% Pd character. This indicates that the bond is covalent. A similar bonding has been observed for **35** and **36**, both of which feature a covalent M-Sb bond. In accordance with the solid state structure, NBO analysis of **77** revealed only a donor-acceptor interaction between Pd and Sb as expected from the rather long Sb-Pd separation. The predominant interaction was found to be the donation of a Pd d-lone pair into a Sb-Cl antibonding orbital. The

other major donor-acceptor interaction was revealed to be the donation of a lone pair on Cl to the antibonding orbital of Sb-Cl.

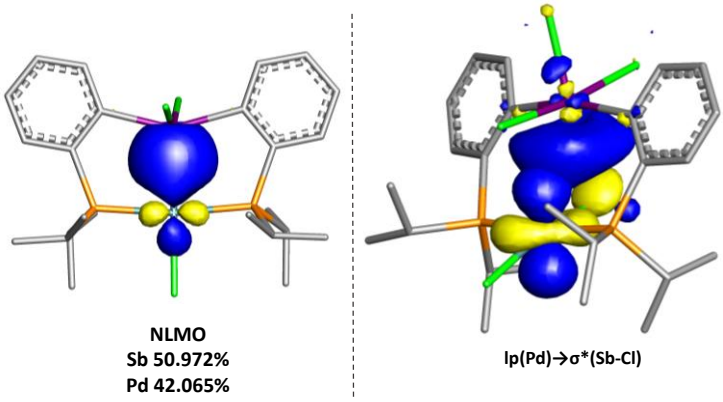

Figure 74. Left: NLMO found in **76**. Principal Pd-Sb interaction in **77.** Hydrogen atoms are omitted for clarity. Isodensity value= 0.5.

Analysis of the molecular orbitals of **77** revealed that the HOMO is based on the Pd-Cl (bridged) bond. The LUMO is however based predominantly on the Sb-Cl antibonding orbitals which is a necessary condition for the photoreductive elimination process (Figure 75). The LUMO and the LUMO+1 orbitals are very close in energy which suggests that both would be equally accessible, at least from an energy point of view.

UV-Vis spectra of **76** and **77** were recorded which revealed an absorption band at 323 nm for **76** and a broad absorption band with two shoulders at 327 nm and 399 nm for **77 (**Figure 75**)**

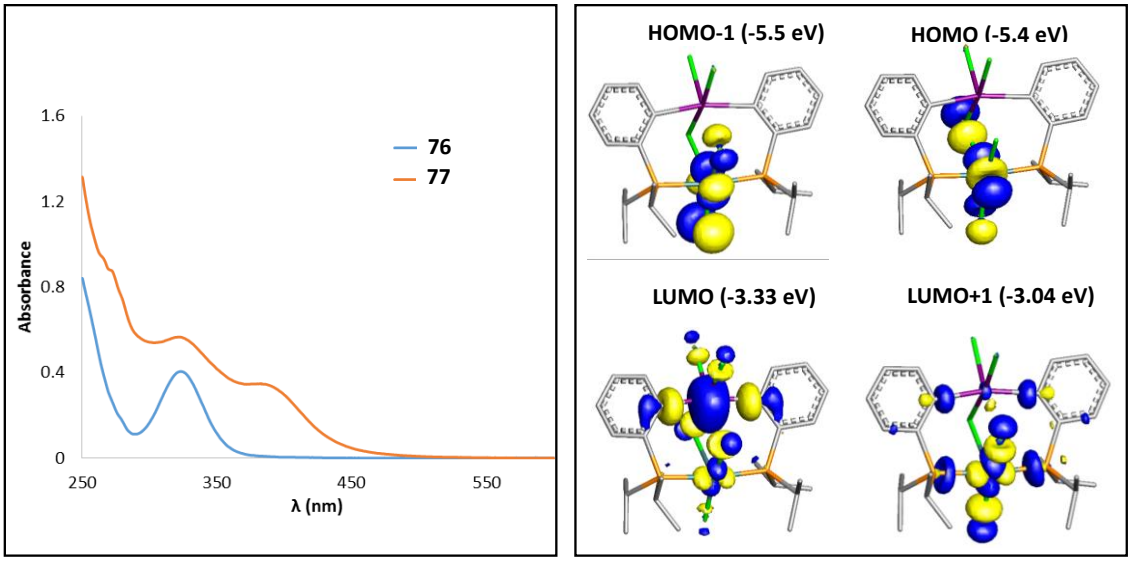

Figure 75. Left: UV-Vis spectrum of a 10^{-4} M solutions of **76** and **77** in THF overlaid with the oscillator strengths. Right: Frontier molecular orbitals of **77** (Hydrogen atoms are omitted for clarity. Isodensity value= 0.5).

5.4.2 Photoreductive elimination reactions of **54**, **75** and **77**

Theoretical analysis of the lowest unoccupied molecular orbitals of complexes **54**, **75** and **77** provided promising insight into the potential of these complexes to undergo clean photoreduction at the antimony center.

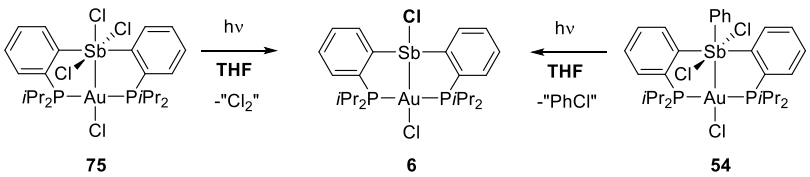

Scheme 12. Photolysis of **54** and **75.**

First, a solution of **75** in THF was irradiated with a mercury lamp and the progress of the reaction was monitored by ^{31}P NMR spectroscopy. The photolytic conversion of **75** into **6** was completed within 45 min with a yield of ~50%. The progressive disappearance of the ^{31}P NMR resonance at 97 ppm corresponding to **75** was observed while the peak corresponding to **6** (64 ppm) appeared indicating the elimination of a chlorine equivalent (Figure 76). The photolysis was accompanied by the formation of unidentified products which show ^{31}P NMR resonances between 80-60 ppm. In an effort to obtain a cleaner photoreduction, the photolysis was performed with 100 equiv. of DMBD in THF. Surprisingly, a very similar photoreactivity profile was observed. As before, the reaction was completed in ~45 min with a yield of ~25%. Even with the radical trap, the formation of impurities could not be avoided (Figure 76). We note in passing that when the photolysis of the analogous trichlorostiborane/gold complex **29** was attempted, it suffered from poor solubility and no conclusive result was obtained.

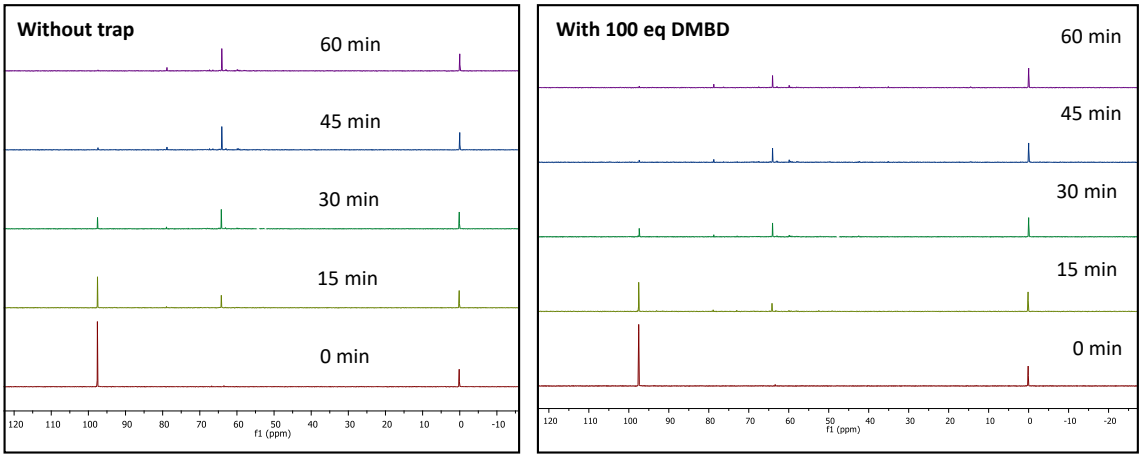

Figure 76. Photolysis of **75** in THF, without a radical trap (left) and with DMBD (right).

Next we sought to study the photolysis of **54**. First, the photolysis was performed in DCM with an excess of DMBD. Surprisingly, the irradiation did not lead to the elimination of chlorine as expected. Instead, elimination of Ph• and Cl• resulting in the formation of **6** was observed as confirmed by ^{31}P NMR spectroscopy. To rule out the possibility of abstraction of halide from the solvent, we performed the photolysis in THF, which lead to identical reactivity. Formation of **6** was observed and the reaction was completed in 2 hr.

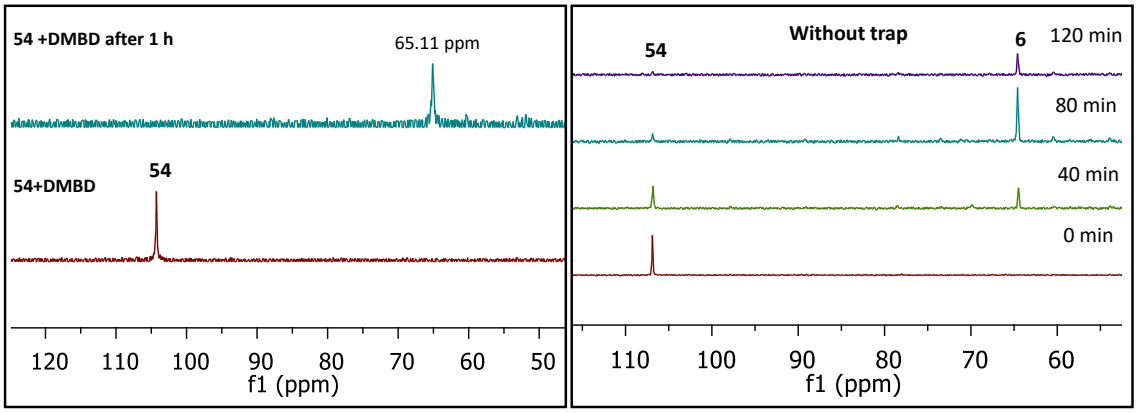

Figure 77. Photolysis of **54**: generation of **6**.

The photolysis in THF was monitored by UV-Vis spectroscopy which revealed a progressive depletion of the absorption band at 365 nm. Although an isobestic point at ~350 nm could be observed for three spectra obtained at 15 min, 45 min and 80 min respectively, (Figure 78), there are other spectra in between that do not pass through the above mentioned isobestic point. The absence of a clean isobestic point suggests that the

photolytic conversion is not quantitative. This was corroborated by the presence of several unidentified peaks observed in the ^{31}P NMR spectra during the photolysis. The elimination of Ph• and Cl• is reminiscent of the Pt-Sb complex **B** (Figure 65). It provides an original demonstration that light can be used to drive the cleavage of Sb-Cl and Sb-Ph bond.

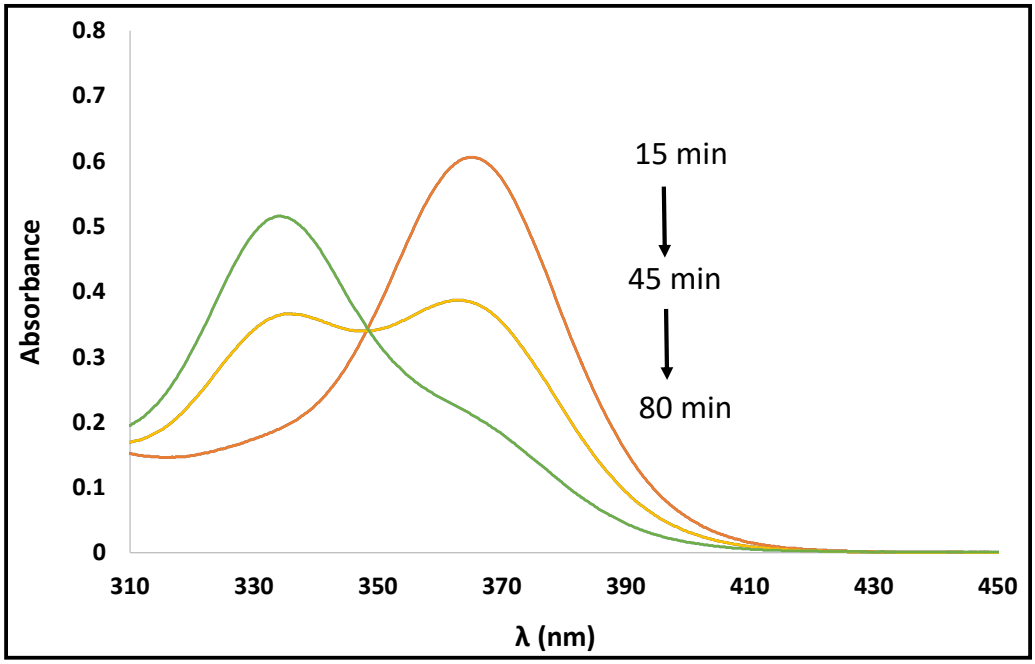

Figure 78. Absorption spectra obtained during the photolysis of **54**.

Motivated by the success of the photolysis reactions of di-*iso*-propylstibine supported gold complexes, we focused on the photoreactivity of the palladium complex **77**. The photolysis of **77** was attempted in DCM with DMBD as a radical trap. The photolysis proceeded smoothly to regenerate **76**, although the solubility of **77** was lowered

by the presence of DMBD. To avoid this issue, we used Ph_2S which emerged as a potent as a radical trap in the photolysis of **38**. Indeed, the use of Ph_2S enhanced the efficiency of the chlorine elimination process and the reaction was completed in 1h as opposed to 3 h in the case where DMBD was used (Figure 79). The yield of **76** was quantitative.

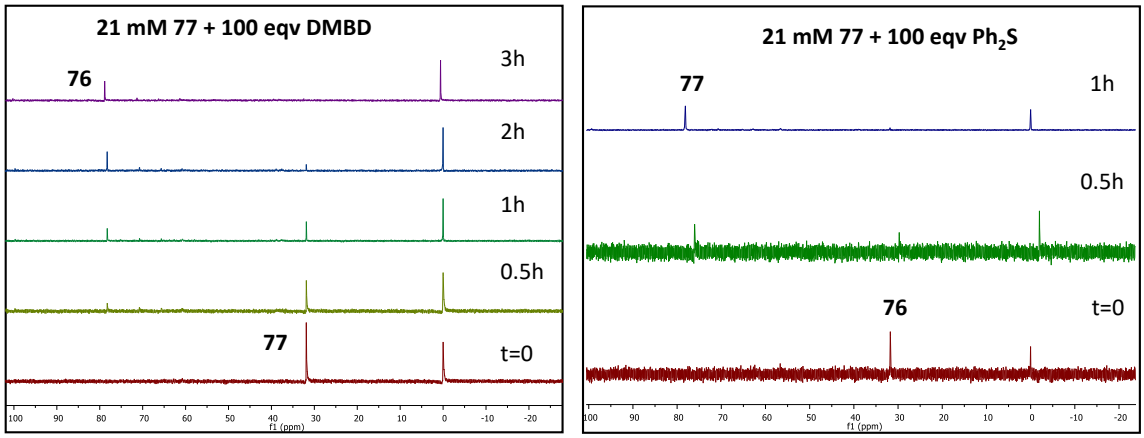

Figure 79. Photolysis of a 21 mM solution of **77**.

5.5 Conclusion

In this project, we have reported the synthesis and characterization of a gold/stiborane complex (**75**) and a palladium/stiborane complex (**77**) supported by a chlorostibine ligand. These complexes feature low lying Sb-Cl σ* orbital which facilitate photo-induced reductive elimination of the halogen. Both these complexes eliminate an equivalent of "Cl_2" to revert back to their reduced counterparts. In the case of the palladium complex, the elimination of chlorine was accompanied by the formation of the Sb-Pd bond.

The photolysis of the complex **54** resulted in the unexpected elimination of one wquivalent of Cl and one equivalent of Ph instead of one equivalent of chlorine. The elimination of chlorobenzene equivalent from a Sb-M platform has been previously observed from Sb-Pt scaffold **B** (Figure 65) but such reactivity from gold-stiborane complexes is unprecedented. It is worth mentioning that the reductive elimination of Ph• and Cl• from a main group element can lead to versatile reactivity.

5.6 Experimental section

General considerations. (tht)AuCl (tht = tetrahydrothiophene),[170] (COD)$PdCl_2$ and (*o*-P*i*Pr_2(C_6H_4)SbCl (**L**^{PiPr}-Cl)[62] were prepared according to the reported procedures. Solvents were dried by passing through an alumina column (pentane and CH_2Cl_2) or by reflux under N_2 over Na/K (Et_2O and THF). All other solvents were used as received. All commercially available chemicals were purchased and used as provided. All air and moisture sensitive manipulations were carried out under an atmosphere of dry N_2 employing either a glove box or standard Schlenk techniques. The photochemical experiments were carried out using a Nikon Microscope 100W mercury lamp, connected with Nikon HBO 100W power supply (Model 78591). During photolysis, the reaction sample was placed in front of a cooling fan (SA-317, SLM Instruments) such that the temperature was maintained at 30°C. UV-vis spectra were recorded in a Shimadzu UV-2501PC spectrophotometer. Ambient temperature NMR spectra were recorded on a Varian Unity Inova 500 FT NMR (499.42 MHz for ^{1}H, 125.58 MHz for ^{13}C, 202.17 MHz for ^{31}P, 469.93 MHz for ^{19}F) spectrometer. Chemical shifts (δ) are given in ppm and are

referenced against residual solvent signals (^{1}H, ^{13}C) or external standards 85 % H_3PO_4 for ^{31}P (δ 0 ppm) and $BF_3.Et_2O$ for ^{19}F (δ -153 ppm). Elemental analyses were performed at Atlantic Microlab (Norcross, GA).

Crystallography. All crystallographic measurements were performed at 110(2) K using a Bruker SMART APEX II diffractometer with a CCD area detector (graphite monochromated Mo Kα radiation, λ = 0.71073 Å, ω-scans with a 0.5° step in ω) at 110 K. In each case, a specimen of suitable size and quality was selected and mounted onto a nylon loop. The semi-empirical method *SADABS* was applied for absorption correction. The structures were solved by direct methods and refined by the full-matrix least-square technique against F^2 with the anisotropic temperature parameters for all non-hydrogen atoms. All H atoms were geometrically placed and refined in riding model approximation. Data reduction and further calculations were performed using the Bruker *Apex2* (2013) and SHELXTL program packages.

Theoretical calculations. Density functional theory (DFT) calculations (full geometry optimization) were carried out on starting from the crystal structure geometries with Gaussian09 program (BP86[174-175] with 6-31G for H, C; 6-31+G(d') for F; 6-31G(d') for P, Cl, cc-pVTZ-PP with Stuttgart relativistic small core for Au,[176-177] Pd and Sb[178-179]). Frequency calculations performed on the optimized geometries found no imaginary frequency, confirming that a local minimum on its potential energy hypersurface had been reached. Optimized geometries were subjected to NBO analysis using NBO 5.9 program.[259] TD-DFT calculations were carried out using the MPW1PW91 functional and

the SMD solvation model, with the same basis sets mentioned above. The molecular orbitals were visualized and plotted using the *Jimp*2 program.[260]

Synthesis of 75. A solution of (tht)AuCl (58.9 mg, 0.183 mmol) in DCM (5 mL) was added dropwise to a solution of (*o*-(*i*Pr_2P)C_6H_4)$_2$SbCl in DCM (2 mL) and the resulting yellow solution was stirred for 30 min. The generation of complex **6** was confirmed by ^{31}P NMR spectroscopy. To the reaction mixture containing **6**, a solution of $PhICl_2$ (75.84 mg, 0.275 mmol) in CH_2Cl_2 (3 mL) was added dropwise at ambient temperature. The color of the solution turned pale yellow. The reaction was stirred for 12h before removing the solvent in vacuo. The resulting yellow solid was washed with Et_2O (2×3 mL) and dried *in vacuo* to afford **75** as pale yellow powder. Yield: 120 mg (77 %). Single crystals of **75** suitable for X-ray diffraction were obtained by vapor diffusion of Et_2O into a solution of the compound in CH_2Cl_2. ^{1}H NMR (499 MHz, $CDCl_3$) δ 9.60 (d, *J* = 8.2 Hz, 2H), 7.88 – 7.73 (m, 4H), 7.67 – 7.53 (m, 2H), 3.68 – 3.14 (m, 4H), 1.49 – 1.37 (dd, *J* = 16.8, 7.3 Hz, 12H), 1.32 (dd, *J* = 16.8, 7.3 Hz, 12H). ^{13}C NMR (126 MHz, $CDCl_3$) δ 180.28 (pseudo-t, $J_{C\text{-}P}$ = 20.3 Hz), 134.62 (s), 133.74 (pseudo-triplet, $J_{C\text{-}P}$ = 8.2 Hz), 131.13 – 130.40 (m), 114.46 (pseudo-t, $J_{C\text{-}P}$ = 27.0 Hz)), 28.57 (pseudo-t, $J_{C\text{-}P}$ = 14.9 Hz), 19.36 (s, C$H_{3i\text{-}Pr}$), 19.03 (s, C$H_{3i\text{-}Pr}$). ^{31}P NMR (202 MHz, $CDCl_3$) δ 97.98. Elemental analysis calcd (%) for $C_{24}H_{36}AuCl_3P_2Sb$: C 34.03, H 4.28; found: C 33.80, H 4.17.

Synthesis of 60. A solution of KF (6 mg, 0.095 mmol) in MeOH (2 mL) was added to a solution of **75** (20 mg, 0.024 mmol) in THF (4 mL) and the resulting solution was stirred at ambient temperature for 30 min. resulting in the precipitation of a white solid. The solvent was removed in vacuo, and the residue extracted with CH_2Cl_2 (5 mL). The

resulting mixture was filtered over Celite and concentrated to 2 mL. Addition of pentane (5 mL) resulted in precipitation of a white powder that was filtered and dried in vacuo to afford **60**. Yield: 12 mg (63%). Single crystals of **60** suitable for X-ray diffraction were obtained by slow evaporation of the compound in CH_2Cl_2/Et_2O (1/1). ^{1}H NMR (499 MHz, $CDCl_3$) δ 8.89 (dd, *J* = 7.9, 3.5 Hz, 2H), 7.85 (d, *J* = 7.2 Hz, 2H), 7.81 – 7.73 (m, 2H), 7.62 (td, *J* = 7.4, 1.1 Hz, 2H), 3.61 – 3.27 (m, 4H), 1.38 (dd, *J* = 18.5, 7.2 Hz, 12H), 1.32 (dd, *J* = 16.9, 7.2 Hz, 12H). ^{13}C NMR (126 MHz, $CDCl_3$) δ 170.22 – 166.29 (m), 135.28 (dd, *J* = 20.5, 10.5 Hz), 133.79 (s), 130.97 (s), 130.13 (s), 119.15 (s), 27.83 (t, *J* = 14.8 Hz), 18.88 (s, $CH_{3i\text{-}Pr}$), 18.70 (s, $CH_{3i\text{-}Pr}$), 18.17 (s, $CH_{3i\text{-}Pr}$).^{31}P{^{1}H} NMR (202.17 MHz; $CDCl_3$): δ 105.01 (d, $^3J_{P\text{-}F}$ = 16 Hz). ^{19}F NMR (469.93 MHz; $CDCl_3$): δ -69.71 (d, 1F, $^2J_{F\text{-}F}$ 17 Hz), -133.78 (dt, 1F, $^2J_{F\text{-}F}$ = 17 Hz, $^3J_{F\text{-}P}$ = 16 Hz). Elemental analysis calcd (%) for $C_{24}H_{36}AuClF_3P_2Sb$: C 36.14, H 4.55; found: C 36.63, H 4.67.

Synthesis of 76. A solution of (COD)$PdCl_2$ (52.51 mg, 0.184 mmol) (COD = 1,5-cyclooctadiene) in CH_2Cl_2 (5 mL) was added dropwise to a stirring solution of (*o*-(*i*Pr_2P)C_6H_4)$_2$SbCl (100 mg, 0.13 mmol) in CH_2Cl_2 (5 mL) at ambient temperature. The color of the solution turned orange immediately. After stirring for an hour, the solvent was evaporated under vacuum and the solid residue was washed with pentane to afford **76** as orange solid. Yield: 130 mg (98%) Single crystals of **76** was obtained by vapor diffusion of Et_2O in to a concentrated solution of **76** in CH_2Cl_2. ^{1}H NMR (500 MHz, $CDCl_3$ δ 8.20 (d, *J* = 7.7 Hz, 2H), 7.80 (t, *J* = 7.4 Hz, 2H), 7.74 (d, *J* = 7.5 Hz, 2H), 7.59 (t, *J* = 7.5 Hz, 2H), 3.04 (tt, *J* = 4.7, 4.0 Hz, 4H), 1.44 (dd, *J* = 17.2, 8.1 Hz, 12H), 1.25 (dd, *J* = 16.0, 7.5 Hz, 12H). ^{13}C NMR (126 MHz, $CDCl_3$) δ 167.07 (pseudo-t, $J_{C\text{-}P}$= 19.5 Hz), 134.27 (s),

132.67 (t, J_{C-P} = 2.4 Hz), 131.33 (t, J_{C-P} = 8.2 Hz), 129.76 (t, J_{C-P} = 2.9 Hz), 125.21 (t, J_{C-P}= 20.5 Hz), 28.40 (t, J_{C-P} = 11.6 Hz, CH_{3i-Pr}), 19.57 (s, CH_{3i-Pr}), 19.06 (s, CH_{3i-Pr}). ^{31}P NMR (202 MHz, cdcl$_3$) δ 78.83. Elemental analysis calcd (%) for $C_{24}H_{36}PdCl_3P_2Sb$: C 39.98, H 5.03; found: C 39.27, H 4.97.

Synthesis of 77. Complex **76** (50 mg, 0.069 mmol) was dissolved in CH_2Cl_2 (2 mL) and a solution of SO_2Cl_2 (25 μL, 0.30 mmol) in CH_2Cl_2 (3 mL) was added dropwise to it. After stirring for 24 h, the solvent was removed under vacuum. The residue was washed with pentane and dried under reduced pressure. The product was obtained as dark yellow solid. Yield: 38 mg (70%). Single crystals were obtained by vapor diffusion of Et_2O into a CH_2Cl_2 solution of **77**. ^1H NMR (500 MHz, $CDCl_3$) δ 8.77 (d, *J* = 8.2 Hz, 1H), 7.67 (t, *J* = 7.4 Hz, 1H), 7.61 – 7.47 (m, 2H), 3.13 – 2.96 (m, 2H), 1.46 (dt, *J* = 34.3, 17.2 Hz, 7H), 1.37 – 1.23 (m, 7H). ^{13}C NMR (100 MHz, $CDCl_3$) δ 175.04 (t, *J* = 6.2 Hz), 134.22 (s), 132.99 (s), 131.67 (s), 129.86 (s), 127.36 (t, *J* = 18.5 Hz), 26.87 (d, *J* = 6.9 Hz), 19.99 (d, *J* = 7.4 Hz), 19.22 (d, *J* = 6.1 Hz). ^{31}P NMR (202 MHz, $CDCl_3$) δ 32.33. Elemental analysis calcd (%) for $C_{24}H_{36}PdCl_5P_2Sb.CH_2Cl_2$: C 34.24, H 4.37; found: C 34.23, H 4.34.

6. AN AMBIPHILIC PHOSPHINE/H-BOND DONOR LIGAND AND ITS APPLICATION TO THE GOLD MEDIATED CYCLIZATION OF PROPARGYLAMIDES

6.1 Introduction

Access to electrophilic transition metal catalysts is typically achieved through the use of a Lewis acid that activates the metal centre by abstraction of an anionic ligand.[10] This strategy has been applied to diverse areas including olefin polymerization catalysis where the role of the Lewis acids is usually fulfilled by strongly Lewis acidic fluorinated boranes. [10, 272-274] The same principles apply to electrophilic late transition metal catalysts which are typically activated by abstraction of a halide anion using a silver salt.[275] While the exposed nature of the resulting cationic transition metal center is usually desired for high catalytic activity, it can also be a source of instability and a conduit for catalyst decomposition, especially in the case of late transition metals that are prone to reduction. [276-277] For this reason, alternative activation methods are being actively pursued, for example with the use of milder Lewis acids. [278-281] It has also been argued that improved catalyst stability could derive from the presence of an ancillary Lewis acidic site positioned within the ligand architecture.[110, 159, 194, 219, 282-284] Analogous approach to activate metal-halogen bond can be conceived by establishing direct non-covalent interaction with the halide.

This idea, combined with recent advances in the field of anion-pairing organocatalysis using hydrogen-bond donor systems[115, 285] which has emerged as a promising new direction due to its broad application in organic transformations, has led us to question whether an intramolecular hydrogen-bond donor functionality could also be used to activate an organometallic catalyst via interaction with a metal-bound anionic ligand.

6.2 Synthesis and characterization of an ambiphilic H-bond donor phosphine ligand

To explore this possibility, we decided to first synthesize an ambiphilic ligand in which the role of the acidic functionality is fulfilled by a hydrogen bond donor group. Reaction of *o*-lithiotrifluoroacetanilide with Ph_2PCl followed by acidic work up produced *o*-(diphenylphosphino)trifluoroacetanilide (**78**) as a pale yellow solid (Scheme 13). The ligand (**78**) was characterized by ^{1}H, ^{19}F and ^{31}P NMR spectroscopy and also by ESI^{-}/MS. Salient spectroscopic features include a ^{1}H NMR resonance at 8.81 ppm corresponding to the amide hydrogen atom and a ^{31}P NMR resonance at -21.9 ppm. The trifluoroacetamide functionality also gives rise to a ^{19}F NMR signal at -76.1 ppm.

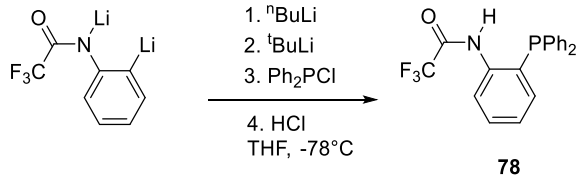

Scheme 13. Synthesis of **78**.

The structure of **78** was also confirmed by X-ray analysis. Ligand **78** crystallizes in the triclinic space group *P*-1 (Figure 80). The phosphorus center is pyramidalized as evidenced by the C-P-C angles around P (103.03(11) for C13-P1-C7, 102.84(14) for C7-P-C1 and 102.31(9) for C1-P1-C13). The P1-C1, P1-C7 and P1-C13 bond distances of 1.836(2) Å, 1.828(4) Å and 1.376(18) Å are comparable to other triphenylphosphines. It is interesting to note that the N-H hydrogen atom is not interacting with the phosphorus atom.

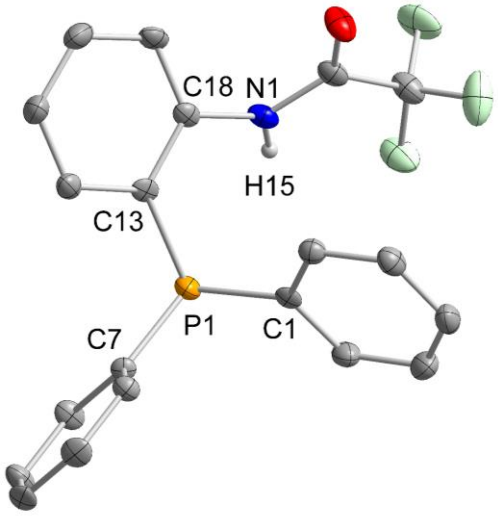

Figure 80. Crystal structure of **78**. Displacement ellipsoids are scaled to the 50% probability level. All the hydrogen atoms except the amide hydrogens are omitted for clarity. Selected bond lengths (Å) and angles (deg) for L: N1-H15 0.85(2), N1-C18 1.428(3), C13-C18- 1.399(3), P1-C1 1.836(2), P1-C7 1.828(4), P1-C13 1.8376(18); C1-P-C7 102.84(14), C1-P1-C13 102.31(9).

6.3 Coordination of **78** to gold (I) synthon

After the successful synthesis of the ligand we sought to test its coordination to the gold(I) center next. Reaction of **78** with one equivalent of (tht)AuCl (tht = tetrahydrothiophene) in THF at room temperature afforded **79** as a light-sensitive white solid (Scheme 14). A peak at 22.2 ppm in the ^{31}P NMR spectrum, downfield to the peak corresponding to the free ligand, confirmed the formation of the gold(I) complex. The ^{1}H NMR resonance corresponding to the N-*H* is observed as a broad singlet at 8.54 ppm. (For the detailed NMR spectra, see Figure 86- Figure 91)

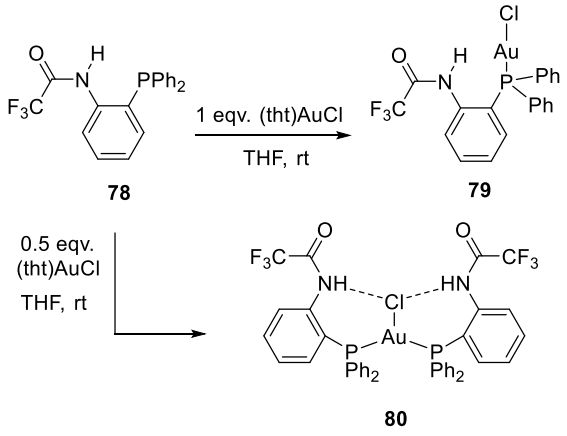

Scheme 14. Synthesis of **79** and **80**.

Complex **79** crystallizes in the $P2_1/c$ space group. The sold state structure of **79** indicates that the complex exists as a dimer held by an aurophilic interaction of 2.997(7) Å (Figure 81).[286] The dimer also benefits from two hydrogen-bonds connecting the N-*H*

proton of one molecule to the chlorine atom of the other one. The presence of these hydrogen bonds is supported by N-H•••Cl hydrogen bonds as confirmed by the Cl1-N1 and Cl1-N1 separations of 3.199(8) Å and 3.164(8) Å which fall in the expected range.[116] The structure of **79** shows no evidence for a hydrogen-bonding interaction involving the gold atom.[287-288]

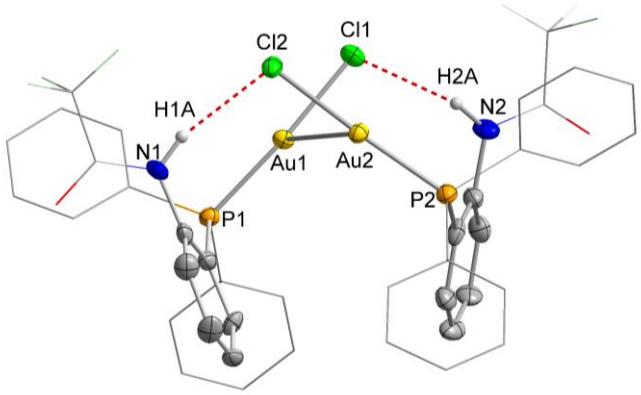

Figure 81. Crystal structure of **79**. Displacement ellipsoids are scaled to the 50% probability level. All the hydrogen atoms except the amide hydrogens are omitted for clarity. Selected bond lengths (Å) and angles (deg) for **79**: Au1-Au2 2.9976(7), Au1-Cl1 2.314(2), Au2-Cl2 2.316(2), N1-H1A 0.8800, N2-H2A 0.8800, H1A---Cl2 2.3802(22), H2A---Cl1 2.4050(24); P1-Au-Cl1 171.93(8), P2-Au2-Cl2 172.94(7).

Next, we decided to investigate the molecularity of **79** in solution using the pulse gradient spin-echo (PGSE) NMR method, which has proved to be well adapted for organometallic compound molecular size determination.[289-292] PGSE measurements were carried out using a solution of **79** in CD_2Cl_2 and its diffusion was compared to that obtained with 1,3,5-tri-tert-butylbenzene (**A**), a molecule that we used as an internal standard (Figure 82). This molecule was chosen because of its apolar nature and inertness

toward **79.** Its molecular size ($V_{X\text{-}ray}$(**A**) = 454 Å^3)[293] is also close to that of monomeric **79** ($V_{X\text{-}ray}$(**79**) = 504 Å^3). Our PGSE measurements indicate that **79** diffuses slower than **A**, in qualitative agreement with the size difference of these two compounds. A quantitative treatment of the diffusion data affords a molecular volume of V_{PGSE}(**79**) = 755 Å^3. This value, which is higher than the value of $V_{X\text{-}ray}$(**79**) = 504 Å^3 but smaller than that of the dimer (1.008 Å^3), could be taken as an indication that the gold complex undergoes a monomer-dimer equilibrium in solution.

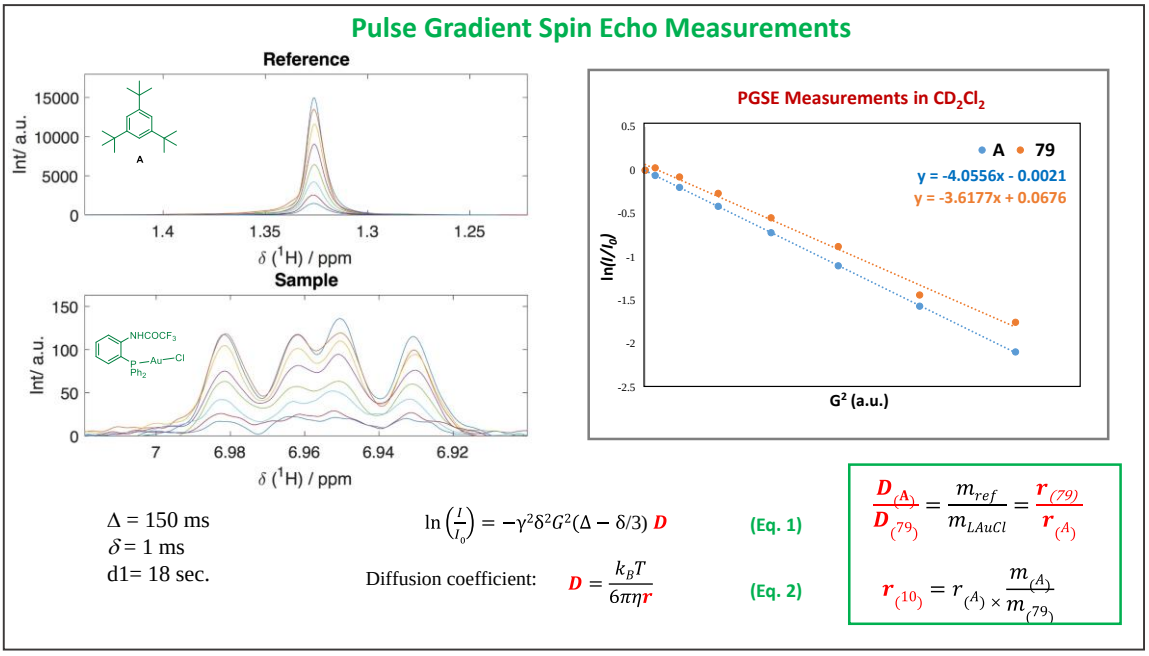

Figure 82. Left: Decay of NMR signal intensity with the progressive increase of the gradient strength. Right: Plot of ln(I/I_0) vs G^2 for the reference **A** (1,3,5-tri-*tert*-butylbenzene) and **79** in the same graph.

We also tested the 2:1 reaction of **78** and (tht)AuCl. This reaction affords the corresponding bis(phosphine) complex **80** (Scheme 14). Complex **80** gives rise to a broad ^{31}P NMR resonance at 35.78 ppm. In the ^{1}H NMR spectrum, the N-*H* proton resonates at 10.55 ppm, indicating its involvement in a hydrogen-bonding interaction. The solid state structure of **80** confirms the formation of the expected complex. The gold center adopts a trigonal planar geometry. The short contact between the amide nitrogen atoms and the gold-bound chlorine atom (Cl1-N1 3.224(5) Å and Cl1-N2 3.197(5) Å) are consistent with the presence of N-H•••Cl interactions. A further evidence for the presence of this interaction comes from the Au-Cl bond distance of 2.6614(14) Å which is significantly longer than that in $(PPh_3)_2AuCl$ (2.526(10) Å).[294] It is also interesting to note that, as a result of this hydrogen bonding motif, the P1-Au-P2 angle in **80** (144.95(5)°) is significantly wider than that in $(PPh_3)_2AuCl$ (136.4(3)°).[294]

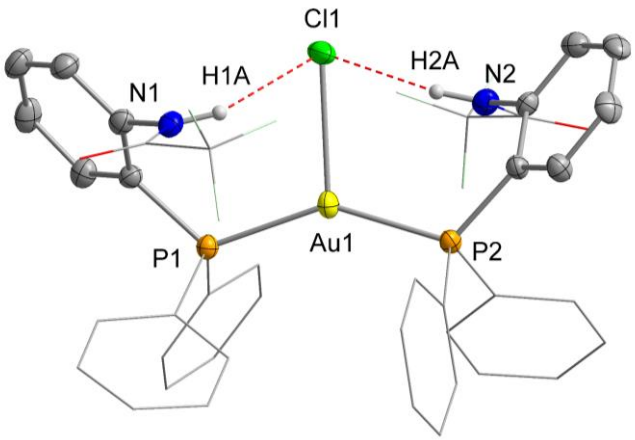

Figure 83. Crystal structure of **80**. Displacement ellipsoids are scaled to the 50% probability level. All the hydrogen atoms except the amide hydrogens are omitted for clarity. Selected bond lengths (Å) and angles (deg) for **80**: Au1-Cl1 2.6614(14), N1-H1A

0.8800, N2-H2A 0.8800, P1-Au-P2 144.90(5), Cl1-A12-P2 108.32(5), Cl1-A12-P2 106.74(5).

To illustrate the extent and significance of H-bondong interaction in **79**, its structure was first optimized using DFT methods (Gaussian09 program: BP86[295-296] functional, with 6-31G for H, C, N and O; 6-31(d') for F, 6-311+G(d) for P, Cl; aug-ccpVTZ for Au[176, 297] and Stuttgart relativistic small core ECPs for Au[297]). The optimized geometry reproduced the solid state structure with reasonable precision (See Table 10).

Table 10. : Selected bond lengths (Å) and angles (°) for 79 as determined crystallographically and optimized computationally.

Parameter	79	79*
Au1-Au2	2.9976(7)	3.26956
Au1-Cl1	2.314(2)	2.32628
Au2-Cl2	2.316(2)	2.32628
N1-H1A	0.8800	1.03979
N2-H2A	0.8800	1.03979
H1A---Cl2	2.3802(22)	2.25096
H2A---Cl1	2.4050(24)	2.25096
P1-Au-Cl1	171.93(8)	170.258
P2-Au2-Cl2	172.94(7)	170.261

The optimized geometry was then subjected to Natural Bond Orbital (NBO) analysis which identified several lp(Cl)→σ*(N-H) interactions contributing a total deletion energy (**E_{del}**) of 21.094 kcal mol^{-1} for each H-bond (Figure 84).

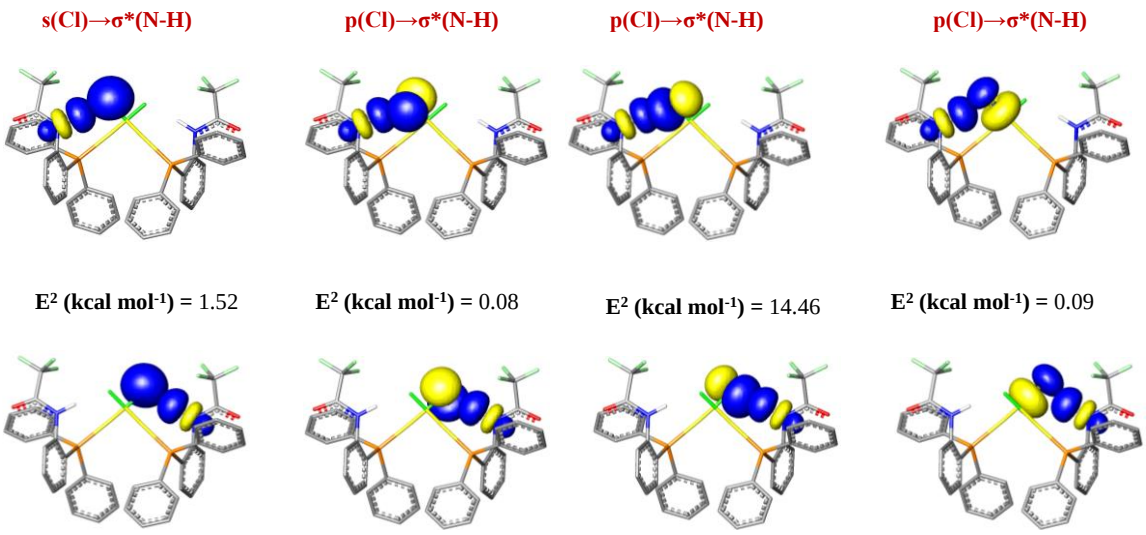

Figure 84. NBO plots of all the lp(Cl)→σ*(N-H) donor-acceptor interactions and calculated second order perturbation energies for each H-bonding interaction in **79** (isodensity value = 0.05). All hydrogen atoms except for N-H atoms are omitted for clarity.

To further establish the H-bonding and aurophilic interactions between the two monomeric units, the optimized electronic structure was subjected to QTAIM calculations using AIMAll program. QTAIM recognized bond paths and bond critical points between the two Au centers and also between the amide hydrogens and chlorides (Figure 85).

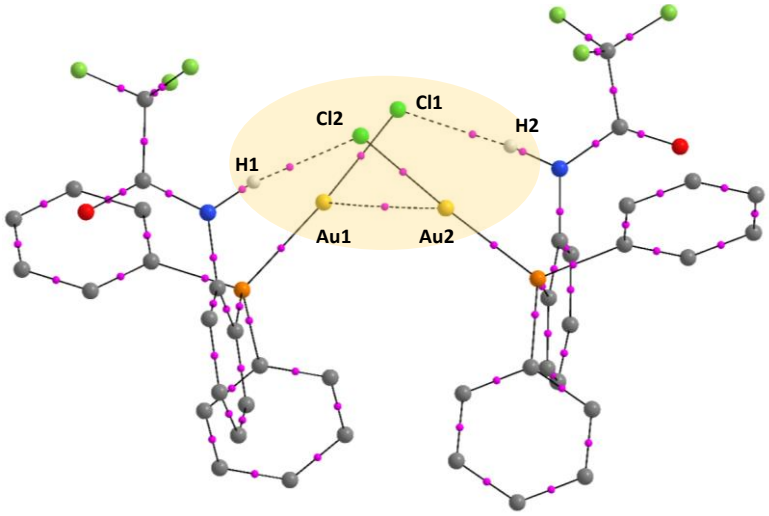

Figure 85. Bond critical points (pink spheres) derived from QTAIM calculation on **79**. All hydrogen atoms except for N-H atoms are omitted for clarity.

Table 11. Relevant parameters of the selected bonding interactions in LAuCl as obtained from QTAIM calculations

Bond	ρ**(r) e Bohr^{-5}**	$\nabla^2 \rho$**(r) e Bohr^{-5}**	**δ (A, B)**
Au1-Au2	0.019648	0.044926	0.22657
Cl2-H1A	0.023372	0.065333	0.102525
Cl1-H2A	0.023373	0.065333	0.1025

6.4 Evaluation of catalytic activity of **79**

Given the demonstrated ability of the trifluoroacetamide functionality to form a hydrogen bond with a gold-bound chloride anion, we questioned whether such an

interaction would be sufficiently strong to render the gold center of these complexes catalytically active. With this in mind, we decided to investigate the catalytic activity of **79** and **80** in the cycloisomerization of propargylamides, without addition of a silver activating agent. Initially, both complexes were tested at room temperature in $CDCl_3$ using *N*-(prop-2-yn-1-yl)benzamide as a substrate. While no cyclisation was observed when 80 was employed as a catalyst, ^{1}H NMR and gas chromatography monitoring showed smooth conversion when **79** was added to the reaction. In all cases, the reactions were accompanied by the slow production of purple gold particles, raising doubt about the nature of the catalytically active species. For this reason, we decided to use a different solvent. We found that **79** is stable in dichloromethane, with no sign of decomposition after 24h as confirmed by visual inspection of the solution and ^{31}P NMR spectroscopy. The catalysis in dichloromethane was monitored by GC and the results are compiled in Table 1. Formation of only one isomer of the cyclized oxazole was observed consistent with the presence of a reactive gold(I) catalytic center.[229-230] A comparison of the percentage conversion of the different starting materials after 24 h, revealed that the reaction occurs faster in the case of electron rich *N*-(prop-2-yn-1-yl)-4-methoxybenzamide in line with the amide functionality acting as the nucleophile toward the activated alkyne. In the case of *N*-(prop-2-yn-1-yl)-2-methylbenzamide, the relatively slow progress of the reaction can be attributed to the steric hindrance resulting from the *o*-Me group.

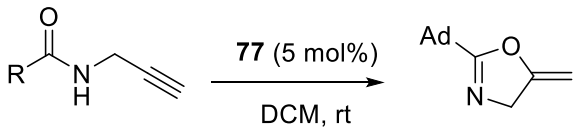

Scheme 15. Catalytic cyclization of propargylic amides by **79**.

Table 12. Catalytic conversion of the propargylic amides by 79 (5 mol%) in CH_2Cl_2 monitored by GC

R	Solvent	Time (h)	Conversion (%)
Ph	CH_2Cl_2	24	36
o-Tolyl	CH_2Cl_2	24	35
p-F-C_6H_4	CH_2Cl_2	24	37
p-OMe-C_6H_4	CH_2Cl_2	24	53

To understand if the presence of an intramolecular hydrogen bond donor group is a prerequisite for catalysis, we also tested the cyclisation of *N*-(prop-2-yn-1-yl)benzamide using $PhNHCOCF_3$ and PPh_3AuCl in $CDCl_3$ and observed no cyclization products even after 48 hours. This experiment shows that the presence of a trifluoroacetamide functionality within the catalyst structure is essential for activity. The lack of activity noted in the case of **80** shows that coordination of a second phosphine ligand to the gold center is also incompatible with substrate activation as previously described.[72]The same explanation may be invoked to rationalize the fact that no reaction is observed when the reactions are carried out in donor solvents such as MeCN and THF. These donor solvent may coordinate to the activated gold center therefore preventing substrate activation.

6.5 Conclusion

In summary, we describe a phosphine gold chloride complex which acts as a self-activating catalyst for the cyclization of propargylamide. The reactivity studies suggests that the self-activating nature of this catalyst originates from the presence of an intramolecular hydrogen bond donor group which activates the gold atom, presumably by interaction with the chloride anion. While the results are compelling, we have not yet been able to ascertain the nuclearity of the catalyst which we presume could be either monomeric or dimeric as suggested by the solid state structure and the PGSE studies. We are currently working on clarifying this point through mechanistic and kinetic analyses.

6.6 Experimental section

General considerations. (tht)AuCl[171], *o*-Bromotrifluoroacetanilide[298], trifluoroacetanilide[299] and the various propargylic amides[230] were prepared according to previously reported procedures. Chloro(triphenylphosphine)gold was obtained from the reaction of (tht)AuCl with triphenylphopshine. *o*-bromoaniline, *n*BuLi (2.2M in hexane) and *t*BuLi (1.5M in pentane) were purchased from Oakwood Chemicals and Alfa Aesar and used as received. All preparations were carried out under an atmosphere of dry N_2 employing either a glove box or standard Schlenk techniques. Solvents were dried by passing through an alumina column (CH_2Cl_2, pentane) or refluxing under N_2 over Na/K (THF, Et_2O). Ambient-temperature NMR spectra were recorded using a Varian Unity Inova 500 FT NMR (499.42 MHz for ^1H, 125.58 MHz for ^{13}C, 469.93 MHz for ^{19}F, 202.17 MHz for ^{31}P) spectrometer. Chemical shifts (δ) are given in ppm and are referenced against

residual solvent signals (^{1}H, ^{13}C) or external $BF_3 \cdot Et_2O$ (^{19}F), H_3PO_4 (^{31}P). GC analysis was carried out using an Agilent GC System (6890 Series) Plus set up equipped with a Rxi-5ms fused silica column from RESTEK (length: 15 m length, id: 0.53 mm, film thickness: 0.50 µm). The column temperature was maintained at 50 °C for 2 min and raised to 250 °C at 25 °C/min. The final temperature (250 °C) was held for 10 min. Elemental analyses were performed by Atlantic Microlab (Norcross, GA).

Crystallography. The crystallographic measurements were performed at 110(2) K using a Bruker APEX-II CCD area detector diffractometer, with graphite-monochromated Mo Kα radiation (λ = 0.71069 Å) and ω scans with a 0.5° step in ω. A specimen of suitable size and quality was selected and mounted onto a nylon loop. The semiempirical method *SADABS* was applied for absorption correction. The structure was solved by direct methods, which successfully located most of the non-hydrogen atoms. The N-H atoms in 1 were located in the electron density map and refined anisotropically. All other hydrogen atoms were placed at calculated positions and refined using a riding model. Subsequent refinement on F2 using the SHELXTL/PC package28 (version 6.1) allowed location of the remaining non-hydrogen atoms. Data reduction and further calculations were performed using the Bruker Apex2 (2013) and SHELXTL program packages.

Theoretical calculations. Density functional theory (DFT) calculations (full geometry optimization) were carried out on starting from the crystal structure geometries with Gaussian09 program (BP86[175, 300] with 6-31G for H, C; 6-31+G(d') for F; 6-31G(d') for P, Cl, cc-pVTZ-PP with Stuttgart relativistic small core for Au[176-177]). Frequency

calculations performed on the optimized geometries found no imaginary frequencies. QTAIM calculations were carried out on the wave functions derived from the optimized structures using the AIMAll program.[180]

Synthesis of 78. *n*-Butyllithium (2.2 M) in hexane (1.69 ml, 3.73 mmol) was added to a solution of *o*-bromotrifluoroacetanilide (1.0 g, 3.73 mmol) in THF (20 mL) at -78ºC. After 1 h, *t*-butyllithium (1.5 M) in pentane (4.97 ml, 7.46 mmol) was added dropwise. The mixture was stirred at -78ºC for another hour, after which PPh_2Cl (0.66 ml, 3.73 mmol) was added. The mixture was allowed to warm to room temperature and stirred overnight. The reaction mixture was quenched with an HCl solution (1M) in diethyl ether (10 ml). All volatiles were evaporated under vacuum and the resulting solid was extracted with pentane. The solvent was evaporated to afford the ligand as pale yellow solid. Yield: 974 mg, 70%. X-ray diffraction quality crystals were obtained by slow evaporation of a concentrated pentane solution. ^{1}H NMR ($CDCl_3$, 499.42 MHz): 8.85 (bs, N-*H*), 8.12 (dd, *J* = 8.2, 4.4 Hz, 1H), 7.45 (td, 1H), 7.39 (td, 6H), 7.31 (td, 4H), 7.19 (t, 1H), 7.03 (t, 1H). ^{13}C NMR ($CDCl_3$, 125.58 MHz): δ 154.75 (q, *J* = 37.3 Hz), 138.16 (d, *J* = 17.7 Hz), 134.11 (d, *J* = 2.4 Hz), 133.76 (s), 133.61 (s), 133.42 (d, *J* = 5.4 Hz), 132.03 (d, *J* = 10.2 Hz), 130.47 (s), 129.61 (s), 128.97 (d, *J* = 7.5 Hz), 128.20 (d, *J* = 12.1 Hz), 126.56 (d, *J* = 1.6 Hz), 122.21 (d, *J* = 1.6 Hz), 115.65 (q, *J* = 289.1 Hz). ^{19}F NMR ($CDCl_3$, 469.93 MHz): -76.11 (s). ^{31}P NMR ($CDCl_3$, 202.17 MHz): -21.42 (s). ESI$^-$/MS for $[C_{20}H_{14}F_3NOP]^-$: m/z calculated 372.08; found 372.0504. Elemental analysis (%) calculated for $C_{20}H_{15}F_3NOP$: C, 64.35; H, 4.05; N, 3.75. Found: C, 63.52; H, 4.37; N, 3.73.

Synthesis of 79. A solution of the ligand **78** (100 mg, 0.26 mmol) in THF (3 ml) was added dropwise to a suspension of (tht)AuCl (85.87 mg, 0.26 mmol) in THF (1 ml) at room temperature. It was left to stir for 2 h in a vessel protected from incident light. The reaction mixture was then layered with pentane. Over the course of 12 h, the product precipitated as a white, light-sensitive solid. The white solid was isolated by filtration and washed with pentane. The product was obtained as a light sensitive white solid. Yield: 130 mg, 83%. Vapor diffusion of pentane in a THF solution afforded clear colorless crystals of **79**. ^{1}H NMR ($CDCl_3$, 499.42 MHz): δ 8.50 (s, 1H, N-*H*), 7.85 (dd, *J* = 7.8, 4.9 Hz, 1H), 7.66 (t, *J* = 7.8 Hz, 1H), 7.63 – 7.50 (m, 10H), 7.33 (t, *J* = 7.7 Hz, 1H), 6.90 (ddd, *J* = 12.8, 7.8, 1.3 Hz, 1H). ^{13}C NMR ($CDCl_3$, 126 MHz). δ 155.02 (q, *J* = 38.2 Hz), 136.35 (d, *J* = 6.3 Hz), 134.36 (d, *J* = 14.3 Hz), 133.51 (d, *J* = 7.1 Hz), 133.28 (d, *J* = 2.0 Hz), 133.03 (d, *J* = 2.7 Hz), 129.84 (d, *J* = 12.4 Hz), 127.68 (d, *J* = 9.7 Hz), 126.95 (d, *J* = 5.4 Hz), 125.80 (s), 125.28 (s), 122.82 (s), 122.34 (s), 115.24 (q, *J* = 289.1 Hz). ^{19}F NMR ($CDCl_3$, 469.93 MHz): δ -75.69 (s). ^{31}P NMR ($CDCl_3$, 202.17 MHz): δ 22.20 (s). ESI$^-$/MS for $[C_{20}H_{14}AuClF_3NOP]^-$: m/z calculated 604.01; found 604.0068. Elemental analysis (%) calculated for $C_{20}H_{15}AuClF_3NOP$: C, 39.66; H, 2.50; N, 2.31. Found: C, 38.65; H, 2.47; N, 2.20.

Synthesis of 80. A solution of the ligand **78** (400 mg, 1.07 mmol) in THF (4 ml) was added dropwise to a suspension of (tht)AuCl (171.75 mg, 0.535 mmol) in THF (1 ml) at room temperature inside the glovebox. It was left to stir for 2 h in a vessel protected from the incident light. The solution was concentrated. Addition of pentane led to the precipitation of the product which was recovered by filtration and washed with pentane.

Yield: 420 mg, 80%. Single crystals were obtained by slow diffusion of pentane into a THF solution of the complex. ^{1}H NMR (499 MHz, cdcl$_3$) δ 10.51 (s, 2H, N-*H*), 7.71 – 7.57 (m, 4H), 7.53 (dd, *J* = 11.5, 4.4 Hz, 12H), 7.41 (t, *J* = 7.6 Hz, 8H), 7.33 (t, *J* = 7.6 Hz, 2H), 6.92 (bs, 2H). ^{13}C NMR (126 MHz, cdcl$_3$) δ 156.33 (s), 156.02 (s), 137.65 (s), 134.25 (s), 133.73 (s), 132.74 (s), 132.05 (s), 129.76 (s), 129.38 (s), 128.13 (s), ^{19}F NMR ($CDCl_3$, 469.93 MHz): δ -75.15 (s). ^{31}P NMR ($CDCl_3$, 202.17 MHz): δ 35.78 (bs). Elemental analysis (%) calculated for $C_{40}H_{30}AuClF_6N_2O_2P_2$: C, 49.07; H, 3.09; N, 2.86. Found: C, 48.21; H, 3.13; N, 2.75.

General procedure for catalytic cyclization of Propargylic Amides in CH_2Cl_2.

5 mol% freshly prepared **79** (5 mg, 0.00825 mmol) was added to a solution of the appropriate propargylic amide (0.1650 mmol) in 2 mL CH_2Cl_2 in a 20 mL vial. The progress of the reaction was monitored by injecting an aliquot of 10 μL in the GC spectrometer and the gas chromatogram was recorded for 18 min at 250°C.

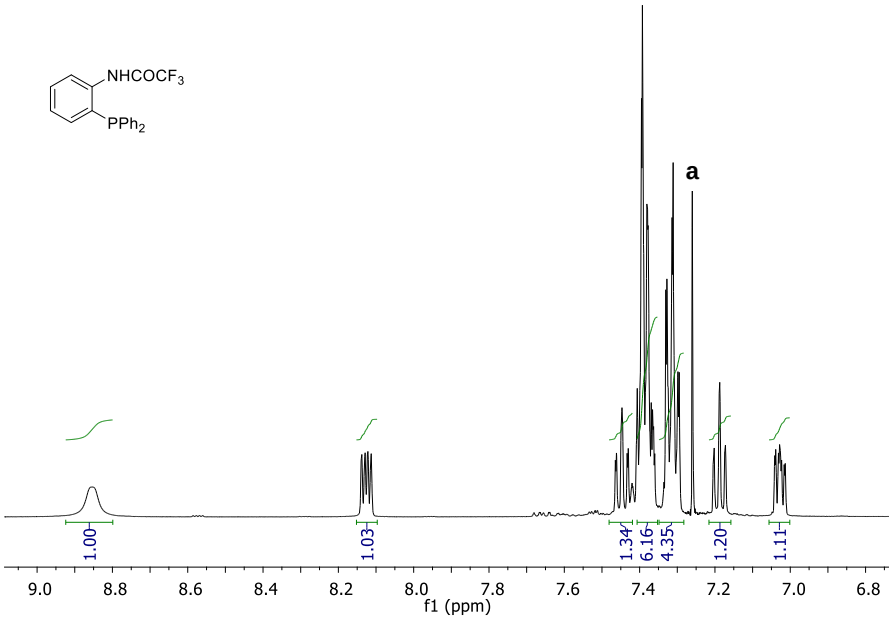

Figure 86. ^{1}H NMR spectrum of **78** in $CDCl_3$. Residual solvent peak is shown in the spectrum. a) $CHCl_3$

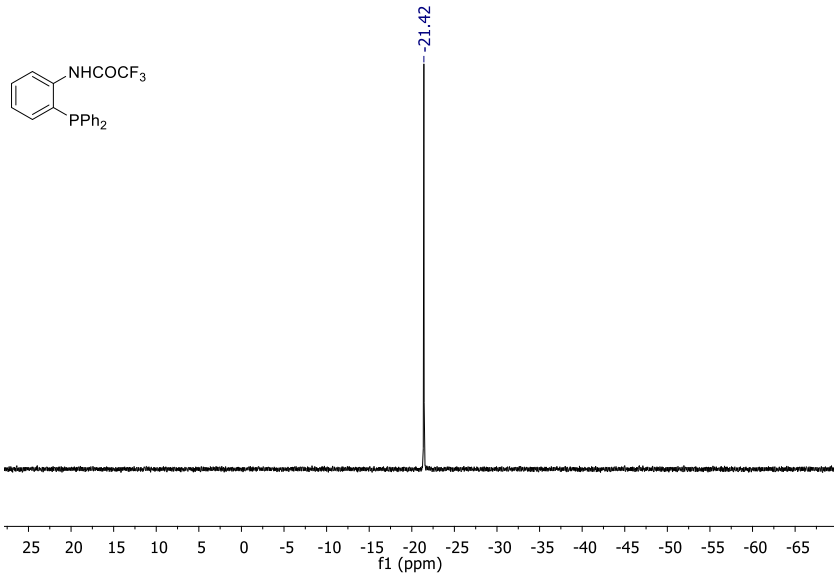

Figure 87. ^{31}P NMR spectrum of **78** in $CDCl_3$

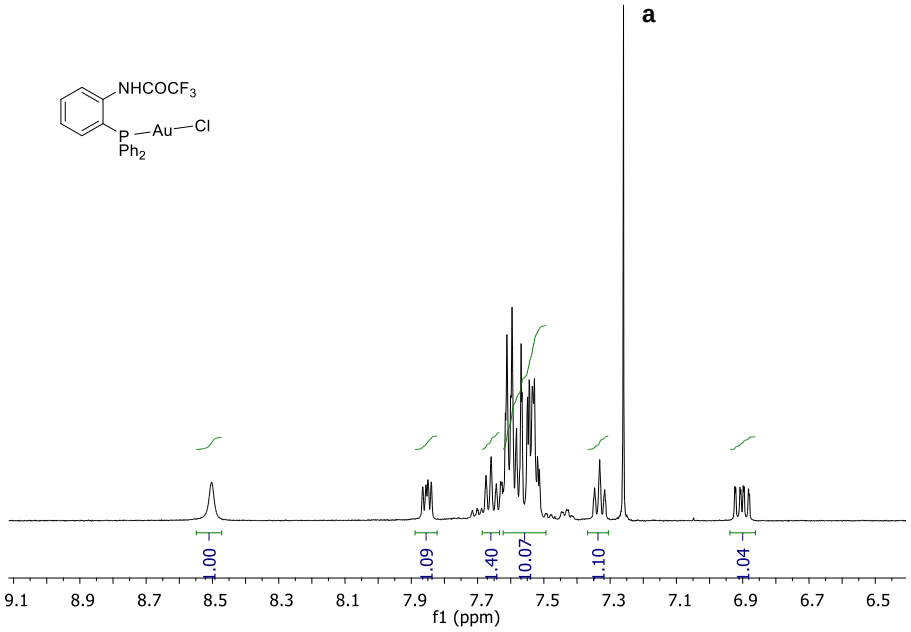

Figure 88. ^{1}H NMR spectrum of **79** in $CDCl_3$. Residual solvent peak is shown in the spectrum. a) $CHCl_3$

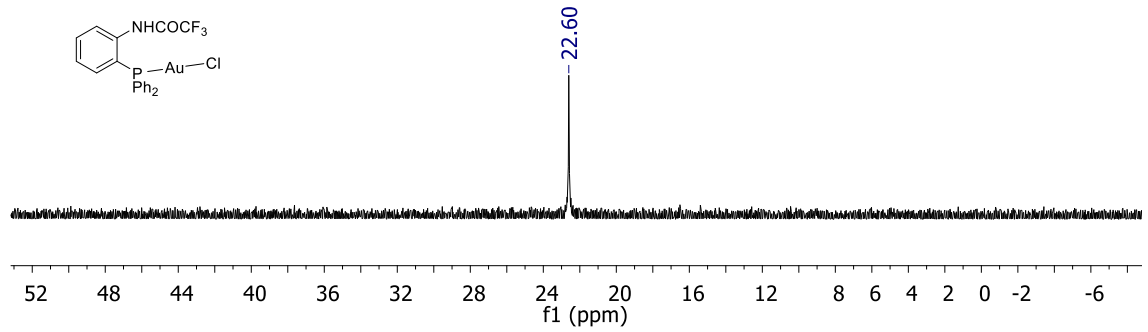

Figure 89. ^{31}P NMR spectrum of **79** in $CDCl_3$.

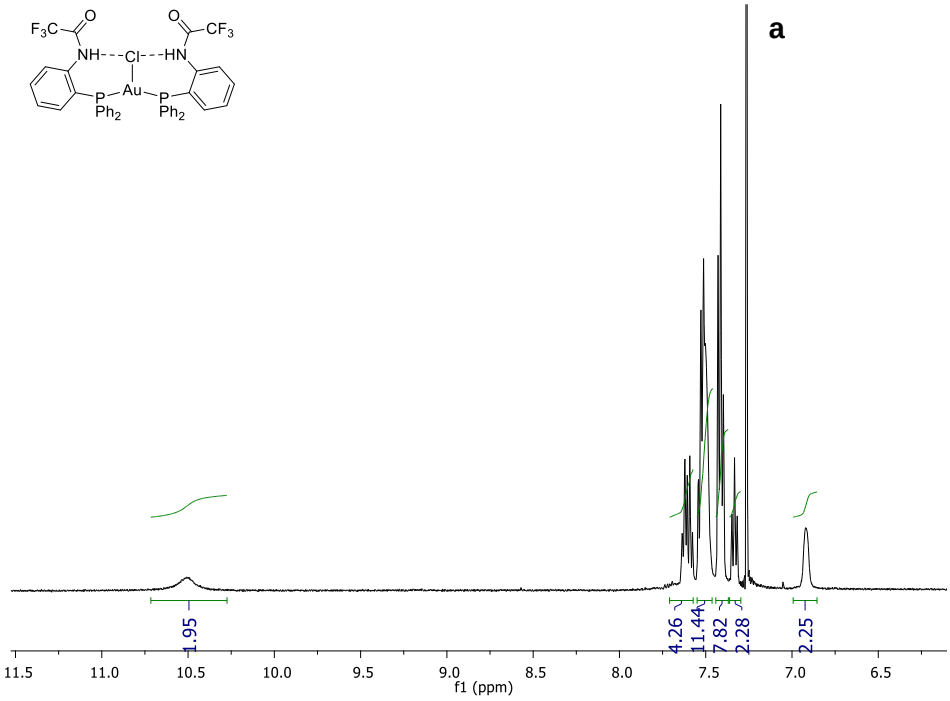

Figure 90. ^{1}H NMR spectrum of **80** in $CDCl_3$

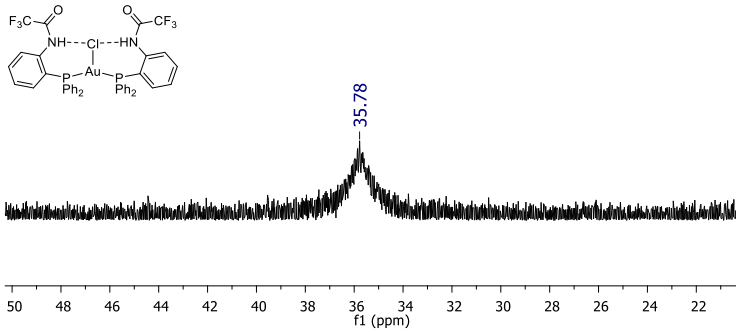

Figure 91. ^{31}P NMR spectrum of **80** in $CDCl_3$.

Determination of relative rate of diffusion of 79 via PGSE Experiment in CD_2Cl_2 with 1,3,5-Tri-*tert*-butylbenzene as a reference.

An NMR tube was charged with 5 mg (0.00825 mmol) of **79**, 2 mg (0.00825 mmol) of 1,3,5-tri-*tert*-butylbenzene (**A**) and 0.5 mL $CDCl_3$. The resulting solution was subjected to Pulse Gradient Spin Echo measurements using a 400MHz Brucker Avance III spectrometer. The gradient strength was incremented in 7% steps from 2% to 72%. The relevant parameters for the experiment were: Δ = 150 ms, δ = 1 ms, d1= 18 sec.

$$\ln (I/I_0) = -\gamma^2\delta^2G^2 (\Delta - \delta/3)\ \mathbf{D} \qquad \text{Eq (1)}$$

$$\mathbf{D} = \frac{kT}{6\pi\eta \boldsymbol{r}} \qquad \text{Eq (2)}$$

According to the Stokes-Einstein equation (Eq. 2), the ratio of the slopes is inversely proportional to the ratio of the corresponding radii. The radius of **79** was determined from the ratio of slopes and the reported value of the radius of 1,3,5-tri-*tert*-butylbenzene.

$\mathbf{V}_{\text{X-ray}}(\mathbf{79})$ = 504 Å^3

$\boldsymbol{r}_{\text{X-ray}}(\mathbf{79})$ = 4.94 Å

$\mathbf{V}_{\text{X-ray}}(\mathbf{A})$ = 454 Å^3

$\boldsymbol{r}_{\text{X-ray}}(\mathbf{A})$ = 4.77 Å

$\boldsymbol{r}_{\text{PGSE}}(\mathbf{79})$ = 4.77 × (4.0556 / 3.6177) Å = 5.65 Å

V_{PGSE} (**79**) = $\frac{4}{3}\pi r^3$ = 755 Å^3

Low resolution MS-ESI$^-$

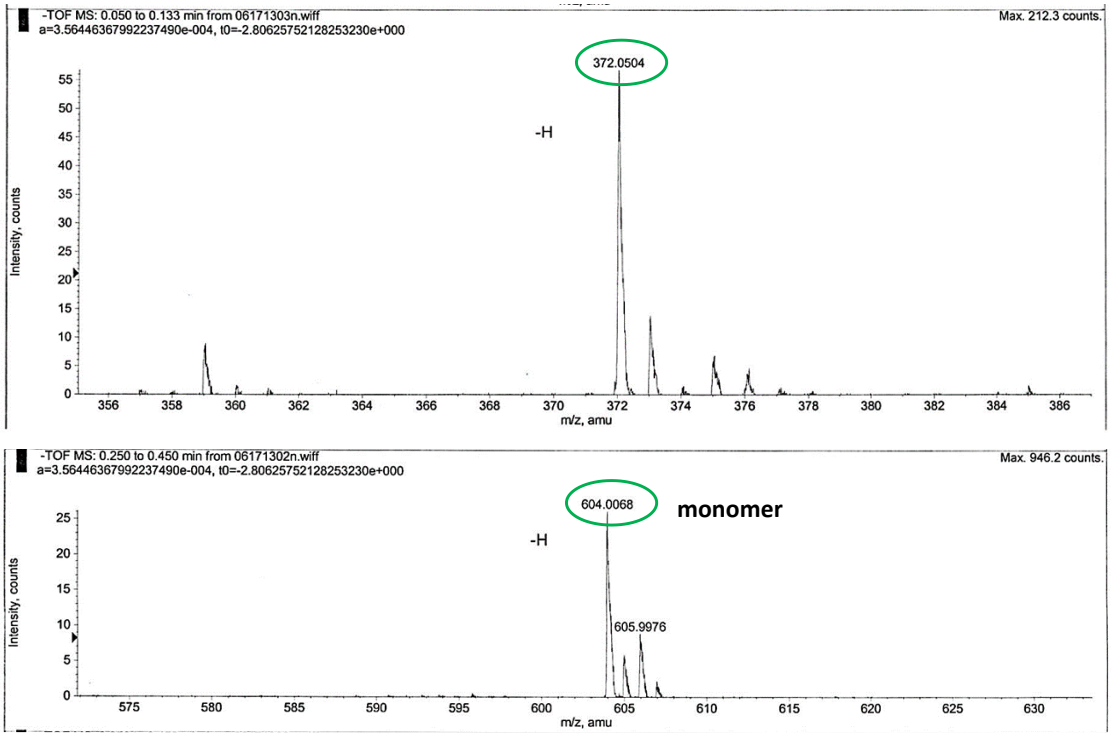

Figure 92. ESI-MS- spectra of the ligand **78** (top) and **79** (bottom).

Catalysis of propargylic amides monitored by Gas Chromatography

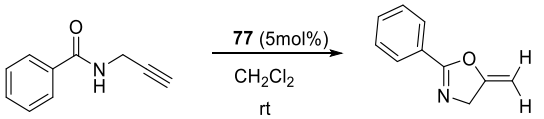

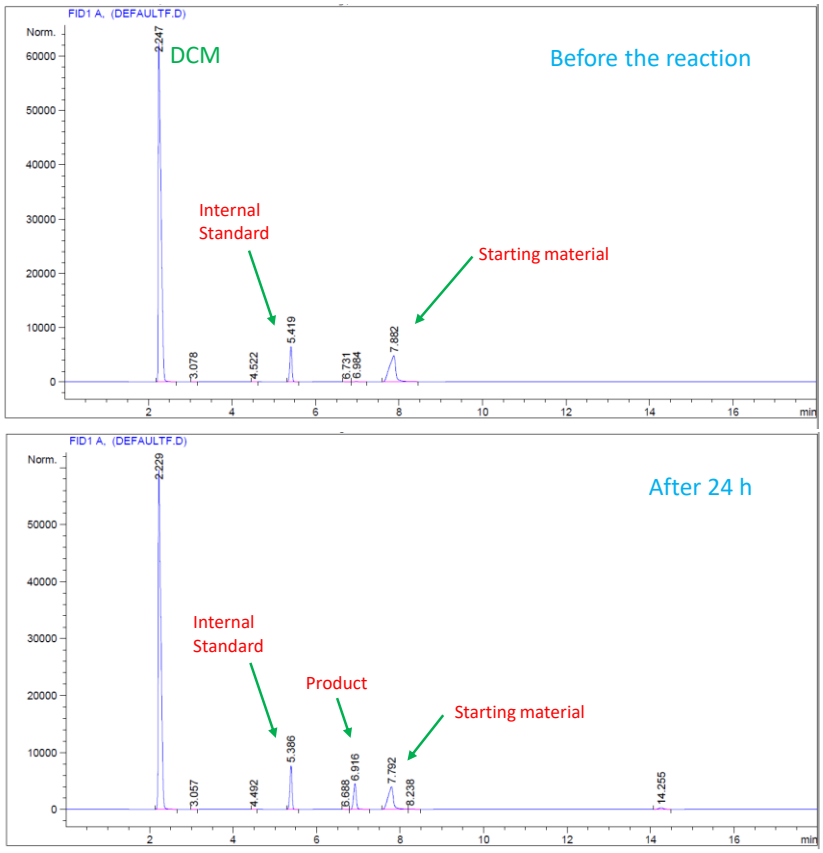

Figure 93. GC trace obtained for the cyclization of N-(prop-2-yn-1-yl)-benzamide catalyzed by **79** in CH_2Cl_2.

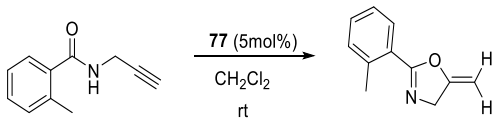

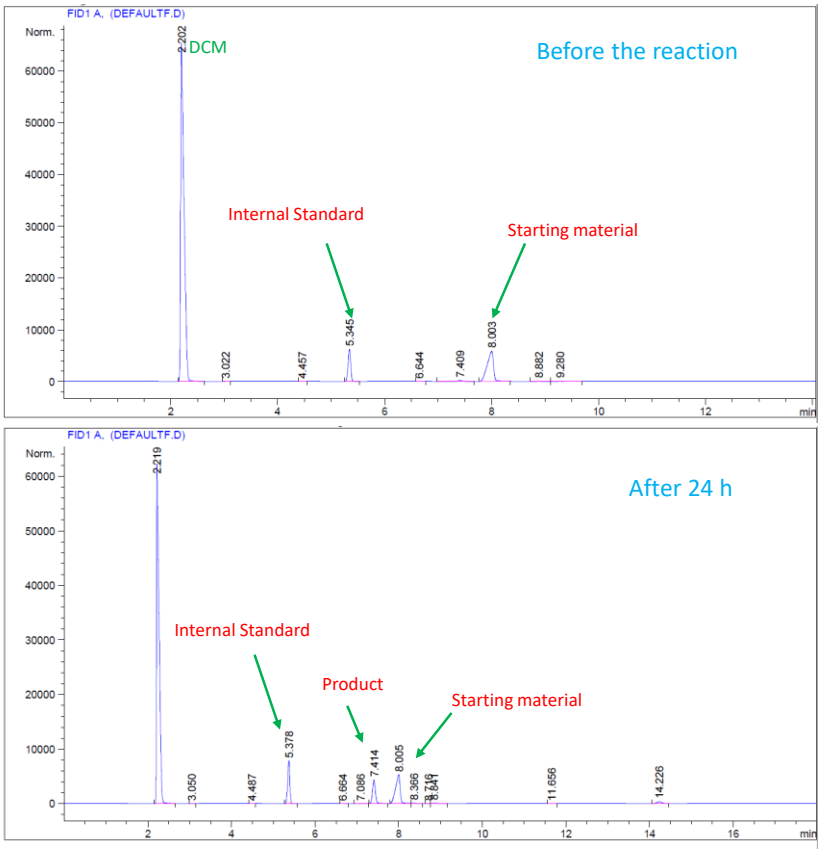

Figure 94. GC trace obtained for the cyclization of N-(prop-2-yn-1-yl)-2-methylbenzamide catalyzed by **79** in CH_2Cl_2.

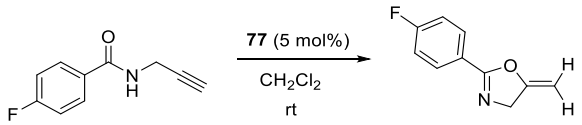

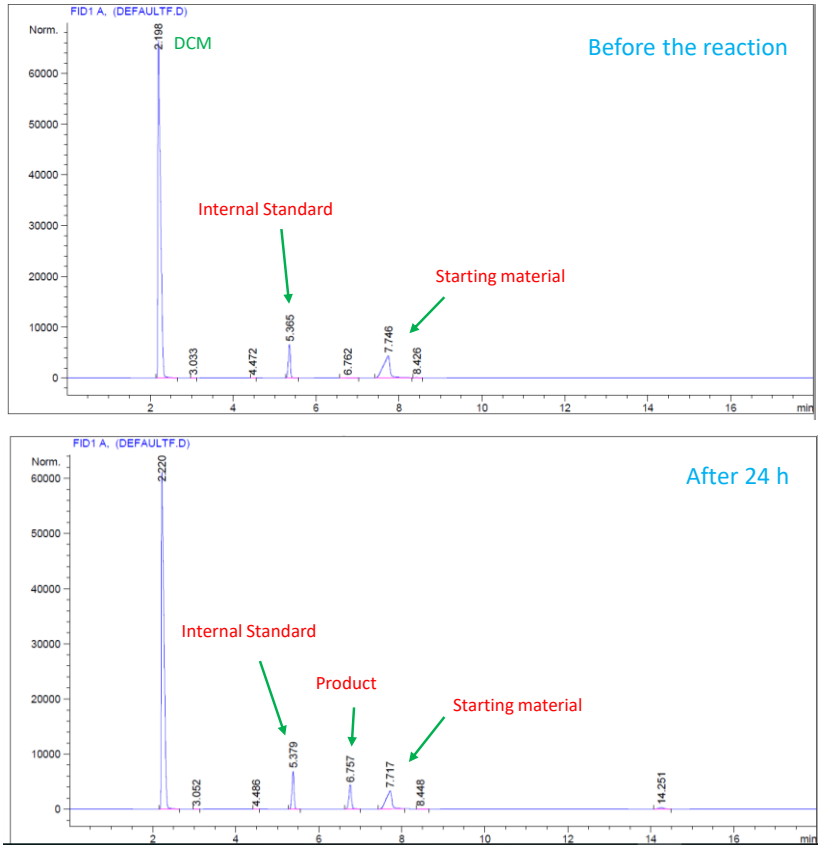

Figure 95. GC trace obtained for the cyclization of N-(prop-2-yn-1-yl)-4-fluorobenzamide catalyzed by **79** in CH_2Cl_2.

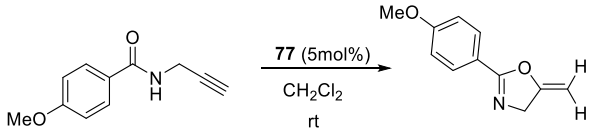

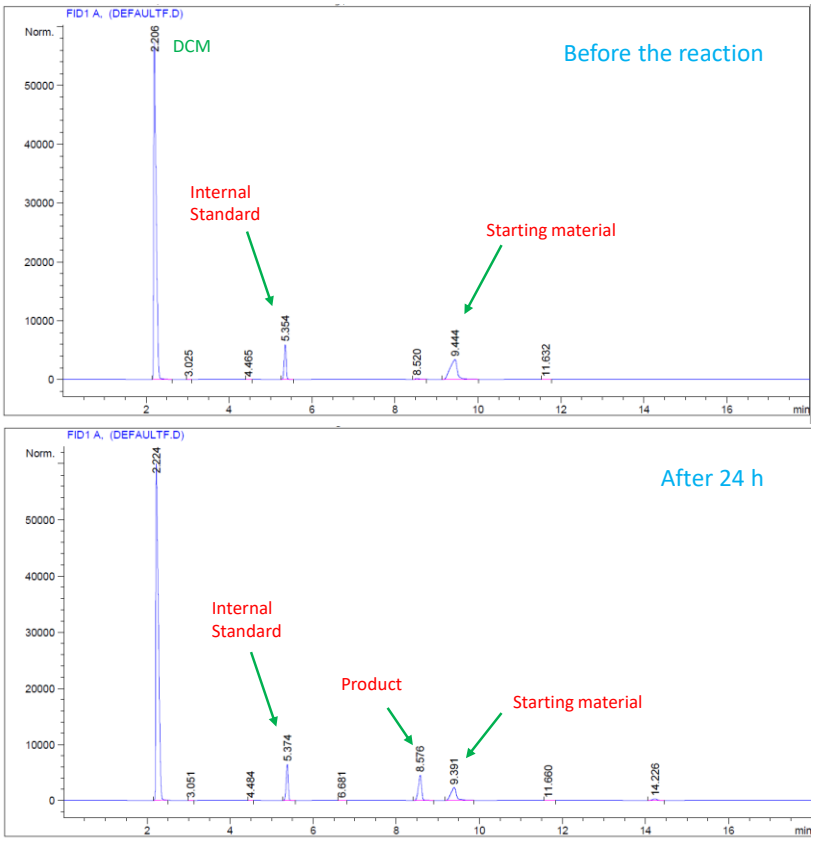

Figure 96. GC trace obtained for the cyclization of N-(prop-2-yn-1-yl)-4-methoxybenzamide catalyzed by **79** in CH_2Cl_2.

7. SUMMARY

7.1 Investigation of anion- and redox control positional switching of a Ph

In this section, I revisited the chemistry that had been developed by my predecessor Dr. Ke who found anion exchange can used to dictate the position of a phenyl ligand around the dinuclear core of a SbAu complex featuring two ancillary phosphine ligands. As part of my work, I found that this structural changes are reversible and **55** can be converted into **54** by stepwise fluoride abstraction using TBDMSCl (Figure 97). I also found that complex **58** is an intermediate in this reaction. This new complex was characterized by heteronuclear NMR and X-ray diffraction studies. By identifying this intermediate, I proved that the dominant factor in the positional switching of the ligands around antimony is the trans influence of the said ligands. Even when only one chloride is replaced by a fluoride anion, the reduced electron density on gold resulting from the electron withdrawing effect of the fluorostibonium moiety forces the strong trans-influencing Ph group to occupy a position perpendicular to the Au-Sb bond vector. I also discovered that the complex connecting **56** to **57** had been mistakenly assigned by Dr. Ke. Rather than being an Au-F complex, I discovered that the intermediate complex **59** is zwitterionic and that it possesses a trifluorotriarylantiminate moiety (Figure 97). The formation of **59** can be explained by the affinity of the hard fluoride anion towards the hard antimony center rather than the soft gold center. Complex **59** is the only compound in this series of gold-stiboaranes which features a disrupted interaction between the cationic linear gold center and an anionic trifluoroantimony center. The migration of the

Ph group from antimony to gold was stimulated by the stability imparted by the formation of the Sb-Au bond in the rearranged product **57** which features the strongest Au→Sb interaction.

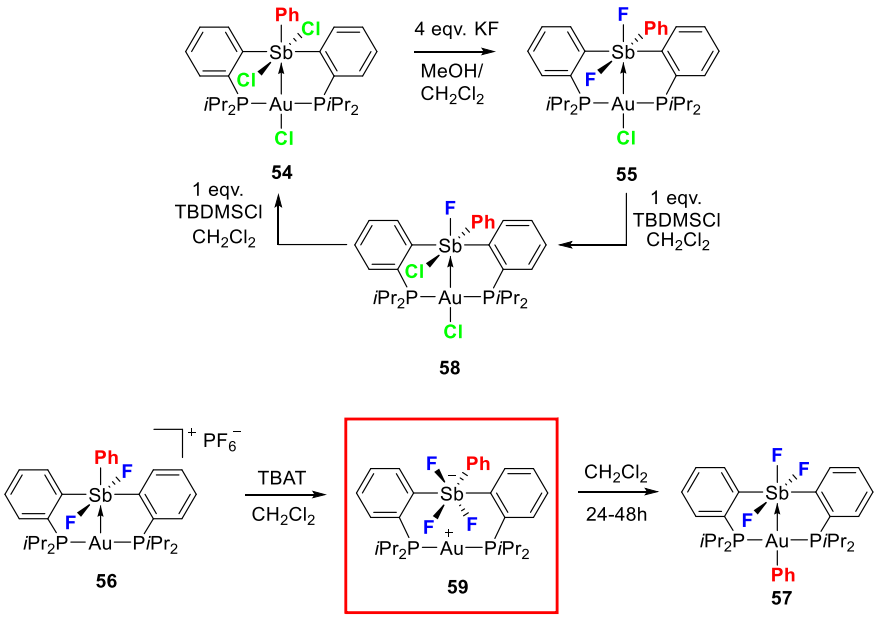

Figure 97. Synthesis of complexes **58** and **59**.

The progression of the three stages were studied computationally to gain insights into the change in the Au→Sb interaction upon the exchange and addition of halides. QTAIM calculations carried out on the series of gold-stiborane complexes **54-59** unambiguously established the effect of the anion exchange reactions on the dinuclear Sb-Au core.

7.2 Effect of peripheral ligands on catalytic activity of gold

To study the influence of peripheral ligands on the reactivity of the gold center, a series of cationic gold/antimony complexes were synthesized. To this end, we oxidized the gold chloride complex **61** using *o*-chloranil to form the corresponding gold/tetrachlorocatecholatestiborane complex **62**. Complex **62** shows depleted electron density on the gold center as a direct manifestation of the increased electrophilicity of the antimony(V) center. Complex **62** differ from the reported complex **20** by the orientation of the Ph group on antimony, which is trans to the gold center in **20** but perpendicular to the Au-Sb bond axis in **62**. As observed in the cases of complexes **54** and **55**, the nature of ligand trans to the gold center affects the strength of the Au→Sb interaction. The presence of the strong electron accepting catecholate oxygen trans to gold intensifies the Au-Sb interaction to such an extent that it can be considered a covalent type interaction, whereas in **62,** the Sb-Au bond fits the donor-acceptor paradigm as a result of the Ph group occupying the trans position.

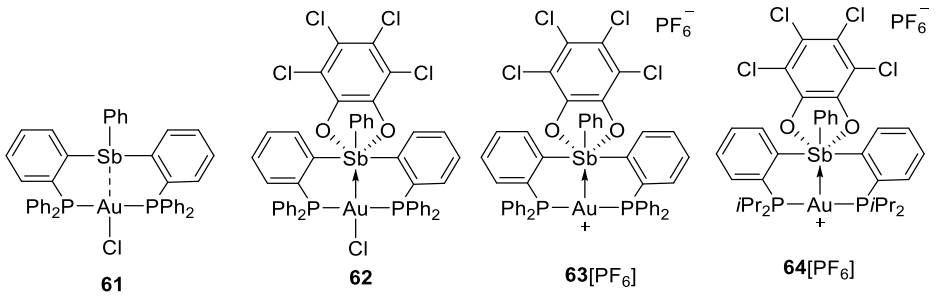

Figure 98. Gold-antimony complexes described in Section 3.

In an effort to produce the potential catalysts, abstraction of the gold-bound chloride was carried out on **62** and **20** resulting in the formation of T-shaped complexes $\mathbf{63}^+$ and $\mathbf{64}^+$ which only differ by the nature of the phosphine substituents. Surprisingly, in both these cations the phenyl group now occupies the trans position which can be rationalized on the basis of the reduced electron density on gold which weakens the Au→Sb donation. Reactivity studies, revealed that $\mathbf{64}^+$ is catalytically inactive in reaction necessitating alkyne activation. This lack of activity is assigned to the steric bulk of the ancillary *i*Pr_2P ligands which block access to the reactive gold center. The use of the less sterically imposing Ph_2P substituents in $\mathbf{63}^+$ makes this complex an effective catalyst for alkyne hydroamination reactions and propargylamide cyclization reactions. These hypothesis regarding the reactivity of $\mathbf{63}^+$ and $\mathbf{64}^+$ was supported by the structural and theoretical studies which helped us understand the influence of the ancillary ligands on the reactivity of gold/stiboranes.

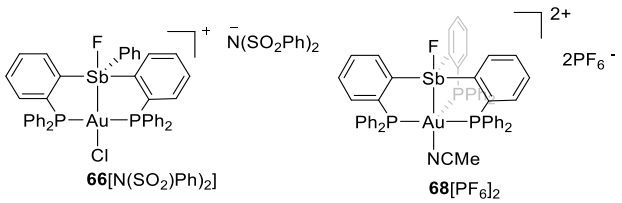

Figure 99. Mono- and dicationic gold-stibonium complexes described in Section 3.

We have also carried out the synthesis of gold(I) complex **66**$[N(SO_2Ph)_2]$ (Figure 99) supported by a stibonium ligand. The effect of the adjoining fluorostibonium moiety

was evident from the strengthening of the gold chloride bond to such an extent that it rendered the abstraction of the gold-bound chloride anion impossible. The successful synthesis of a diacationic gold complex **68**$[PF_6]_2$ featuring both a cationic gold center and a stibonium was achieved using a tetradentate phosphinostibine ligand (Figure 99). Unfortunately, σ-electron withdrawing strength of the fluorostibonium in the case of was insufficient to overcome the electron donating effect of the coordinating phosphines around gold. Thus, complex **68**$[PF_6]_2$ showed poor catalytic reactivity in hydromaination of alkynes due to the mild electrophilicity of the gold center as well as the steric crowding around the gold atom. Altogether, these results demonstrated that different routes can be used to access novel mono- and dicationic gold/stibonium complexes.

7.3 Activation of a Sb/Pt catalyst with Brønsted acid

Antimony based Lewis acidic ligands have shown remarkable reactivity when coordinated to metal centers. Hypervalent stiboranes have played an important role in inducing catalytic reactivity in the coordinated cationic gold centers via strong metal-ligand interactions. Such reactivity can be considered to be achieved in related transition metals such as platinum. We have revisited the synthesis of trifluorostiborane platinum(0) complexes with the aim of finding a stable derivative capable of activating small molecules. A stable, easily synthesized and tractable trifluorostiborane platinum complex **73** was obtained by the reaction of **35** with excess TlF and PhCN. In this complex, the PhCN coordinates to the Pt center, thus stabilizing this molecule towards spectroscopic

and elemental analysis. The interaction between the antimony and the metal center was investigated computationally.

Despite a strong Sb→Pt interaction, this complex failed to activate alkynes due to the stable coordination of the nitrile. However, addition of HBF_4 turns the catalysis on, presumably because of Sb-F bond protonolysis leading to a more electrophilic complex.

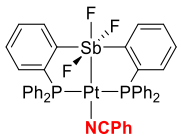

73

Figure 100. Trifluorstiborane-platinum(0) complex described in Section 4.

7.4 Photoreductive elimination from Sb/Au and Sb/Pd platforms

Photoredox reactions are of relevance to the field of solar fuel productions. In this thesis, I have investigated several main group-late transition metal complexes with the objective of observing photoreduction of the main group center. I synthesized the pincer gold complex **75** which features a chlorostibine ligand with two di-*iso*-propylphosphines coordinated to gold. Complex **75** eliminated one equivalent of chlorine upon photolysis in THF to produce the corresponding reduced stibine complex 6 (Figure 101). The photoreductive elimination process was monitored by ^{31}P NMR spectroscopy and UV-Vis spectroscopy. The use of di-*iso*-propylphosphinostibine increases the solubility of the species compared to its diphenylphosphinostibine analog leading to a more efficient

chlorine elimination process. This is the first example of a main group element based photoreductive elimination of halogen from a gold complex.

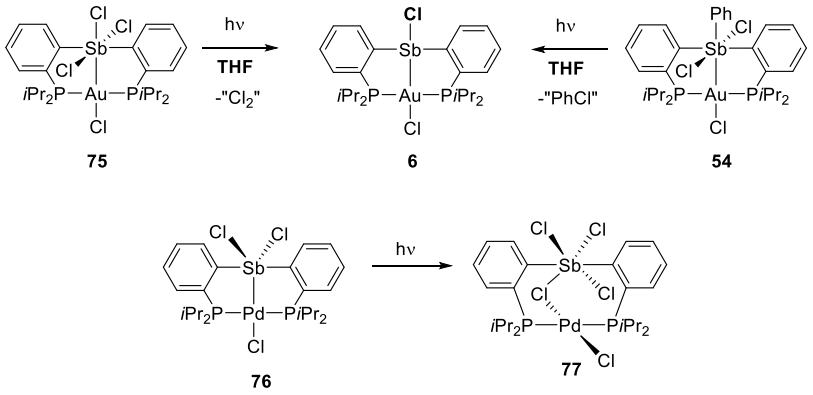

Figure 101. Photolysis of **54**, **75** and **77**.

Similar reactivity was also observed in the case of a Pd complex **77** (Figure 101), whose solubility was also significantly improved compared to that of the reported analog **38**. Inspired by the success of this platform, we investigated the possibility of chlorobenzene elimination from a gold/stiborane platform **54**. We were excited to observe the elimination of Ph• and Cl• from complex **54** (Figure 101).

7.5 Self-activation of Au-Cl by pendant H-bond donor functionality

Activation of an Au-Cl bond without an external activator has become the new challenge in the domain of gold catalysis. To overcome the synthetic challenges posed by the use of silver additive in gold catalysis, several alternate methods have been developed by organometallic chemists. Drawing inspiration from the fast-developing field of anion-

abstraction catalysis, we decided to employ H-bond donor functionalities for the activation of gold catalysts. In this project, we have explored the possibility of activating an Au-Cl bond using a newly designed ambiphilic phosphine/H-bond donor ligand **78** in which the H-bond donor functionality is a trifluoroacetamide.

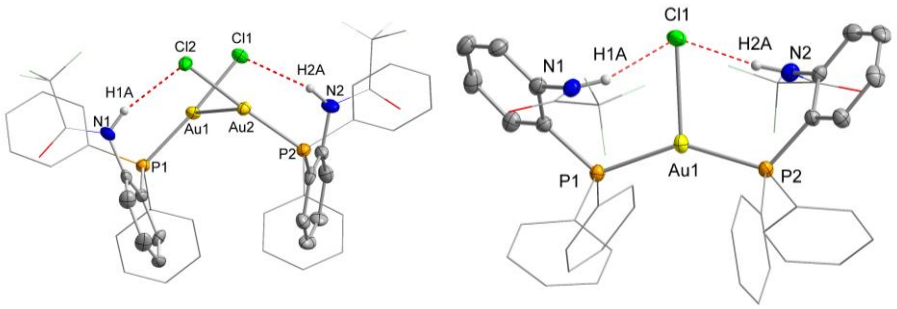

Figure 102. Solid state structures of **79** and **80** featuring H-bonding interaction.

The coordination chemistry of **78** with gold(I) has been studied both structurally and spectroscopically. The solid state structures of the gold(I) complexes **79** and **80** show the presence of NH---Cl hydrogen bonding interactions (Figure 102). We have also found that complex **79**, which is dimeric in nature in the solid state, behaves as a self-activating catalyst for the cycloisomerization of propargyliamides. In an effort to probe the identity of the catalytically active species in solution, we performed Pulse Gradient Spin Echo measurements by using diffusion NMR spectroscopy. The PGSE experiment revealed that the complex establishes a monomer-dimer equilibrium in $CDCl_3$ and in CH_2Cl_2. Further control experiments proved that the presence of the H-bond donor functionality in close proximity of the gold center is necessary for the self-activation process. We believe that

this work establishes an interesting bridge between the area of gold catalysis and that of anion-pairing organocatalysis.

REFERENCES

1. Lewis, G. N., *Valence and the structure of atoms and molecules*. Dover Publications: New York, 1966.
2. Weicker, S. A.; Stephan, D. W., *Bull. Chem. Soc. Jpn.* **2015,** *88*, 1003.
3. Sivaev, I. B.; Bregadze, V. I., *Coord. Chem. Rev.* **2014,** *270–271*, 75.
4. Guo, Z.; Shin, I.; Yoon, J., *Chem. Commun.* **2012,** *48*, 5956.
5. Wade, C. R.; Broomsgrove, A. E. J.; Aldridge, S.; Gabbaï, F. P., *Chem. Rev.* **2010,** *110*, 3958.
6. Ishihara, K. In *Chiral B(III) Lewis acids*, Wiley-VCH Verlag GmbH: 2000; pp 135.
7. Ishihara, K. In *Achiral B(III) Lewis acids*, Wiley-VCH Verlag GmbH: 2000; pp 89.
8. Ishihara, K.; Yamamoto, H., *Eur. J. Org. Chem.* **1999**, 527.
9. Yao, M.-L.; Kabalka, G. W. In *Organic synthesis using boron and organoboron halides*, CRC Press: 2012; pp 579.
10. Chen, E. Y.-X.; Marks, T. J., *Chem. Rev.* **2000,** *100*, 1391.
11. Erker, G., *Chem. Commun.* **2003**, 1469.
12. Simocko, C.; Wagener, K. B., *Organometallics* **2013,** *32*, 2513.
13. McCahill, J. S. J.; Welch, G. C.; Stephan, D. W., *Angew. Chem. Int. Ed.* **2007,** *46*, 4968.
14. Chuit, C.; Corriu, R. J. P.; Reye, C.; Young, J. C., *Chem. Rev.* **1993,** *93*, 1371.
15. Holmes, R. R., *Chem. Rev.* **1996,** *96*, 927.
16. Olah, G. A.; Schlosberg, R. H., *J. Am. Chem. Soc.* **1968,** *90*, 2726.

17. Olah, G. A.; Klopman, G.; Schlosberg, R. H., *J. Am. Chem. Soc.* **1969,** *91*, 3261.

18. Olah, G. A., *J. Org. Chem.* **2005,** *70*, 2413.

19. Gutmann, V.; Hubacek, H.; Steininger, A., *Monatsh. Chem.* **1964,** *95*, 678.

20. Krossing, I.; Raabe, I., *Chem. Eur. J.* **2004,** *10*, 5017.

21. Yi, W.; Tan, N., *Acta Crystallogr., Sect. E* **2011,** *67*, 917.

22. Ohkata, K.; Takemoto, S.; Ohnishi, M.; Akiba, K.-y., *Tetrahedron Lett.* **1989,** *30*, 4841.

23. Althaus, H.; Breunig, H. J.; Lork, E., *Organometallics* **2001,** *20*, 586.

24. Copolovici, D.; Isaia, F.; Breunig, H. J.; Rat, C. I.; Silvestru, C., *RSC Adv.* **2014,** *4*, 26569.

25. Hirai, M.; Gabbai, F. P., *Chem. Sci.* **2014,** *5*, 1886.

26. Hirai, M.; Gabbaï, F. P., *Angew. Chem. Int. Ed.* **2015,** *54*, 1205.

27. Hirai, M.; Myahkostupov, M.; Castellano, F. N.; Gabbaï, F. P., *Organometallics* **2016**.

28. Chen, C.-H.; Gabbaï, F. P., *Angew. Chem. Int. Ed.* **2017,** *56*, 1799.

29. Ke, I.-S.; Myahkostupov, M.; Castellano, F. N.; Gabbaï, F. P., *J. Am. Chem. Soc.* **2012,** *134*, 15309.

30. Green, M. L. H., *J. Organomet. Chem.* **1995,** *500*, 127.

31. Bouhadir, G.; Bourissou, D., Coordination of Lewis acids to transition metals: Z-type ligands. *Struct. Bond.*, 2017; Vol. 171, pp 141.

32. Kameo, H.; Nakazawa, H., *Chem. Rec.* **2017,** *17*, 268.

33. Amgoune, A.; Bourissou, D., *Chem. Commun.* **2011,** *47*, 859.

34. Werner, H., *Angew. Chem. Int. Ed. Engl.* **1983,** *22*, 927.

35. Shriver, D. F., *J. Am. Chem. Soc.* **1963,** *85*, 3509.

36. Shriver, D. F., *Acc. Chem. Res.* **1970,** *3*, 231.

37. Shriver, D. F.; Sailor, M. J., *Acc. Chem. Res.* **1988,** *21*, 374.

38. Muir, K. W.; Ibers, J. A., *Inorg. Chem.* **1969,** *8*, 1921.

39. Burlitch, J. M.; Leonowicz, M. E.; Petersen, R. B.; Hughes, R. E., *Inorg. Chem.* **1979,** *18*, 1097.

40. Braunschweig, H.; Gruss, K.; Radacki, K., *Angew. Chem. Int. Ed.* **2007,** *46*, 7782.

41. Braunschweig, H.; Gruss, K.; Radacki, K., *Inorg. Chem.* **2008,** *47*, 8595.

42. Bontemps, S.; Bouhadir, G.; Miqueu, K.; Bourissou, D., *J. Am. Chem. Soc.* **2006,** *128*, 12056.

43. Bontemps, S.; Gornitzka, H.; Bouhadir, G.; Miqueu, K.; Bourissou, D., *Angew. Chem. Int. Ed.* **2006,** *45*, 1611.

44. Bontemps, S.; Bouhadir, G.; Dyer, P. W.; Miqueu, K.; Bourissou, D., *Inorg. Chem.* **2007,** *46*, 5149.

45. Bontemps, S.; Sircoglou, M.; Bouhadir, G.; Puschmann, H.; Howard, J. A. K.; Dyer, P. W.; Miqueu, K.; Bourissou, D., *Chem. Eur. J.* **2008,** *14*, 731.

46. Sircoglou, M.; Bontemps, S.; Bouhadir, G.; Saffon, N.; Miqueu, K.; Gu, W.; Mercy, M.; Chen, C.-H.; Foxman, B. M.; Maron, L.; Ozerov, O. V.; Bourissou, D., *J. Am. Chem. Soc.* **2008,** *130*, 16729.

47. Gualco, P.; Lin, T.-P.; Sircoglou, M.; Mercy, M.; Ladeira, S.; Bouhadir, G.; Pérez, L. M.; Amgoune, A.; Maron, L.; Gabbaï, F. P.; Bourissou, D., *Angew. Chem. Int. Ed.* **2009,** *48*, 9892.

48. Gualco, P.; Mallet-Ladeira, S.; Kameo, H.; Nakazawa, H.; Mercy, M.; Maron, L.; Amgoune, A.; Bourissou, D., *Organometallics* **2015,** *34*, 1449.

49. Gualco, P.; Mercy, M.; Ladeira, S.; Coppel, Y.; Maron, L.; Amgoune, A.; Bourissou, D., *Chem. Eur. J.* **2010,** *16*, 10808.

50. Kameo, H.; Ikeda, K.; Bourissou, D.; Sakaki, S.; Takemoto, S.; Nakazawa, H.; Matsuzaka, H., *Organometallics* **2016,** *35*, 713.

51. Kameo, H.; Kawamoto, T.; Sakaki, S.; Bourissou, D.; Nakazawa, H., *Chem. Eur. J.* **2016,** *22*, 2370.

52. Lin, T.-P.; Gabbaï, F. P., *Polyhedron* **2017,** *125*, 18.

53. Levason, W.; McAuliffe, C. A., *Acc. Chem. Res.* **1978,** *11*, 363.

54. Hope, E. G.; Levason, W.; Powell, N. A., *Inorg. Chim. Acta* **1986,** *115*, 187.

55. Cavaglioni, A.; Cini, R., *Polyhedron* **1997,** *16*, 4045.

56. Srivastava, K. V.; Bhatt, D. S.; Shukla, S. R.; Bajaj, C. H.; Jasra, V. R., *React. Kinet. Catal. Lett.* **2005,** *85*, 3.

57. Wache, S.; Herrmann, W. A.; Artus, G.; Nuyken, O.; Wolf, D., *J. Organomet. Chem.* **1995,** *491*, 181.

58. Benjamin, S. L.; Levason, W.; Reid, G.; Warr, R. P., *Organometallics* **2012,** *31*, 1025.

59. Benjamin, S. L.; Levason, W.; Light, M. E.; Reid, G.; Rogers, S. M., *Organometallics* **2014,** *33*, 2693.

60. Wade, C. R.; Lin, T.-P.; Nelson, R. C.; Mader, E. A.; Miller, J. T.; Gabbaï, F. P., *J. Am. Chem. Soc.* **2011,** *133*, 8948.

61. Lin, T.-P.; Wade, C. R.; Pérez, L. M.; Gabbaï, F. P., *Angew. Chem. Int. Ed.* **2010,** *49*, 6357.

62. Ke, I.-S.; Gabbaï, F. P., *Inorg. Chem.* **2013,** *52*, 7145.

63. Wade, C. R.; Ke, I.-S.; Gabbaï, F. P., *Angew. Chem. Int. Ed.* **2012,** *51*, 478.

64. Jones, J. S.; Wade, C. R.; Gabbaï, F. P., *Organometallics* **2015,** *34*, 2647.

65. Burton, J. W., *Sci. Synth.* **2002,** *4*, 53.

66. Malisch, W.; Kuhn, M., *J. Organometal. Chem.* **1974,** *73*, C1.

67. Wade, C. R.; Gabbaï, F. P., *Angew. Chem. Int. Ed.* **2011,** *50*, 7369.

68. Harman, W. H.; Peters, J. C., *J. Am. Chem. Soc.* **2012,** *134*, 5080.

69. MacMillan, S. N.; Hill Harman, W.; Peters, J. C., *Chem. Sci.* **2014,** *5*, 590.

70. Barnett, B. R.; Moore, C. E.; Rheingold, A. L.; Figueroa, J. S., *J. Am. Chem. Soc.* **2014,** *136*, 10262.

71. Bouhadir, G.; Bourissou, D., *Chem. Soc. Rev.* **2016,** *45*, 1065.

72. Inagaki, F.; Matsumoto, C.; Okada, Y.; Maruyama, N.; Mukai, C., *Angew. Chem. Int. Ed.* **2015,** *54*, 818.

73. Nocera, D. G., *Inorg. Chem.* **2009,** *48*, 10001.

74. Powers, D. C.; Anderson, B. L.; Nocera, D. G., *J. Am. Chem. Soc.* **2013,** *135*, 18876.

75. Yang, H.; Gabbai, F. P., *Nat Chem* **2015,** *7*, 12.

76. Cook, T. R.; Dogutan, D. K.; Reece, S. Y.; Surendranath, Y.; Teets, T. S.; Nocera, D. G., *Chem. Rev.* **2010,** *110*, 6474.

77. Cook, T. R.; McCarthy, B. D.; Lutterman, D. A.; Nocera, D. G., *Inorg. Chem.* **2012,** *51*, 5152.

78. Cook, T. R.; Surendranath, Y.; Nocera, D. G., *J. Am. Chem. Soc.* **2009,** *131*, 28.

79. Powers, D. C.; Chambers, M. B.; Teets, T. S.; Elgrishi, N.; Anderson, B. L.; Nocera, D. G., *Chem. Sci.* **2013,** *4*, 2880.

80. Elgrishi, N.; Teets, T. S.; Chambers, M. B.; Nocera, D. G., *Chem. Commun.* **2012,** *48*, 9474.

81. Heyduk, A. F.; Nocera, D. G., *Science* **2001,** *293*, 1639.

82. Powers, D. C.; Hwang, S. J.; Anderson, B. L.; Yang, H.; Zheng, S.-L.; Chen, Y.-S.; Cook, T. R.; Gabbai, F. P.; Nocera, D. G., *Inorg. Chem.* **2016,** *55*, 11815.

83. Cook, T. R.; Esswein, A. J.; Nocera, D. G., *J. Am. Chem. Soc.* **2007,** *129*, 10094.

84. Jahnke, A. A.; Howe, G. W.; Seferos, D. S., *Angew. Chem. Int. Ed.* **2010,** *49*, 10140.

85. Detty, M. R.; Friedman, A. E., *Organometallics* **1994,** *13*, 533.

86. Detty, M. R.; Friedman, A. E.; McMillan, M., *Organometallics* **1994,** *13*, 3338.

87. McCormick, T. M.; Jahnke, A. A.; Lough, A. J.; Seferos, D. S., *J. Am. Chem. Soc.* **2012,** *134*, 3542.

88. Carrera, E. I.; McCormick, T. M.; Kapp, M. J.; Lough, A. J.; Seferos, D. S., *Inorg. Chem.* **2013,** *52*, 13779.

89. Carrera, E. I.; Seferos, D. S., *Dalton Trans.* **2015,** *44*, 2092.

90. Carrera, E. I.; Lanterna, A. E.; Lough, A. J.; Scaiano, J. C.; Seferos, D. S., *J. Am. Chem. Soc.* **2016,** *138*, 2678.

91. Li, P.-F.; Carrera, E. I.; Seferos, D. S., *ChemPlusChem* **2016,** *81*, 917.

92. Yang, H.; Gabbaï, F. P., *J. Am. Chem. Soc.* **2014,** *136*, 10866.

93. Sahu, S.; Gabbai, F. P., *J. Am. Chem. Soc.* **2017,** *139*, 5035.

94. Khusnutdinova, J. R.; Milstein, D., *Angew. Chem. Int. Ed.* **2015,** *54*, 12236.

95. Grützmacher, H., *Angew. Chem. Int. Ed.* **2008,** *47*, 1814.

96. Owen, G. R., *Chem. Soc. Rev.* **2012,** *41*, 3535.

97. Tsoureas, N.; Kuo, Y.-Y.; Haddow, M. F.; Owen, G. R., *Chem. Commun.* **2011,** *47*, 484.

98. Ekkert, O.; Miera, G. G.; Wiegand, T.; Eckert, H.; Schirmer, B.; Petersen, J. L.; Daniliuc, C. G.; Froehlich, R.; Grimme, S.; Kehr, G.; Erker, G., *Chem. Sci.* **2013,** *4*, 2657.

99. Anderson, J. S.; Rittle, J.; Peters, J. C., *Nature* **2013,** *501*, 84.

100. Crevier, T. J.; Bennett, B. K.; Soper, J. D.; Bowman, J. A.; Dehestani, A.; Hrovat, D. A.; Lovell, S.; Kaminsky, W.; Mayer, J. M., *J. Am. Chem. Soc.* **2001,** *123*, 1059.

101. Sircoglou, M.; Saffon, N.; Miqueu, K.; Bouhadir, G.; Bourissou, D., *Organometallics* **2013,** *32*, 6780.

102. Sircoglou, M.; Mercy, M.; Saffon, N.; Coppel, Y.; Bouhadir, G.; Maron, L.; Bourissou, D., *Angew. Chem. Int. Ed.* **2009,** *48*, 3454.

103. Sircoglou, M.; Bouhadir, G.; Saffon, N.; Miqueu, K.; Bourissou, D., *Organometallics* **2008,** *27*, 1675.

104. Derrah, E. J.; Sircoglou, M.; Mercy, M.; Ladeira, S.; Bouhadir, G.; Miqueu, K.; Maron, L.; Bourissou, D., *Organometallics* **2011,** *30*, 657.

105. Fischbach, A.; Bazinet, P. R.; Waterman, R.; Tilley, T. D., *Organometallics* **2008,** *27*, 1135.

106. Boone, M. P.; Stephan, D. W., *J. Am. Chem. Soc.* **2013,** *135*, 8508.

107. Boudreau, J.; Fontaine, F.-G., *Organometallics* **2011,** *30*, 511.

108. Fontaine, F.-G.; Zargarian, D., *J. Am. Chem. Soc.* **2004,** *126*, 8786.

109. Fontaine, F.-G.; Boudreau, J.; Thibault, M.-H., *Eur. J. Inorg. Chem.* **2008**, 5439.

110. Devillard, M.; Nicolas, E.; Appelt, C.; Backs, J.; Mallet-Ladeira, S.; Bouhadir, G.; Slootweg, J. C.; Uhl, W.; Bourissou, D., *Chem. Commun.* **2014,** *50*, 14805.

111. Jones, J. S.; Gabbai, F. P., *Chem. Eur. J.* **2017,** *23*, 1136.

112. You, D.; Gabbaï, F. P., *J. Am. Chem. Soc.* **2017,** *139*, 6843.

113. Ford, D. D.; Lehnherr, D.; Kennedy, C. R.; Jacobsen, E. N., *ACS Catal.* **2016,** *6*, 4616.

114. Kennedy, C. R.; Lehnherr, D.; Rajapaksa, N. S.; Ford, D. D.; Park, Y.; Jacobsen, E. N., *J. Am. Chem. Soc.* **2016,** *138*, 13525.

115. Brak, K.; Jacobsen, E. N., *Angew. Chem. Int. Ed.* **2013,** *52*, 534.

116. Dahl, E. W.; Szymczak, N. K., *Angew. Chem. Int. Ed.* **2016,** *55*, 3101.

117. Geri, J. B.; Szymczak, N. K., *J. Am. Chem. Soc.* **2015,** *137*, 12808.

118. Moore, C. M.; Bark, B.; Szymczak, N. K., *ACS Catal.* **2016,** *6*, 1981.

119. Moore, C. M.; Szymczak, N. K., *Chem. Sci.* **2015,** *6*, 3373.

120. Moore, C. M.; Szymczak, N. K., *Chem. Commun.* **2015,** *51*, 5490.

121. Hudnall, T. W.; Melaïmi, M.; Gabbaï, F. P., *Org. Lett.* **2006,** *8*, 2747.

122. Hudnall, T. W.; Bondi, J. F.; Gabbaï, F. P., *Main Group Chemistry* **2007,** *5*, 319.

123. Bowman-James, K.; Bianchi, A.; Garcia-Espana, E.; Editors, *Anion Coordination Chemistry*. Wiley-VCH Verlag GmbH & Co. KGaA: 2012; p 559 pp.

124. Busschaert, N.; Caltagirone, C.; Van Rossom, W.; Gale, P. A., *Chem. Rev.* **2015,** *115*, 8038.

125. Santos-Figueroa, L. E.; Moragues, M. E.; Climent, E.; Agostini, A.; Martinez-Manez, R.; Sancenon, F., *Chem. Soc. Rev.* **2013,** *42*, 3489.

126. Madhuprasad; Bhat, M. P.; Jung, H.-Y.; Losic, D.; Kurkuri, M. D., *Chem. Eur. J.* **2016,** *22*, 6148.

127. Lee, M. H.; Kim, J. S.; Sessler, J. L., *Chem. Soc. Rev.* **2015,** *44*, 4185.

128. Gale, P. A.; Busschaert, N.; Haynes, C. J. E.; Karagiannidis, L. E.; Kirby, I. L., *Chem. Soc. Rev.* **2014,** *43*, 205.

129. Chang, K.-C.; Sun, S.-S.; Odago, M. O.; Lees, A. J., *Coord. Chem. Rev.* **2015,** *284*, 111.

130. Zhou, Y.; Zhang, J. F.; Yoon, J., *Chem. Rev.* **2014,** *114*, 5511.

131. Hudson, Z. M.; Wang, S., *Dalton Trans.* **2011,** *40*, 7805.

132. Galbraith, E.; James, T. D., *Chem. Soc. Rev.* **2010,** *39*, 3831.

133. Xu, Z.; Chen, X.; Kim, H. N.; Yoon, J., *Chem. Soc. Rev.* **2010,** *39*, 127.

134. Jäkle, F., *Chem. Rev.* **2010,** *110*, 3985.

135. Zhao, H.; Leamer, L. A.; Gabbai, F. P., *Dalton Trans.* **2013,** *42*, 8164.

136. Hudnall, T. W.; Chiu, C.-W.; Gabbaï, F. P., *Acc. Chem. Res.* **2009,** *42*, 388.

137. Hirai, M.; Cho, J.; Gabbaï, F. P., *Chem. Eur. J.* **2016,** *22*, 6537.

138. Pan, B.; Gabbaï, F. P., *J. Am. Chem. Soc.* **2014,** *136*, 9564.

139. Ghorab, M. F.; Winfield, J. M., *J. Fluorine Chem.* **1990,** *49*, 367.

140. Erker, G., *Dalton Trans.* **2005**, 1883.

141. Piers, W. E., *Adv. Organomet. Chem.* **2005,** *52*, 1.

142. Robertson, A. P. M.; Chitnis, S. S.; Jenkins, H. A.; McDonald, R.; Ferguson, M. J.; Burford, N., *Chem. Eur. J.* **2015,** *21*, 7902.

143. Sharutin, V. V.; Sharutina, O. K.; Pakusina, A. P.; Platonova, T. P.; Zadachina, O. P.; Gerasimenko, A. V., *Russ. J. Coord. Chem.* **2003,** *29*, 89.

144. Fukin, G. K.; Zakharov, L. N.; Domrachev, G. A.; Fedorov, A. Y.; Zaburdyaeva, S. N.; Dodonov, V. A., *Russ. Chem. Bull.* **1999,** *48*, 1722.

145. Dodonov, V. A.; Fedorov, A. Y.; Fukin, G. K.; Zaburdyaeva, S. N.; Zakharov, L. N.; Ignatenko, A. V., *Main Group Chemistry* **1999,** *3*, 15.

146. Holmes, R. R.; Day, R. O.; Chandrasekhar, V.; Holmes, J. M., *Inorg. Chem.* **1987,** *26*, 157.

147. Breunig, H. J.; Koehne, T.; Moldovan, O.; Preda, A. M.; Silvestru, A.; Silvestru, C.; Varga, R. A.; Piedra-Garza, L. F.; Kortz, U., *J. Organomet. Chem.* **2010,** *695*, 1307.

148. Nishii, N.; Matsumura, Y.; Okawara, R., *J. Organomet. Chem.* **1971,** *30*, 59.

149. Nishii, N.; Hashimoto, K.; Okawara, R., *J. Organomet. Chem.* **1973,** *55*, 133.

150. Tunde Bamgboye, T.; Begley, M. J.; Bryan Sowerby, D., *J. Organomet. Chem.* **1 989,** *362*, 77.

151. Jean, M., *Anal. Chim. Acta* **1971,** *57*, 438.

152. Bowen, L. H.; Rood, R. T., *J. Inorg. Nucl. Chem.* **1966,** *28*, 1985.

153. Benjamin, S. L.; Reid, G., *Coord. Chem. Rev.* **2015,** *297–298*, 168.

154. Chao, S. T.; Lara, N. C.; Lin, S.; Day, M. W.; Agapie, T., *Angew. Chem. Int. Ed.* **2011,** *50*, 7529.

155. Ke, I.-S. Organoantimony Lewis Acid as Flouride Receptors and Ligands towards Transition Metals Texas A & M University, 2013.

156. Sircoglou, M.; Mercy, M.; Saffon, N.; Coppel, Y.; Bouhadir, G.; Maron, L.; Bourissou, D., *Angew. Chem. Int. Ed.* **2009,** *48*, 3454.

157. Cowie, B. E.; Emslie, D. J. H.; Jenkins, H. A.; Britten, J. F., *Inorg. Chem.* **2010,** *49*, 4060.

158. Cowie, B. E.; Emslie, D. J. H., *Organometallics* **2015,** *34*, 2737.

159. Yang, H.; Gabbaï, F. P., *J. Am. Chem. Soc.* **2015,** *137*, 13425.

160. Laitar, D. S.; Müller, P.; Gray, T. G.; Sadighi, J. P., *Organometallics* **2005,** *24*, 4503.

161. Wyss, C. M.; Tate, B. K.; Bacsa, J.; Wieliczko, M.; Sadighi, J. P., *Polyhedron* **2014,** *84*, 87.

162. Macchi, P.; Sironi, A., *Coord. Chem. Rev.* **2003,** *238-239*, 383.

163. Bader, R. F. W.; Stephens, M. E., *J. Am. Chem. Soc.* **1975,** *97*, 7391.

164. Schmider, H. L.; Becke, A. D., *J. Chem. Phys.* **2002,** *116*, 3184.

165. Schmider, H. L.; Becke, A. D., *J. Mol. Struct.: THEOCHEM* **2000,** *527*, 51.

166. Tsipis, A. C.; Gkekas, G. N., *Dalton Trans.* **2013,** *42*, 8307.

167. Forniés, J.; Fortuño, C.; Ibáñez, S.; Martín, A.; Mastrorilli, P.; Gallo, V.; Tsipis, A., *Inorg. Chem.* **2013,** *52*, 1942.

168. Sircoglou, M.; Bouhadir, G.; Saffon, N.; Miqueu, K.; Bourissou, D., *Organometallics* **2008,** *27*, 1675.

169. Bruno, I. J.; Cole, J. C.; Kessler, M.; Luo, J.; Motherwell, W. D. S.; Purkis, L. H.; Smith, B. R.; Taylor, R.; Cooper, R. I.; Harris, S. E.; Orpen, A. G., *J. Chem. Inf. Comput. Sci.* **2004,** *44*, 2133.

170. Uson, R.; Laguna, A.; Laguna, M.; Briggs, D. A.; Murray, H. H.; Fackler, J. P., (Tetrahydrothiophene)Gold(I) or Gold(III) Complexes. In *Inorg. Synth.*, John Wiley & Sons, Inc.: 2007; pp 85.

171. Korshin, E. E.; Leitus, G.; Shimon, L. J. W.; Konstantinovski, L.; Milstein, D., *Inorg. Chem.* **2008,** *47*, 7177.

172. Zhao, X.-F.; Zhang, C., *Synthesis* **2007,** *2007*, 551.

173. Chalmers, B. A.; Bühl, M.; Athukorala Arachchige, K. S.; Slawin, A. M. Z.; Kilian, P., *Chem. Eur. J.* **2015,** *21*, 7520.

174. Becke, A. D., *Phys. Rev. A* **1988,** *38*, 3098.

175. Perdew, J. P., *Phys. Rev. B* **1986,** *33*, 8822.

176. Peterson, K. A.; Puzzarini, C., *Theor. Che. Accounts Theor. Comput. Model Theor. Chim. Acta.* **2005,** *114*, 283.

177. Figgen, D.; Rauhut, G.; Dolg, M.; Stoll, H., *Chem. Phys.* **2005,** *311*, 227.

178. Peterson, K. A., *J. Chem. Phys.* **2003,** *119*, 11099.

179. Metz, B.; Stoll, H.; Dolg, M., *J. Chem. Phys.* **2000,** *113*, 2563.

180. Keith, T. A. *AIMAll (Version 14.06.21)*, TK Gristmill Software: Overland Park KS, USA, 2014.

181. Lu, T.; Chen, F., *J. Mol. Graphics Modell.* **2012,** *38*, 314.

182. Lu, T.; Chen, F., *J. Comput. Chem.* **2012,** *33*, 580.

183. Shriver, D. F., *Acc. Chem. Res.* **1970,** *3*, 231.

184. Parkin, G., *Organometallics* **2006,** *25*, 4744.

185. Hill, A. F., *Organometallics* **2006,** *25*, 4741.

186. Bouhadir, G.; Amgoune, A.; Bourissou, D., *Adv. Organomet. Chem.* **2010,** *58*, 1.

187. Amgoune, A.; Bourissou, D., *Chem. Commun.* **2011,** *47*, 859.

188. Braunschweig, H.; Dewhurst, R. D., *Dalton Trans.* **2011,** *40*, 549.

189. Kameo, H.; Nakazawa, H., *Chem. Asian J.* **2013,** *8*, 1720.

190. Jones, J. S.; Gabbaï, F. P., *Acc. Chem. Res.* **2016,** *49*, 857.

191. Jones, J. S.; Gabbaï, F. P., *Chem. Lett.* **2016,** *45*, 376.

192. Benjamin, S. L.; Krämer, T.; Levason, W.; Light, M. E.; Macgregor, S. A.; Reid, G., *J. Am. Chem. Soc.* **2016,** *138*, 6964.

193. Vollmer, M. V.; Xie, J.; Lu, C. C., *J. Am. Chem. Soc.* **2017,** *139*, 6570.

194. Bouhadir, G.; Bourissou, D., *Chem. Soc. Rev.* **2016,** *45*, 1065.

195. Kameo, H.; Kawamoto, T.; Sakaki, S.; Bourissou, D.; Nakazawa, H., *Chem. Eur. J.* **2016,** *22*, 2370.

196. Kameo, H.; Ikeda, K.; Bourissou, D.; Sakaki, S.; Takemoto, S.; Nakazawa, H.; Matsuzaka, H., *Organometallics* **2016,** *35*, 713.

197. Cammarota, R. C.; Lu, C. C., *J. Am. Chem. Soc.* **2015,** *137*, 12486.

198. Schindler, T.; Lux, M.; Peters, M.; Scharf, L. T.; Osseili, H.; Maron, L.; Tauchert, M. E., *Organometallics* **2015,** *34*, 1978.

199. Fong, H.; Moret, M.-E.; Lee, Y.; Peters, J. C., *Organometallics* **2013,** *32*, 3053.

200. Anderson, J. S.; Rittle, J.; Peters, J. C., *Nature* **2013,** *501*, 84.

201. Shih, W.-C.; Gu, W.; MacInnis, M. C.; Timpa, S. D.; Bhuvanesh, N.; Zhou, J.; Ozerov, O. V., *J. Am. Chem. Soc.* **2016,** *138*, 2086.

202. Ugarte, R. A.; Hudnall, T. W., *Green Chemistry* **2017,** *19*, 1990.

203. Chitnis, S. S.; Sparkes, H. A.; Annibale, V. T.; Pridmore, N. E.; Oliver, A. M.; Manners, I., *Angew. Chem. Int. Ed.* **2017,** *56*, 9536.

204. Tofan, D.; Gabbai, F. P., *Chem. Sci.* **2016,** *7*, 6768.

205. Hirai, M.; Myahkostupov, M.; Castellano, F. N.; Gabbaï, F. P., *Organometallics* **2016,** *35*, 1854.

206. Arias Ugarte, R.; Devarajan, D.; Mushinski, R. M.; Hudnall, T. W., *Dalton Trans.* **2016,** *45*, 11150.

207. Li, N.; Qiu, R.; Zhang, X.; Chen, Y.; Yin, S.-F.; Xu, X., *Tetrahedron* **2015,** *71*, 4275.

208. Robertson, A. P. M.; Burford, N.; McDonald, R.; Ferguson, M. J., *Angew. Chem. Int. Ed.* **2014,** *53*, 3480.

209. Holthausen, M. H.; Mehta, M.; Stephan, D. W., *Angew. Chem. Int. Ed.* **2014,** *53*, 6538.

210. Caputo, C. B.; Hounjet, L. J.; Dobrovetsky, R.; Stephan, D. W., *Science* **2013,** *341*, 1374.

211. Wade, C. R.; Gabbaï, F. P., *Organometallics* **2011,** *30*, 4479.

212. Wade, C. R.; Lin, T.-P.; Nelson, R. C.; Mader, E. A.; Miller, J. T.; Gabbaï, F. P., *J. Am. Chem. Soc.* **2011,** *133*, 8948.

213. Ke, I.-S.; Jones, J. S.; Gabbaï, F. P., *Angew. Chem. Int. Ed.* **2014,** *53*, 2633.

214. Yang, H.; Gabbaï, F. P., *J. Am. Chem. Soc.* **2014,** *136*, 10866.

215. Sahu, S.; Gabbaï, F. P., *J. Am. Chem. Soc.* **2017,** *139*, 5035.

216. Green, M. L. H., *J. Organomet. Chem.* **1995,** *500*, 127.

217. Wade, C. R.; Gabbaï, F. P., *Angew. Chem. Int. Ed.* **2011,** *50*, 7369.

218. Sen, S.; Ke, I.-S.; Gabbaï, F. P., *Inorg. Chem.* **2016,** *55*, 9162.

219. Inagaki, F.; Matsumoto, C.; Okada, Y.; Maruyama, N.; Mukai, C., *Angew. Chem. Int. Ed.* **2015,** *54*, 818.

220. Inagaki, F.; Nakazawa, K.; Maeda, K.; Koseki, T.; Mukai, C., *Organometallics* **2017**, Ahead of Print.

221. Smith, C. E.; Smith, P. S.; Thomas, R. L.; Robins, E. G.; Collings, J. C.; Dai, C.; Scott, A. J.; Borwick, S.; Batsanov, A. S.; Watt, S. W.; Clark, S. J.; Viney, C.; Howard, J. A. K.; Clegg, W.; Marder, T. B., *J. Mater. Chem.* **2004,** *14*, 413.

222. Wang, Y.; Wang, Z.; Li, Y.; Wu, G.; Cao, Z.; Zhang, L., *Nat. Comm.* **2014,** *5*, 3470.

223. Malhotra, D.; Mashuta, M. S.; Hammond, G. B.; Xu, B., *Angew. Chem. Int. Ed.* **2014,** *53*, 4456.

224. Lavallo, V.; Wright, J. H.; Tham, F. S.; Quinlivan, S., *Angew. Chem. Int. Ed.* **2013,** *52*, 3172.

225. Alvarado, E.; Badaj, A. C.; Larocque, T. G.; Lavoie, G. G., *Chem. Eur. J.* **2012,** *18*, 12112.

226. Leyva, A.; Corma, A., *Adv. Synth. Catal.* **2009,** *351*, 2876.

227. Lavallo, V.; Frey, G. D.; Donnadieu, B.; Soleilhavoup, M.; Bertrand, G., *Angew. Chem. Int. Ed.* **2008,** *47*, 5224.

228. Mizushima, E.; Hayashi, T.; Tanaka, M., *Org. Lett.* **2003,** *5*, 3349.

229. Hashmi, A. S. K.; Weyrauch, J. P.; Frey, W.; Bats, J. W., *Org. Lett.* **2004,** *6*, 4391.

230. Weyrauch, J. P.; Hashmi, A. S. K.; Schuster, A.; Hengst, T.; Schetter, S.; Littmann, A.; Rudolph, M.; Hamzic, M.; Visus, J.; Rominger, F.; Frey, W.; Bats, J. W., *Chem. Eur. J.* **2010,** *16*, 956.

231. Tolman, C. A., *Chem. Rev.* **1977,** *77*, 313.

232. Grobe, J.; Krummen, N.; Wehmschulte, R.; Krebs, B.; Laege, M., *Z. Anorg. Allg. Chem.* **1994,** *620*, 1645.

233. Wagler, J.; Brendler, E., *Angew. Chem. Int. Ed.* **2010,** *49*, 624.

234. Wagler, J.; Hill, A. F.; Heine, T., *Eur. J. Inorg. Chem.* **2008**, 4225.

235. Baker, L.-J.; Rickard, C. E. F.; Taylor, M. J., *J. Chem. Soc., Dalton Trans.* **1995**, 2895.

236. Egorova, I. V.; Zhidkov, V. V.; Grinishak, I. P.; Rakhanskii, A. A., *Russ. J. Gen. Chem.* **2014,** *84*, 1371.

237. Ivanov, M. A.; Sharutin, V. V.; Ivanov, A. V.; Gerasimenko, A. V.; Antsutkin, O. N., *Russ. J. Coord. Chem.* **2008,** *34*, 527.

238. Knop, O.; Vincent, B. R.; Cameron, T. S., *Can. J. Chem.* **1989,** *67*, 63.

239. Rüther, R.; Huber, F.; Preut, H., *J. Organomet. Chem.* **1985,** *295*, 21.

240. Sharutin, V. V.; Molokova, O. V.; Sharutina, O. K., *Russ. J. Inorg. Chem.* **2013,** *58*, 400.

241. Sharutin, V. V.; Molokova, O. V.; Sharutina, O. K.; Akimova, T. I.; Gerasimenko, A. V.; Pushilin, M. A., *Russ. J. Coord. Chem.* **2004,** *30*, 559.

242. Sharutin, V. V.; Pakusina, A. P.; Egorova, I. V.; Platonova, T. P.; Bukvetskii, B. V.; Popov, D. Y., *Russ. J. Coord. Chem.* **2001,** *28*, 827.

243. Sharutin, V. V.; Pakusina, A. P.; Senchurin, V. S.; Gerasimenko, A. V.; Gerasimenko, E. A., *Russ. J. Coord. Chem.* **2002,** *28*, 540.

244. Sharutin, V. V.; Pakusina, A. P.; Smirnova, S. A.; Fukin, G. K., *Russ. J. Coord. Chem.* **2004,** *30*, 392.

245. Sharutin, V. V.; Pakusina, A. P.; Zadachina, O. P.; Sharutina, O. K.; Gerasimenko, A. V.; Pushilin, M. A., *Russ. J. Coord. Chem.* **2004,** *30*, 397.

246. Sharutin, V. V.; Sharutina, O. K.; Bondar', E. A.; Pakusina, A. P.; Adonin, N. Y.; Starichenko, V. F.; Fukin, G. K.; Zakharov, L. N., *Russ. J. Coord. Chem.* **2001,** *27*, 393.

247. Sharutin, V. V.; Sharutina, O. K.; Bondar', E. A.; Pakusina, A. P.; Gatilov, Y. V.; Adonin, N. Y.; Starichenko, V. F., *Russ. J. Coord. Chem.* **2002,** *28*, 333.

248. Sharutin, V. V.; Sharutina, O. K.; Molokova, O. V.; Ettenko, E. N.; Krivolapov, D. B.; Gubaidullin, A. T.; Litvinov, I. A., *Russ. J. Gen. Chem.* **2004,** *71*, 1243.

249. Sharutin, V. V.; Sharutina, O. K.; Osipov, P. E.; Platonova, T. P.; Pakusina, A. P.; Fukin, G. K.; Zakharov, L. N., *Russ. J. Coord. Chem.* **2001,** *27*, 483.

250. Sharutin, V. V.; Sharutina, O. K.; Senchurin, S. V., *Russ. J. Inorg. Chem.* **2014,** *59*, 951.

251. Shen, K.-W.; McEwen, W. E.; La Placa, S. J.; Hamilton, W. C.; Wolf, A. P., *J. Am. Chem. Soc.* **1968,** *90*, 1718.

252. Wang, G.-C.; Xiao, J.; Yu, L.; Li, J.-S.; Cui, J.-R.; Wang, R.-Q.; Ran, F.-X., *J. Organomet. Chem.* **2004,** *689*, 1631.

253. Wade, C. R. Synthesis and Study of Boron and Antimony Lewis Acids as Small Anion Receptors and Ligands Towards Transition Metals. Texas A&M University, 2012.

254. Sheldrick, G. M., SADABS.

255. Dolomanov, O. V.; Bourhis, L. J.; Gildea, R. J.; Howard, J. A. K.; Puschmann, H., *J. Appl. Crystallogr.* **2009,** *42*, 339.

256. Spek, A., *Acta Crystallogr., Sect. C* **2015,** *71*, 9.

257. Spek, A., *Acta Crystallogr., Sect. D* **2009,** *65*, 148.

258. Norman, N.; Mathisen, H., *Acta Chem. Scand.* **1964,** *18*, 353.

259. Glendening, E. D.; Badenhoop, J. K.; Reed, A. E.; Carpenter, J. E.; Bohmann, J. A.; Morales, C. M.; Weinhold, F., *NBO 5.9*, Theoretical Chemistry Institute, University of Wisconsin, Madison, WI, 2011.

260. Manson, J.; Webster, C. E.; Pérez, L. M.; Hall, M. B., http://www.chem.tamu.edu/jimp2/index.html.

261. Braunschweig, H.; Gruss, K.; Radacki, K., *Angew. Chem. Int. Ed.* **2009,** *48*, 4239.

262. Braunschweig, H.; Radacki, K.; Schwab, K., *Chem. Commun.* **2010,** *46*, 913.

263. Bertermann, R.; Böhnke, J.; Braunschweig, H.; Dewhurst, R. D.; Kupfer, T.; Muessig, J. H.; Pentecost, L.; Radacki, K.; Sen, S. S.; Vargas, A., *J. Am. Chem. Soc.* **2016,** *138*, 16140.

264. Jones, J. S. Coordination Non-innocence and Redox Chemistry of Antimony Ligands. Texas A&M University, 2016.

265. Yang, H. Antimony and Tellurium Non-innocent Z-ligands for Transition Metals and Their Application in Photoredox Chemistry and Electrophilic Catalysis. Texas A&M University, 2016.

266. Alzoubi, B. M.; Walther, M.; Puchta, R.; van Eldik, R., *Dalton Trans.* **2012,** *41*, 6932.

267. Teets, T. S.; Cook, T. R.; McCarthy, B. D.; Nocera, D. G., *Inorg. Chem.* **2011,** *50*, 5223.

268. Hwang, S. J.; Powers, D. C.; Maher, A. G.; Anderson, B. L.; Hadt, R. G.; Zheng, S.-L.; Chen, Y.-S.; Nocera, D. G., *J. Am. Chem. Soc.* **2015,** *137*, 6472.

269. Teets, T. S.; Nocera, D. G., *J. Am. Chem. Soc.* **2009,** *131*, 7411.

270. Powers, D. C.; Benitez, D.; Tkatchouk, E.; Goddard, W. A.; Ritter, T., *J. Am. Chem. Soc.* **2010,** *132*, 14092.

271. Vigalok, A., *Chem. Eur. J.* **2008,** *14*, 5102.

272. Van der Eide, E. F.; Piers, W. E.; Romero, P. E.; Parvez, M.; McDonald, R., *Organometallics* **2004,** *23*, 314.

273. Yang, X.; Stern, C. L.; Marks, T. J., *J. Am. Chem. Soc.* **1991,** *113*, 3623.

274. Piers, W. E.; Chivers, T., *Chem. Soc. Rev.* **1997,** *26*, 345.

275. Guérinot, A.; Fang, W.; Sircoglou, M.; Bour, C.; Bezzenine-Lafollée, S.; Gandon, V., *Angew. Chem. Int. Ed.* **2013,** *52*, 5848.

276. Ranieri, B.; Escofet, I.; Echavarren, A. M., *Org. Biomol. Chem.* **2015,** *13*, 7103.

277. Zhdanko, A.; Maier, M. E., *ACS Catal.* **2015,** *5*, 5994.

278. Fang, W.; Presset, M.; Guerinot, A.; Bour, C.; Bezzenine-Lafollee, S.; Gandon, V., *Organic Chemistry Frontiers* **2014,** *1*, 608.

279. Fang, W.; Presset, M.; Guérinot, A.; Bour, C.; Bezzenine-Lafollée, S.; Gandon, V., *Chem. Eur. J.* **2014,** *20*, 5439.

280. Alcarazo, M., *Acc. Chem. Res.* **2016,** *49*, 1797.

281. Wegener, M.; Huber, F.; Bolli, C.; Jenne, C.; Kirsch, S. F., *Chem. Eur. J.* **2015,** *21*, 1328.

282. Jones, J. S.; Gabbai, F. P., *Chem. Eur. J.* **2017,** *23*, 1136.

283. Devillard, M.; Bouhadir, G.; Bourissou, D., *Angew. Chem. Int. Ed.* **2015,** *54*, 730.

284. You, D.; Gabbai, F. P., *J. Am. Chem. Soc.* **2017,** *139*, 6843.

285. Auvil, T. J.; Schafer, A. G.; Mattson, A. E., *Eur. J. Org. Chem.* **2014,** *2014*, 2633.

286. Angermaier, K.; Schmidbaur, H., *Z. Naturforsch., B: Chem. Sci.* **1996,** *51*, 879.

287. Berger, R. J.; Schoiber, J.; Monkowius, U., *Inorg. Chem.* **2017,** *56*, 956.

288. Scherf, L. M.; Baer, S. A.; Kraus, F.; Bawaked, S. M.; Schmidbaur, H., *Inorg. Chem.* **2013,** *52*, 2157.

289. Pregosin, P. S.; Kumar, P. G. A.; Fernández, I., *Chem. Rev.* **2005,** *105*, 2977.

290. Zuccaccia, C.; Stahl Nicholas, G.; Macchioni, A.; Chen, M.-C.; Roberts John, A.; Marks Tobin, J., *J. Am. Chem. Soc.* **2004,** *126*, 1448.

291. Hoefelmeyer, J. D.; Brode, D. L.; Gabbaï, F. P., *Organometallics* **2001,** *20*, 5653.

292. Valentini, M.; Pregosin, P. S.; Ruegger, H., *Organometallics* **2000,** *19*, 2551.

293. Sakai, T., *Acta Crystallogr., Sect. B* **1978,** *34*, 3649.

294. Khan, M.; Oldham, C.; Tuck, D. G., *Can. J. Chem.* **1981,** *59*, 2714.

295. Becke, A. D., *Phys. Rev. A* **1988,** *38*, 3098.

296. Perdew, J. P., *Phys. Rev. B* **1986,** *33*, 8822.

297. Figgen, D.; Rauhut, G.; Dolg, M.; Stoll, H., *Chem. Phys.* **2005,** *311*, 227.

298. Pietraszuk, C.; Rogalski, S.; Powała, B.; Miętkiewski, M.; Kubicki, M.; Spólnik, G.; Danikiewicz, W.; Woźniak, K.; Pazio, A.; Szadkowska, A.; Kozłowska, A.; Grela, K., *Chem. Eur. J.* **2012,** *18*, 6465.

299. Huchel, U.; Tiwari, P.; Schmidt, R. R., *J. Carbohydr. Chem.* **2010,** *29*, 61.

300. Becke, *Phys. Rev. A: Gen. Phys.* **1988,** *38*, 3098.